

December 2017

# Semi-Open Space and Micro-Environmental Control for Improving Thermal Comfort, Indoor Air Quality, and Building Energy Efficiency

Meng Kong  
*Syracuse University*

Follow this and additional works at: <https://surface.syr.edu/etd>



Part of the [Engineering Commons](#)

---

## Recommended Citation

Kong, Meng, "Semi-Open Space and Micro-Environmental Control for Improving Thermal Comfort, Indoor Air Quality, and Building Energy Efficiency" (2017). *Dissertations - ALL*. 810.  
<https://surface.syr.edu/etd/810>

This Dissertation is brought to you for free and open access by the SURFACE at SURFACE. It has been accepted for inclusion in Dissertations - ALL by an authorized administrator of SURFACE. For more information, please contact [surface@syr.edu](mailto:surface@syr.edu).

## **Abstract**

Local air delivery, heating, and cooling combined with local space partition and confinement (called semi-open space or SOS) have the potential to provide micro-environment that is tailored to the individual preference of the occupants, and hence increase the percentage of satisfied occupancy from currently 80% to near 100%. This research investigates the use of a micro-environmental control system ( $\mu X$ ) and semi-open space (SOS) to efficiently provide the desired thermal comfort and air quality conditions for individual occupants while the ambient air temperature set-points were relaxed for reducing the overall energy consumption of the building. A computational fluid dynamics (CFD) model was developed and validated. The model in combination with the results from full-scale chamber experiments was used to evaluate the performance of proposed cooling/heating delivery system and the role of the SOS. During summer time, a cooler air was supplied locally. It was found that the cooling performance increased more by increasing the supply air flow rate than reducing the supply air temperature when the total cooling power is constant, and the cooling performance of the Air Terminal Devices (ATDs) was highly dependent on the shooting angle. The cooling efficiency increased dramatically with the supply air temperature. Also, both the CFD model simulation and experimental work has demonstrated that the heat loss by the manikin was sensitive to the distance between the diffuser and the manikin. However, this effect was also related to the clothing material on the manikin. During the winter time, the idea of heating a person with only a warm air jet was shown to be not efficient, but the confinement box was able to improve the heating performance by two to three times. A more ergonomically-friendly warming foot mat with a reflective box was very effective to restore people's thermal

comfort when the ambient space air was maintained at a lower temperature set-point for energy saving. The existence of the cubicle, as an SOS, significantly changed the airflow pattern in the office, and hence the thermal environment and air quality distribution. The cubicle could “protect” the occupants from the background air flow by reducing the average velocity as well as increasing the average temperature in the occupied space. The openness of the cubicle weakened the “protection” of the cubicle depending on the opening’s orientation and size. The “protection” may not be favored regarding thermal comfort and air quality when the emission is inside the cubicle, but it should be encouraged when the emission is outside the cubicle. The combination of the  $\mu X$  with the SOS can create an independent micro-environment regarding thermal comfort and air quality as well as maintain the privacy of the occupant. As a secondary goal, the ability of the CFD model to adequately predict the local heat transfer from the human body and its limitation were also investigated. The case without the  $\mu X$  compared better with the experiment than the case with the  $\mu X$  from the heat transfer point of view. The effect of the clothing material could be properly represented by a constant temperature difference or as a layer of thermal resistance. Moreover, it was found the fidelity of the surface temperature control for the manikin affected the validation of the CFD model. The concept of SOS was defined for the first time in this study and SOS’s role in shaping the microenvironment with and without local heat, cooling and ventilation were investigated both numerically and experimentally. The detailed CFD model developed has accurate representation of the effects of the manikin’s geometry and the effect of clothing thermal resistance on the boundary conditions for the CFD simulation, which can be used for the investigation of effects of air velocity, temperature, room air flow pattern and clothing on the local and

overall average heat loss from human bodies and the resulting thermal comfort of the building occupants under various internal room and partition configurations.

Semi-Open Space and Micro-Environmental Control for Improving Thermal  
Comfort, Indoor Air Quality, and Building Energy Efficiency

by

Meng Kong

B.S., Beijing University of Civil Engineering and Architecture, 2010  
M.S., Syracuse University, 2013

Dissertation

Submitted in partial fulfillment of the requirements for the degree of  
Doctor of Philosophy in *Mechanical and Aerospace Engineering*.

Syracuse University  
December 2017

Copyright © Meng Kong 2017  
All Rights Reserved

## **Acknowledgements**

Seven years ago, when I stepped into the classroom of Syracuse for the first time, I did not expect that I could eventually accomplish both my Master and Ph.D. degree so fast. Within those seven years, I gained tremendous knowledge and research experience. I would like to take this opportunity to express my sincere gratitude to all the people who helped me during my study in Syracuse since I came here. Without them, I would not certainly survive and succeed in this marathon.

My foremost and most sincere gratitude should definitely go to my advisor, Dr. Jianshun Zhang, whom I met during the most difficult time in my life. He recruited me, a rookie in research at that time, into his team, and guided me with his rich experience, extensive knowledge and great patience on the road to a qualified engineer and scientist. His lessons, talks and even the typical smile have helped build the foundation of my career and reconstructed my confidence in life. He is not only a good advisor in my study but also an extraordinary mentor in my life.

I would like to thank Dr. H. Ezzat Khalifa and Dr. Thong Q. Dang for supporting and co-advising me during the last two years of my study. From the discussions and constructive criticism at our weekly meeting and in the classroom, I learned not only the fundamental knowledge but also the attitude and respect to the science. I would also like to thank Dr. Ashok Shantilal Sangani, Dr. Can Isik, and Dr. Shalabh Chandra Maroo for serving on my defense committee and great comments on my dissertation.

I would like to express my gratitude to many graduate students and colleagues for their help during my research. My appreciation goes to Dr. Lihui Wang, Dr. Nhan Huu Phan, Jingjing Wang, Zhimin Jiang, Rui Zhang and Fan Zhang for their contribution to my work in these

years. I would like to give my special thanks to all the members of BEESL group intensively for their support during my stay in Syracuse, especially Ms. Beverly Guo, who keeps helping us manage the lab, share experimental skills, and make logistic arrangements. Finally, I would like to thank my family. My father, Yun Kong, who used to encourage me to come to the US to study, has built the foundation of my life and used his whole life to show me how a real man should behave. My Mother, Xiping Jia has given endless love to her son but asked nothing in return. My two little cats, Coke and Sprite, have accompanied me during this period of time. I also thank all my friends for their continuous encouragement and support.

Most of the information, data, or work presented herein was through a research project funded by the Advanced Research Projects Agency-Energy (ARPA-E), U.S. Department of Energy, under Award Number **DE-AR0000526**. The views and opinions of authors expressed herein do not necessarily state or reflect those of the United States Government or any agency thereof.

Meng Kong

Syracuse, October 2017



## Table of Contents

Abstract .....	1
Acknowledgements .....	vi
Table of Contents .....	vii
List of Figures .....	xi
List of Tables .....	xiv
List of Symbols .....	xv
1. Introduction.....	1
1.1. Background and Problem Definition.....	1
1.1.1. Motivation.....	1
1.1.2. Semi-open Space.....	5
1.1.3. Micro-Environmental Control Strategy .....	10
1.1.4. Multi-scale Zones in a Ventilated Room .....	15
1.1.5. Problem definition .....	19
1.2. Goal and Objectives .....	21
1.3. Scope of Work and Dissertation Roadmap .....	21
2. Thermal Comfort, Indoor Air Quality and Room Air Distribution .....	25
2.1. Thermal Environment .....	25
2.1.1. Thermal Comfort .....	25
2.1.2. Thermal Comfort Evaluation .....	27
2.2. Air Quality.....	43
2.2.1. Delivering the Fresh Air .....	44
2.2.2. Removing the Pollutant.....	46
2.3. Room Air and Contaminant Distribution.....	48
2.4. Indoor Environment Evaluation and Design Methods.....	52
2.4.1. Analytical Model .....	52
2.4.2. Empirical Models.....	52
2.4.3. Nodal Model .....	53
2.4.4. Zonal Model.....	53
2.4.5. Design Chart .....	55
2.4.6. Computational Fluid Dynamics Model.....	57
3. Performance Evaluation of Different Room Air Distribution Systems .....	59
3.1. Field Experimental Evaluation of Three Kinds of Ventilation Systems.....	59

3.1.1.	Overview.....	59
3.1.2.	Flow Field Characteristics .....	64
3.1.3.	Thermal Comfort Analysis .....	65
3.1.4.	Air Quality Analysis .....	66
3.2.	CFD Model Development .....	68
3.2.1.	Overview.....	68
3.2.2.	Experiment Data Set for Model Validation .....	69
3.2.3.	Governing Equations for CFD Model.....	70
3.2.4.	Post Processing .....	73
3.2.5.	Verification and Validation.....	73
3.2.6.	PV and UFAD Comparison .....	79
3.2.7.	PV Performance under Different Airflow Rates.....	82
3.3.	Summary and Conclusions.....	86
4.	Micro-environmental Control for Efficient Local Cooling .....	88
4.1.	Overview .....	88
4.1.1.	Experimental Facility.....	90
4.1.2.	Computational Model .....	93
4.1.3.	Boundary Conditions Used in CFD Simulation .....	95
4.1.4.	Determination of the Convective Heat Transfer Coefficient.....	99
4.1.5.	Heat Removal Performance and Thermal Comfort .....	100
4.2.	Results and Discussion.....	102
4.2.1.	Validation.....	102
4.2.2.	Convective Heat Transfer Coefficient of Different Body Segments .....	105
4.2.3.	Determination of Suitable Air Supply Temperature and Flow Rates .....	106
4.2.4.	Evaluation of ATDs .....	109
4.2.5.	Effect of Furniture.....	115
4.2.6.	Effect of the Surface Temperature .....	116
4.2.7.	Other Considerations .....	120
4.3.	Summary and Conclusions.....	120
5.	Micro Environmental Control for Efficient Heating .....	122
5.1.	Overview .....	122
5.1.1.	Boundary Conditions for CFD Simulations.....	123
5.1.2.	Clothing Assembly.....	129
5.1.3.	Thermal Comfort .....	130

5.2.	Results and Discussion.....	131
5.2.1.	Split Diffuser.....	131
5.2.2.	Effect of Confinement Box.....	138
5.2.3.	Footwarmer.....	142
5.3.	Summary and Conclusions.....	145
6.	Experimental Evaluation of the Micro-Environmental Control in a Semi-Open Space	148
6.1.	Overview.....	148
6.1.1.	Experimental Facility.....	148
6.1.2.	Experimental Conditions.....	154
6.2.	Micro-Environmental Control System in Cooling Condition.....	160
6.2.1.	Effects of the Distance between the Diffuser and the Manikin.....	160
6.2.2.	Effect of the Shooting Angle.....	163
6.2.3.	Effect of the Supply Flow Rate and Supply Temperature.....	165
6.2.4.	Effect of the Clothing Material.....	168
6.3.	Effects of the Semi-Open Space.....	171
6.3.1.	With v.s. Without the Cubicle.....	172
6.3.2.	Effect of the Opening Size of the Cubicle.....	179
6.3.3.	Cubicle with $\mu X$ .....	181
6.4.	Thermal Response Evaluation.....	184
6.5.	Summary and Conclusions.....	187
7.	CFD Study of the Ventilated Semi-Open Space.....	189
7.1.	Overview.....	189
7.2.	Effects of the SOS.....	191
7.2.1.	Pollutant Mass Fraction Level in the Breathing Zone and the Cubicle.....	192
7.2.2.	Contaminant Removal Efficiency.....	196
7.2.3.	Blocking Coefficient.....	201
7.3.	Summary and Conclusions.....	202
8.	Performance Evaluation of the Selected Cooling/Heating Delivery Devices.....	205
8.1.	Performance Evaluation of Three Different ATDs for Cooling.....	205
8.2.	Performance Evaluation of the Heating Delivering Device (HDDs).....	210
8.3.	Summary and Conclusions.....	214
9.	Conclusions and Recommendations for Future Study.....	216
9.1.	Effects of the SOS and $\mu X$ on Thermal Comfort and Air Quality Conditions.....	216

9.2. Validity of CFD Models.....	220
9.3. Recommendations for Future Work.....	222
Reference .....	225

## List of Figures

Figure 1-1 Summary of average HVAC energy saving in 5 climates(Hoyt et al. 2015).....	3
Figure 1-2 Examples of Semi-open Space.....	7
Figure 1-3 Categories of micro-environmental control strategy.....	15
Figure 1-4 Micro-environment zone definition .....	18
Figure 2-1 Thermal comfort.....	26
Figure 2-2 Physiological model development .....	31
Figure 2-3 Timeline of psychological rational model’s development .....	40
Figure 2-4 Different air distribution systems for cooling with high (left) and low (right) location of supply openings (Nielsen 2011) .....	56
Figure 2-5 Design chart of the "Family Tree" (Nielsen 2011) .....	57
Figure 3-1 Prototype Room Layout .....	60
Figure 3-2 Target Cubicle .....	60
Figure 3-3 Terminal of ventilation system: UFAD (left), PV (center), CV (Right).....	62
Figure 3-4 Measurement Setup .....	63
Figure 3-5 Velocity comparison of three systems .....	64
Figure 3-6 Temperature comparison of three systems.....	65
Figure 3-7 Equivalent Temperature .....	66
Figure 3-8 Local Ventilation Efficiency, Ventilation Efficiency and Blocking Coefficient .....	67
Figure 3-9 Target cubicle (left) and TIEQ (right).....	68
Figure 3-10 Terminal of ventilation system: UFAD (a), PV (b) .....	70
Figure 3-11 Cubicles Configuration .....	<b>Error! Bookmark not defined.</b>
Figure 3-12 Grid resolution (a) and velocity in front of the face (b).....	75
Figure 3-13 Velocity validation (a) of different boundary conditions; (b) of different simulation space.....	78
Figure 3-14 Temperature validation along the right front pole (a) of different boundary conditions; (b) of different simulation space .....	79
Figure 3-15 Equivalent temperature .....	80
Figure 3-16 AQI (a) and cooling efficiency (b) comparison .....	81
Figure 3-17 PV outlet velocity profile .....	82
Figure 3-18 Temperature distribution on the manikin symmetry plane .....	83
Figure 3-19 Back view of the temperature distribution .....	84
Figure 3-20 Velocity field on the manikin symmetry plane .....	85
Figure 3-21 Tracer gas mass fraction field at manikin symmetry plane.....	86
Figure 4-1 Computational domain and three types of ATDs studied .....	90
Figure 4-2 Schematic of the test chamber.....	92
Figure 4-3 Experimental Facility .....	93
Figure 4-4 Mesh grids of the CFD model.....	94
Figure 4-5 Velocity traverse grid and profile of the diffuser (Type I).....	98
Figure 4-6 Comparison between CFD and experimental results .....	104
Figure 4-7 Convective heat transfer coefficient of different segments of the human body .....	106
Figure 4-8 Local operative temperature and air velocity.....	108

Figure 4-9 Movement range of the occupant (left) and the shooting angle of the ATDs (right) .....	110
Figure 4-10 Cooling performance of Type I ATD shooting at different angles with the manikin sitting along the center line .....	111
Figure 4-11 Velocity field at the symmetric plane of the manikin when it sits 0.45m and 0.61m away from the desk .....	112
Figure 4-12 Summary of the cooling performance of the three ATDs .....	114
Figure 4-13 Velocity field behind the manikin .....	116
Figure 4-14 Surface temperature measurement on the manikin .....	117
Figure 4-15 Surface temperature distribution on the manikin .....	118
Figure 5-1 Split diffuser to the feet .....	124
Figure 5-2 Split diffuser with the confinement box (a) CFD model; (b) Example of the strip door ( <a href="http://www.ganikpvcurtains.com/">http://www.ganikpvcurtains.com/</a> ) .....	127
Figure 5-3 Footwarmer heating .....	128
Figure 5-4 Surface heat flux of the cases with different supply velocities .....	133
Figure 5-5 Mean Thermal Vote of the cases with different supply velocities .....	135
Figure 5-6 Surface heat flux of the cases with different supply combinations .....	137
Figure 5-7 Mean Thermal Vote of the cases with different supply combinations .....	138
Figure 5-8 Surface heat flux of the cases with confinement box .....	140
Figure 5-9 Mean Thermal Vote of the cases with confinement box .....	141
Figure 5-10 Surface heat flux of the cases with footwarmer .....	143
Figure 5-11 Mean Thermal Vote of the cases with footwarmer .....	145
Figure 6-1 Flow diagram of the IEQ chamber .....	150
Figure 6-2 Clothed multi-segment thermal manikin .....	151
Figure 6-3 Diffuser with louvers installed .....	151
Figure 6-4 Partition of the cubicle .....	152
Figure 6-5 Cubicle around the workstation .....	154
Figure 6-6 IEQ chamber (a) and its HVAC system (b) .....	156
Figure 6-7 Segmental heat flow rates of the cases with different distances .....	163
Figure 6-8 Effect of the shooting angle .....	165
Figure 6-9 Effect of the supply flow rate .....	166
Figure 6-10 Effect of the supply temperature .....	167
Figure 6-11 Cooling efficiency .....	168
Figure 6-12 Manikin dressed in a polo shirt (left) and a sports shirt (right) .....	169
Figure 6-13 Segmental heat flow rates of the cases with different clothing material .....	171
Figure 6-14 Velocity in the occupied space (26.1 °C) (FO: fully open; FC: fully closed) .....	173
Figure 6-15 Temperature in the occupied space with v.s. without cubicle (26.1 °C) .....	174
Figure 6-16 Velocity in the occupied space (23.9 °C) .....	175
Figure 6-17 Temperatures at different heights from the floor in the occupied space with v.s. without cubicle (return air temperature: 23.9 °C) .....	176
Figure 6-18 Temperature in the occupied space with opening in the front (26.1 °C) .....	180
Figure 6-19 Temperature in the occupied space with opening in the front (23.9 °C) .....	181
Figure 6-20 Percentage of increased heat loss compared with the case with fully closed cubicle .....	182

Figure 6-21 Whole-body MTV prediction of the cases with different distances .....	184
Figure 6-22 Whole-body MTV prediction of the cases with different supply temperatures and flow rates .....	185
Figure 6-23 Whole-body MTV prediction with and without the cubicle .....	186
Figure 7-1 Simulation domain with SOS .....	190
Figure 7-2 Sampling grid in the breathing zone .....	191
Figure 7-3 SF <sub>6</sub> mass fraction in the breathing zone with desk emission .....	193
Figure 7-4 SF <sub>6</sub> mass fraction in the breathing zone with wall emission .....	194
Figure 7-5 SF <sub>6</sub> mass fraction in the cubicle with desk emission .....	195
Figure 7-6 SF <sub>6</sub> mass fraction in the cubicle with wall emission .....	196
Figure 7-7 Contaminant Removal Efficiency in the breathing zone .....	197
Figure 7-8 Contaminant Removal Efficiency with desk emission .....	199
Figure 7-9 Contaminant Removal Efficiency with wall emission .....	201
Figure 7-10 Blocking Coefficient of the cubicle .....	202
Figure 8-1 Layout of diffuser/manikin experiment .....	206
Figure 8-2 Three types of diffusers (ATDs) tested .....	206
Figure 8-3 Manikin test with the heating delivering device .....	211
Figure 8-4 Heating delivering device .....	211
Figure 8-5 Prediction of the performance of the HDD using linear regression .....	214

## List of Tables

Table 1-1 Temperature inside and outside SOS (data from Bauman et al. 1991) .....	10
Table 1-2 Micro-zone regarding different exposure .....	16
Table 2-1 Summary of the physiological models .....	32
Table 2-2 Summary of the rational psychological models .....	41
Table 2-3 Summary of the ventilation systems.....	50
Table 3-1 Grid Summary .....	74
Table 3-2 Manikin Boundary Condition.....	76
Table 3-3 Cubicle Setting for Whole Room Simulation.....	77
Table 4-1 Boundary Conditions for Validation .....	95
Table 4-2 Cooling ability of different combinations of supply temperature and flow rates .....	107
Table 4-3 Comparison between set-point temperature and measured temperature .....	119
Table 5-1 Summary of the boundary conditions of split diffuser test .....	124
Table 5-2 Summary of the boundary conditions using confinement box .....	125
Table 5-3 Summary of the boundary conditions using footwarmer .....	128
Table 5-4 Local clothing insulation .....	129
Table 5-5 Summary of heating with hot jet at different velocities .....	131
Table 5-6 Summary of heating with hot jet of different supply combinations .....	135
Table 5-7 Summary of heating with hot jet and confinement box .....	139
Table 5-8 Summary of heating with footwarmer.....	142
Table 6-1 Summary of the garment dressing the manikin.....	149
Table 6-2 Experiment conditions of the $\mu$ X tests .....	157
Table 6-3 Experimental conditions of the cubicle tests .....	159
Table 6-4 Experimental results of the cases with different distances between the diffuser and the manikin.....	161
Table 6-5 Experimental results with different clothing material .....	170
Table 6-6 Summarized test results of the partitioned office without $\mu$ X at 26.1 °C return air temperature .....	177
Table 6-7 Summarized test results of the partitioned office without $\mu$ X at 23.9 °C return air temperature .....	178
Table 6-8 Summarized test results of the partitioned office with $\mu$ X at 26.1 °C return air temperature .....	183
Table 8-1 Performance of single rectangular diffuser at 23 cfm and 50 W.....	207
Table 8-2 Performance of single rectangular and split round diffusers at 23 cfm and 50 W .....	208
Table 8-3 Performance of single rectangular and split round diffusers at 17 cfm and 50 W .....	209
Table 8-4 Test results of the heating mat only.....	212
Table 8-5 Test results of the heating mat and bulb.....	213



## List of Symbols

$A$	Area ( $\text{m}^2$ )
$A_1$	Area of surface 1 ( $\text{m}^2$ )
$A_2$	Area of surface 2 ( $\text{m}^2$ )
$A_{cov,i}$	Covered body area of clothing element $i$ ( $\text{m}^2$ )
$A_{Open}$	Open area of the semi-open space ( $\text{m}^2$ )
AQI	Air Quality Index
$ASF_i$	Area Summation Factors for region $i$
$A_S^{n_s,p}$	Accessibility of the supplied air from diffuser $n_s$
$A_{Total}$	Total surface area of the semi-open space ( $\text{m}^3$ )
$A_t$	Total body surface area ( $\text{m}^2$ )
$\overline{a_0}^{Re}$	Parameters in calculating porous media resistance coefficient
$a_1, a_2$	Linear regression constants of the clothing independent thermal comfort model
$b$	Height of the jet (m)
$C$	Tracer gas concentration at target point ( $\text{kg}/\text{m}^3$ )
$C_\infty$	Ambient concentration ( $\text{kg}/\text{m}^3$ )
$C_d$	Flow coefficient ( $\text{m}/\text{s} \cdot \text{Pa}^{-n}$ )
$C_e$	Tracer gas concentration in the exhaust ( $\text{kg}/\text{m}^3$ )
$C_s$	Tracer gas concentration in the supply air ( $\text{kg}/\text{m}^3$ )
$C_p(t)$	Tracer gas concentration at the location $p$ at time $t$ ( $\text{kg}/\text{m}^3$ )
$C_S^{n_s}$	Concentration of the tracer gas of the air supplied by diffuser $n_s$

$C_{SOS}$	Contaminant concentration of the Semi-Open Space ( $\text{kg}/\text{m}^3$ )
$c_p$	Specific heat capacity ( $\text{J}/(\text{kg}\cdot^\circ\text{C})$ )
$DTS$	Dynamic Thermal Stimulus
$d_k$	Diffusion rate of turbulent kinetic energy (W)
$d_h$	Hydraulic diameter of the orifices (m)
$e$	Contaminant Removal Efficiency or Ventilation Efficiency
$F_{p-i}$	Angle factor between a person and surface $i$
$F_{1,2}$	View factor from surface 1 to 2
$\bar{f}$	Porosity
$G_k$	Gravity production of turbulent kinetic energy (W)
$g$	Gravitational acceleration ( $\text{m}/\text{s}^2$ )
$\Delta H$	Pressure loss ( $\text{kg}/\text{m}^2$ )
$HL_{SOS}$	Heat Load of the semi-open space
$HL_{Total}$	Heat Load of the whole space
$h$	Convective heat transfer coefficient ( $\text{W}/(\text{m}^2\cdot\text{K})$ )
$h_i$	Height of the cell $i$ (m)
$h_{teq}$	Dry heat transfer coefficient ( $\text{W}/^\circ\text{C}$ )
$iF$	Intake Fraction
$K_{s,i}$	Static constant of region $i$
$K_{d,i}$	Dynamic constant of region $i$
$k$	Turbulent kinetic energy (J)
$L$	Thermal load

$L_1$	Horizontal distance from the outlet (m)
$L_2$	Height from the floor to the head level (m)
$l$	Length between the centers of two zones
$l_c$	Characteristic length (m)
$l_\mu, l_\varepsilon$	Characteristic lengths (m)
$M$	Metabolic rate of an occupant
$\dot{m}_{j \rightarrow i}$	Mass flow from zone $j$ to zone $i$ (kg/s)
$n$	Flow exponent
$P$	Cooling Power (W)
$PMV$	Predicted Mean Vote
$P_i$	Absolute pressure in zone $i$ (Pa)
$P_k$	Shear production of the turbulent kinetic energy (W)
$PPD$	Predicted Percent Dissatisfied
$Pr$	Prandtl number
$p$	Hydrostatic pressure (Pa)
$Q$	Supply volume flow rate (m <sup>3</sup> /s)
$\dot{Q}_{1-2}$	Radiant heat transfer between surface 1 and 2 (W)
$\dot{Q}_{adj.}$	Adjusted total heat loss (W)
$\dot{Q}_{meas}$	Measured total heat loss (W)
$\dot{Q}_{total, BL}$	Total heat loss of the baseline case (W)
$\dot{Q}_{total, i}$	Total heat loss of the case $i$ (W)
$q''$	Heat flow rate from the human body (W)

$\dot{q}_t$	Total heat flux (W/m <sup>2</sup> )
$\dot{q}_r$	Radiant heat flux (W/m <sup>2</sup> )
$\dot{q}_c$	Convective heat flux (W/m <sup>2</sup> )
$q_T''$	Measured heat loss (W)
$R$	Total sensible thermal resistance (m <sup>2</sup> ·K/W)
$R_T$	Total insulation, including resistance of clothing and air layer (m <sup>2</sup> ·K/W)
$R_{cl,local,i}$	Local clothing resistance of segment $i$ (m <sup>2</sup> ·K/W)
$R_{cl,whole,i}$	Whole-body clothing resistance of a clothing element $i$
$Re$	Reynolds number
$r$	Gas constant J/(kg·K), 287 J/(kg·K) for air
$S$	Corresponding source term
$Sc$	Schmidt number
$S_j$	Momentum source term (N/m <sup>3</sup> )
$T$	Temperature at target point (°C)
$T_0$	Surface temperature of the occupant (°C)
$T_1$	Room air temperature (°C)
$T_2$	Raised room air temperature (°C)
$T_\infty$	Ambient temperature (°C)
$T_{clo}$	Temperature of the clothes surface (°C)
$\Delta T_i$	Temperature difference between skin surface and supply (°C)
$T_{jet}$	Supply air jet temperature (°C)
$T_{r,meas}$	Measured return air temperature

$T_{r,set}$	Set-point of the return air temperature (°C)
$T_s$	Temperature of the supply air (°C)
$T_{s1}$	Absolute temperature of surface 1 (K)
$T_{s2}$	Absolute temperature of surface 2 (K)
$T_{sk,face}$	Temperature of the skin of the face (°C)
$T_{skin,i}$	Temperature of the skin of region $i$ (°C)
$TSV$	Thermal Sensation Vote
$t$	Time (s)
$t_a$	Average air temperature (°C)
$t_{eq}$	Equivalent temperature (°C)
$t_{eq,i}$	Equivalent temperature of segment $i$ (°C)
$t_i$	Temperature of surface $i$ (°C)
$t_o$	Operative temperature (°C)
$\bar{t}_r$	Mean radiant temperature (°C)
$t_s$	Manikin surface temperature (°C)
$U_0$	Initial jet velocity (m/s)
$U_c$	Characteristic free isothermal jet velocity (m/s)
$U_m$	Maximum velocity in a cross-section of a jet (m/s)
$u_i$	Mean velocity in $i$ direction (m/s)
$u'$	Fluctuating velocity (m/s)
$V$	Total volume of the room (m <sup>3</sup> )
$\dot{V}$	Supply volume flow rate (m <sup>3</sup> /s)

$\dot{V}_i$	Supply flow rate of case $i$ ( $\text{m}^3/\text{s}$ )
$V_c$	Characteristic velocity of the buoyancy ( $\text{m}/\text{s}$ )
$V_i$	Volume of zone $i$ ( $\text{m}^3$ )
$v$	Stream velocity ( $\text{m}/\text{s}$ )
$x_i$	Coordinate in $i$ direction ( $\text{m}$ )
$\Phi_{j \rightarrow i}$	Energy flow from zone $j$ to zone $i$ ( $\text{W}$ )
$\Phi_{source}$	Energy generation rate in zone $j$ ( $\text{W}$ )
$a_v$	Thermal expansion coefficient ( $1/\text{K}$ )
$\beta$	Blocking Coefficient
$v_r$	Relative velocity ( $\text{m}/\text{s}$ )
$\gamma_t$	Thermal turbulent diffusivity ( $\text{m}^2/\text{s}$ )
$\varepsilon$	Turbulence dissipation rate ( $\text{W}$ )
$\epsilon_1$	Emissivity of surface 1
$\epsilon_2$	Emissivity of surface 2
$\sigma$	Stefan-Boltzmann constant ( $5.67 \times 10^{-8} \text{ W}/(\text{m}^2 \cdot \text{K}^4)$ )
$\mu_t$	Turbulent viscosity ( $\text{Pa} \cdot \text{s}$ )
$\tau_{ij}$	Reynolds' stress ( $\text{kg}/(\text{m} \cdot \text{s}^2)$ )
$\tau_n$	Nominal time constant of the room ( $\text{s}$ )
$\tau_p$	Mean age of air ( $\text{s}$ )
$\bar{\tau}_p'$	Room average age of air under piston flow ventilation ( $\text{s}$ )
$\Gamma$	Corresponding diffusion coefficient
$\lambda$	Thermal conductivity ( $\text{W}/(\text{m} \cdot \text{K})$ )

$\eta_a$	Air Exchange Efficiency
$\eta_T$	Temperature cooling efficiency
$\eta_v$	Flow rate cooling efficiency
$\mu$	Dynamic viscosity (Pa·s)
$\nu$	Kinematic viscosity (m <sup>2</sup> /s)
$\rho$	Density (kg/m <sup>3</sup> )
$\phi$	Scalar variable (energy, enthalpy, concentration, etc.)
$\xi$	Porous media resistance coefficient
$\xi_0$	Parameters in calculating porous media resistance coefficient
$\xi_\varphi$	Parameters in calculating porous media resistance coefficient

## **1. Introduction**

### **1.1. Background and Problem Definition**

#### **1.1.1. Motivation**

Buildings, since they were created for the first time, have been offering a shelter to protect humans against the natural weather for thousands of years. With the development of human society, buildings have been upgraded to provide people with better indoor environment by using heating, ventilating and air conditioning (HVAC) systems. Nowadays people spend more than 80% of their time indoors. The indoor thermal and air quality conditions play a key role in human health, comfort, and performance.

Since the beginning of the 1970s, energy crisis first came in developed country and then spread to the whole world, which led to the need to save energy. More recently, concern over climate change has led to a renewed worldwide effort in reducing building energy consumption to reduce CO<sub>2</sub> emissions. It was reported that heating, ventilation and air conditioning (HVAC) for buildings consume approximately 20% of the total energy use in developed countries (Hoyt et al. 2009, 2015) and about 13% in the United States (EIA 2014). Reducing energy consumption by HVAC systems plays a major role in improving the building's overall energy efficiency. The conventional HVAC system typically uses total volume heating, cooling, and ventilation system in which the entire indoor air space is well mixed and conditioned to achieve the set-point temperature set by a thermostat for the space. Since occupants only occupy a fraction of the total air volume in the building, this type of system wastes a significant amount of energy to condition the unoccupied space. It also creates inevitable discomfort and poor air quality for some occupants because



it cannot tailor the condition for individual occupant according to their preferences. It was reported that individuals had different thermal sensations under the conventional HVAC system due to variation in gender, age, body mass, clothing habits, metabolic rate, and thermal adaptation (Indraganti et al. 2015; Karjalainen 2012; Kim et al. 2013). Moreover, there are also individual differences between occupants regarding perceived air quality (Summer 1971). ASHRAE Standard 55 (ASHRAE 2013c) defines thermal comfort conditions under which 80% of the occupants would be satisfied, and ASHRAE Standard 62 (ASHRAE 2013d) specifies the minimum outdoor air amount per occupant and floor area of the indoor space. However, in a large office building survey study, only 11% and 26% of the buildings achieved the 80% of occupants satisfaction criteria for thermal comfort and air quality, respectively (Huizenga et al. 2006). The large interpersonal variability in thermal sensation and perceived air quality makes the buildings unable to satisfy many people's thermal comfort requirement, even though a large amount of energy has been used to maintain the narrow temperature band and condition the outdoor air.

Building energy consumption is mainly driven by the cooling or heating load which is proportional to the temperature difference between indoor and outdoor air according to the Fourier's law for heat transfer (Mills 1999). The typical thermostat set-point range inside a building is within 2.2 °C<sup>[1]</sup>. Several published findings have indicated the significant energy saving potential by expanding the temperature set-point range (increasing the set-point in the summer and reducing the set-point in the winter) (Hoyt et al. 2009, 2015). Simulation analysis has shown that expanding the set-point range from 21.4-23.9 °C to

---

<sup>[1]</sup> (X) °C = (X × 9/5 + 32) °F.

18.9-26.1 °C in a conventional HVAC building would reduce HVAC energy consumption by at least 20% depending on the location and climate (Hoyt et al. 2009).

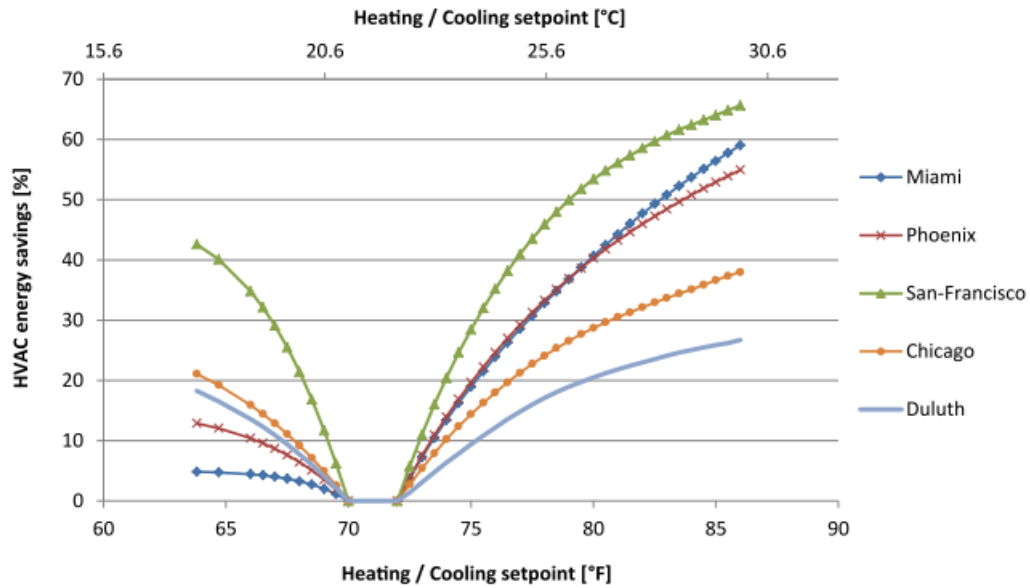


Figure 1-1 Summary of average HVAC energy saving in 5 climates(Hoyt et al. 2015)

Expanding the temperature band of the building will also adversely impact the occupants' thermal comfort as expected (Hoyt et al. 2015; Verhaart et al. 2015). Broader set-point range sacrifices thermal comfort, which affects occupants' productivity. A study supported by the Finnish and American government concluded that an average 2% decrement in work performance per °C increment in room temperature was reported by multiple studies when the temperature is above 25.0 °C (Seppanen et al. 2004). Moreover, a few studies also show that when the temperature dropped below 20.0 °C, 0.5-3% reduction in productivity per °C decrement was also observed (Lan et al. 2012). One should keep in mind that the salary costs of office workers are usually about two orders of magnitude more expensive than the building facility cost (de Dear et al. 2013). Therefore, efforts have to be made to restore

people's thermal comfort locally when the expanded temperature band was applied to save energy.

A personalized environmental control system (PEC) or micro-environmental control system, which was first defined by Khalifa (Khalifa 2017), has the potential to restore people's thermal comfort as well as provide fresh outdoor air to the people directly, and hence save energy. In recent years, many new methods and systems for improving personal environmental quality and reducing energy consumption (Cao et al. 2015; Khalifa 2006; Kong et al. 2014; Nielsen 2007), have found applications in the real offices after studied in the research laboratories.

Different from the conventional total volume ventilation, the air supply devices of these types of systems are mostly mounted in cubicles created by open office partitions. This kind of arrangement does not only give relatively independent environment on the remaining office space and other cubicles but allow the interaction between them. Depending on the configuration of the cubicle and PEC system, the environment in the cubicle as well as around the manikin may differ a lot and influence the thermal sensation and inhaled air quality, as well as the overall efficiency of heating or cooling. It was shown that with local air distribution systems, the cubicle could prevent the contaminant from coming into it when the source is outside the cubicle and can partially confine the contaminant in it when the source is in the cubicle (Kong et al. 2014). The space in the cubicle semi-confined by the office partitions is defined as the *Semi-open Space* (SOS), which plays a key role in determining the micro-environment experienced by the occupant

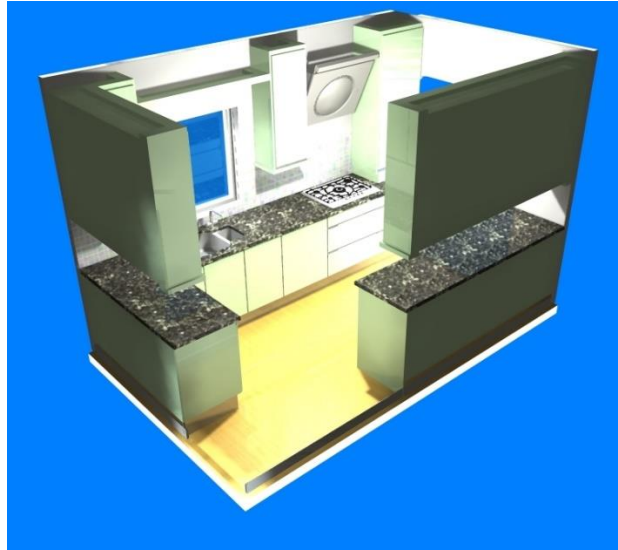
in the cubical. This study aims at studying how SOS and the micro-environmental control system can be optimized for improving thermal comfort and indoor air quality while reducing building energy consumptions.

### 1.1.2. Semi-open Space

**Semi-open Space** is defined as a subspace created by semi-enclosed partitions in a larger open space. Based on this definition, there are a lot of applications of SOS, for instance cubicles in the office (Figure 1-2a), hoods in the kitchens (Figure 1-2b), blocked wards in the hospital (Figure 1-2c), blocks in the restroom (Figure 1-2d), et al.



(a)



(b)



(c)



(d)

Figure 1-2 Examples of Semi-open Space

(a) office cubicles (“Office cubicles” 2014); (b) residential kitchens (“Residential kitchens” 2014); (c) hospital wards (“Hospital wards” 2014); (d) restroom blocks (“Restroom blocks” 2014).

These applications may look quite different at first sight; however, they share some features from the ventilation and pollution control point of view. A semi-open space, on the one hand, is a partially open space with connections between one SOS and the others as well as the outside space. On the other hand, SOS also provides a relatively independent space. Integrated with an appropriate PEC system, SOS has a big potential of saving energy while improving thermal comfort level and air quality around occupants as well as providing sound, light, and spatial privacy.

However, so far most of the ventilation studies are focused on the air distribution in open space. Only a few researches were done to investigate the performance of SOS (Demetriou et al. 2008; Zhang et al. 2007). Jiang et al. (1997) studied two kinds of office configurations

with five ventilation strategies numerically and found that the use of partitions significantly affects the uniformity of the supply air distribution. Some work has been done to show the influence of partition of workstations on air distribution. However, these workstations were neither individually ventilated nor adequately enclosed. Bauman (F.S. Bauman et al. 1991; Fred S. Bauman et al. 1992) did a very comprehensive work on the ventilation in an office with workstations. In his work the influence of a range of partition configurations and environmental parameters, including partition height, solid or airflow partitions, airflow gap size, supply air volume, supply/room temperature difference, supply diffuser location, heat load density, workstation size and cooling or heating mode, was investigated in a ceiling-ventilated room in terms of thermal environment and ventilation efficiency. Many useful and interesting results are found (F.S. Bauman et al. 1991):

- The magnitude of partition effect should diminish with increasing workstation size, toward the limiting case—i.e., having the air movement conditions found with no partitions present;
- Air flow partitions may result in small increases in air velocity within small workstations, but very limited;
- The effect of supply air flow rate appears to be very small on the average air velocity;
- The locations of the diffuser and return vent affect the performance of the partitioning very much. The temperature and velocity distribution differs a lot when the position is different;
- In total volume ventilated room, the effect of the partition (gap size) is unpredictable;
- The existence of air-flow partitions has a negligible effect on temperature (and even velocity) distributions in all workstations;

- When the test condition is the same (heat load, supply temperature, supply air flow rate), the most acceptable comfort conditions are obtained in the larger cubicle;
- No comfort improvements are predicted due to airflow partitions;
- Comfort conditions are identical in all three workstations when no partitions are present;
- The existence of the partition increases the mean radiant temperatures;
- Short circuiting may occur when the partitions are present;
- The presence of the partitions is a reason for non-uniformity;
- Heat loads in partitioned workstations had a significant effect on air temperatures, mean radiant temperatures, and overall comfort conditions.

Based on the results of their experiments, data are collected, and the performance of the SOS can be analyzed (Table 1-1). In a cooling mode with a constant heat source in the workstation, most of the temperature inside the workstation is lower than the temperature in the outside space, and the largest difference can be as high as 1.1 °C, which means SOS can partition the space at least regarding temperature distribution. After this study, another work done by Shaw et al. (Shaw, Vaculik, et al. 1993; Shaw, Zhang, et al. 1993) investigated the effect of the cubicle partition on the air quality. It was concluded that the existence of a cubicle could cause a dead air space inside the cubicle and, hence, an increase of mean age of air. Nevertheless, due to the non-uniformity of the mixing ventilation, different configurations of the workstation and different supply conditions, the partition effect cannot be generalized.



Table 1-1 Temperature inside and outside SOS (data from Bauman et al. 1991)

Case #	Room Temp (°C)	WS1 Temp (°C)		WS2 Temp (°C)		WS3 Temp (°C)	
		Avg	$\Delta T$	Avg	$\Delta T$	Avg	$\Delta T$
1A	24.20	23.47	-0.73	23.50	-0.70	23.57	-0.63
1B	24.20	23.63	-0.57	23.77	-0.43	23.80	-0.40
3A	26.40	25.60	-0.80	25.67	-0.73	25.93	-0.47
4A	21.90	21.40	-0.50	21.57	-0.33	21.27	-0.63
4B	22.10	21.27	-0.83	21.50	-0.60	21.33	-0.77
5A	23.60	23.43	-0.17	23.43	-0.17	23.10	-0.50
5B	23.20	22.73	-0.47	23.10	-0.10	22.10	-1.10

### 1.1.3. Micro-Environmental Control Strategy

Total volume HVAC (T-HVAC) system and local/personalized ventilation system provide clean and conditioned air to the room but in different ways. T-HVAC systems have diffusers located outside the semi-open space. Different air distribution systems offer different strategies in providing thermal comfort condition and protection of people against pollutants. The pollutants are almost fully mixed in the occupied zone in a room or in a vehicle ventilated by mixing ventilation, and they are removed by a diluting process (P. V. Nielsen et al. 2003). The displacement ventilation aims for displacing but not mixing the polluted room air with clean air, which is supplied close to the floor at a low velocity. In

this system, the thermal flows induced by the heat source dominate the air movement in the room and an obvious vertical temperature gradient exists in the whole space (P. V. Nielsen 2011). Often, occupants in rooms with mixing or displacement ventilation have to compromise between preferred thermal comfort and perceived air quality, because some people are very sensitive to air movement while others are more sensitive to the air quality. The disadvantage of the total-volume ventilation principle is that often room air movement is changed due to furniture rearrangement and this may increase occupants' complaints of discomfort and poor air quality (Melikov et al. 2002).

The strategy of using a PEC system to improve occupants' thermal comfort is suggested by many standards (Melikov et al. 2013) and is also an effective way to reduce the building's total energy cost. The PEC system is reported to be capable of improving the thermal comfort and air quality around the subject, reducing the intensity of SBS symptoms and increasing the performance of the subjects (Arens et al. 2006a; Kaczmarczyk et al. 2004; A. K. Melikov 2004; H. Zhang 2003). Usually, the micro-environmental control strategies are classified into three different categories: air quality control, thermal comfort control and comprehensive control which includes both air quality and thermal comfort. Air quality control is accomplished by supplying fresh/purified air to the people locally, exhausting the contaminated air locally, separating the contaminating source from the occupants (Khalifa et al. 2009; Khalifa et al. 2008; Russo et al. 2008; Russo and Khalifa 2010; Russo et al. 2009; Russo and Khalifa 2010). These systems are also called personalized ventilation (PV) system (Kaczmarczyk et al. 2004). In the space where occupants are less movable, for example, offices, theaters, and vehicles, the local-supply-fresh/purified-air system can be

applied. Moreover, this kind of system is usually designed to provide comfort to occupants at the same time, especially in summer, which makes it qualified to be the third category of the micro-environmental control strategy. Since it can satisfy the individual needs of each occupant by customizing the environment around the human body, it has a big advantage over both displacement and mixing ventilation. It was also found that a PV system supplying only one fourth amount of fresh air of the displacement ventilation could be more effective regarding users' satisfaction (Cermak et al. 2006; N. Gao and Niu 2005). The same conclusion was obtained by Melikov that this kind of system may reduce significantly the number of occupants dissatisfied with inhaled air quality (Dalewski et al. 2013; Melikov et al. 2002). The local exhaust system is typically utilized in the space where pollutant source is strong and clustered, like the kitchen. Some other applications use air or partition to separate the pollutants from the occupants, for example, protective ventilation (Cao et al. 2015). This kind of system is usually used in space when the pollutants are distributed. Several kinds of personalized ventilation devices have been developed recently. It is proven that some of them can improve the air quality as well as thermal comfort while the others cannot. A push-and-pull kind of PV is invented and applied to the aircraft cabin seat. The result showed a dramatic decrease (77%) of contaminant concentration inhaled by the exposure manikin when the local supply of clean air existed and the contaminant exhaled can only be exhausted effectively when the local exhaust and the local supply are used simultaneously (Melikov and Dzhartov 2013). A local exhaust ventilation system with a privacy cell in air cabin developed by Dygert also shows an advantage compared with back seat exhaust, reducing the passenger exposure to 60% no matter where the infectious source is (Dygert and Dang 2012). A lot of personalized ventilation terminals have been developed

and tested by Nielsen, and the performance of these systems was proved to be significant (Kong et al. 2015; Nielsen et al. 2008, 2013; Nielsen et al. 2007; Nielsen et al. 2007).

Another kind of micro-environmental control strategy is only for the control of thermal comfort condition. These systems use recirculation air, radiation or conduction to provide local cooling or heating to the occupants. Recirculation air is a more common method that provides warm or cool air to the person and sometimes helps improve perceived air quality, especially in summer condition. The performance of using this system to deliver clean, cool and dry air to the breathing zone of each occupant and maintain the thermal comfort level depends on the interaction among the supply airflow, occupants-initiated flows (free convection flow around the body and the flow of respiration), the airflow of exhalation and the room airflow outside workspaces (Melikov 2004). Radiant or conductive heating and cooling are realized by using a surface that is hotter or cooler than the surface of a human body. The difference between them is that the surface for radiation is usually away from the occupant and of higher temperature and the one for conduction is usually touching the body closely and of lower temperature. Over the past few years, many kinds of PEC systems for controlling thermal comfort have been developed and tested either physically or physiologically. Arens and Zhang from U.C. Berkeley made many efforts in this field by testing many kinds of PEC systems in their lab including using footwarmers in cold environment (Zhang et al. 2015), using moving air for cooling during moderate exercise (Zhai et al. 2015) and in offices (Arens et al. 1998; F. Bauman et al. 1993; Pasut et al. 2014; Zhai et al. 2013), a heated/cooled chair (Pasut et al. 2013, 2015), and an integrated task-ambient conditioning system (Zhang et al. 2010). Melikov from DTU also made some

contributions to this field by testing a heated/cooled seat on acceptable ambient temperature range (Zhang et al. 2007), facially-supply warm air in cold environment (Kaczmarczyk et al. 2010), local convective and radiant cooling in warm environment (Melikov et al. 2013), and a ductless personalized ventilation (Halvonova and Melikov 2010), and designing an integrated locally controlled system for optimal comfort (Melikov and Knudsen 2007; Watanabe et al. 2010). Some other researchers have also done related work in this field. Huang et al. investigated the demand for air movement in a warm environment (Huang et al. 2013). Foda and Sirén developed a design strategy for maximizing the energy-efficiency of a localized floor-heating system (Foda and Sirén 2012). Moreover, Deng et al. tested a heated seat for improving comfort with the human subject (Deng et al. 2016).

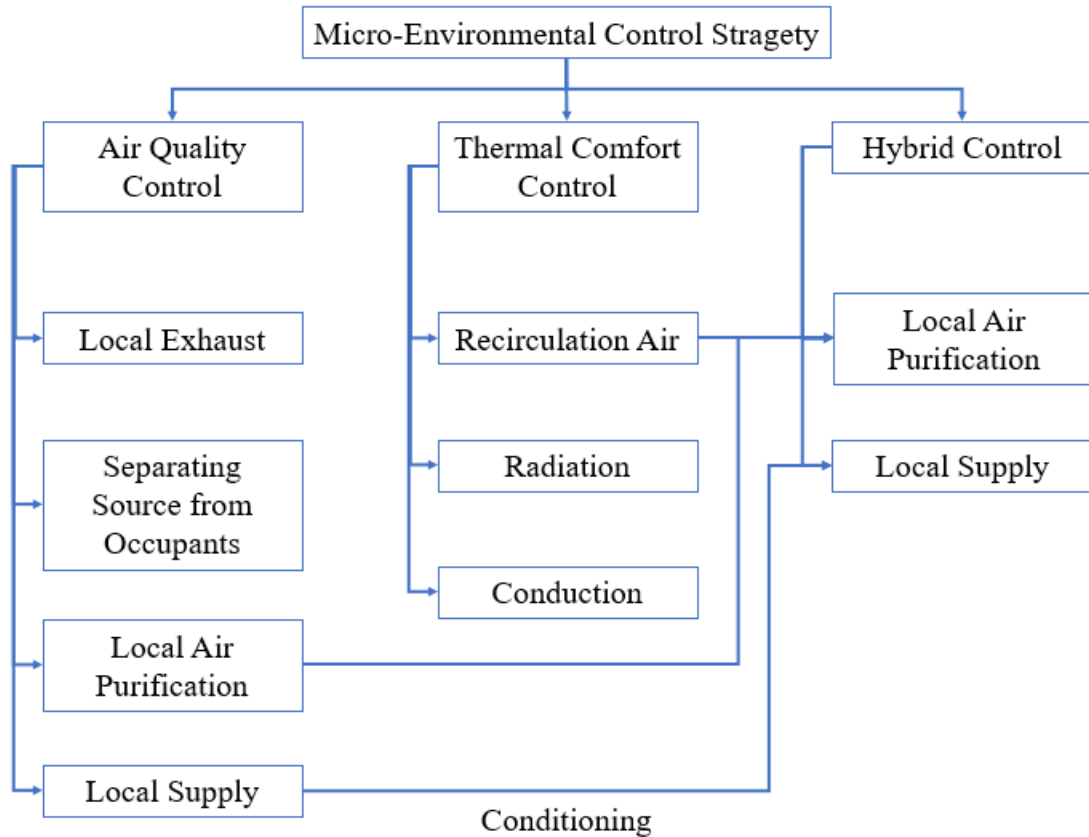


Figure 1-3 Categories of micro-environmental control strategy

#### 1.1.4. Multi-scale Zones in a Ventilated Room

In a room with semi-open spaces, space can be divided into several zones with different scales. Typically, three zones are involved: the micro-(environment) zone, the meso-(environment) zone, and the macro-(environment) zone. The micro-environment zone is defined as the perceived real and conceptual space around a person that directly impact his/her personal environmental quality/exposure to the total indoor environment. The meso-environment zone is the zone in the SOS enclosed by the semi-open partitions excluding the micro-environment. The macro-environment zone is the zone outside the SOS. Besides,

depending on the environmental control strategy or air distribution strategy, there are non-occupied zones in the three zones, including the space above 1.8 m from the floor and within 1.0 m from external walls/windows or fixed heating, ventilating or air-conditioning equipment and 0.3 m from internal walls (ASHRAE 2013c) (Figure 1-4).

In fact, among the three zones, micro-zone is the most important one. However, the configuration of the specific micro-zone differs regarding the category of the exposure. Imagine one is sitting in a room (Figure 1-4), all the surrounding environment has some influence on the sensation of the people. The air of certain temperature flows around his/her body, exchanges the energy with it and brings the draft effect to his/her exposed skin. The surrounding surfaces exchanges energy with the human body by radiation. People take in the air from the vicinity of the nose and mouth, and also expire the stale air back to the ambience. In some cases, the contaminant in the air can even harm the human body through the exposed skin, for example, the ozone can lead to the irritation of the skin, VOC can significantly dehydrate and irritate the skin (Brasche et al. 2004). The lamps as well as the sunshine through the window project lights to space. Windows on the wall also provide the view of the outdoor scenery that affects the mood of people to some degree. Noise transmitted in the space interferes the thinking of people and also affects the productivity of building occupants. Depending on the specific exposure aspect, the micro-zone is defined differently, and the following table provides a summary of the definition of micro-zones for different exposure considerations.

Table 1-2 Micro-zone regarding different exposure

Exposure of interest	Related Micro-zone
Thermal Comfort	The space around the body in which the temperature and velocity of the air can be felt and surrounding surfaces which exchanges energy with occupant by radiation.
Air Quality	The vicinity of the nose and mouth and space around the exposed skin when certain kind of contaminant is considered.
Lighting Condition	The space in the work place in front of the occupant.
View	Inside and outside the semi-open space which can be seen by the occupant.
Noise	The space close to the occupant's ear which the noise can be perceived.



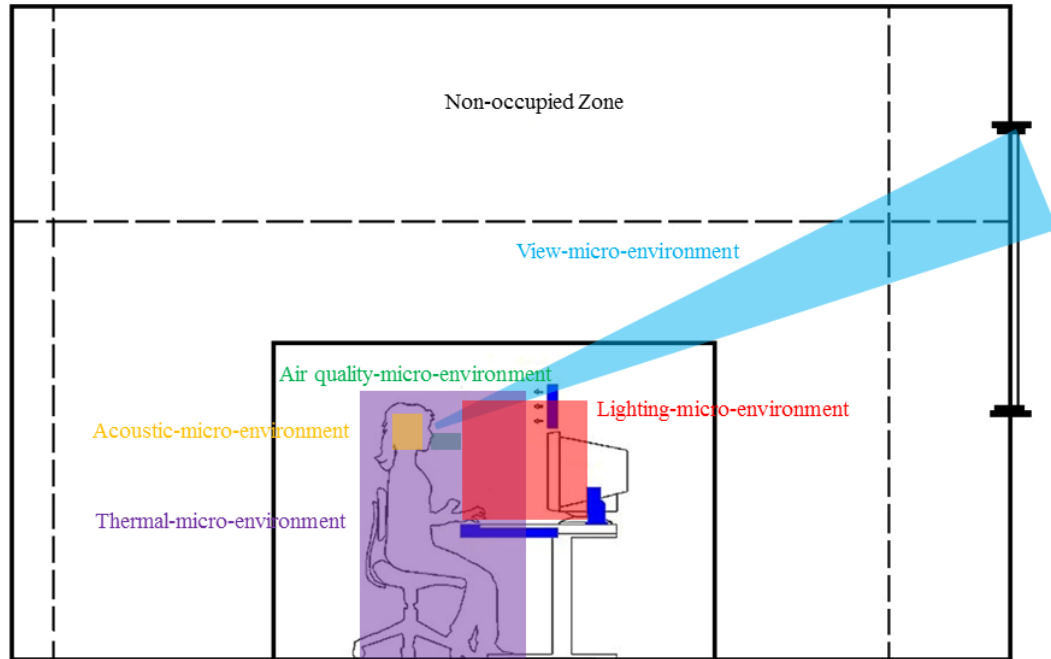


Figure 1-4 Micro-environment zone definition

Technically “micro-environment” is a big term, but in this work, it is limited to be referred to the thermal and air exposures of the occupants.

The multi-scale zones can be geometrically separated but still interact with each other from the performance point of view. These zones also differ regarding the human activity within the zones. The micro-environment zone is the zone in which occupants spend most of their time, while the macro-environment zone is the zone in which occupant spend occasionally and is considered as circulation zone. Different requirements of the environment can be made according to the purpose of the zones. The multi-scale concept is especially applicable to the case with semi-open space since in an open space, the meso-environment zone is the buffer zone between the micro- and the macro-environment zone.

### **1.1.5. Problem definition**

The fundamental research question is how to use semi-open space and micro-environmental control to efficiently provide the desired thermal comfort and air quality conditions for individual occupants while reducing the overall energy consumption of the building. Extending the temperature set-points can reduce the temperature differential across the envelope, which reduces the heating and cooling loads of the HVAC system and reduces energy consumption for air conditioning. Delivering cooling or heating locally to the space confined by a semi-open space surrounding the occupant in principle enables the micro-environmental control of the thermal and air quality conditions for the individual occupant. The effectiveness and efficiency of such a micro-environmental control system depend on the SOS configuration, methods of local heating and cooling, and air distribution design. Air supplied from a local air diffuser tends to entrain and mix with the ambient air, and hence its ability to cool or heat is reduced when reaching the human body. On the other hand, having a too cold air reaching the human body can cause draft and make the occupant thermally uncomfortable. The airflow through the openings of the semi-open space can also significantly affect the performance of the micro-environmental control system. This research will address these issues, and is designed to focus on the following specific questions:

- 1) How different the local air delivery methods perform comparing to the total air volume system?
- 2) How effective is the local air-cooling for micro-environmental control? Can it remove the additional heat from the occupant when the ambient temperature in the general

space is increased for energy saving? What are optimal design and operating parameters (supply air distribution, flow rate, and temperature)?

- 3) How to provide local heating? How effective are different local heating methods?
- 4) What is the role of the semi-open space for micro-environmental control? How the SOS configuration affect the effectiveness of the micro-environmental control system?

## **1.2. Goal and Objectives**

The primary goal of the proposed study is to investigate why and how semi-open space (SOS) and micro-environmental control system (MECS) can improve thermal comfort and IAQ while saving energy. Specific objectives are:

- 1) Develop experimental and numerical methods for evaluating the performance of the micro-environmental control system (MECS) in semi-open space (SOS) for improving thermal comfort and indoor air quality in the micro-environment while the set-point temperature in the macro-environment is relaxed (increased in case of cooling or reduced in case of heating applications) for reducing building energy consumption;
- 2) Improve the understanding of the various factors affecting the performance, including SOS configurations and MECS design and operation parameters, such as air supply conditions of the air supply terminal for cooling and working heat flux of the heating mat for heating.
- 3) Develop guidelines for the application of SOS and MECS.

As a secondary goal, the ability of CFD to adequately predict the local heat transfer from the human body and its limitation is also investigated. Since the application of the semi-open space is diverse, only the office with cubicles is studied in this work.

## **1.3. Scope of Work and Dissertation Roadmap**

To achieve the objectives above, the following research works have been performed:

- 1) A review of the fundamentals on thermal comfort, indoor air quality, and room air distribution methods have been conducted, and the results are presented in Chapter 2.
- 2) A series of preliminary studies were conducted to help improve the understanding of the work scope and methods. Three different local air distribution methods have been evaluated by conducting full-scale experiments, and the results are presented in Chapter 3.
- 3) A CFD model was developed primarily based on previous studies at Syracuse University as well as some other researchers. The performance of three proposed air terminal devices (ATDs) and different kinds of heating delivering devices (HDDs) for the micro-environment control system were evaluated. Specifically, the following subjects were studied:

For cooling condition:

- a) Influence of the supply air condition, including supply air temperature and flow rates;
- b) Effect of the shooting angle, i.e., air supply directions;
- c) Effect of the manikin location relative to the supply air diffuser;

For heating condition:

- d) The performance of using warm air, i.e., convection, to heat the manikin.
- e) The performance of using radiation and conduction to heat the manikin.

These studies were conducted using a 3-dimensional domain representing a typical office environment with expanded ambient temperature set-points. Results are presented in Chapter 4 and 5 of this dissertation for cooling and heating, respectively.

- 4) To further validate the CFD model and provide additional experimental data of using a micro-environmental control system to restore thermal comfort while saving energy, a full-scale experimental mock-up system of a single workstation equipped with micro-environmental control system was constructed subsequently. Hot-sphere anemometer and thermistor temperature sensor were used to monitor the micro-environment around the manikin, and embedded heat flux sensors were used to monitor the heat flow rates from different segments of the manikin. The results were compared to the CFD simulation, and further analysis was conducted to address the issue about the discrepancy between CFD and experiments and improve the understanding of the fluid mechanics and heat transfer processes involved. Results are presented in Chapter 4 of this dissertation.
  
- 5) Upon completion of the experimental facility, a more thorough study of using a micro-environmental control system with or without semi-open space was conducted. The mock-up micro-environmental control system with adjustable air diffuser was tested with a dressed manikin. The effects of shooting angle, manikin location, supply air flow rates and supply air temperature were tested, and a design chart was developed to help with the application of the micro-environmental control system. Then a typical semi-open space, office cubicle, was created around the workstation, the effect of the semi-open space of different configurations on the micro-environment was investigated through a series of experimental measurements. Results are presented in Chapter 6 of this dissertation.

- 6) The performance of the semi-open space was further evaluated by CFD simulation regarding air quality and thermal environment management. The effects of opening size, opening location/orientation, pollutant source and ventilation strategies were investigated, and some guidelines for designing the SOS for micro-environmental control were developed. Results are presented in Chapter 7 of this dissertation.
  
- 7) Chapter 8 of the dissertation summarizes the conclusions from this study and identify areas for further investigation on the subject.

## **2. Thermal Comfort, Indoor Air Quality and Room Air Distribution**

Indoor environment refers to the building's environment about the health and wellbeing of those who occupy space within it. The purpose of the HVAC system is to provide the occupant satisfactory thermal comfort and air quality conditions. Since the modern HVAC system was created for the first time, thousands of studies about monitoring, evaluating, predicting, and designing indoor environment have been conducted in the past few decades. The understanding of the related concepts needs to be clarified to obtain a meaningful conclusion.

### **2.1. Thermal Environment**

Thermal comfort is defined as the condition of mind that expresses satisfaction with the thermal environment, which is the environment that affects a person's heat loss (ASHRAE 2013c). Evaluating and predicting the thermal environment requires an understanding of thermal comfort and existing evaluation methods.

#### **2.1.1. Thermal Comfort**

Thermal comfort is a plurality of sensations and is secured by all factors influencing the thermal condition experienced by the occupant (Croitoru et al. 2015). The judgment of thermal comfort is a cognitive process which involves many inputs influenced by physical, physiological, psychological, and other processes (ASHRAE 2013a).

The common-sense people have is that one feels comfortable at certain temperature and humidity and uncomfortable when they exceed the certain range. Thermal comfort is a



direct response of the body to some environmental factors, including air temperature, humidity, velocity, radiation, conduction, etc. Also, thermal comfort depends on behaviors that are initiated by one's thermal sensation. For example, people put on more clothes when they feel cold and take off clothes when they feel hot. In addition, the difference of individual cognition of thermal comfort has already been found to be related to age, gender, weight, metabolic rate, mood, etc. Based on these, the factors which affect thermal comfort can be classified as environmental, adaptive, and intrinsic factors (Figure 2-1).

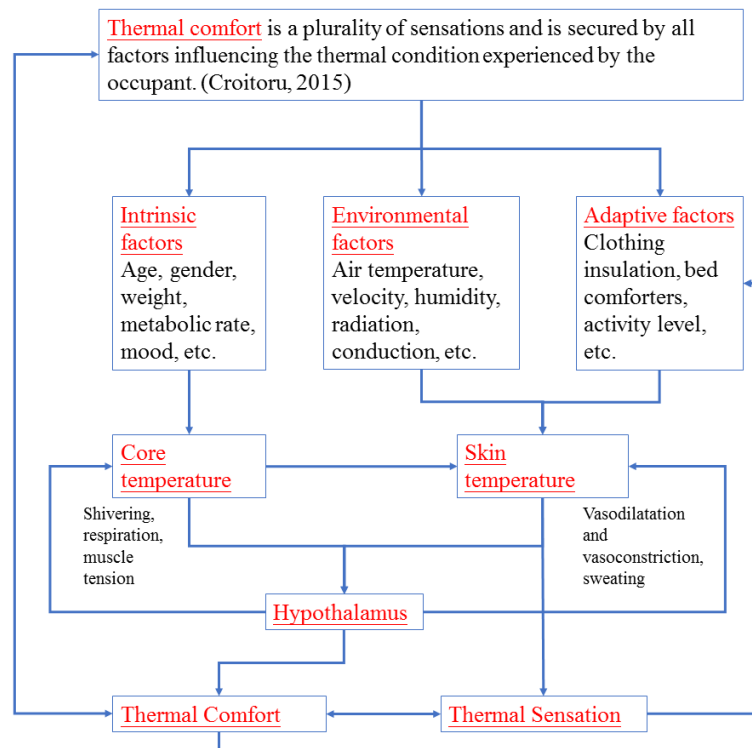


Figure 2-1 Thermal comfort

Thermal comfort is the result of thermoregulation to maintain thermal balance. To achieve thermal balance, the body behaves in a strongly non-linear manner and contains multiple

sensors, multiple feedback loops and multiple outputs (Hensen 1990). The controlled variables are core temperature and skin temperature. The signal received by the skin or deep body is returned to the hypothalamus and triggers the adaption algorithm – shivering, respiration, muscle tension, vasodilatation, vasoconstriction, and sweating – to continuously make the heat balance.

### **2.1.2. Thermal Comfort Evaluation**

During the past four decades, hundreds of researchers have been continuously putting efforts in explaining and predicting thermal comfort of people. The first thermal comfort model was developed for military and aerospace applications. Over the past 30 years, many kinds of thermal comfort model have been developed to help with the design and evaluation of both the indoor and outdoor environments. Fanger (1970) developed the first widely-used thermal comfort model – Predicted Mean Vote (PMV) and Predicted Percent Dissatisfied (PPD) – by relating the thermal comfort to a steady state heat balance equation. This model was then referred by many comfort standards and is still widely used all over the world. However, this model also has its limitations, for example, it is mostly accurate for clothing insulation between 0.3 and 1.2 clo, for activity level below 1.4 met, and for air-conditioned buildings (Charles 2003). Therefore, other models have come up afterward.

As mentioned above, since thermal comfort is a cognitive process which involves many inputs influenced by physical, physiological, psychological, and other processes (ASHRAE 2013a), thermal comfort models are categorized as physiological models – explains and simulates the physiological response of the human body – and psychological models –

explains and predicts the cognitive process for thermal comfort.

#### **2.1.2.1. Physiological Models**

The physiological models simulate the autonomic thermoregulation response of the human body to the external stimuli. The first model which explains and gives a prediction of thermoregulation process is the 25-node model developed by Stolwijk (Stolwijk 1971). This model divided the human body into one central blood compartment and six segments each of which has four layers in the radial direction. Because of the division into six parts, the model can be used in non-uniform condition, but the environment was still considered as a steady state. However, although this model had well constructed a reasonable procedure for predicting the thermoregulatory behavior, it was not widely used at that time because of the lack of computational resource. This model was originally developed for aerospace applications. Some simplified models were developed instead. One of them was developed in 1971 by Givoni and Goldman (Givoni and Goldman 1971, 1972). This model treated the entire human body as one node and helped predict the core and corresponding skin temperature empirically based on any given metabolic rate, environment, and clothing. This model is only applicable to a hot environment. Afterward, the well-known Pierce two-node model was developed by Gagge et al. (Gagge 1973; Gagge et al. 1986). This model simplified Stolwijk's model to a lumped two-node model which represented the skin and core of body separately. It calculated the heat generation rate based on metabolic rate and additional shivering and muscle tension heat generation. The blood flow, sweating rate, and additional heat generation rate are all calculated based on the skin and core temperature deviation from the set-point. Different from the 25-node model, this model enables the

prediction in transient condition by adding the time derivative of skin and core temperature but disables the prediction in non-uniform condition because of the simplification. Another well-known two-node model is the KSU two-node model developed by Kansas State University (Azer and Hsu 1977). This model is very similar to the Pierce two-node model, and the only difference is the control equations for sweating and blood flow. In order to address the issue of prediction in nonuniform condition with a simpler model, Kohri et al. developed a dispersed two-node mode based on Gagge's two-node model integrated with the model of the distribution of the metabolic heat and the skin blood flow rate developed by Yokoyama (Kohri and Mochida 2002, 2003; Yokoyama et al. 1997; YOKOYAMA et al. 2000). In this model, the body is divided into 11 parts, and each part has a core layer and a skin layer. With the development of computing ability, people started to come back to Stolwijk's model and continued his work. Several direct derivatives include IESD-Fiala model (Fiala et al. 1999, 2001), Tanabe's 65-node model (Tanabe et al. n.d.) and Multi-element model (Yi et al. 2004). In Fiala's model, the body is divided into 20 elements, most of which consist of 3 sectors. Same with Stolwijk's model, this model includes a passive system, which represents the physical body and heat transfer inside it and with the surrounding environment, and an active system, which predicts the thermoregulatory reactions. Tanabe divided the human body into 16 elements, each of which has four layers: core, muscle, fat, and skin, with a central blood compartment. The convective and radiant heat transfer coefficient through the manikin is determined by manikin experiment. The multi-element model is the most complicated and realistic human thermoregulation model which decomposes the human body into 15 cylindrical parts using 3000 nodes. With several significant improvements based on Tanabe's model, Huizenga et al. developed another

model – the UC Berkeley Comfort Model. This model has the potential to simulate an arbitrary number of segments. Blood flows through limbs to the extremities with counter-current heat exchange. Each segment is represented by multiple nodes and a blood object with heat exchanged between the adjacent nodes, node and blood and artery and vein. The summary of these models was presented in Figure 2-2 and Table 2-1.

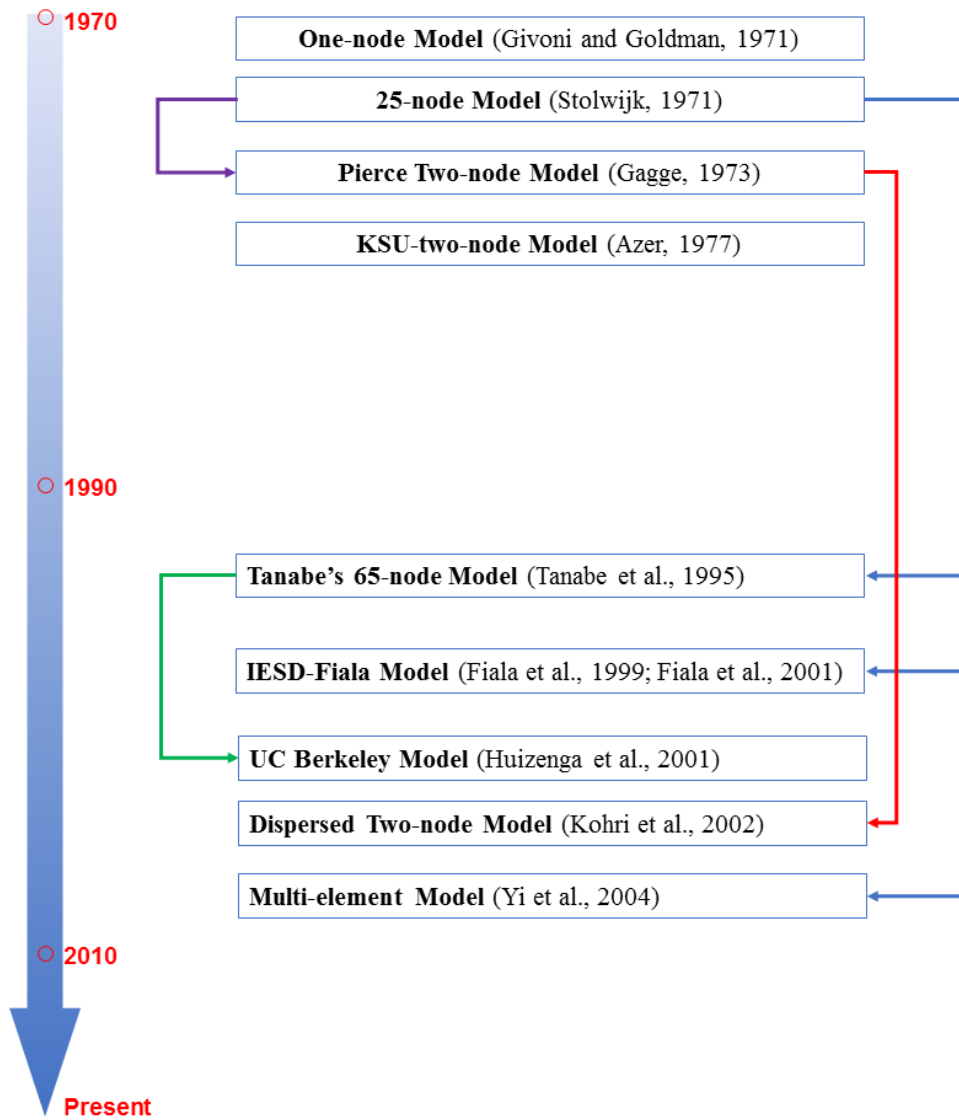


Figure 2-2 Physiological model development

Table 2-1 Summary of the physiological models

<b>Model</b>	<b>Temperature</b>	<b>Metabolic rate</b>	<b>Static</b>	<b>Dynamic</b>	<b>Uniform</b>	<b>Nonuniform</b>
<b>One-node Model</b> (Givoni and Goldman, 1971)	Hot environment	N/A	√	×	√	×
<b>25-node Model</b> (Stolwijk, 1971)	N/A	N/A	√	×	√	√
<b>Pierce Two-node Model</b> (Gagge, 1973)	Cool to very hot	Low and moderate	√	√	√	×
<b>KSU-two-node Model</b> (Azer, 1977)	Cool to very hot	Low and moderate	√	√	√	×
<b>Tanabe's 65-node Model</b> (Tanabe et al., 1995)	N/A	N/A	√	×	√	√
<b>IESD-Fiala Model</b> (Fiala et al., 1999; Fiala et al., 2001)	5-50 °C	0.8-10 met	√	√	√	√
<b>UC Berkeley Model</b> (Huizenga et al., 2001)	N/A	N/A	√	√	√	√
<b>Dispersed Two-node Model</b> (Kohri et al., 2002)	Cool to very hot	Low and moderate	√	√	√	√

<b>Multi-element Model</b> (Yi et al., 2004)	N/A	N/A	√	√	√	√
--	-----	-----	---	---	---	---



### **2.1.2.2. Psychological Models**

Normally a heat balance type thermal comfort model includes: a detailed multi-segmented, multi-layer physical heat exchange model and clothing model that deals with the thermal interaction between the human body and its environment; a multi-segmented physiological thermoregulation model that simulates the human body in terms of the passive and active thermal system; and a psychological thermal sensation model that predicts both local and whole body thermal sensation (Cheng et al. 2012; Guan et al. 2003). However, since the thermal comfort assessment is a cognitive process, after all, the last one is the essential part of the thermal comfort model. During the past few decades, many efforts have been made in this area, and many models have been developed. These models are further categorized as rational (objective) models and adaptive (subjective) models.

The principle of the rational model is that all the rational models make the inherent assumption that there is some predictable comfort response for a given physiological state of the body, which means that the psychological comfort response is exclusively related to the physiological behavior of the human body (Croitoru et al. 2015). Some of the rational models have to work with the physiological model while the others do not. The development of rational model starts from the early 1920s, when the “Effective Temperature (ET)” was proposed for the first time (Houghton 1923). Moreover, during the next fifty years, several indices were developed including “Wet Bulb Globe temperature (WBGT)” (Yaglou and Minaed 1957) and “Equatorial Comfort Index (ECI)” (Webb 1959). The study performed by Fanger is a milestone for thermal comfort study (Fanger 1970). Predicted mean vote (PMV) and Predicted Percent Dissatisfied (PPD) model he developed

has affected all the studies afterward and adopted by many standards until now. PMV is an index which is used to predict the mean response of a large group according to the ASHRAE thermal sensation scale. PMV uses the energy imbalance of the human body to give the comfort prediction of the occupants in a given environment:

$$PMV = [0.303 \exp(-0.036M) + 0.028]L \quad (2 - 1)$$

Where  $M$  is the metabolic rate and  $L$  is the thermal load on the body, defined as the difference between internal heat production and heat loss to the actual environment for a person hypothetically kept at comfort values of skin temperature and evaporative rate. After PMV is determined, the PPD can be estimated using

$$PPD = 100 - 95 \exp[-(0.03353PMV^4 + 0.2179PMV^2)] \quad (2 - 2)$$

The PMV and PPD model is widely used by many designs and assessment standards, such as ASHRAE and ISO standard. In ASHRAE Standard 55, an acceptable thermal environment is defined with more than 80% of the occupant feel thermally comfortable. Albeit the PMV and PPD model has been used for more than 40 years, its validity has been questioned because the space we lived in mostly is highly nonuniform and transitional and the model failed when used in extreme condition. Therefore, many other models have been developed to fill the gap.

During a long time after that, the focus of the research was still on the prediction of thermal sensation to the uniform environment. The Pierce two-node model and KSU two-node model both came with a model predicting thermal sensation. The Pierce two-node model use the calculated skin temperature, core temperature and skin wetness to predict thermal sensation (TSENS) and thermal discomfort (DISC) (Gagge et al. 1986). The KSU model

determines the thermal sensation directly from the physiological strain (Azer and Hsu 1977). After entering 1990s, many researchers started to work on predicting human response to asymmetrical and transient environments. However, during the first ten years, the prediction was still made on the whole-body basis even in nonuniform environment. Taniguchi developed a model to relate the average temperature of the facial skin and its rate of change to the whole body thermal sensation (Taniguchi et al. 1992):

$$TSV = 0.81 \times (T_{sk,face} - 33.9) + 39.1 \times dT_{sk,face}/dt \quad (2 - 3)$$

where the overall thermal sensation vote (TSV) was only correlated with the sensation of the facial part. This model ignored the influence of other body parts on the overall thermal sensation, but it indicated the fact that some body part had a higher impact factor than others and it made it possible to evaluate the transient thermal sensation by adding a time derivative term. Matsunaga developed an index named equivalent temperature (AET) to calculate PMV and evaluate the overall comfort (Matsunaga et al. 1993). The AET is a surface area-weighted value for three regions of the human body: head (0.1), abdomen (0.7), and feet (0.2). It seems crude that his model assigned the impact factor of each body part based on the surface area, but it still reflected the different impact factor of each body part. Almost at the same time, de Dear et al. developed a receptor model named Dynamic Thermal Stimulus (DTS) Model, which assigned different thermal sensation Area Summation Factors (ASFs) to different regions based on thermal sensitivities (de Dear et al. 1993):

$$DTS = \sum ASF_i (K_{s,i} T_{skin,i} + \frac{K_{d,i} dT_{skin,i}}{dt}) \quad (2 - 4)$$

Compared with the AET model, this model is more reasonable and can be used to predict

the response to the transient environment. Another transient thermal sensation model was proposed by Wang. In this model, the thermal sensation is calculated in two parts-static and dynamic (X. Wang 1994):

$$\text{Thermal Sensation} = U_0 + \Delta U \quad (2 - 5)$$

Where  $U_0$  is Fanger's PMV model, and  $\Delta U$  is based on the rate of heat storage in the skin and depends on the whole-body net heat gain. Based on the regression analysis of large amount of experiments and physiological IESD-Fiala model, a model named Dynamic Thermal Sensation (DTS) Model was developed (Lomas et al. 2003). Different with Wang's model, this model predicts the response to transient condition by including the changing rate of the mean skin temperature and predicts the static part by the error signals of the skin surface temperature and body core temperature. But the same with Wang's model, it does not consider nonuniform environments. The most advanced and complicated model was developed in the new century by the group of U.C. Berkeley (H. Zhang, Arens, Huizenga, et al. 2010a, 2010b, 2010c). This psychological model is used together with the physiological model developed by them to give the prediction of thermal sensation and comfort to both dynamic and nonuniform environment. Different with the model presented before, the model contained local sensation and comfort for each body segment. The thermal sensation is predicted with four inputs: local skin temperature, mean skin temperature and the time derivatives of skin and core temperatures, which can all be obtained by using the physiology model. And the comfort is calculated using thermal sensation. This model was developed and validated based on a large amount of experimental data representing all the major effects that have been observed about the human response to the thermal environment and it is the first model addressing human

responses to simultaneous nonuniform and transient thermal conditions. Another model which can treat people's response to nonuniform thermal condition is the clothing independent thermal comfort model based on the equivalent temperature ( $t_{eq}$ ) proposed by Nilsson. Equivalent temperature is defined as the temperature of an imaginary enclosure with the mean radiant temperature equal to air temperature and still air in which a person has the same sensible heat exchange by convection and radiation as in the actual conditions. The definition of the equivalent temperature can be related to the whole body as well as local parts of a human being. The principle of this model is that the heat loss corresponding to a certain level of comfort, or discomfort, is consequently to be the same (Håkan O. Nilsson 2007). The model was developed based on the comparison of thermal manikin tests and human subject tests in the same conditions. Correlations were constructed between the thermal sensation vote for the local or whole body and the heat loss from the corresponding manikin segment. Compared with the Berkeley's model, this method only considers the sensible heat loss from the human body and not suitable for transient condition, but it can also be used to evaluate the thermal response of local body part as well as the whole body to the nonuniform environments. In addition, this model has a prominent feature: the model is empirical, and it does not involve the use of the human body thermal physical and physiological modelling. Both a thermal manikin for experimental study and numerical manikin for CFD simulation with simple constant temperature boundary condition can be employed to obtain the evaluation of the thermal environment (Cheng et al. 2012). Because of these features, this current study will utilize this method for predicting the thermal response.

One of the most sweeping changes across the field of thermal comfort research in the past 20 years is the acceptance of a fundamentally different model of comfort – adaptive model. This concept derives from an idea of taking the building occupant as an integral component of the comfort ‘system’ (R. de Dear et al. 2013). The adaption process was classified as physiological (acclimatization), behavioral (using operable windows, fans, doors, awnings, etc.), and psychological (adjusting comfort expectations toward climatic conditions prevailing indoors and outdoors) (de Dear, Richard J., Brager 1998). The principle of the model is that the occupant cannot only sense the comfort level but also react to achieve comfort (F. Nicol and Humphreys 2007). The most important ways for the occupants to reach the comfort level were clothes changing and the air movement improvement (J. F. Nicol and Raja 1997). The feeling of being in control psychologically leads to faster adaption to different conditions and a more extended range of the comfort temperature (de Dear, Richard J., Brager 1998). Different with the rational model, this concept loosens the restriction of indoor temperature control, but unfortunately current standard only allowed it to be applied to natural ventilation buildings.

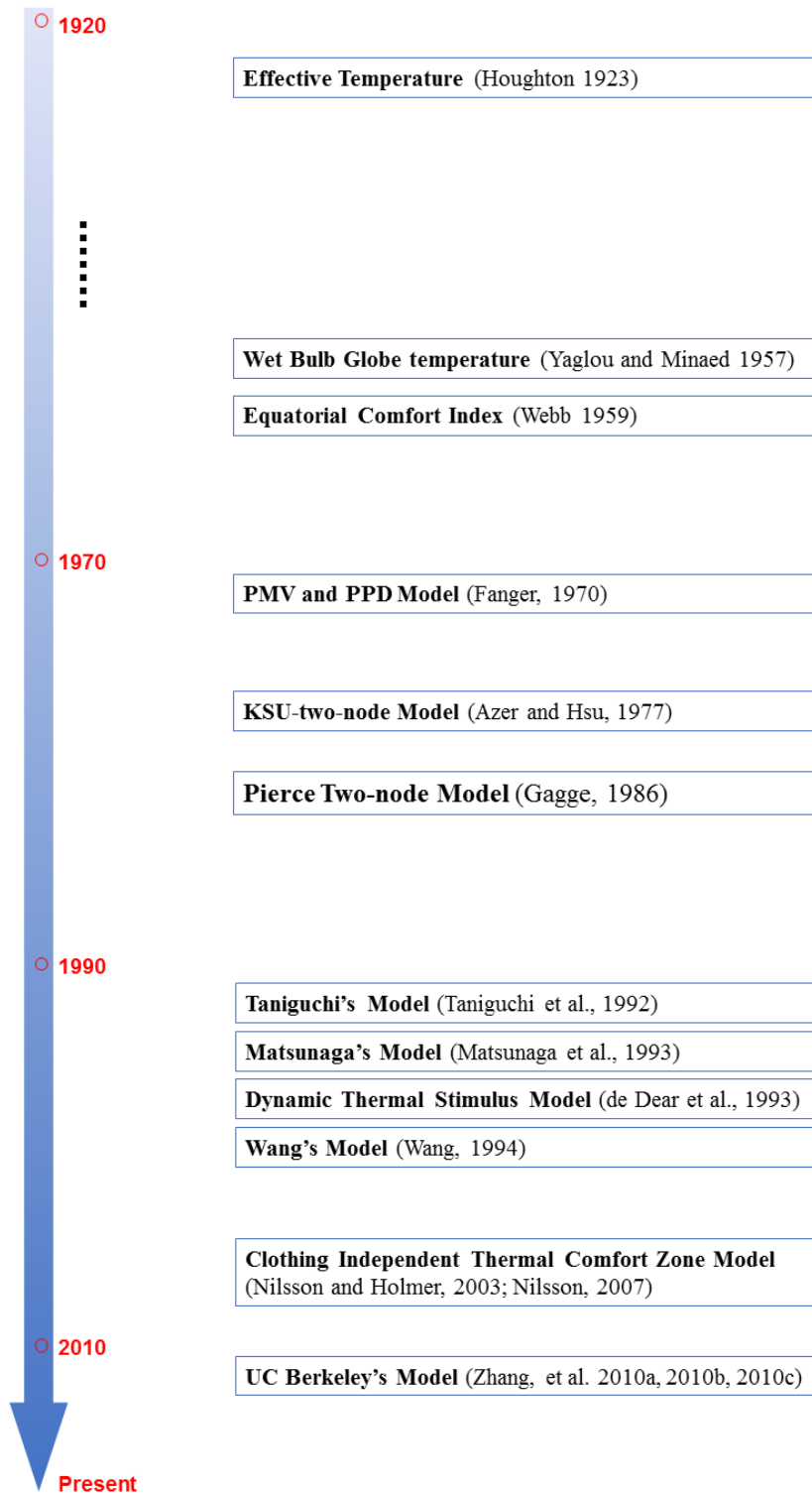


Figure 2-3 Timeline of psychological rational model's development

Table 2-2 Summary of the rational psychological models

<b>Model</b>	<b>Environmental Condition</b>	<b>Static</b>	<b>Dynamic</b>	<b>Uniform</b>	<b>Nonuniform</b>	<b>Local Response</b>	<b>Other Limitations</b>
<b>Effective Temperature</b> (Houghton 1923)	N/A	√	×	√	×	×	No clothing and metabolic rate effect included
<b>Wet Bulb Globe Temperature</b> (Yaglou and Minaed 1957)	Hot condition	√	×	√	×	×	N/A
<b>Equatorial Comfort Index</b> (Webb 1959)	Applicable also to extreme condition	√	×	√	×	×	N/A
<b>PMV and PPD Model</b> (Fanger, 1970)	N/A	√	×	√	×	×	Mechanical ventilated buildings; 0.3-1.2 clo; <1.4 met
<b>KSU-two-node Model</b> (Azer, 1977)	Cool to very hot	√	√	√	×	×	Low and moderate
<b>Pierce Two-node Model</b> (Gagge, 1973)	Cool to very hot	√	√	√	×	×	Low and moderate



<b>Taniguchi's Model</b> (Taniguchi et al., 1992)	Vehicle cabin	√	×	√	×	×	Only consider the face
<b>Matsunaga's Model</b> (Matsunaga et al., 1993)	N/A	√	×	√	√	×	N/A
<b>Dynamic Thermal Stimulus Model</b> (de Dear et al., 1993)	N/A	√	√	√	√	×	N/A
<b>Wang's Model</b> (Wang, 1994)	N/A	√	√	√	×	×	N/A
<b>DTS Model</b> (Lomas et al., 2003)	13-48 °C, 1-10 met	√	√	√	×	×	N/A
<b>Clothing Independent Thermal Comfort Model</b> (Nilsson and Holmer, 2003; Nilsson, 2007)	Regular clothing	√	×	√	√	√	No evaporation effects involved, not suitable for zero or heavy clothing
<b>UC Berkeley's Model</b> (Zhang, et al. 2010a, 2010b, 2010c)	N/A	√	√	√	√	√	More focused on locally cooling in warm condition

## 2.2. Air Quality

ASHRAE Standard 62.1-2016 defines acceptable Indoor Air Quality (IAQ) as “*air in which there are no known contaminants at harmful concentrations as determined by cognizant authorities and with which a substantial majority (80% or more) of the people exposed do not express dissatisfaction*”. The ventilation systems, creating different patterns of airflow field, determine the distribution of fresh air and pollutants, including gaseous and particulate components. A good ventilation system should be able to maintain the gaseous and particulate contaminants below some acceptable level. Some common indoor pollutants include carbon dioxide, carbon monoxide, radon, volatile organic compounds (VOCs), mycotoxins, microorganisms, viruses, allergens, and suspended particulate matter. Different contaminants have different aerodynamic features and toxicity. Therefore, the threshold concentration varies in a wide range. Usually, in order to evaluate the indoor air quality, several methods are used by the scientists and engineers: physical measurement, subjective evaluation, and computational simulation.

Physical measurement is the most accurate method to evaluate the indoor air quality. The actual level of any specific pollutant can be measured either in the field or the lab. This method is widely used in many research and engineering projects (Cao et al. 2015; Kong et al. 2014; Nielsen et al. 2013). However, the cost of it is expensive and sometimes limits its application. Subjective evaluation is the most straight-forward method to determine the level of indoor air quality. However, this method can only be used in an environment with non-harmful substance, like CO<sub>2</sub> or odor. One should note that the air quality perceived by the occupants is not necessarily correlated with the actual air quality, since the perceived

air quality is affected by not only the pollutant concentration but also the humidity, temperature, and velocity of the air. A survey has suggested that increased air movement improves occupant's perceived air quality (Zhang et al. 2007). Another widely used method to evaluate indoor air quality is computational simulation, mostly computational fluid dynamics (CFD). This method is the cheapest one but requires the most knowledge about the pollutant distribution as well as computational calculation, but a big advantage of this method is that more detailed results about the distribution of the pollutant could be obtained easily.

By using physical measurement and computational simulation, researchers can get the specific contaminant's concentration in the occupied space. However, since there is always more than one kind of contaminant in the indoor space, the specific concentration might not be that useful. In order to evaluate the ventilation performance more easily, a lot of indices have been developed. These indices are classified into two categories: one for evaluating the efficiency of delivering the fresh air and one for evaluating the performance of removing the pollutant.

### **2.2.1. Delivering the Fresh Air**

The indices for evaluating the efficiency of delivering the fresh air look into how the fresh air is distributed in the indoor space. These indices include Mean Age of Air, Air Exchange Efficiency, and Accessibility of Supplied Air.

*Mean Age of Air* is developed by Sandberg in 1980s (Sandberg 1981). It is defined as “the

time, that has elapsed since the air entered the room (Sandberg 1981).” When the supplied air is clean and fresh, the smaller the local mean age of air is, the fresher and cleaner the air is. The actual Mean Age of Air can be measured using tracer gas. With the development of the CFD techniques, Mean Age of Air  $\tau_p$  can also be calculated by using the following transport equation (Li and Jiang 1998):

$$\frac{\partial}{\partial x_j} (u_j \tau_p) = \frac{\partial}{\partial x_j} \left( \Gamma \frac{\partial \tau_p}{\partial x_j} \right) + 1 \quad (2 - 6)$$

where  $\Gamma$  is the diffusion coefficient of the tracer gas.

***Air Exchange Efficiency***  $\eta_a$  denotes the efficiency of the external air flushing a ventilated room (Hang and Li 2011). It is defined as the ratio between the room mean age of air under piston flow ventilation and the local mean age of air.

$$\eta_a = \frac{\bar{\tau}_p'}{\tau_p} \times 100\% \quad (2 - 7)$$

where  $\bar{\tau}_p'$  is the room average age of air under piston flow ventilation. Usually in room, the shortest possible time to replace the air is defined as the nominal time constant of the room:

$$\tau_n = \frac{V}{Q} \quad (2 - 8)$$

where  $V$  is the total volume of the room and  $Q$  is the supply volume flow rate. And under the piston flow ventilation,

$$\bar{\tau}_p' = \frac{1}{2} \tau_n \quad (2 - 9)$$

***Accessibility of Supplied Air*** is a time-related parameter which reflects the capability of

the supplied fresh air to reach a certain location at any time. It can be determined by injecting a tracer gas to the supply and monitor the concentration at the target location from the time the tracer gas is injected ((Kato et al. 1994)):

$$A_S^{n_s,p}(\tau) = \frac{\int_0^\tau C_p(t)dt}{C_S^{n_s}\tau} \quad (2 - 10)$$

where  $A_S^{n_s,p}$  is the Accessibility of the Supplied Air from diffuser  $n_s$  to reach the location  $p$  at time  $\tau$ ,  $C_p(t)$  is the tracer gas concentration at the location  $p$  at time  $t$ , and  $C_S^{n_s}$  is the concentration of the tracer gas of the air supplied by diffuser  $n_s$ . Accessibility of Supplied Air reflects the dynamic feature of the indoor flow field. After a sufficient long time, the summation of  $A_S^{n_s,p}$  of each diffuser will reach 1 and not change.

### 2.2.2. Removing the Pollutant

The indices for evaluating the performance of removing the pollutant look into how the pollutant travels in the indoor flow field. These indices include Contaminant Removal Efficiency, Intake Fraction, and Air Quality Index.

**Contaminant Removal Efficiency** ( $e$ ), or **Ventilation Efficiency**, reflects the capability of a ventilation system to remove contaminants. It is defined as

$$e = \frac{C_e - C_s}{C_p - C_s} \quad (2 - 11)$$

where  $C_e$  is the contaminant concentration in the exhaust air, and  $C_s$  is the contaminant concentration in the supply air. The Contaminant Removal Efficiency of a room is therefore defined as

$$e = \frac{C_e - C_s}{\bar{C} - C_s} \quad (2 - 12)$$

where  $\bar{C}$  is the averaged contaminant concentration of the room space.

However, due to the existence of the SOS and individual supply system, a relatively independent environment is created inside it, which will likely prevent the air inside and outside the cubicle from interacting. Together with the different ventilation system, the SOS “protect” the environment inside it to different degrees. Therefore, another index named Blocking Coefficient which indicates the blocking effect of the SOS is defined as

$$\beta = \frac{C_e - C_s}{C_{SOS} - C_s} \quad (2 - 13)$$

where  $C_{SOS}$  is the contaminant concentration of the SOS.

Air with pollution is taken in by the occupants through breathing. Exposure to pollutants through breathing can be indicated by the index ***Intake Fraction*** (iF), which is defined as the integrated incremental intake of a pollutant, summed over all exposed individuals, and occurring over a given exposure time, released from a specified source or source class, per unit of pollutant emitted (Bennett et al. 2002):

$$iF = \frac{\sum_{people,time} \text{intake of pollutant by an individual (mass)}}{\text{mass released into the environment (mass)}} \quad (2 - 14)$$

When there are multiple occupants in a room, the Intake Fraction of each occupant is defined as individual Intake Fraction.

***Air Quality Index*** (AQI) (Russo et al. 2008; Russo and Khalifa 2010; Russo and Khalifa

2010) indicates the level of air quality. It is defined as

$$AQI = \frac{1 - C - (1 - C_e)}{1 - C_s - (1 - C_e)} = \frac{C_e - C_p}{C_e - C_s} \quad (2 - 15)$$

AQI is hence a measure of how effectively the fresh supply air is delivered to the target point (e.g., the breathing zone). If the supply air of the PV system is all outdoor air, when  $AQI = 1.0$ , clean air is present at the target point, and when  $AQI = 0.0$ , the air at a certain point is perfectly mixed (as it would be in an ideal mixing-ventilation system). The smaller AQI means worse air quality. AQI is converted to Ventilation Efficiency (VE) or Contaminant Removal Efficiency by:

$$VE = e = \frac{C_e - C_s}{C - C_s} = \frac{1}{1 - AQI} \quad (2 - 16)$$

This current work looks into the contaminant distribution in a room equipped with SOS under steady state condition, and no breathing effects is going to be considered. Therefore, Contaminant Removal Efficiency was chosen to describe the spatial distribution of the air quality.

### **2.3. Room Air and Contaminant Distribution**

Room air and contaminant distribution is determined by the configuration of the ventilation system, including the location and size of the supply and return vents, the supply conditions, the contaminant source, and the room layout. Depending on those factors, Cao et al.

classified the existing ventilation systems into eight categories (Cao et al. 2014). The feature of each system is summarized in **Table 2-3**.



Table 2-3 Summary of the ventilation systems

<b>Ventilation System</b>	<b>Principle</b>	<b>Advantage</b>	<b>Disadvantage</b>	<b>Application</b>
Mixing Ventilation (MV)	Dilute the contaminated room air by mixing the supplied fresh air with indoor air	Uniform room condition; Widely used	Wasting energy in unoccupied zone; airborne infection	Almost everywhere
Displacement Ventilation (DV)	Displace the contaminated room air with fresh and cool air by buoyancy	Higher ventilation effectiveness	Not applicable to heating mode; the flow far away from the supply becomes distorted; cold feet	Offices
Personalized Ventilation (PV)	Supply fresh and conditioned air locally	Improve individual thermal comfort and air quality level; have the potential to save energy	High initial cost and maintenance fee	Offices, theaters, vehicles, airplanes, etc.
Hybrid Ventilation (HV)	Combine MV and DV to overcome the shortcomings of DV	Higher ventilation efficiency than DV and MV	Possible draught issue at foot level	Offices
Stratum Ventilation	Supply at the height of breathing zone	Allow higher room temperature and save energy; better air quality	Potential airborne infection	Building in East Asia (offices, classrooms, etc.)

Protected Occupied Zone Ventilation	Use a low-turbulent plane jet to separate an office environment into several subzones	Prevent possible polluted air from moving from one subzone to another	Draught issue	Offices
Local Exhaust Ventilation	Exhaust the pollution locally from the source	Very effective when contaminant/heat source can be identified	Only applicable when the contaminant/heat source is clustered	Kitchens, laboratories
Piston Ventilation	Use low velocity and turbulence air supply to create a piston flow	Very effective way to remove contaminants in the room	Costly and require a very high air change rate	Clean rooms, hospital operating rooms

This current work is focused on the performance of the micro-environment control system and the semi-open space in a MV background.

## **2.4. Indoor Environment Evaluation and Design Methods**

Various modeling approaches have been used for modeling the thermal distribution and air-flow movement. The type of approach used depends on the complexity of the phenomena observed, the modeling objectives, the parameters investigated, and the degree of required accuracy (Megri and Haghightat 2007). A brief account of each approach is given below.

### **2.4.1. Analytical Model**

Analytical Models are derived from fundamental equations of fluid dynamics and heat transfer, such as mass, momentum, energy and chemical-species conservation equations. The analytical models use simplifications in both geometry and thermo-fluid boundary conditions to obtain a solution. The analytical models are probably the oldest method for predicting ventilation performance. This method is still widely used today due to its simplicity, rich in physical meaning and little requirement in computing resource, although it may not be accurate for complicated ventilation cases and results may not be sufficiently informative (Chen 2009).

### **2.4.2. Empirical Models**

The empirical model is a model also based on the fundamental laws of transport phenomena. However, different from the analytical method, some of the coefficients or forms of the

formula come from experiments or experience. For instance, Cho (Cho et al. 2008) investigated the behavior of a wall confluent jet by experiment and simulation. The maximum velocity of the jet is determined by

$$\frac{U_m}{U_0} = 2.96l_c^{-0.79} \quad (2 - 17)$$

in which the throw constant (2.96) is obtained empirically. Similar to analytical models, empirical models are valid only for simplified conditions for which they are developed, though the empirical models may apply to a wider range of conditions by adjusting the empirical model coefficients.

### **2.4.3. Nodal Model**

Nodal model is the most simplified model for simulating the indoor environment. Usually, it is used in the building simulation software when the rooms or zones which share the same setting point will be represented by a single node. The heat transfer and air and contaminant flow between each two connected nodes are calculated based on the fundamental or empirical laws. CONTAMN and COMIS are two typical programs which are using a nodal network to calculate the airflow, pressure and contaminant distribution in a building (Chen 2009). Typically, the local transport phenomena inside each zone or room are ignored, and the environment inside them is considered to be uniform.

### **2.4.4. Zonal Model**

A zonal model is an intermediate approach between nodal model and Computation Fluid Dynamic (CFD) model. It deals with the internal transport phenomena inside the room by

dividing the room into several subzones. The perfect mixing assumption is adopted for each subzone. Individual temperature, contaminant concentration, and mass are assigned to each subzone to represent the non-uniform distribution in the space. Challenge in developing a zonal model is to define and construct subzones with the corresponding representation of mass and energy flow. The zonal models had been developed based on measured airflow patterns or mass and energy balance equations (Chen 2009). The former one divides the room space based on the knowledge of flow pattern and usually only fit in the specific ventilation system and room configuration. The latter one used energy and mass conservation laws to calculate the inter-zonal flux and is used more widely. Zonal models are a promising way to predict air movement in a room concerning comfort conditions and gradient of temperature because they require extremely little computer time and could easily be included in multi-zone air movement models (Ahmed Chérif Megri and Mark Snyder 2005; Megri and Haghghat 2007; Teshome and Haghghat 2004).

Most of the present zonal model are implemented based on the mass and energy conservation laws (Eqn. 2 and 3) in every subzone with several complementary equations including ideal gas equation (Eqn. 4), mass flow- pressure difference equation (Eqn. 5 and 6) and heat exchange fluxes equation (Eqn. 7) (Megri and Haghghat 2007). When the moisture or contaminant is involved, some other equations can be utilized to calculate the distribution (Mendonça and Inard 2002; Wurtz et al. 2006).

$$\sum_j \dot{m}_{j \rightarrow i} = 0 \quad (2 - 18)$$

$$\sum_j \Phi_{j \rightarrow i} + \Phi_{source} = \rho_i V_i c_p \frac{\partial T_i}{\partial t} \quad (2 - 19)$$

$$P_i = \rho_i r T_i \quad (2 - 20)$$

$$\dot{m}_{j \rightarrow i} = \rho_{j,i} A C_d (P_j - P_i)^n \quad (2 - 21)$$

$$\dot{m}_{j \rightarrow i} = \rho_{j,i} A C_d \left[ P_j - P_i - \frac{1}{2} (\rho_j h_j + \rho_i h_i) \right]^n \quad (2 - 22)$$

$$\Phi_{j \rightarrow i} = c_p (\dot{m}_{j \rightarrow i}^+ T_j + \dot{m}_{j \rightarrow i}^- T_i) - \frac{\lambda A}{l} (T_j - T_i) \quad (2 - 23)$$

Due to the simplification of the transport equation, momentum transport equation is absent in most of the zonal model which means these model can only be applied to the flow of low velocity. Some researchers (Haghighat et al. 2001) also developed a simplified numerical model in which the jet characteristic equation was introduced to generalize its application to the mechanically ventilated building. However, this kind of model would increase significantly the complexity of the zonal model which will make the zonal model more expensive.

#### 2.4.5. Design Chart

Nielsen developed a method to help to predict and design the total volume air distribution system based on discussions of air flow pattern in a range of ventilation systems, which is called “Family Tree” of air distribution systems (Nielsen 1980, 2006, 2011; Nielsen et al. 2007; Nielsen and Jakubowska 2009; Skistad et al. 2002). The influence of supplied momentum flow versus buoyancy forces is discussed, and geometries for high ventilation effectiveness are indicated as well as geometries for fully mixed flow. Long time work on

the research of various ventilation systems and rich experience makes it possible for him to find the key factor of designing a ventilation system. Geometrically the ventilation systems are based on the location of supply openings, and the opening ratio of the supply diffuser to the wall area (Figure 2-4). For each specific configuration the flow pattern, ventilation effectiveness, and comfort level are analysed based on the operation parameters – temperature difference between the supply and return air and supply airflow rate.

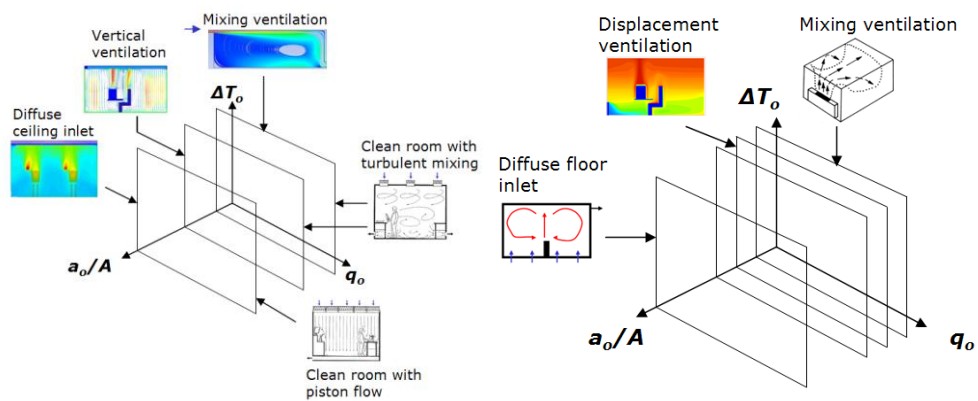


Figure 2-4 Different air distribution systems for cooling with high (left) and low (right) location of supply openings (Nielsen 2011)

The goal of implementing a ventilation system is to maintain the environment in the occupied space comfortable and clean with appropriate supply flow rate and temperature. Therefore, a limit will be applied to the air flow rate and supply temperature to fulfil the requirement of thermal comfort and air quality, such as minimum outdoor air, acceptable draught and acceptable temperature gradient. To help make the decisions more qualified, a design chart is developed and by using this chart, user can find the optimal systems based on their demands (Figure 2-5)(Nielsen 2011).

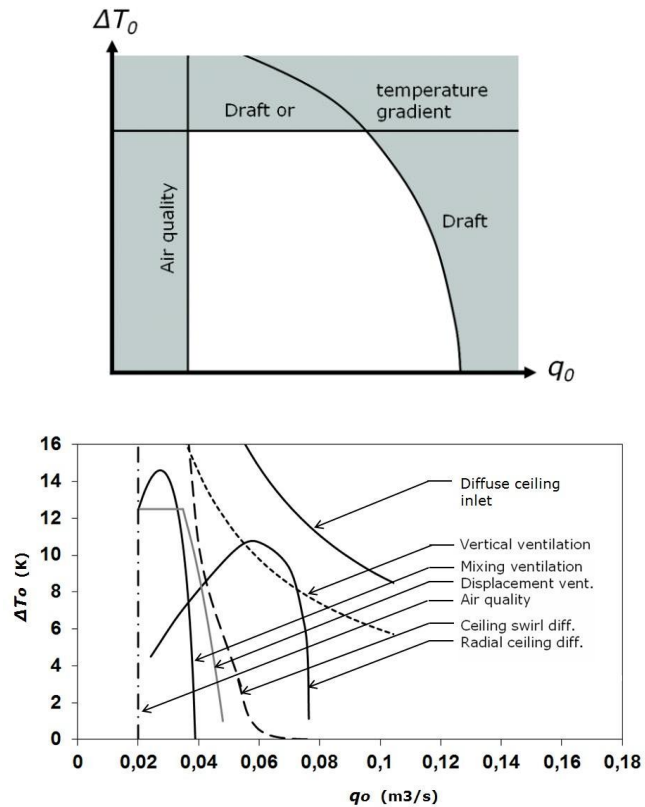


Figure 2-5 Design chart of the "Family Tree" (Nielsen 2011)

#### 2.4.6. Computational Fluid Dynamics Model

Computational Fluid Dynamics (CFD) Model is a numerical method to model the indoor environment by solving a set of partial differential equations. In this way, all the details of the indoor environment can be obtained if proper boundary conditions, appropriate computational mesh, and turbulence model are used. CFD model used to be an expensive way for modeling indoor environment, but thanks to the development of computer science, the difficulty of representing complex geometry and dealing with dense mesh has been overcome. Increasing numbers of work have been done using CFD in many engineering fields and with the time going on the commercial CFD software has been the most popular



method in modeling indoor environment due to its powerful capability and friendly user interfaces. This work utilized the CFD simulation to help design and evaluate the micro-environment system. More details will be discussed in the next few chapters.

### **3. Performance Evaluation of Different Room Air Distribution Systems**

Before jumping into the systemic study of using micro-environment control system and semi-open space for thermal comfort and air quality control, a series of preliminary studies were conducted to help improve the understanding of the work scope and methods. Both experimental and CFD simulation works were performed to compare the performance of a different room air distribution/ventilation systems in a full-scale office room containing 12 cubicles. The objectives were to improve the understanding of characteristics of the various micro-environmental control system and the role of semi-open space for indoor environmental control and to develop a CFD model for performance prediction.

#### **3.1. Field Experimental Evaluation of Three Kinds of Ventilation Systems**

##### **3.1.1. Overview**

###### **3.1.1.1. Experimental Setup**

The prototype room is the Total Indoor Environmental Quality (TIEQ) Lab located in the Syracuse Center of Excellence (COE) Building, which is depicted in Figure 3-1 with a full size of 6.25 m × 10.52 m × 3.15 m <sup>[2]</sup>. There are 12 cubicles in this room arranging along two side walls and two doors on each end. Three ventilation systems are equipped with it: a displacement ventilation system with four floor-diffusers in the corridor, a under-floor air distribution (UFAD) ventilation system with one floor-diffuser in each cubicle and a personalized ventilation system with a PV Exhausto diffuser (referred as “PV” in the following) in each cubicle.

---

<sup>[2]</sup> (Y) m = (Y × 100) cm = (Y × 3.28) ft = (Y × 39.37) in

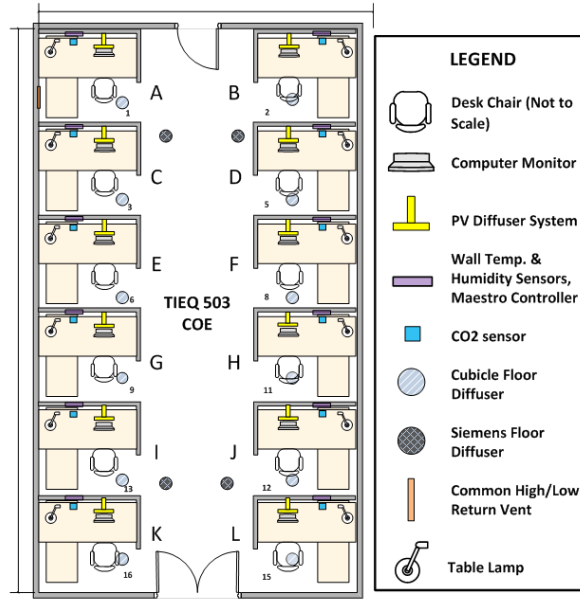


Figure 3-1 Prototype Room Layout



Figure 3-2 Target Cubicle

Figure 3-2 shows the test cubicle which has a full size of 1.91 m × 1.84 m × 1.71 m. A desk is located in front of the chair with a monitor on it and a computer processor below it. Moreover, a lower desk is set on the left-hand side of the chair with a storage box below it. The sensor and temperature controller is installed on the front partition of the cubicle while

the PV and UFAD are installed above the monitor and at the right back side of the chair, respectively.

The fresh and clean air is supplied to the work place through the UFAD system (Figure 3-3 left), PV system (Figure 3-3 center) or chair ventilation (CV) system (Figure 3-3 right). The UFAD diffuser is mounted on the floor of the cubicle fed by a variable-air volume box in the under-floor plenum. It consists of 16 long slots and 16 short slots arranged in a ring of a 6.35 cm internal diameter and a 19.69 cm external diameter. The PV diffuser is mounted 1.33 m above the floor with a tube connected from back to the air handler. It has a total length of 36.83 cm and a diameter of 6.86 cm with two grill openings symmetrically on both wings. Each opening is 11.43 cm long, divided into six parts by grill evenly. The supply air direction can be adjusted by rotating each wing about the central axle of the diffuser. A CV terminal consists of an air bag of an area  $0.52 \text{ m}^2$  <sup>[3]</sup>, which covers the chair and two tubes connected on the two sides. A box was used to connect the tube to the supply of the air system. A total flow rate of  $0.047 \text{ m}^3/\text{s}$  <sup>[4]</sup> is used for UFAD and  $0.009 \text{ m}^3/\text{s}$  flow rate is applied to both PV and CV.

---

<sup>[3]</sup>  $(Z) \text{ m}^2 = (Z \times 10.76) \text{ ft}^2$

<sup>[4]</sup>  $(W) \text{ m}^3/\text{s} = (W \times 2118.88) \text{ cfm}$



Figure 3-3 Terminal of ventilation system: UFAD (left), PV (center), CV (Right)

During the experiment, the flow field around the manikin is monitored regarding both velocity and temperature at different heights (0.1 m, 0.6 m, 0.8 m, 1.1 m, 1.4 m and 1.6 m) and locations (left front, left, right front and right). A tracer gas test is also conducted in the lab using CO<sub>2</sub>. Four injecting tubes are located at the entrances of the four corner cubicles (A, B, K, and L), and another injecting tube is either located under the chair in the cubicle or outside the cubicle at the center of the corridor to represent the different location of contaminant source. Five sampling ports are placed respectively in the breathing zone of the manikin, in the occupied cubicle, in the corridor, in the supply duct, and in the return duct. INNOVA-1301\_Multipoint Sampler and Doser is used to both inject the CO<sub>2</sub> and sample the air. INNOVA-1412i\_Photoacoustic Gas Monitor is used to analyze the sampled air from the lab.



Figure 3-4 Measurement Setup

### 3.1.1.2. Equivalent Temperature

The personalized ventilation does not only increase the air quality around the people, but also improve the thermal comfort. Clothing independent equivalent temperature ( $t_{eq}$ ) was used to evaluate the thermal comfort level with manikin. As mentioned before, this index is defined as the temperature of an imaginary enclosure with the mean radiant temperature equal to air temperature and still air in which a person has the same heat exchange by convection and radiation as in the actual conditions which can be determined using the following equation:

$$t_{eq} = t_s - \frac{q_T''}{h_{cal}} \quad (3 - 1)$$

where  $q_T''$  is the measured manikin heat loss during the actual condition,  $h_{teq}$  is the dry heat transfer coefficient, determined during calibration in a standard environment,  $t_s$  is the

manikin surface temperature and  $t_{eq}$  is the temperature of the uniform homogeneous environment which is the equivalent temperature (Nilsson 2004).

### 3.1.2. Flow Field Characteristics

Both velocity and temperature were measured close to the surface of the manikin (within 0.1 m to the closest surface) to give us some concepts of the flow field in the vicinity of the manikin. The velocity comparison (Figure 3-5) shows a much smaller velocity of the CV system compared with the other two systems. The max velocity in the CV case is about 0.09 m/s, which might be due to the large area of the chair ventilation terminal. Based on the ASHRAE Standard 55, in the room temperature of 26.0 °C, the mean room velocity is suggested to be lower than 0.2 m/s for mixing ventilation system, which is higher than most of the velocities measured in either the PV or UFAD case.

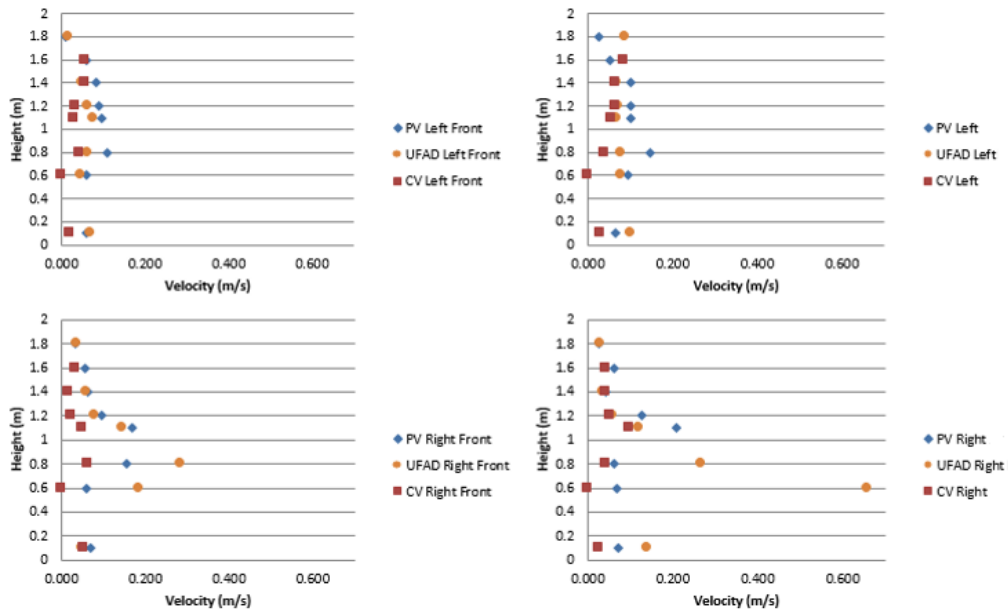


Figure 3-5 Velocity comparison of three systems

The temperature field of CV was more uniform than the other two (Figure 3-6). Moreover, there existed a slight gradient vertically. In the UFAD and PV system, an obvious obstacle of the temperature at the waist level could be found, but in CV system there wasn't any, which might be resulted from the fact that the CV supply flow of uniform and low velocity did not impact the temperature stratification induced by the thermal plume.

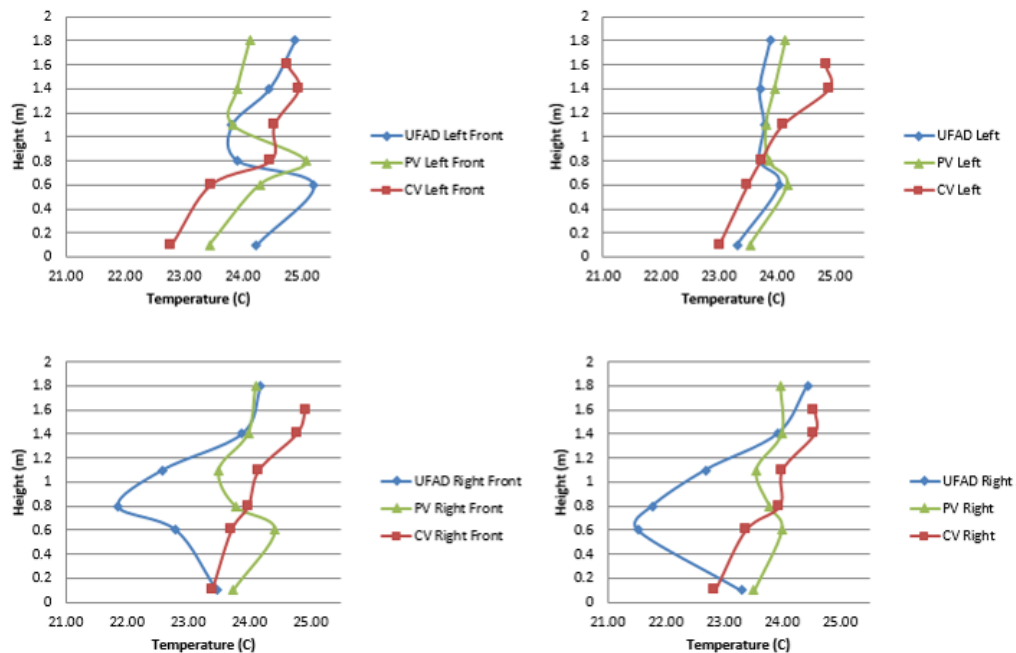


Figure 3-6 Temperature comparison of three systems

### 3.1.3. Thermal Comfort Analysis

Figure 3-7 showed the equivalent temperature along the body of the manikin in three systems. The thermal sensation of the whole body was neutral for all the three systems (22.0-23.0 °C), although a little cooler in CV case. However, an intense variation of equivalent temperature for different parts existed for each system. Right upper arm (18.4



°C) is the part feeling the coldest in UFAD case, so as the face (15.8 °C) in the PV case and the back (16.0 °C) in the CV case. In general, the parts with low equivalent temperature are always close to the supply opening and exposed to the cooler supply air more directly, and the parts with high equivalent temperature are always far away from the supply.

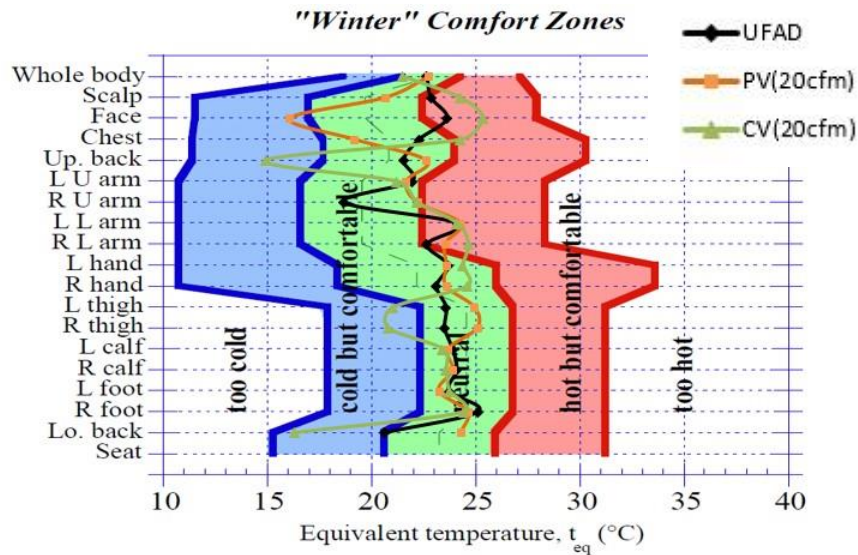


Figure 3-7 Equivalent Temperature

### 3.1.4. Air Quality Analysis

Figure 3-8 gives the Ventilation Efficiency, Blocking Coefficient and Local Ventilation Efficiency for both dosing inside and outside the cubicle. The Local Ventilation Efficiency is defined as

$$LVE = \frac{\varepsilon}{\beta} = \frac{C_{SOS} - C_s}{C_p - C_s} \quad (3 - 2)$$

which could be used to evaluate the performance of the local ventilation system in the SOS. For dosing inside the cubicle, CV gave the best LVE (a little higher than PV) and moderate VE which was because more contaminant was held in the cubicle (the Blocking Coefficient

was the lowest). For dosing outside the cubicle, PV gave the best LVE but worst VE which was because too much contaminant was “sucked” into the cubicle (the Blocking Coefficient was the only half of the others’).

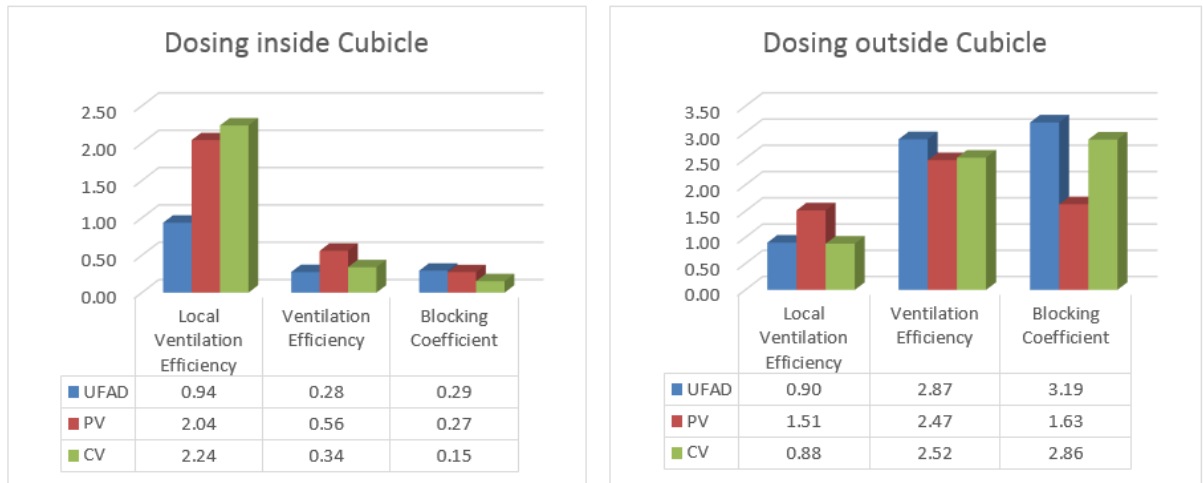


Figure 3-8 Local Ventilation Efficiency, Ventilation Efficiency and Blocking Coefficient

## 3.2. CFD Model Development

### 3.2.1. Overview

This subsection presents the development of the CFD model for simulating the flow field in the cubicle as discussed in the previous section. The prototype room studied is an office room (6.25 m×10.52 m×3.15 m) with 12 cubicles arranged in 2 rows, located in the Syracuse Center of Excellent (COE) Building (Figure 3-9). Each cubicle has approximately the same configuration and size. The target cubicle was occupied by a manikin and has dimensions of 1.91 m×1.84 m×1.71 m high. The air and air contaminant movement in the cubicle was simulated by using a commercial CFD software STAR-CCM. The CFD model was verified by sensitivity analysis and validated by experimental results. Analysis of the flow characteristics in the cubicle was conducted to provide detailed information of the performance of the personalized ventilation.



Figure 3-9 Target cubicle (left) and TIEQ (right)

### 3.2.2. Experiment Data Set for Model Validation

#### Moved to experiment part

Experiments were conducted previously to give us some basic ideas of the flow field as well as validate the CFD model. A cubicle on the west (right in **Error! Reference source not found.**) side of the office was selected to be the test cubicle. A 20 body segments thermal manikin was used to simulate a real person. The manikin was seated in an office chair in front of the computer at a distance approximately 0.10 m from the front desk. A side desk and a storage box were placed to the left side of the chair. A monitor with a keyboard and a mouse was placed on the front desk and a processor beneath the front desk (Figure 3-1). The fresh and clean air was supplied to the work place through UFAD (Figure 3-10 a) and PV (Figure 3-10 b) which yielded airflow rates of 55.10 l/s and 9.44 l/s at temperatures of 18.6°C and 18.4°C. The UFAD was mounted on the floor of the cubicle fed by a variable-air volume box in the under floor plenum. Detailed information about the configuration of the diffusers is presented in Sec. 3.1.1.1. During the test, the manikin was set under a comfort mode. Regular light clothes were applied on it. Both the temperature and heat flux of the manikin were monitored and recorded.

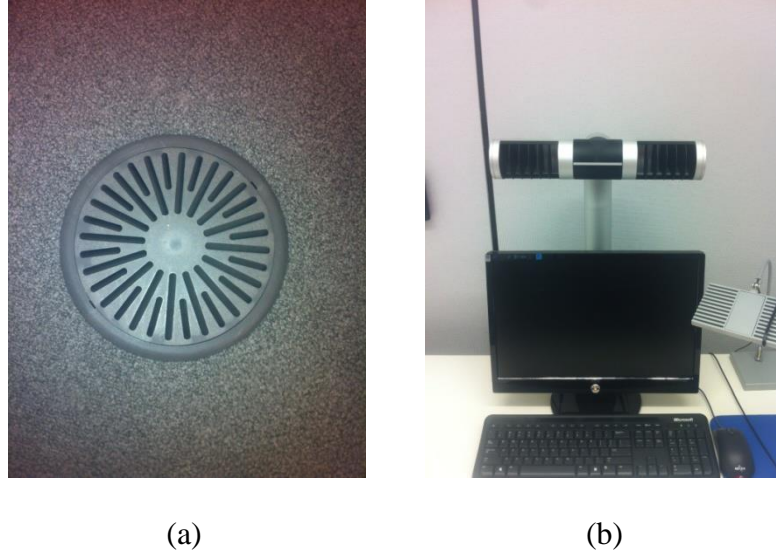


Figure 3-10 Terminal of ventilation system: UFAD (a), PV (b)

During the experiment, the flow field around the manikin was monitored regarding both velocity and temperature at different heights (0.1 m, 0.6 m, 0.8 m, 1.1 m, 1.4 m and 1.6 m) and locations (left front, left, right front and right). The velocity in front of the PV was also measured to validate the CFD model.

### 3.2.3. Governing Equations for CFD Model

The eddy-viscosity RANS model is the most popular class of turbulence model utilized for indoor environment simulations (Dyert et al. 2009). The basic equations include mass, momentum and transport equation of other quantities.

$$\frac{\partial}{\partial x_i}(\rho u_i) = 0 \quad (3-3)$$

$$\frac{\partial}{\partial t}(\rho u_j) + \frac{\partial}{\partial x_i}(\rho u_i u_j) = -\frac{\partial p}{\partial x_j} + \frac{\partial}{\partial x_i} \left( \mu \frac{\partial u_j}{\partial x_i} - \rho \overline{u'_j u'_i} \right) + S_j \quad (3-4)$$

$$\frac{\partial}{\partial t}(\rho\phi) + \frac{\partial}{\partial x_i}(\rho u_i \phi) = \frac{\partial}{\partial x_i} \left( \Gamma \frac{\partial \phi}{\partial x_i} - \rho \overline{u'_i \phi'} \right) + S \quad (3-5)$$

Boussinesq and Reynolds' analogies are used to model the turbulent term.

$$\tau_{ij} = -\rho \overline{u'_i u'_j} = \mu_t \frac{\partial u_i}{\partial x_j} \quad (3-6)$$

$$H_i = \rho c_p \overline{u'_i T'} = -\rho c_p \gamma_t \frac{\partial T}{\partial x_i} \quad (3-7)$$

For RANS-based CFD methods, the most difficult task in setting up a CFD simulation is the selection of a turbulence model. Researchers have used a wide range of turbulence models when studying micro-environment around human body (Dygert et al. 2009; Khalifa et al. 2006) which include the zero-equation model (Xu and Chen 2001a, 2001b), standard  $k-\varepsilon$  model (Gao and Niu 2004; Hayashi et al. 2002), the RNG  $k-\varepsilon$  model (Gao and Niu 2006; Khalifa 2006), the  $v^2-f$  model (Dang 2008), the realizable  $k-\varepsilon$  model (Russo et al. 2009), and the SST  $k-\omega$  model (Deevy et al. 2008). By comparing different turbulence models including  $k-\varepsilon$  family and  $k-\omega$  family models, Dygert found the  $k-\varepsilon$  family gave similar predictions and compared well with the test data while  $k-\omega$  turbulence models showed bad agreement in predicting the jet development. In this case, the realizable  $k-\varepsilon$  turbulence model is used.

Another challenge in CFD modeling of room airflows is the simulation of flow close to solid surfaces due to the transition of turbulence flow to the flows dominated by viscous

effect near the surfaces. The two-layer approach which is developed by Xu is used as an alternative to the low-Reynolds' number approach that allows the one-equation turbulence model to be applied in the near-wall region and the two-equation  $k$ - $\varepsilon$  model to be applied in the region away from the wall (Xu and Chen 2001a). With this approach, the whole flow field is divided into two regions – the near-wall layer and the far field. In the first layer, the turbulent kinetic energy  $k$  is calculated by

$$\frac{\partial k}{\partial t} + u_i \frac{\partial k}{\partial x_i} = d_k + P_k + G_k - \varepsilon \quad (3 - 8)$$

The eddy viscosity is calculated by

$$\nu_t = \sqrt{u'u'} l_\mu \quad (3 - 9)$$

The turbulence dissipation rate  $\varepsilon$  by

$$\varepsilon = \frac{\sqrt{u'u'} k}{l_\varepsilon} \quad (3 - 10)$$

where  $G_k$  is the gravity production of turbulent kinetic energy,  $P_k$  is the shear production of the turbulent kinetic energy and  $l_\mu$  and  $l_\varepsilon$  are characteristic lengths which are defined well in Xu's work (Xu and Chen 2001a).

The values of  $\varepsilon$  specified in the near-wall layer are blended smoothly with the values computed from solving the  $k$ - $\varepsilon$  equations far from the wall. The equation for the turbulent kinetic energy is solved in the entire flow. This explicit specification of  $\varepsilon$  and  $\mu_t$  is arguably no less empirical than the low-Reynolds' number approach, and the results are often as good or better. In STAR-CCM+, the two-layer formulations will work with either low-Reynolds number type meshes  $y^+ \sim 1$  or wall-function type meshes  $y^+ > 30$  (CD-Adapco 2015).

#### **3.2.4. Post Processing**

Cooling efficiency of the ventilation system is examined using Cooling/Heating Efficiency Index  $\Phi$ , an indication of the extent to which the cool supply air reaches the target point (e.g., occupied zone),  $\Phi$ :

$$\Phi = \frac{T - T_{clo}}{T_s - T_{clo}} \quad (3 - 11)$$

#### **3.2.5. Verification and Validation**

A computational model was developed using a commercial CFD code (STAR-CCM). To simulate the flow field in the cubicle, a seated computer simulated manikin (SCSM) was imported into STAR-CCM. The configuration of the SCSM was developed by Khalifa et al. (2009). In order to make it easier to simulate and to align with a desk, the hair and hands were removed. A single cubicle case was created to represent the target cubicle. The



polyhedral mesh was used in this study instead of the tetrahedral mesh because it provides a balanced solution for complex mesh generation problems. It is relatively easy and efficient to build, requiring no more surface preparation than the equivalent tetrahedral mesh. It also contains approximately four times fewer cells than a tetrahedral mesh for a given starting surface (CD-Adapco 2015).

To obtain valid simulation results, an appropriate grid is necessary. However, increasing the number of cells results in much more time for computing. Therefore, an optimal mesh is needed to balance the number of cells and the accuracy of the calculation. Creating every grid mesh requires meshing the surface of the manikin first. Then a proper boundary layer representation can be employed for the manikin surfaces. Next, the remaining surfaces including walls, inlets, outlets and floor need to be meshed. Finally, the volume mesh will be created. Five grids were created for the grid independence study. The velocity distribution and the flow structure of the symmetric plane were compared (Figure 3-11). A summary of the five grids is provided in Table 3-1. All the cases consist of polyhedral cells with polygonal surface elements, except the prism layer attached on the boundary (Figure 3-11).

Table 3-1 Grid Summary

<b>Grid Label</b>	<b>Base Size (m)</b>	<b>Number of cells</b>	<b>Number of elements on the manikin</b>	<b>Prism layer</b>	<b>Average Wall Y+</b>
<b>A</b>	0.1( <b>0.1</b> )	107,846	2,128	5	1.21
<b>B</b>	0.07( <b>0.07</b> )	181,925	3,966	5	1.18

<b>C</b>	0.05( <b>0.05</b> )	336,326	4,290	5	1.58
<b>D</b>	0.05( <b>0.02</b> )	929,342	4,617	15	1.51
<b>E</b>	0.05( <b>0.015</b> )	1,857,385	7,556	15	1.42

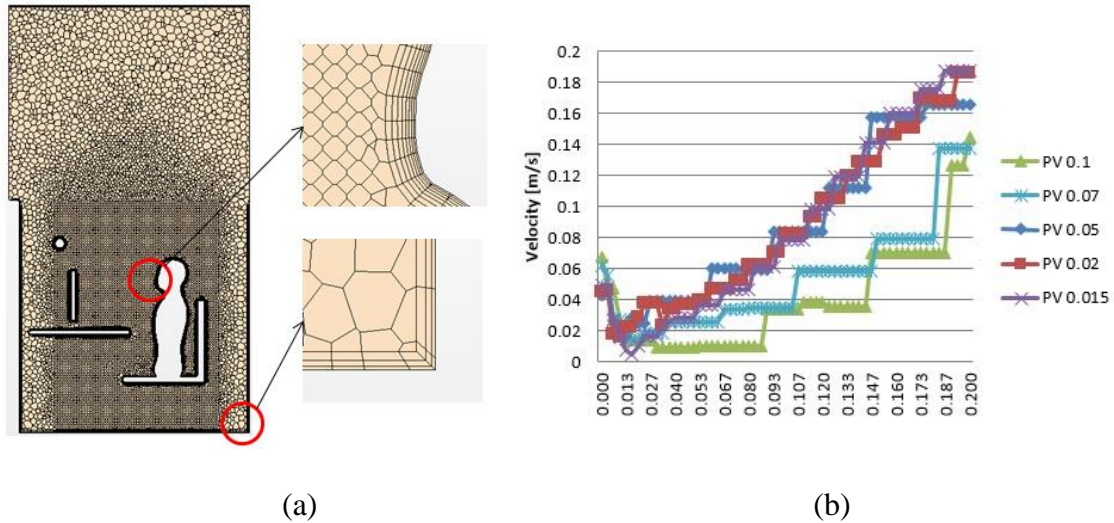


Figure 3-11 Grid resolution (a) and velocity in front of the face (b)

The accuracy of the calculation mostly depends on the density of volume mesh grids. In STAR-CCM, it is controlled by the base size, which other size is defined compared to it. Cases with base grid size 0.05 m, 0.02 m and 0.015 m gave acceptable grid independence and were better than 0.07 m and 0.10 m. Considering the time consumed in the simulation, a base grid size of 0.05 m was used.

In order to validate the simulation model, several cases were conducted and used to compare with the experimental results. Since in the experiment, a thermal comfort model,

as well as casual clothing, was applied to the manikin, an identical boundary condition could not be created in the CFD model. Instead, two approximation methods were used to replace the thermal comfort boundary condition: specified heat flux and specified surface temperature for individual body parts (Table 3-2). A whole-room case (Table 3-3), as well as the single cubicle case, were tested simultaneously.

Table 3-2 Manikin Boundary Condition

Manikin Parts	PV		UFAD	
	Temp [°C]	Q/A[W/m <sup>2</sup> ]	Temp [°C]	Q/A[W/m <sup>2</sup> ]
Face	30.0	126.55	32.5	81.22
Head	31.8	95.50	32.5	82.76
R Upper Arm	31.4	51.75	32.6	64.01
L Upper Arm	31.4	55.75	32.6	54.89
R Forearm	33.6	50.57	33.5	53.81
L Forearm	33.7	66.99	34.5	67.88
R Hand	32.5	81.18	32.4	83.98
L Hand	32.5	84.58	32.4	84.31
Chest	31.4	72.53	32.3	60.12
Shoulders	34.4	47.66	34.2	51.38
Stomach	34.6	44.12	34.2	50.49
Back	32.5	50.37	31.1	64.87
R Up Thigh	32.0	34.49	30.2	41.33

<b>L Up Thigh</b>	32.0	34.92	30.2	37.09
<b>R Low Thigh</b>	32.9	40.28	30.6	45.58
<b>L Low Thigh</b>	33.6	39.47	31.6	43.94
<b>R Calf</b>	29.3	49.75	30.0	49.05
<b>L Calf</b>	29.5	48.02	30.2	47.31
<b>R Foot</b>	29.2	47.21	34.5	45.41
<b>L Foot</b>	29.2	51.38	31.2	49.60

Table 3-3 Cubicle Setting for Whole Room Simulation

UFAD @ 23.9 °C (A person seated in the cubicle D (ATM5))						
	ATM1	ATM2	ATM3	ATM5(Occ)	ATM6	ATM8
Flowrate (L/s)	55.83	58.83	46.53	48.77	18.21	42.22
SA Temp (°C)	25.1	25.0	28.9	24.3	23.7	24.4
RA Temp (°C)	24.2					
	AMT9 (Manikin)	ATM11	ATM12	ATM13	ATM15	ATM16
Flowrate (L/s)	55.14	46.36	42.49	43.72	44.24	55.83
SA Temp (°C)	15.3	24.4	24.6	15.9	24.5	24.7
RA Temp (°C)	24.2					
PV @ 23.9 °C (A person seated in the cubicle D (ATM5))						
	ATM1	ATM2	ATM3	ATM5(Occ)	ATM6	ATM8
Flowrate (L/s)	7.40	7.40	38.75	9.44	2.62	7.60
SA Temp (°C)	22.4	22.8	28.9	21.7	23.3	22.4
RA Temp (°C)	24.5					
	AMT9 (Manikin)	ATM11	ATM12	ATM13	ATM15	ATM16
Flowrate (L/s)	9.44	8.70	6.50	8.50	35.15	10.25

SA Temp (°C)	15.7	16.8	17.0	15.8	15.9	16.2
RATemp (°C)	24.5					

Velocity measurements were taken on the symmetric plane of the PV. The following showed the velocity comparison at the symmetric plane of the PV and manikin between the experiment and simulation (Figure 3-12). Similar results were obtained with the two different boundary conditions, which also agreed well with the measurements (Figure 3-12 a). Both the single cubicle case and the whole-room case showed quite similar results of jet development (Figure 3-12 b) which had dominant effects on the flow pattern around the manikin.

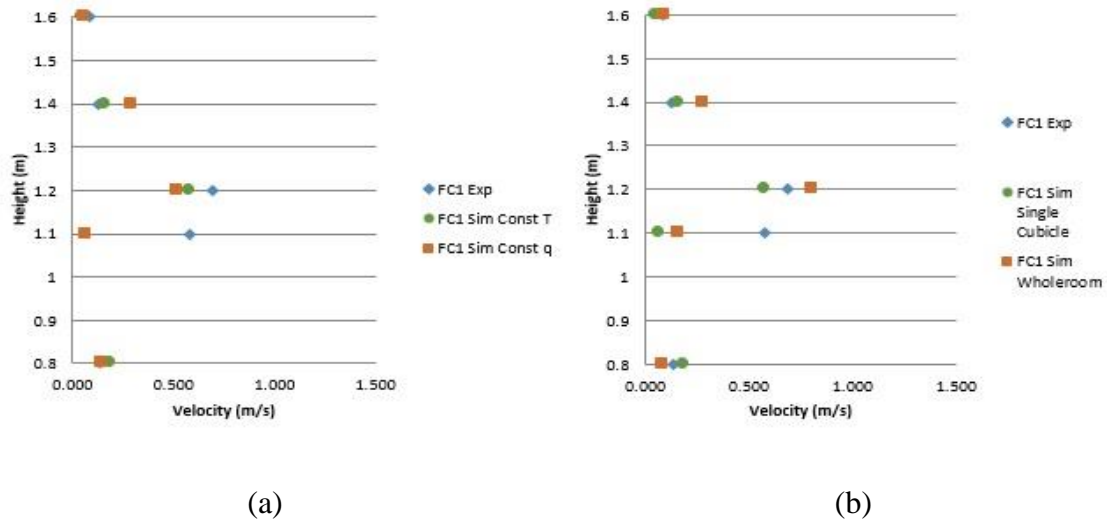


Figure 3-12 Velocity validation (a) of different boundary conditions; (b) of different simulation space

Temperature measurements were taken along the four vertical poles around the manikin. The results showed a better agreement obtained by the specified surface temperature

compared with the specified surface heat flux (Figure 3-13 a). The whole-room case gave almost the same agreement as the single cubicle case did (Figure 3-13 b), which means a simplified single cubicle case is good enough to represent the flow field.

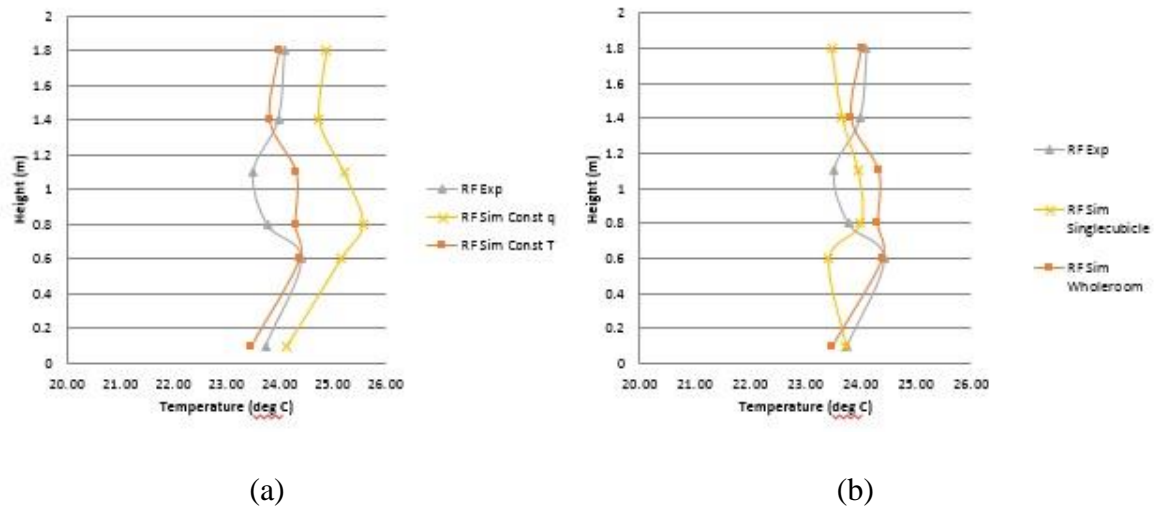


Figure 3-13 Temperature validation along the right front pole (a) of different boundary conditions; (b) of different simulation space

### 3.2.6. PV and UFAD Comparison

Based on the experiment results, an evaluation of thermal comfort based on the equivalent temperature is calculated. Defined by the ASHRAE 62 (1989), “the equivalent temperature is the temperature of an imaginary enclosure with the mean radiant temperature equal to air temperature and still air in which a person has the same heat exchange by convection and radiation as in the actual conditions.” After calibration, the heat transfer coefficients for each part has been obtained. Using Eqn. 3-1, the equivalent temperature for each part can be calculated. The thermal comfort zone given by Nilsson (H O Nilsson 2004) with the

calculated equivalent temperature indicates a thermal comfort evaluation for each part. Overall, PV and UFAD give almost the same thermal comfort level for most parts of the manikin, while for the chest, face, and scalp, PV gives cooler impact on the manikin, and for the right upper arm UFAD gives lower equivalent temperature because a part of the supply air from the UFAD blew through the upper arm (Figure 3-14).

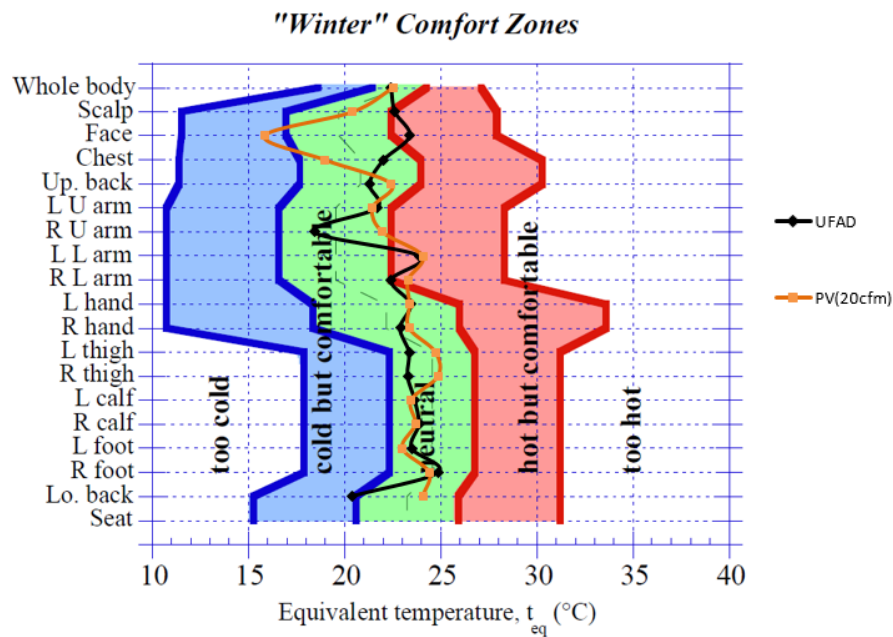


Figure 3-14 Equivalent temperature

The AQI for the air quality is calculated with the software. A better performance was achieved by the PV (Figure 3-15 a). In UFAD case, a uniform profile was created in most space of the cubicle due to the strong mixing performance of the UFAD. In contrast, an obvious PV jet with cleaner air provided a local dilution in the breathing zone. The lowest AQI took place near the floor for both cases but in PV case, another low AQI region showed up below the front desk which is a stagnation region. The AQI in the vicinity of the mouth

and nose which PV can provide (0.483) is about four times of that UFAD can provide (0.115).

As shown in Figure 3-15 (b), cooling effect took place differently in different cases. For the UFAD case, the cooler air was supplied from the floor, some part of the supplied air was obstructed by the chair and front desk. Moreover, then the air spread out and was transported to the region where the manikin was. However, for the PV case, the cooler air was transported to the manikin face directly with a little entrainment which led to the lower equivalent temperature at the head, face and chest level which needs to be cooled the most (Figure 3-15). Some part of the cooler air went around the head and then sank down to the floor level due to the heavier density caused by lower temperature.

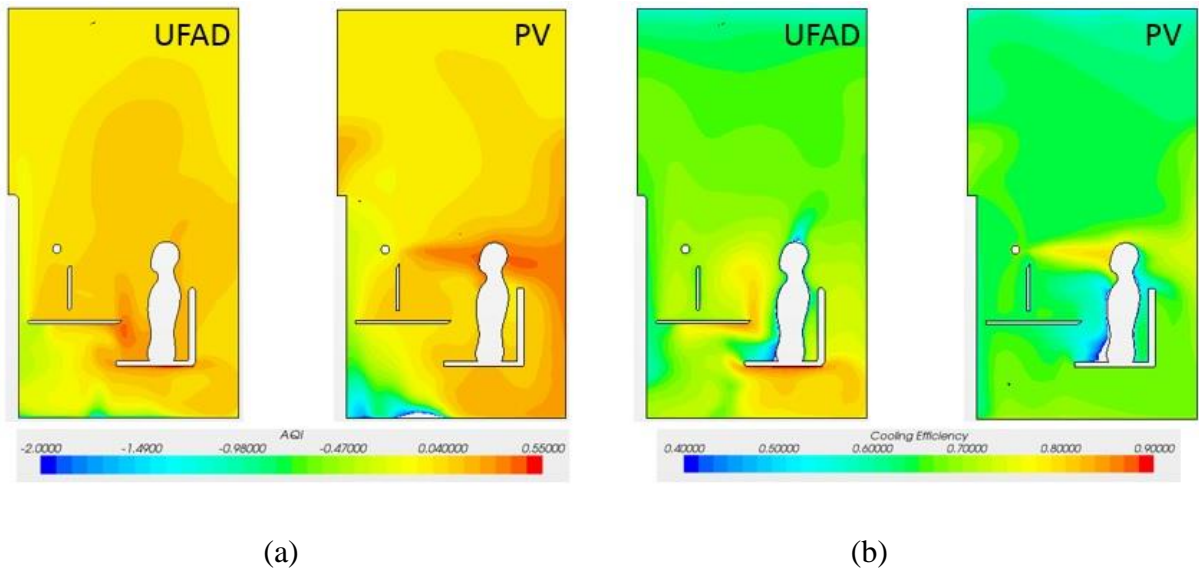


Figure 3-15 AQI (a) and cooling efficiency (b) comparison



### 3.2.7. PV Performance under Different Airflow Rates

In order to investigate the flow field and performance of the PV under different airflow rates. A velocity profile measurement was conducted to give a velocity distribution over the PV outlet. The velocity was measured on a  $12 \times 5 (\times 2)$  grid. Based on the measurement, a boundary condition was created in the STAR-CCM (Figure 3-16). One can see that the largest velocity took place in the central two slots of the PV especially for the large flow rate (7.08 L/s and 9.44 L/s).

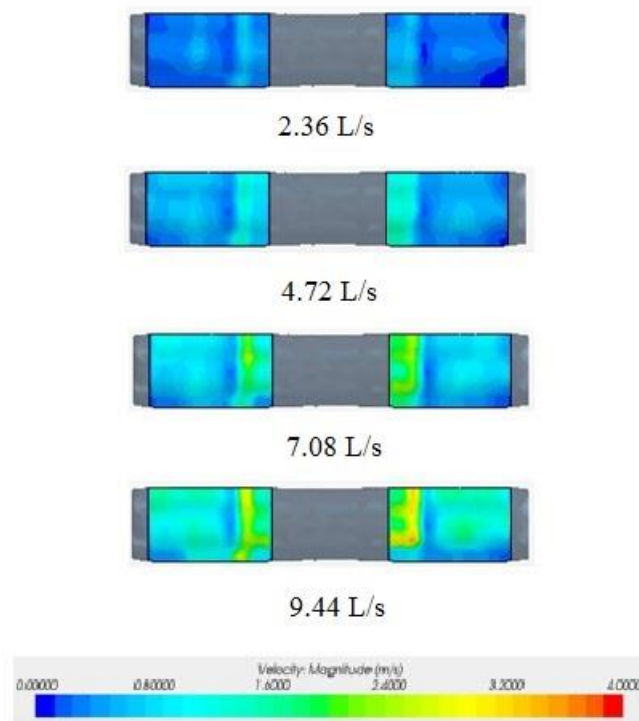


Figure 3-16 PV outlet velocity profile

Under different air flow rates, the same specified surface temperature is given for each case. A clear increasing temperature (22-25 °C) can be seen with decreasing air flow rate in

Figure 3-17. A jet detouring occurred in the case of 2.36 L/s, and 4.72 L/s which is due to a larger density difference and the local cooling region is also changed from head level to stomach. In the case of 7.08 L/s and 9.44 L/s, a remaining jet showed up behind the head of the manikin and spread through the partition of the cubicle, but in the case of 4.72 L/s and 2.36 L/s, the jet is stopped by the manikin and descended to the lower level. The thermal plume at the head level of the manikin has been destroyed by the jet of 4.72, 7.08 and 9.44 L/s, but only the one in the 2.36 L/s case still existed.

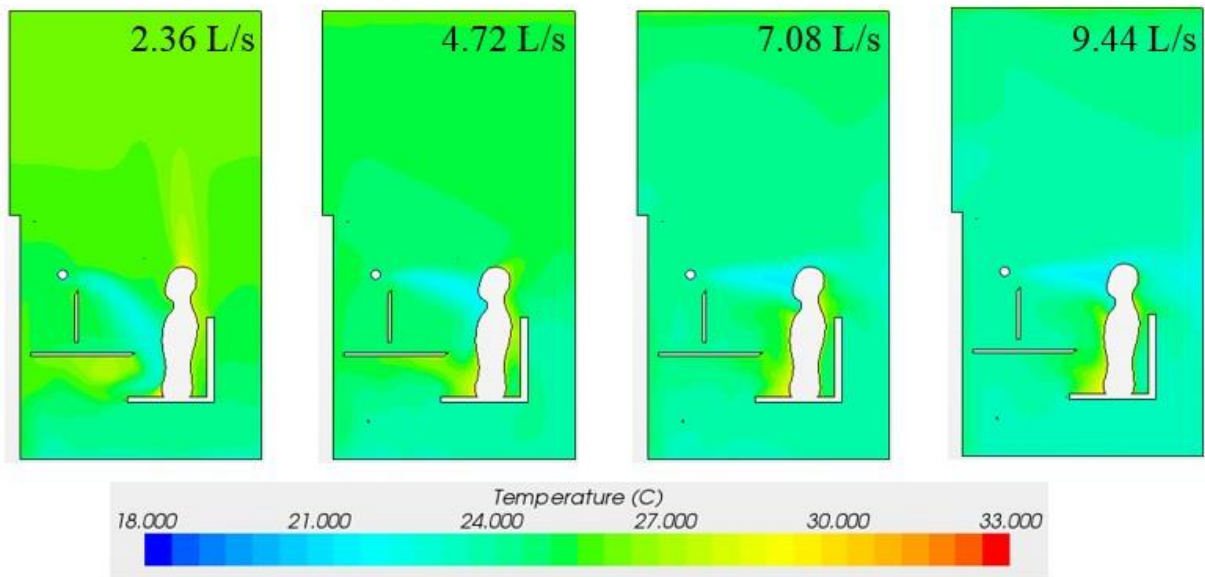


Figure 3-17 Temperature distribution on the manikin symmetry plane

In the view from the back of the manikin (Figure 3-18), our observation was confirmed: a cooler region existed around the manikin head in the cases 7.08 L/s and 9.44 L/s, with a thermal plume going up above the head in the case 2.36 L/s. Moreover, the thermal plumes of the cases 7.08 L/s and 9.44 L/s are stopped from the shoulder level, but the one of 4.72 L/s has been destroyed at a lower level.

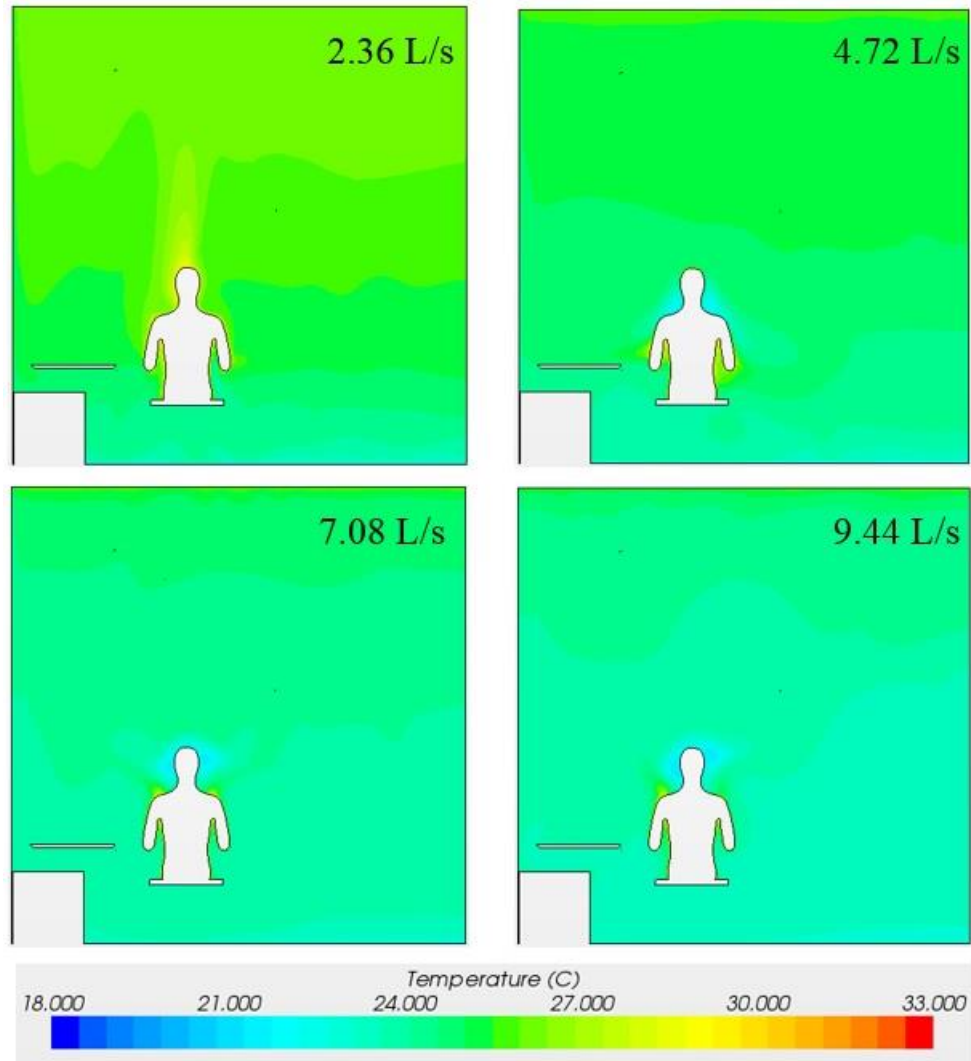


Figure 3-18 Back view of the temperature distribution

From the velocity field (Figure 3-19), a more obvious flow field is indicated. For the cases of 7.08 L/s and 9.44 L/s, the air supplied by the PV went through the head and spread over the back partition, most part dropped to the lower level beneath the chair and was driven back up by the thermal plume. For the cases 4.72 L/s and 2.36 L/s, the jet was prevented by the manikin and flushing to the lower level through the slot between the manikin and

the front desk. Based on ASHRAE standard 55 (2013), in the room temperature of 26 °C, the mean room velocity is suggested to be lower than 0.2 m/s which is not satisfied in the case of 4.72, 7.08 and 9.44 L/s.

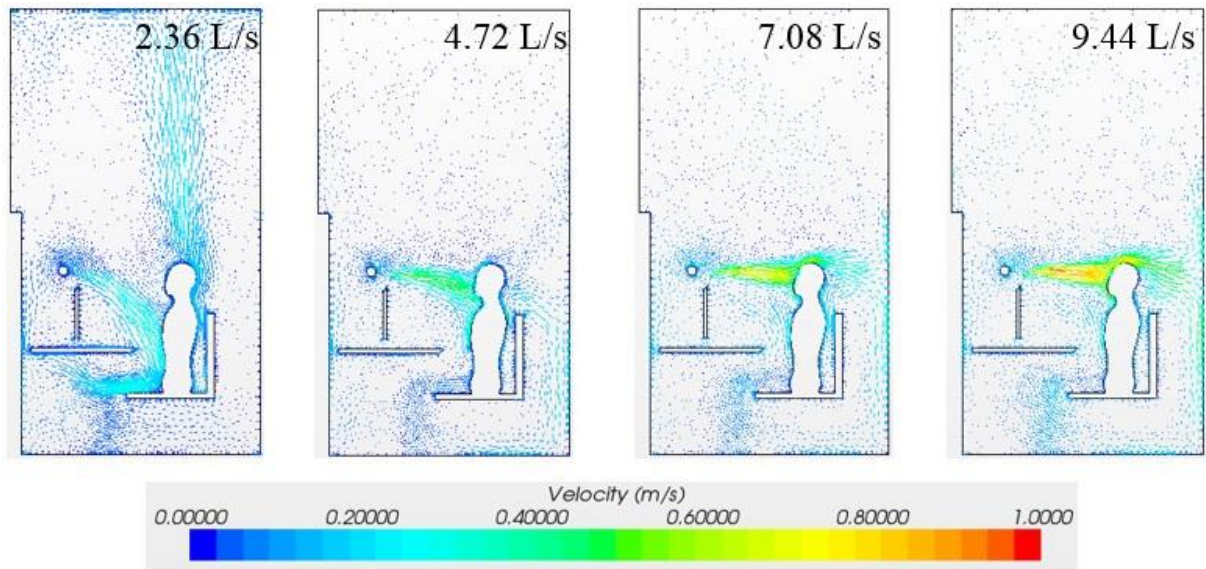


Figure 3-19 Velocity field on the manikin symmetry plane

Air quality is also tested with the tracer gas simulation. SF<sub>6</sub> is emitted from the floor uniformly as the tracer gas at a rate of 1E-6 kg/(m<sup>2</sup>s). After getting to steady state, the mass fraction field at the symmetry plane of the manikin was tested (Figure 3-20). One can easily find that, with the air flow rate increasing, the average mass fraction of the contaminant decreased a lot. The highest fraction always took place near the floor. Moreover, due to the recirculation flow at the lower part, most of the contaminant was pushed to the front partition. The contaminant fraction at the breathing zone in the 2.36 L/s case (0.29%) was much larger than the other three (0.093%, 0.040% and 0.032% for 4.72, 7.08 and 9.44 L/s)

which is resulted from the fact that the jet of 2.36 L/s descended too fast to reach the breathing zone.

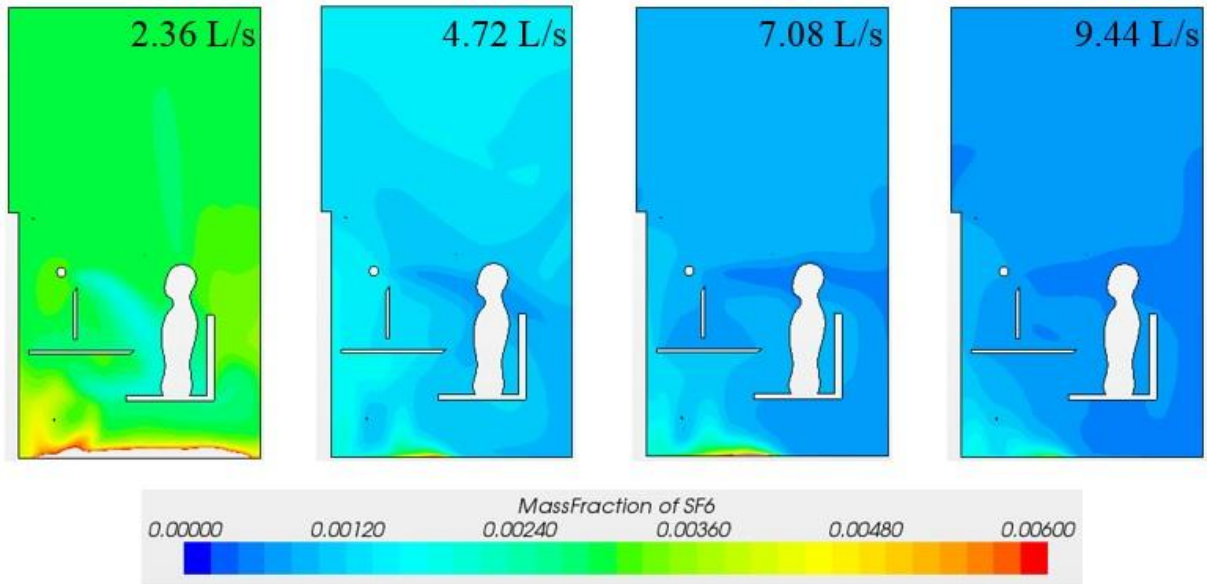


Figure 3-20 Tracer gas mass fraction field at manikin symmetry plane

### 3.3. Summary and Conclusions

This work shows a comparison of three local ventilation systems regarding flow field characteristics, thermal comfort performance and air quality improvement and develops a validated CFD case to help evaluate the detailed performance of two ventilation systems. The measurement results indicate that a better or at least equivalent micro-environment around the manikin, regarding thermal comfort and air quality, will be created by either the PV or CV system with only 1/5 amount of the air provided by the UFAD system. This work also shows that the performance of each system depends on the location of the contaminant source and correlation with the cubicle configuration though how it works is still

ambiguous. A computational mesh with a base grid size of 0.05 m was found to have sufficient grid independence in the simulation results. Based on the comparison between experiment and simulation, the CFD model with the realizable  $k$ - $\epsilon$  turbulence model in combination with the two layer-model for boundary layer over solid surfaces was found to provide satisfactory predictions.

#### **4. Micro-environmental Control for Efficient Local Cooling**

The concept of using the micro-environmental control system ( $\mu X$ ) to save energy has just been raised for several years, and there are still many unanswered questions. The main issues about using the  $\mu X$  include the capability of the  $\mu X$  to restore thermal comfort with affordable energy consumption, the best configurations of the  $\mu X$  under different condition (cooling and heating), and ergonomic and aesthetic concerns. To address these issues, this chapter is focused on developing and validating a CFD model and using it to help investigate the effect of the supply condition on the jet cooling performance and evaluate the performance of three existing Air Terminal Devices (ATDs) which can be implemented in the  $\mu X$  for supplying sufficient cooling.

##### **4.1. Overview**

A  $\mu X$  has been developed under the ARPA-E project (Khalifa and Koz 2016). It consists of a micro-scale vapor compression system, of which the evaporator is embedded in the phase change material (PCM). The compression system is designed to run during the night to freeze the PCM to avoid dumping heat around the occupants as well as reduce the peak electricity rate. A certain amount of cooling is stored in the PCM and released as a cool breeze through a proper air terminal device (ATD) to make the office worker comfortable for up to 10 hours during the day when the office room temperature is increased from 23.9 °C to 26.1 °C (Khalifa 2017). In this way, although an extra portion of energy is consumed by the  $\mu X$  during the night, the total cooling energy consumption is reduced by around 20% based on the in-house simulation results for in 7 different climates in the U.S. based on an unpublished work done by our group.

The computational and experimental domain represented a full-scale office, 4.88 m × 3.66 m × 3.05 m high, with a linear diffuser mixing system (Figure 4-1). A workstation was located in the center of the room. A laptop was placed on the desk, and a  $\mu X$  was put under the desk to provide local cooling to a manikin. The  $\mu X$  was of the size 0.42 m × 0.19 m × 0.48 m, which was about the size of a desktop computer. It sucked the air through the holes on two sides and supplied the air through an ATD. The cooling power,  $P$ , provided by the mockup  $\mu X$  is calculated as

$$P = \rho \cdot \dot{V} \cdot c_p \cdot (T_1 - T_{jet}) \quad (4 - 1)$$

where  $\rho$  is the density of the air (kg/m<sup>3</sup>),  $\dot{V}$  is the supply air volume flow rate (m<sup>3</sup>/s),  $c_p$  is the specific heat of the air (J/(kg·°C)),  $T_1$  is the room air temperature, and  $T_{jet}$  is the supply air jet temperature (°C).

The  $\mu X$  is designed to supply 50 W cooling power during a summer day, different combinations of supply flowrate and supply temperature were tested using CFD model. The operating condition of the  $\mu X$  was selected based on the evaluation of the cooling performance as well as the thermal comfort. Three types of ATDs were investigated (Figure 4-1). Type I was a single-diffuser ATD placed under the desk which has a diffuser area of 13.10 cm × 7.20 cm. Type II was a round-diffuser ATD placed above the desk facing the occupant, and the diffuser had a radius of 5.50 cm. Type III is a split-diffuser ATD placed under the desk, which had two diffusers with an area of 6.05 cm × 7.20 cm each. A manikin with 20 separately heated segments was seated in an office chair in front of the desk to simulate an occupant working in the office.



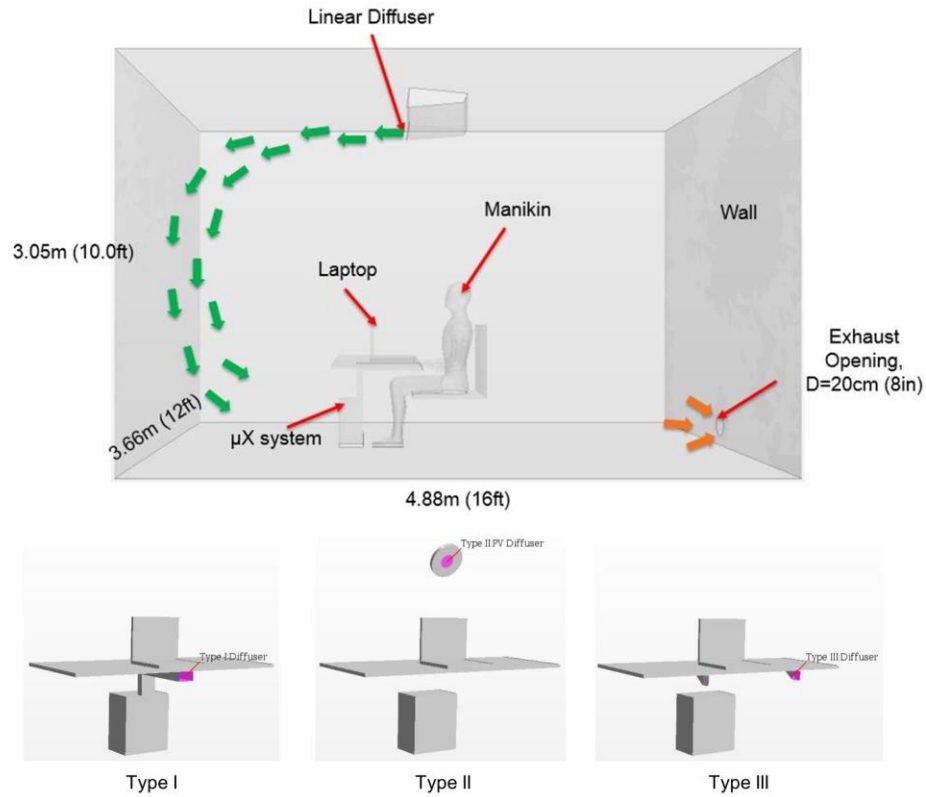


Figure 4-1 Computational domain and three types of ATDs studied

#### 4.1.1. Experimental Facility

Full-scale laboratory testing has been used as a reliable testing method for indoor air quality, thermal management, and associated energy estimation studies (Cao et al. 2015; Kong et al. 2016; Nilsson et al. 2007). The present work utilized a full-scale polished stainless-steel chamber system which the CFD model simulated (Figure 4-2). An HVAC system was used for conditioning the chamber, and the room temperature was controlled by the return air temperature. A linear air diffuser was constructed to provide better-defined boundary conditions for comparison with the CFD simulations. The outlet had the dimensions of  $0.017 \text{ m} \times 0.900 \text{ m}$ . The supply air flow rate was set at  $0.075 \text{ m}^3/\text{s}$  which corresponded to an air change rate of  $5 \text{ h}^{-1}$ . The supply air jet was directed to the wall of

the chamber and then distributed to the rest of the room before it was exhausted. The supply velocity is around 4.9 m/s which is a little higher than the design velocity of 4.1 m/s. However, the main purpose of the linear diffuser is to create a uniformly mixing condition in the occupied space as well as minimize the local draft on the manikin.

In order to ascertain that the environment inside the chamber is fully mixed, three temperature trees using thermistors were placed around the manikin, measuring the temperature at six different heights, 0.10 m, 0.40 m, 0.70 m, 1.00 m, 1.30 m, and 1.50 m. Since it was reported that the thermal plume of the manikin was about 0.20 m thick (Bolashikov et al. 2010; Licina et al. 2014), two temperature trees were placed 0.30 m away from the side of the manikin, and the other one was placed 1.00 m behind the manikin. Ten thermocouples were also used in this study to monitor the surface temperature of the chamber wall (two on the floor, two on the ceiling, two on each side wall and one on each end wall). To ascertain no draft except the  $\mu$ X supply air was perceived by the manikin, air velocity measurement was taken with hot-sphere anemometers on the left of the manikin at the same heights of the temperature measurement. A 20-segment manikin, which was made to represent a 50<sup>th</sup> percentile Western Male body form with a total surface area of 1.8 m<sup>2</sup> and height of 1.80 m, was seated by the desk to simulate a working person. Temperature and heat flux sensors were distributed over each segment of the manikin to monitor or control the surface temperature and heat flux. In this study, the manikin's surface temperatures were controlled at set-points, while allowing the heat flux to vary with the environmental condition. The head, face, and forearms were set to be 33.9 °C to represent exposed skin surface, and the other segments were set to be 31.7 °C which represents

surfaces of light clothing (Dygart et al. 2009; Kong et al. 2015). The heat flux through each segment was monitored and recorded for comparison with the CFD simulation results.

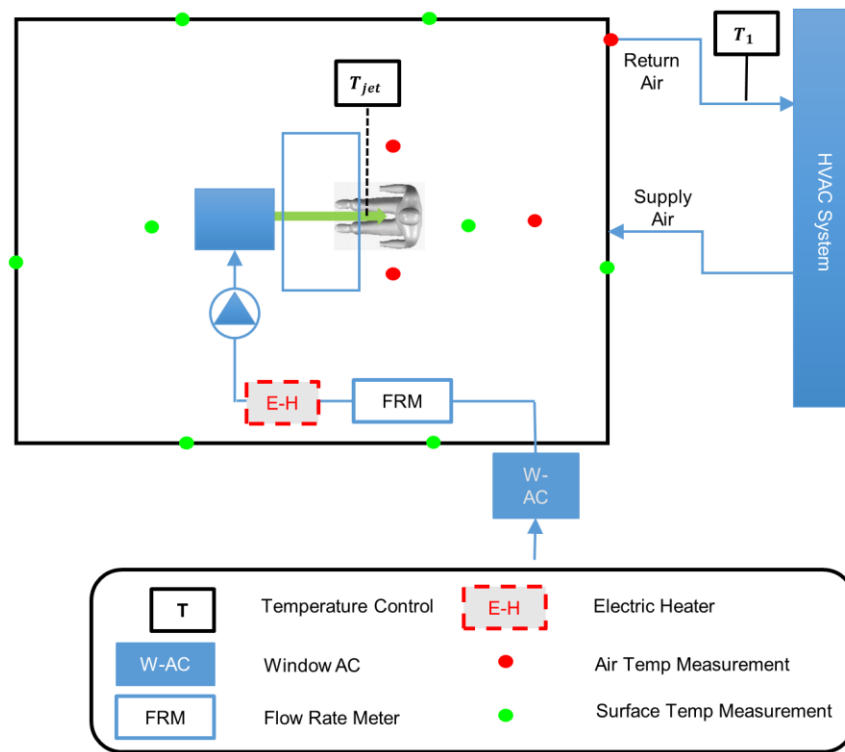


Figure 4-2 Schematic of the test chamber

Inside the chamber, a mockup  $\mu X$  was built. The system consisted of a window air conditioning unit, an orifice flange flow rate meter, an in-duct fan, a plenum box, an electric heater, an air diffuser and connecting ducts between them (Figure 4-2). Different from the real  $\mu X$ , instead of sucking air from its immediate surroundings inside the room, the window air conditioner was placed outside the chamber to supply overcooled air ( $\sim 10^\circ\text{C}$ ) through a hole in the chamber wall in order to minimize the disturbance to the chamber's airflow and prevent the exhaust heat from the window air conditioner from going into the chamber. The overcooled air was reheated to the set-point before it was supplied to the manikin.



Figure 4-3 Experimental Facility

#### 4.1.2. Computational Model

All CFD simulations in this study were performed using a commercial CFD software (STAR-CCM+ 9.04.011). This software utilizes a more user-friendly interface and includes almost every function needed for CFD simulation including creating the geometry, generating the mesh, calculating and post-processing. It has been used more and more in recent years and performed well compared to other software (Peng et al. 2016). The flow field was calculated as incompressible ideal gas based on the standard  $k - \varepsilon$  turbulence model in combination with a two-layer wall treatment model. It enables the turbulent dissipation rate  $\varepsilon$  and turbulent viscosity  $\nu_t$  to be calculated smoothly from the freestream

through the buffer layer to the viscous sub-layer (Kong et al. 2015). All the equations were solved with the SIMPLE algorithm and a second-order accurate scheme. Since the chamber space is symmetric, the computational domain of half of the chamber was first created using the commercial grid-generation software Pointwise and then the grids were regenerated using STAR-CCM+. Polyhedral grids with prism layer mesh were used in this study. A rather fine grid (around 5M cells) was applied around the manikin (Figure 4-4). In order to generate a mesh with good discretization, the surface and volume mesh was generated based on the guideline given by Russo (Russo 2011). The surface cells on the manikin varied from 2.50 mm to 10.00 mm and twenty layers of prism cells were distributed all over the surface in a total thickness of 25.00 mm with a stretching ratio of 1.2. This gave a  $y^+$  value on the surface of the manikin lower than 0.8 which was considered to be sufficiently good. A relatively uniform mesh was applied in the mixing region between the manikin and the diffuser. The length scale of the surface cell of the diffuser was on the order of 2.00 mm.

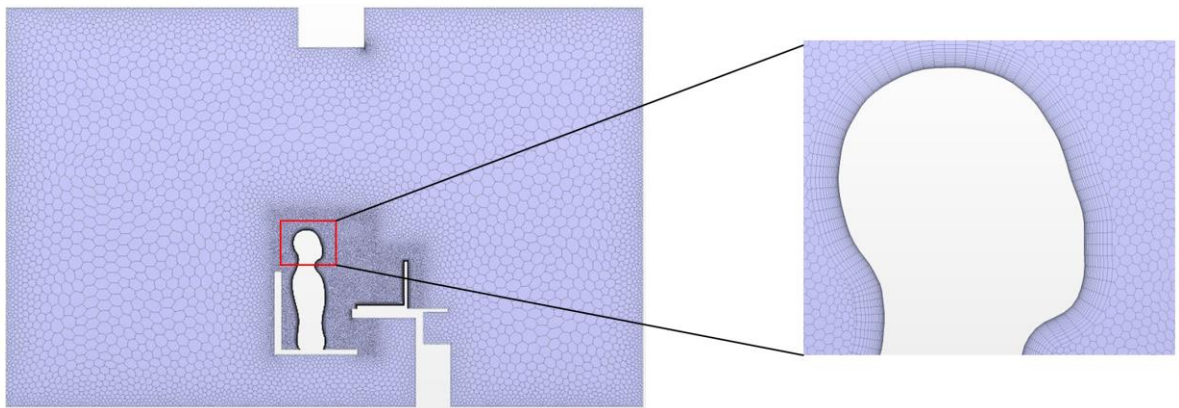


Figure 4-4 Mesh grids of the CFD model

### 4.1.3. Boundary Conditions Used in CFD Simulation

This chapter summarized two parts of this work. The first part was validating the CFD model. In this part of work, CFD simulation results were compared with experimental measurements. Two validation cases were run and compared with experimental data. One was for the manikin sitting in a room of raised temperature (26.1 °C) without the  $\mu$ X (Case I), and the other one was for the manikin sitting in a room of raised temperature (26.1 °C) with the  $\mu$ X (Case II). The boundary conditions of the cases for validation are summarized in Table 4-1.

Table 4-1 Boundary Conditions for Validation

Surface	Boundary Condition Type	Setting
Ceiling	Constant Temperature	25.7 °C for Case I; 25.5 °C for Case II
Floor	Constant Temperature	24.3 °C for Case I; 24.5 °C for Case II
Manikin Head, Face, and Forearm	Constant Temperature	33.9 °C
Remaining Manikin Surface	Constant Temperature	31.7 °C
Linear Diffuser	Velocity Inlet	5 m/s, Turbulence Intensity (T.I.) = 0.1; Turbulent Length Scale = 0.0023 m;

		27.8 °C for Case I; 28.3 °C for Case II
Exhaust Opening	Pressure Outlet	N/A
μX Diffuser (Type I)	Velocity Inlet	Measured Vel. & T.I.; Turbulent Length Scale= 0.0065 m; 23.09 °C for Case II
Laptop	Heat Source	17.0 W
Symmetric Plane	Symmetry Plane	N/A
The Other Surfaces	Adiabatic Wall	N/A

The percentage of radiant heat loss from an occupant is significant, ranging from 50% to 66% (Wang et al. 2014). It is, therefore, important to get an accurate account of the radiant heat loss for predicting the total heat loss. According to the law of radiant heat transfer between gray surfaces, the radiant heat transfer  $\dot{Q}_{1-2}$  between surface 1 and 2 is governed by:

$$\dot{Q}_{1-2} = \frac{\sigma(T_{s1}^4 - T_{s2}^4)}{\frac{1 - \epsilon_1}{\epsilon_1 A_1} + \frac{1}{A_1 F_{1,2}} + \frac{1 - \epsilon_2}{\epsilon_2 A_2}} \quad (4 - 2)$$

where  $\sigma$  is the Stefan-Boltzmann constant ( $5.67 \times 10^{-8} \text{ W}/(\text{m}^2 \cdot \text{K}^4)$ ), and  $T_{s1}$  and  $T_{s2}$  are the absolute temperature of surface 1 and 2 (K),  $\epsilon_1$  and  $\epsilon_2$  are the emissivity of surface 1 and 2,  $A_1$  and  $A_2$  are the area of surface 1 and 2 ( $\text{m}^2$ ), and  $F_{1,2}$  is the view factor from surface 1 to 2. Therefore, the emissivity and temperature of all the surfaces have to be determined

ahead of the simulation. In this study, the emissivity of the manikin surface was given by the manufacturer as 0.92, and the emissivity of the surrounding chamber wall was assumed to be 0.27 (polished stainless steel, obtained from the material specification). The surface temperature used in the simulation was obtained from experimental measurements.

The inlet velocity (Figure 4-5) of the  $\mu$ X diffuser was set in the computational model to match the experimental setup. A total air flow rate of  $0.014 \text{ m}^3/\text{s}$  was used in the simulation with a maximum velocity of  $2.2 \text{ m/s}$ . Values for turbulent intensity varied in the experiment from 5.0 % to 15.0 %. A value of 10.0 % was used in the simulation throughout for simplification.



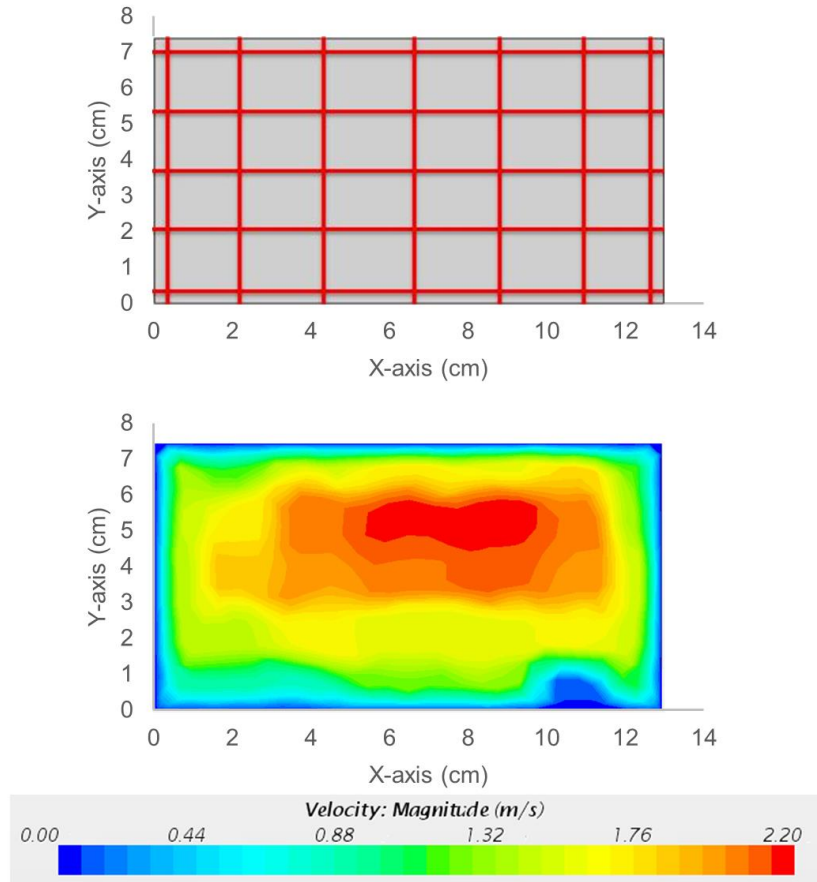


Figure 4-5 Velocity traverse grid and profile of the diffuser (Type I)

The second part of this work is evaluating the performance of different ATDs in cooling the manikin. The CFD cases simulated the scenario that the office room was kept at 26.1 °C, i.e., 2.2 °C higher than the normal set-point for cooling. Room supply air of certain temperature was provided to the chamber to make the exhaust air temperature to be 26.1 °C. In this study, for the case without  $\mu X$ , the supply temperature was kept at 25.4 °C, and for the case with the  $\mu X$ , the supply temperature was kept at 26.0 °C. Also, since for a conditioned building the wall temperature (mostly internal walls) should be close to room temperature according to the heat balance, it is reasonable to apply 26.1 °C as the wall surface temperature. The  $\mu X$  was designed to supply constant 50.0 W cooling power during

the day in the summer. Different combinations of supply air temperatures and flow rates reflecting the 50 W cooling power according to Eqn. 4-1 were tested first and then the best combination was selected based on cooling performance and thermal comfort.

#### **4.1.4. Determination of the Convective Heat Transfer Coefficient**

This study calculated the natural convective heat transfer coefficient of each segment of a seated manikin using the results of the CFD simulations. The total heat flux of each segment  $\dot{q}_t$  consists of radiant heat flux  $\dot{q}_r$  and convective heat flux  $\dot{q}_c$ . And the convective heat flux equals to the product of the convective heat transfer coefficient  $h$  and temperature difference between the surface  $T_0$  and room air  $T_1$ .

$$\dot{q}_t = \dot{q}_r + \dot{q}_c = \dot{q}_r + h \cdot (T_0 - T_1) \quad (4 - 3)$$

The convective heat transfer coefficient obtained in this study was compared with some previous studies (de Dear et al. 1997; Sørensen and Voigt 2003; Yang et al. 2009). de Dear et al. (1997) used a purely experimental approach which measured the total sensible heat flux with a thermal manikin and isolated the convective part from it by covering the manikin with the low-emissivity material. The accuracy of this method depended on the measurement accuracy, including temperature and heat flux measurements. Yang et al. (2009) used a hybrid method, with which they measured the total sensible heat flux using a thermal manikin and subtracted the radiant heat flux obtained from numerical simulation to get the convective heat flux. The accuracy of this method also depended on the accuracy of the measurement since obtaining the radiant heat flux by numerical simulation also required accurate surface temperature measurement. Sørensen and Voigt (2003), as well as the current work, used CFD models to calculate the convective heat flux by solving a

series of fluid mechanics equations. The accuracy of this method depended on the use of the turbulence model and grid quality.

#### 4.1.5. Heat Removal Performance and Thermal Comfort

To raise the room air set-point from 23.9 °C to 26.1 °C, the  $\mu X$  is needed to manage the local thermal envelop so as to not sacrifice thermal comfort. Since from Fanger's work, most of the thermal comfort models evaluated the thermal comfort based on the heat balance, in this current chapter the approach used for evaluating whether the  $\mu X$  can restore thermal comfort is according to the thermal balance analysis. A person sitting in an office is assumed to generate a total of 115 W (seated, very light work in offices), which is equal to the amount of heat that needs to be released to the surrounding environment to achieve thermal balance for the occupant. Among the 115 W, 70 W is considered to be sensible heat loss (convective and radiant) and 45 W is considered to be latent heat loss (evaporative and respiratory) (ASHRAE 2013b). This study only focused on the sensible part. The heat flow rate from the human body  $q''$  under steady state can be expressed as:

$$q'' = A \cdot (1/R) \cdot (T_0 - T_1) \quad (4 - 4)$$

Where  $A$  is the body surface area ( $m^2 / ft^2$ ),  $T_0$  is the averaged human surface temperature (°C),  $T_1$  is the ambient temperature (assuming the mean radiant temperature equals to the air temperature, °C) and  $R$  is the total sensible thermal resistance ( $m^2 \cdot K/W$ ). If the thermal resistance does not change when  $T_1$  changes to the raised set-point  $T_2$ , the change in heat flow rate  $\Delta q''$  is:

$$\Delta q'' = A \cdot (1/R) \cdot (T_2 - T_1) \quad (4 - 5)$$

Divide Eqn. 2 by Eqn. 1,

$$\Delta q'' = q \cdot (T_2 - T_1) / (T_0 - T_1) \quad (4 - 6)$$

Assuming that the surface temperature at a comfortable state is around 33.9 °C (Cheng et al. 2012) for exposed parts (head and forearm) and 31.7 °C for clothed parts (Dygert et al. 2009; Houdas and Ring 1982; Kong et al. 2015) which gives an averaged surface temperature around 32.0 °C (Russo et al. 2009), when the ambient temperature changes from 23.9 °C to 26.1 °C, a difference of 19.2 W needs to be removed by the  $\mu$ X.

The objective of this chapter is to develop and validate a CFD model, and use it to help investigate the effect of the supply condition on the jet cooling performance and evaluate the performance of three existing ATDs which can be implemented in the  $\mu$ X for supplying sufficient cooling to remove a minimum of 19.2 W to restore an occupant's thermal balance when the ambient room air is raised by 2.2 °C.

## **4.2. Results and Discussion**

### **4.2.1. Validation**

As mentioned earlier, the validation work included two cases, with and without the  $\mu X$ . Case I dealt with the flow field without the  $\mu X$ , in which the natural convection dominated the heat exchange between the manikin and ambiance. Case II focused on the flow field with the  $\mu X$ , in which both the natural and forced convection played important roles.

The total heat loss from the manikin as well as the averaged heat flux of each segment was recorded and compared with the CFD results. For the case without the  $\mu X$ , the total heat loss predicted by CFD was 74.4 W. Compared to the total heat loss by experiment 74.0 W, the error was about 0.5 %. The heat flux distribution over the 20 segments also agreed well with the measured data (Figure 4-6). For the case with the  $\mu X$ , the CFD simulation gave a total heat loss of 108.3 W. Compared to the total measured heat loss of 115.1 W, the error was around 5.9 %. These errors are smaller than those found in previous studies (Martinho et al. 2008). The heat flux distribution gave a more detailed description of the source of the error. A significant discrepancy was observed for the stomach as well as the back part of the manikin, which the air was blowing onto. One explanation would be that the CFD model under-predicted the forced convective heat transfer from the manikin. Another explanation was that the manikin did not maintain the same surface temperature as in the simulation. According to the description of the manufacturer, the manikin surface temperature of each segment was controlled by a distributed sensor wire and a distributed heating wire. Even though they claimed that the temperature distribution over each segment was very uniform, an obvious non-uniformity of temperature was still observed because it is not possible to

control the surface temperature everywhere. This non-uniform surface temperature distribution was different with the boundary condition used in the CFD case, and therefore, was very likely to result in the difference in heat flux prediction. More discussion is included in Section 4.2.6. Nonetheless, the difference between the predicted and measured heat fluxes are relatively small and is considered to be acceptable to evaluate different ATDs.

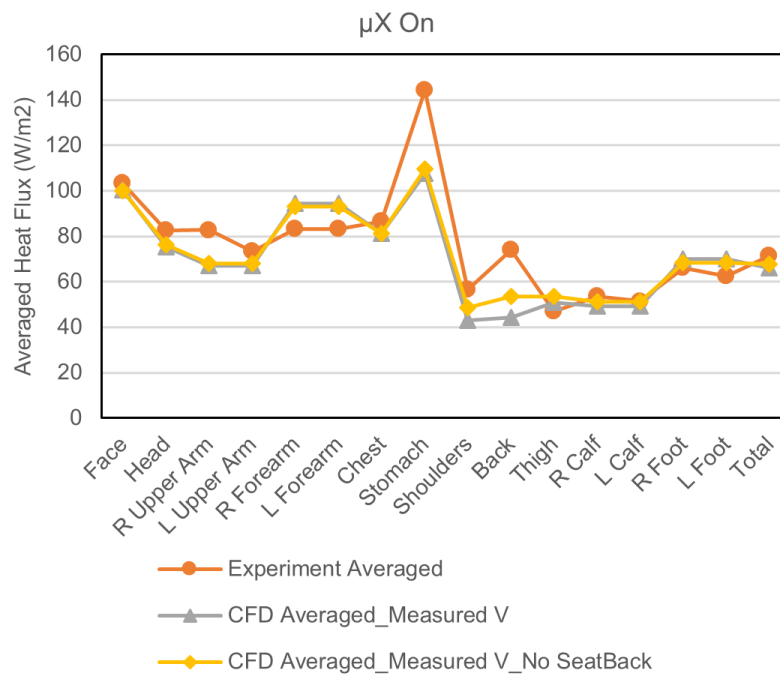
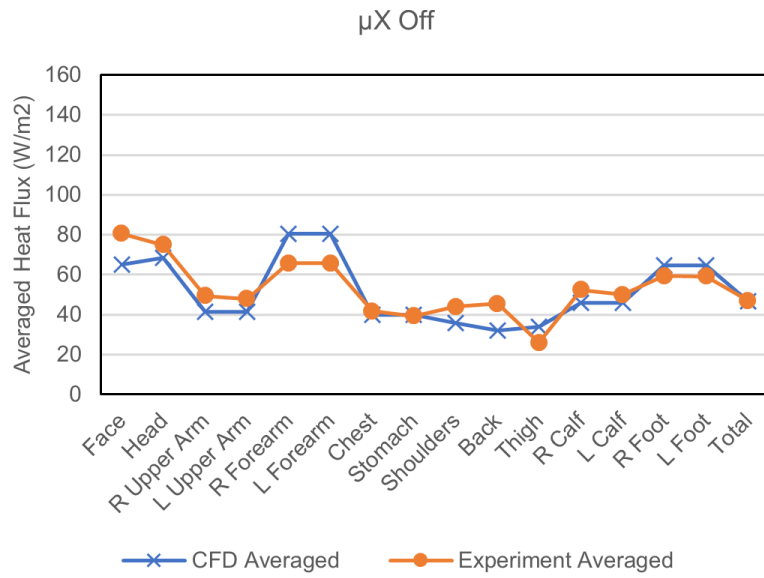


Figure 4-6 Comparison between CFD and experimental results

#### **4.2.2. Convective Heat Transfer Coefficient of Different Body Segments**

The current work calculated the convective heat transfer coefficient of each segment of a seated manikin. Different from the work done by other researchers, this work was the only one using a manikin representing an adult male instead of a female. Figure 4-7 shows the comparison between the results of this study and their results. The comparatively better agreement was observed for the chest, back, thigh, pelvic, and foot while larger variances were obtained for the head, arm, and calf. This difference partially results from the different shape of the manikin. The difference in height, surface area and shape could change the development of the thermal boundary layer and thus the convective heat transfer coefficient. However, considering the difference between three previous studies, this reason may not be the primary one. A more convincing explanation could be that the ways used to calculate the convective heat flux were different in these works. As mentioned in Sec. 4.1.4, three methods were utilized in these works including the current work. Among these three methods, de Dear et al. (de Dear et al. 1997) using the pure experiment seems to be the most reliable method assuming all the measurements were accurate enough because the other two methods involved numerical errors which were hard to quantify.



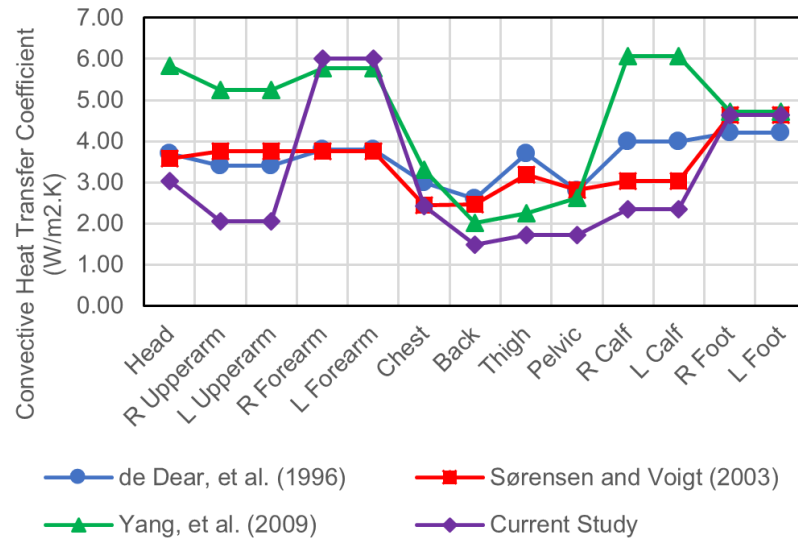


Figure 4-7 Convective heat transfer coefficient of different segments of the human body

#### 4.2.3. Determination of Suitable Air Supply Temperature and Flow Rates

Localized cooling provided by the  $\mu X$  sometimes can cause insufficient cooling or local discomfort if the supply condition, such as the target area, supply velocity, supply temperature, is not controlled properly. Since the  $\mu X$  is designed to give 50.0 W of cooling during the work hours in the summer, several combinations of supply air temperature and flow rates (Table 4-2) were tested using the validated CFD model. The ambient air and surface temperature were kept at 26.1 °C, and the manikin was placed 0.20 m away from the desk. A rectangular air diffuser (13.1 cm  $\times$  7.2 cm) was mounted under the desk aiming at the stomach of the manikin. The manikin surface was set as a constant temperature boundary which had a temperature of 33.9 °C on the head and 31.7 °C on the remaining surface. The total heat loss of each case with the  $\mu X$  was subtracted by the total heat loss without the  $\mu X$  to give the extra heat removed by the air jet.

#### 4.2.3.1. Cooling Ability

Table 4-2 shows the relationship between the extra heat removed by the air jet and the supply air flow rates as well as supply air temperature. While the flow rate ranged from 0.008-0.038 m<sup>3</sup>/s, the extra heat removed by the jet varied linearly with it even though the supply temperature was reduced. It is because when the flow rate increased, the velocity of the air blowing onto the manikin was also increased, resulting in an increase in the convective heat transfer coefficient.

Table 4-2 Cooling ability of different combinations of supply temperature and flow rates

Case	A	B	C	D	E
Supply Temperature	21 °C	22 °C	23 °C	24 °C	25 °C
Flow Rate	0.008 m <sup>3</sup> /s	0.010 m <sup>3</sup> /s	0.014 m <sup>3</sup> /s	0.020 m <sup>3</sup> /s	0.038 m <sup>3</sup> /s
Extra Heat Removed (W)	22.5	25.8	33.5	44.9	78.1

#### 4.2.3.2. Thermal Comfort

According to the tested result, all the combinations could fulfill the requirement of removing 19.2 W extra heat from the manikin, but the further concern should be paid to the comfort. ASHRAE standard 55 suggests a method of using operative temperature to determine the limits of local air speed. “Operative temperature is the uniform temperature of an imaginary black enclosure and air within it in which an occupant would exchange the

same amount of heat by radiation plus convection as in the actual non-uniform environment.” It is determined based on the local air temperature and mean radiant temperature (ASHRAE 2013c). In this study, the local operative temperature and air speed were collected along a vertical line 1.00 cm away from the manikin. Figure 4-8 shows the simulation obtained operative temperature and air velocity in front of the manikin. The region enclosed by the solid (red) lines represents the acceptable conditions for thermal comfort (ASHRAE 2013c). The measured velocities for Cases A and B were lower than the upper limit (1.2 m/s) while Case D and E were much higher. Case C showed a maximum velocity approximating to the limit. Moreover, because it is reported that supply air from a personalized ventilation system should have a temperature ranging from 23.0 to 26.0 °C to avoid significant discomfort to occupants (Melikov 2004), the selected combination used in the following study was Case C.

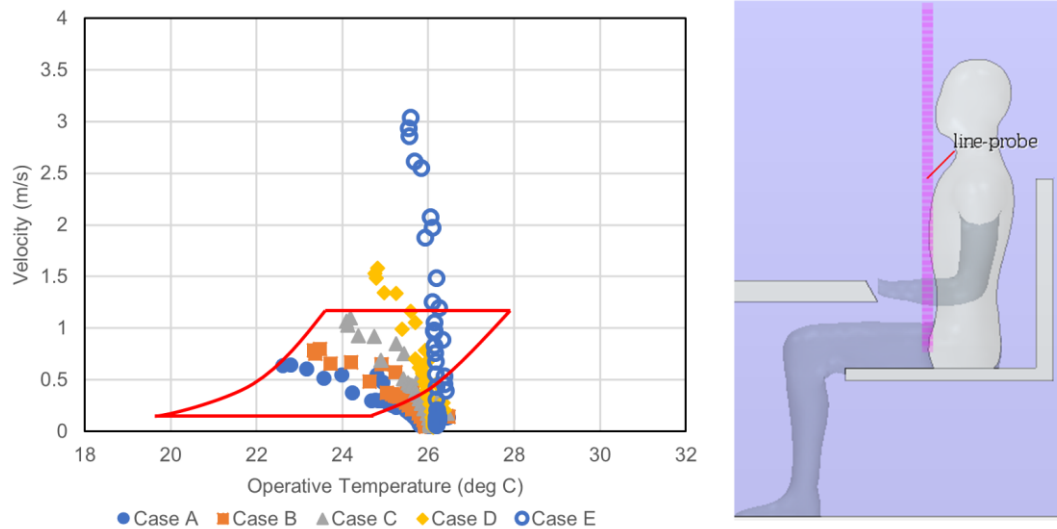


Figure 4-8 Local operative temperature and air velocity

#### **4.2.4. Evaluation of ATDs**

Once the supply condition is determined, the next challenge would be how to manage the air flow properly. A good ATD is supposed to have excellent performance on thermal comfort, perceived air quality, and ergonomics (Kaczmarczyk et al. 2006). Many kinds of ATDs have been designed and studied by other researchers, for example, desk mounted ATDs (Melikov et al. 2002), seat embedded ATDs (Kong et al. 2014, Nielsen, et al. 2007), pillow ATDs (Nielsen et al. 2008), etc.. In this study, three types of desk mounted ATDs were selected and tested using the validated CFD model (Figure 4-1).

In the current section, the CFD model had the same configuration as used in the validation work. The computational domain represented a workstation for one office worker. The room's background temperature was maintained at 26.1 °C with an air exchange rate of 5 h<sup>-1</sup> and the supply condition of the  $\mu$ X is 0.014 m<sup>3</sup>/s and 23.0 °C. It was assumed that the office worker could move by the desk in a semicircle with a radius of 0.61 m. The direction of the supply air could be adjusted for all the three ATDs.

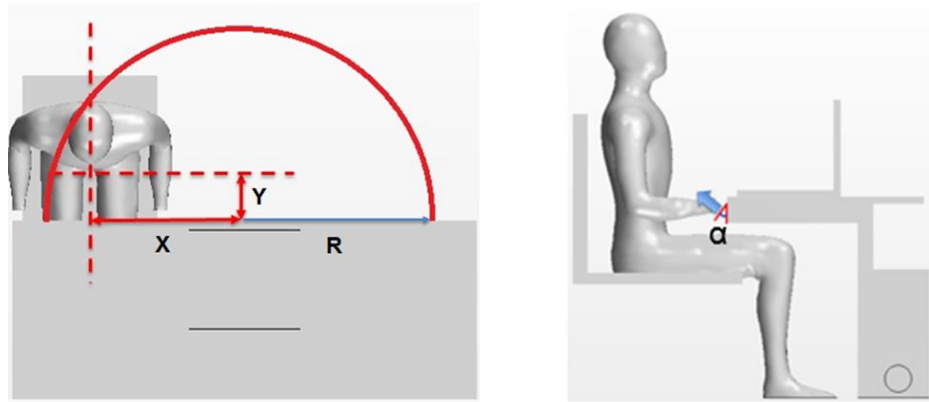


Figure 4-9 Movement range of the occupant (left) and the shooting angle of the ATDs  
(right)

The performance of the three ATDs was evaluated while the manikin was located within the movement range and the jet was shooting at different angles. Figure 4-10 illustrates the cooling performance of the Type I ATD while the manikin was sitting along the center line. Six different angles, 0°, 5°, 10°, 20°, 30°, and 40° were tested. The optimal angle for cooling always lay between 0° and 10° regardless of the distance from the diffuser (Y). The most extra heat removed by the  $\mu X$  while the manikin was sitting 0.20m, 0.45m, and 0.61m away from the desk was respectively 33.6 W, 32.4 W, and 30.3 W. When the manikin was sitting very close to the desk (0.20 m), the jet from the diffuser could work in a rather broad angle ( $> 40^\circ$ ). Even when the manikin was sitting at the edge of the semi-circular movement range, within 23°, the  $\mu X$  would still work.

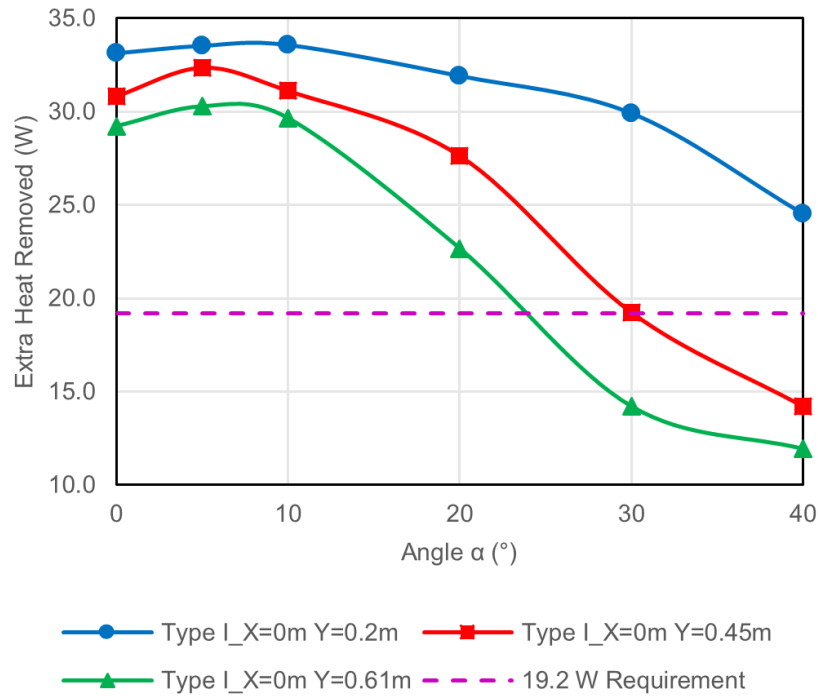


Figure 4-10 Cooling performance of Type I ATD shooting at different angles with the manikin sitting along the center line

Based on the results shown in Figure 4-10, the performance of the ATD was highly dependent on the target region which the jet blew onto. For those three locations, the target region of the jet moved upwards when the angle increased. Within 10° the jet was always blowing to the stomach region. When the angle was increased to larger than 10°, the jet started to blow onto the chest, and the heat loss started to decrease. This is mainly because when the angle increased, the jet blew on a smaller part of the body and some part of the jet even could not touch the body when the angle is too large. The extra heat removed by the jet was still higher than 19.2 W until the target zone moved to the upper part of the chest (30° for Y=0.45 m and Y=0.61 m, Figure 4-11). After that, some part of the jet missed the human body and detoured around to the back of it.

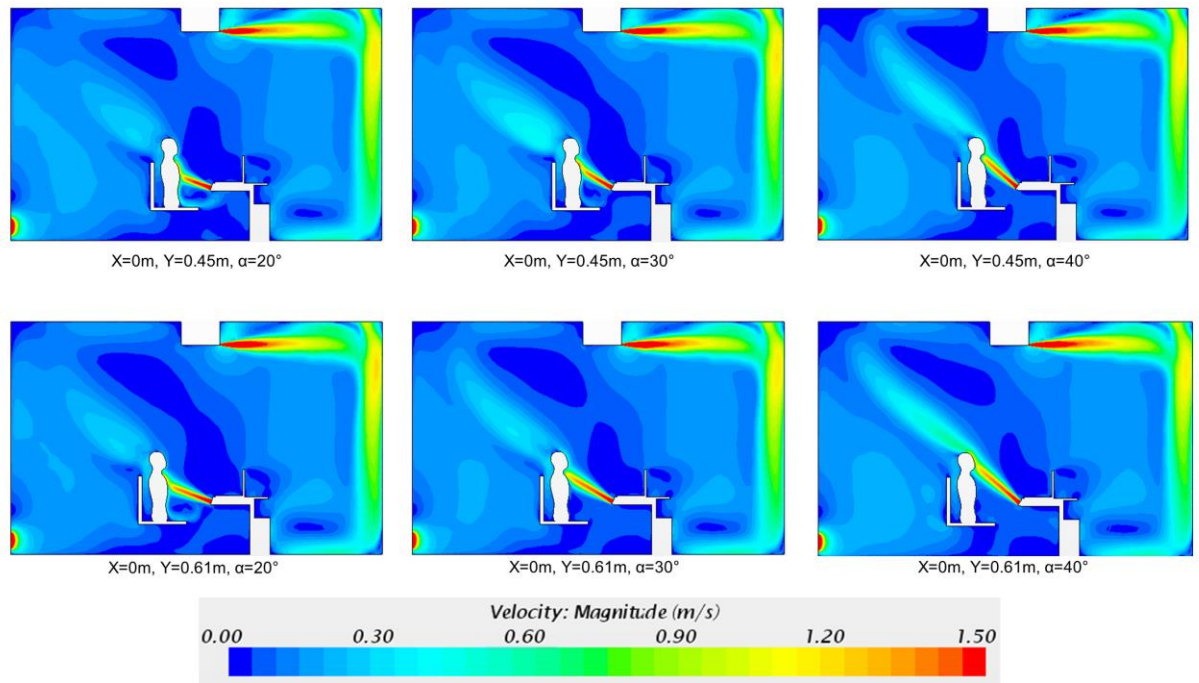


Figure 4-11 Velocity field at the symmetric plane of the manikin when it sits 0.45m and 0.61m away from the desk

When the manikin was placed to one side, the jet had to be adjusted horizontally also. According to the previous results, the jet was always aimed at the stomach region to ensure the best cooling performance. The results were shown in Figure 4-12. The bold red figures indicated the best cooling performance of the jet shooting at the optimal angle at each location. For example, for Type I ATD, when the manikin was put 0.45 m away from the manikin, the column of data shown by the side of the black star of 0.45 m indicates the extra heat removed by the jet when the shooting angle was respectively 0°, 5°, 10°, 20°, 30°, and 40° from the bottom to the top. The highest extra heat removed was obtained when the manikin sat in the 10-o'clock direction of the diffuser (30° angle).

Similar studies have been done for the other two ATDs (Figure 4-12). For Type II and Type III ATDs, only the results of the jet shooting at the stomach were shown in the figure. It turns out that all three ATDs could fulfill the requirement to remove 19.2 W from the manikin. The worst scenario always appeared at the edge of the movement range. Among the three ATDs, Type I ATD worked the best in terms of the extra heat removed.



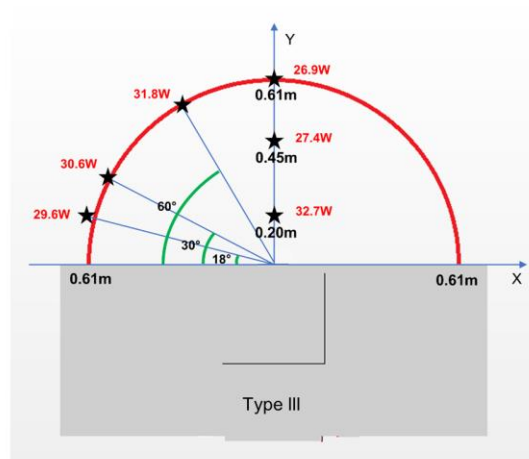
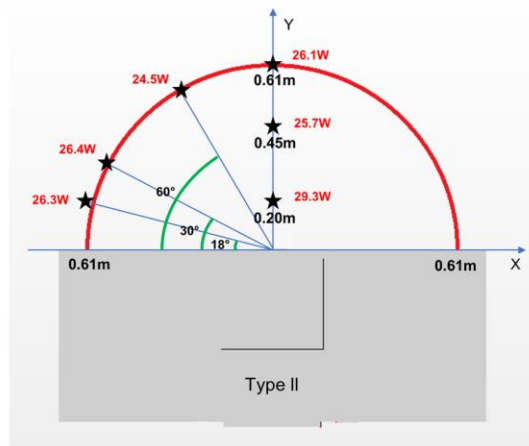
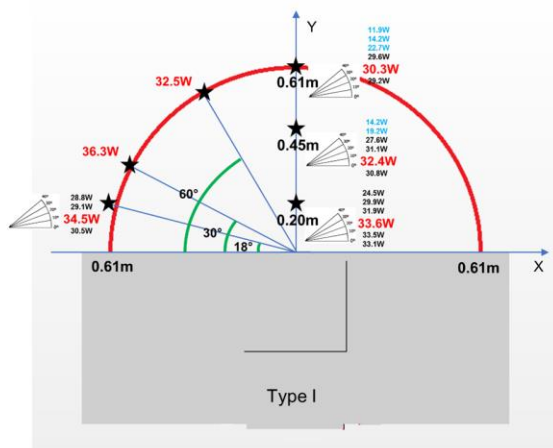


Figure 4-12 Summary of the cooling performance of the three ATDs

#### 4.2.5. Effect of Furniture

As mentioned by previous researchers (Dygert et al. 2009), the presence of the furniture can influence the interaction between the thermal plume and the jet, resulting in a discrepancy in the performance of the jet. For example, the seat on which the manikin sat can prevent the thermal plume around the legs from rising up, leading to a weaker thermal plume around the upper part of the body. In this study, the effect of the seat backrest was evaluated. In the experiment, the manikin was sitting in a chair with a perforated backrest. Different from having a solid backrest, in this case, the jet was able to penetrate the backrest. So a case without a backrest was run and compared with the case with a solid backrest. The yellow line in Figure 4-6 shows the averaged heat flux of each segment in the case without the backrest, and the gray line shows the averaged heat flux of each segment in the case with a solid backrest. The comparison indicates a difference in the heat flux ( $\sim 10 \text{ W/m}^2$ ) from the back. Figure 4-13 shows the velocity field behind the manikin, and it is believed that with the solid backrest, the air which came to the back of the manikin was split into two portions. One was transported away from the manikin, and the other one was converged to the center of the back. However, without the solid backrest, most of the air was converged to the region behind the back and took more heat from the back. Therefore, the solid backrest provided some “insulation” to the people, especially when the people were laid back. This “insulation” protects the people from being cold in cold environment but may exacerbate the discomfort in a hot environment. In addition to the backrest, it is noted that factors such as chair handles, clothing, and hair, can also influence

the heat transfer by changing the surface temperature, creating obstacles for the thermal plume and even changing the shape of the manikin.

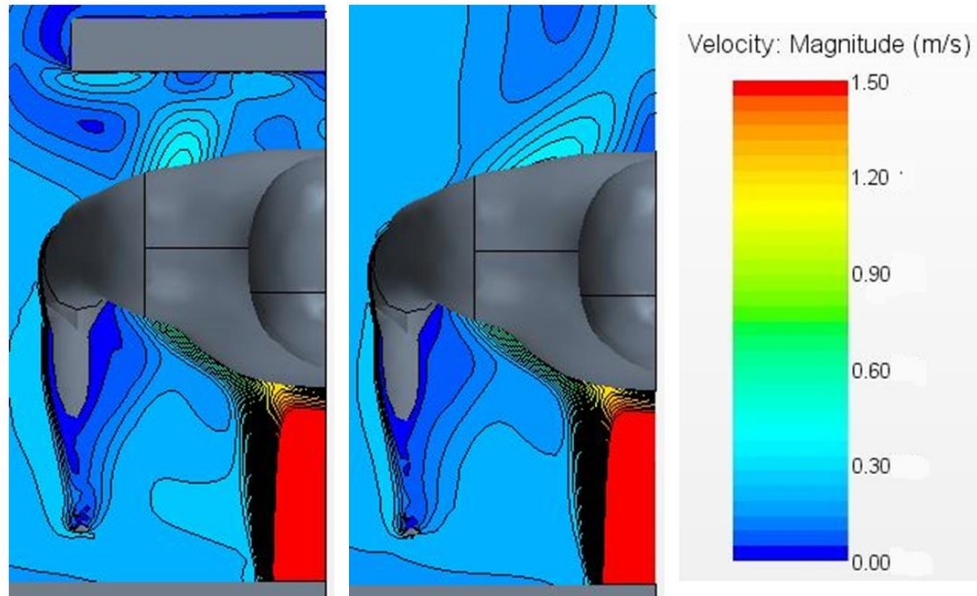


Figure 4-13 Velocity field behind the manikin

#### 4.2.6. Effect of the Surface Temperature

As mentioned in Section 4.2.1, in addition to the turbulence-model effect as noted by previous work (Martinho et al. 2008), the discrepancy between the experimental and CFD results was possibly because of the non-uniform temperature distribution on the manikin surface. The CFD simulation used constant surface temperature on the manikin skin. To properly validate the CFD model, the experiment should have had the same setting as the CFD simulation. However, creating an absolutely uniform surface temperature on a manikin in the experiment is almost impossible, since it is impractical to monitor and control the temperature of every point of the manikin's surface. The manufacturer states

that “every segment of the manikin has one distributed sensor wire, zig-zagging the entire area of the segment. The accuracy of measurement and control of the temperature is  $\pm 0.1$  °C”. However, much larger differences have been found during the experiment. In order to show that, a thermocouple was used to measure the surface temperature of the manikin during the experiment (Figure 4-14).

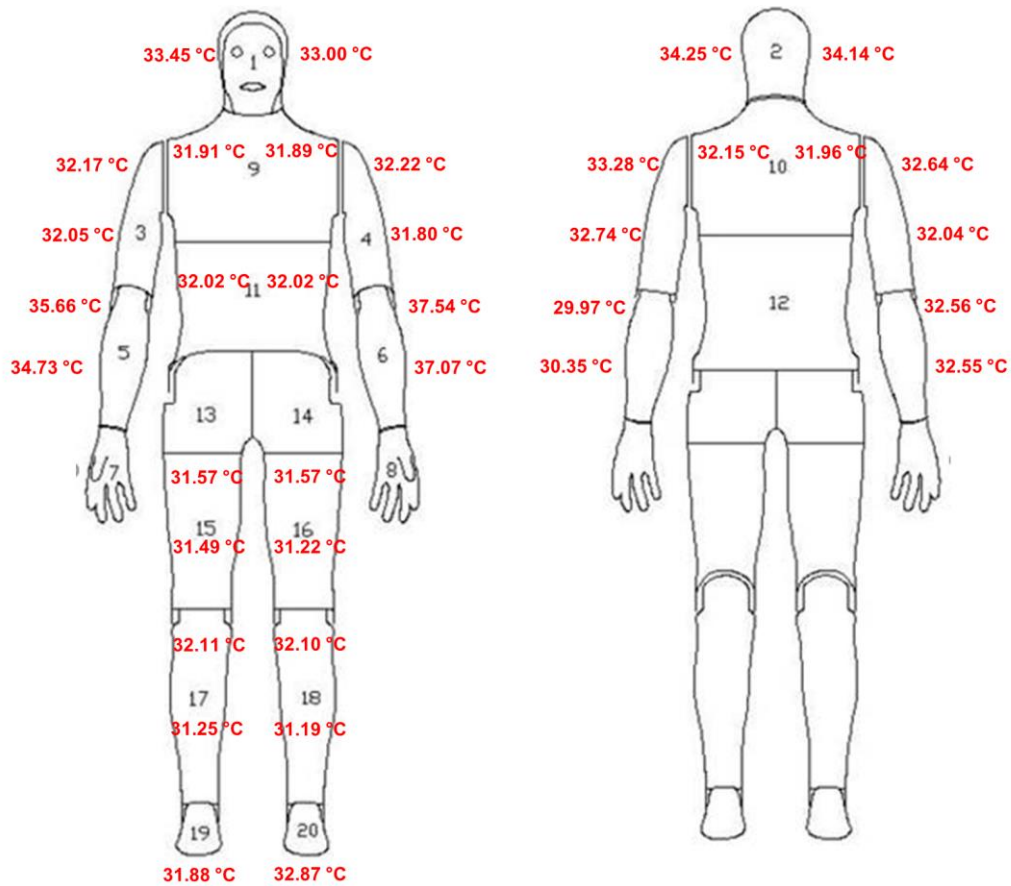


Figure 4-14 Surface temperature measurement on the manikin

The surface temperature within one segment was found to vary quite a bit. The smallest one was found on the stomach, while the largest one was found on the left forearm. Since only very limited numbers of points were measured for each segment, it may not be able to represent the true variance, but it still proved that the surface temperature was non-uniform.

A clearer surface temperature distribution on the manikin could be seen by using a thermal camera (Figure 4-15). The non-uniform surface temperature distribution was confirmed, and at least a 1.0 °C surface temperature difference was found on almost all the segments. Each segment always had a higher temperature in the central part and lower temperature at the edge.

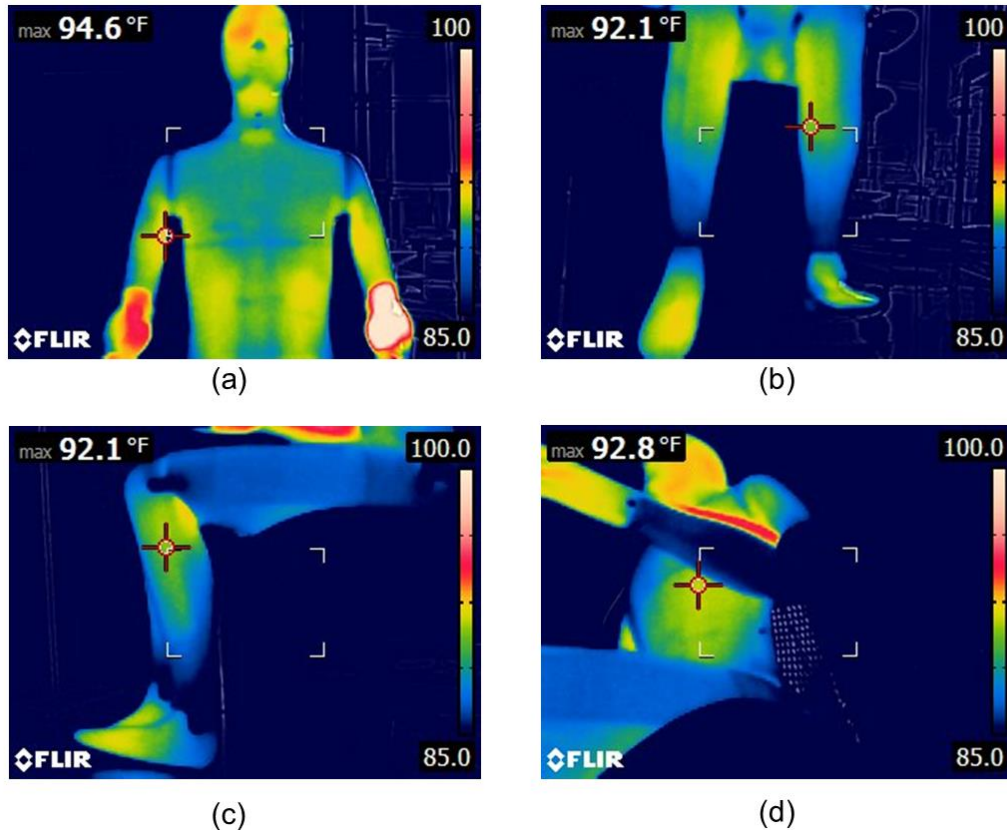


Figure 4-15 Surface temperature distribution on the manikin

The difference between the measured surface temperature and temperature set-point has also been observed (Figure 4-14, Figure 4-15). Average values of the measured surface temperature were used to represent the temperature for each segment. More segments were experiencing a higher temperature than the set-point (Table 4-3).

Table 4-3 Comparison between set-point temperature and measured temperature

	Set-point Temp., °C	Measured Temp., °C	Temp. Difference, °C
Face	33.9	33.2	-0.7
Head	33.9	34.2	0.3
Shoulder	31.7	32.1	0.4
Chest	31.7	31.9	0.2
Back	31.7	32.1	0.4
Stomach	31.7	32.0	0.3
Right Upperarm	31.7	32.2	0.5
Left Upperarm	31.7	32.5	0.8
Right Forearm	33.9	33.9	0.0
Left Forearm	33.9	33.7	-0.2
Right Thigh	31.7	31.5	-0.2
Left Thigh	31.7	31.5	-0.2
Right Calf	31.7	31.7	0.0
Left Calf	31.7	31.7	0.0
Right Foot	31.7	31.9	0.2
Left Foot	31.7	32.9	1.2

Note: **Red** value means the measured temperature is higher than the set-point;

**blue** value means the measured temperature is lower than the set-point.

In order to show the effect of the surface temperature on the heat loss of the manikin, a CFD case using the measured surface temperature was run to compare with the case using the set-point temperature. A better agreement was found by using the measured surface temperature. The difference of total heat loss between the CFD and experiment was reduced from 4.6 W to 2.1 W compared with the case using set-point temperature. This study indicates that accurate prediction of the heat loss from the manikin requires a surface temperature that is as close to the experiment as possible.

#### **4.2.7. Other Considerations**

The application of the ATDs is not only based on physical measurement, such important factors as ergonomics and aesthetics could also play an important role in human judgment and general perception (Kaczmarczyk et al. 2006). Among the three ATDs tested, the Type I ATD worked the best since it could remove the most extra heat from the manikin with the same amount of cooling power. However, it may interfere with people's thighs and bring some difficulties if people use a keyboard tray. The round panel (Type II ATD) was reported to be able to provide thermal comfort as well as perceived air quality (Kaczmarczyk et al. 2006), but implementing this type of ATD requires drilling a hole on the desk to connect the diffuser with the  $\mu X$  which can be disruptive and unfavorable. Type III ATD leaves more space under the desk, and also avoids making any modification to the furniture. However, this kind of diffuser needs more complex duct connection and may have the problem of balancing the air of two openings.

#### **4.3. Summary and Conclusions**

A CFD model has been developed, validated and applied to evaluate the performance of three types of ATDs selected for a micro-environment control system ( $\mu X$ ). It was found:

- 1) The CFD-predicted heat loss from the manikin agreed within 6% of the measured results from the full-scale chamber tests. Also, it was found that the heat loss of the manikin was very sensitive to the furniture placement and surface temperature of the manikin.
- 2) Convective heat transfer coefficients of all the segments of the manikin were calculated in the current work and compared with previous studies. The difference

in height, surface area, and shape of the manikin could change the development of the thermal boundary layer and thus the convective heat transfer coefficient. However, more discrepancy was due to the methods of measurement.

- 3) Cooling performance was increased more by increasing the supply air velocity than reducing the supply air temperature when the total cooling power was constant. Considering the extra heat removed and discomfort caused by the jet, the combination of 23.0 °C supply air temperature and 0.014 m<sup>3</sup>/s flow rate was recommended as the operating condition for the micro-environment control system.
- 4) The performance of three types of ATDs (Air Terminal Devices) was evaluated using the validated CFD model over a semicircle range of 0.61 m radius around the  $\mu$ X diffuser. The manikin could be cooled sufficiently in the movement range using any of the three ATDs tested, while Type I ATD (a single diffuser in the center) worked the best. The cooling performance of the ATDs is highly dependent on the shooting angle (target area). The best performance was always achieved when the jet was blown onto the stomach of the manikin because in this case, the jet could blow onto the largest area of the body.

Based on this study, one of the three ATDs has been selected for incorporation into the  $\mu$ X. The final product will be tested with a thermal manikin and 32 human subjects in the near future. More discussion in terms of thermal sensation and comfort for each individual body part, draft effect, perceived air quality is going to be addressed based on more measurements and evaluation of the subjects.



## **5. Micro Environmental Control for Efficient Heating**

This chapter is focused on using the previously validated CFD model to help evaluate different methods of heating the occupant locally for restoring thermal comfort, including convection, radiation, and conduction.

### **5.1. Overview**

The focus of application of the micro-environmental control system has been on cooling the person in the warm environment. There were only quite few studies looking into the use of it in the cool condition (Deng et al. 2016; Pasut et al. 2015; Verhaart et al. 2015; Zeiler et al. 2015; Zhang et al. 2015). Different from cooling the person in the warm environment, in a cool condition the occupants tend to wear more clothes (long sleeve shirt and thicker trousers), which gives a total clothing value of around 1.0 clo (compared to 0.5 clo in summer) (ASHRAE 2013c). In addition, since in a cool environment the ambient air temperature is much cooler than the body temperature, there is no “free convection” available for adding heat to the body, and one can only reduce heat loss from the body from convective heat transfer mechanism. To add heat to the body, conduction or radiation is necessary. Furthermore, the sensitivity of different part of the human body to the cool environment is significant. All these facts combine to make personalized heating more complicated than cooling.

This chapter used the validated CFD model developed in the previous chapter for evaluating different heating methods. The computational domain represented a full-scale office, 4.88 m × 3.66 m × 3.05 m, with a linear diffuser mixing system (Figure 4-1). A

workstation with a laptop on top of it was in the center of the room. The  $\mu X$  for heating is designed to provide 60 W heating power constantly during the day of winter. Based on some previous study, the feet are significantly sensitive to the cool environment and dominate the discomfort of the entire body in a cool environment (Arens et al. 2006b). Warm feet are essential for the perception of comfort in a cool environment (Zhang et al. 2015). Therefore, in any form, the heating power was supplied to the feet first. This 60 W heating power was converted firstly to a blow of warm air to heat the occupant by convection. The supply flow rate and supply temperature were determined using Eqn. 4-1. Different supply air velocities were tested as well as the supply temperature. Then the idea of using a confinement box with the warm air was tested. In the end, another method using a footwarmer to heat the feet by conduction and radiation was evaluated.

### **5.1.1. Boundary Conditions for CFD Simulations**

This chapter summarized three parts of work. The first part talks about determining the supply condition of using convection to heat the occupant. In this part, two split diffusers were located in front of the feet of the occupant (Figure 5-1). First of all, the effect of the supply velocity was evaluated. A total amount of 0.0024 m<sup>3</sup>/s air at 40 °C was supplied to the feet. The opening size of the supply diffusers was 0.0500 m × 0.0500 m, 0.0625 m × 0.0500 m, and 0.0833 m × 0.0500 m based on different supply velocity (0.3 m/s, 0.4 m/s and 0.5 m/s). Then different combinations of the supply temperature and supply flow rates were tested. The temperature varied from 40 °C to 36.8 °C and 31.3 °C, and the flow rate changed according to the supply temperature based on Eqn. 4-1. The optimal supply velocity was applied to all the three cases and the opening size of the supply diffusers

respectively  $0.0500\text{ m} \times 0.0500\text{ m}$ ,  $0.0625\text{ m} \times 0.0500\text{ m}$ , and  $0.0833\text{ m} \times 0.0500\text{ m}$ . The boundary condition of this first part was summarized in Table 5-1.

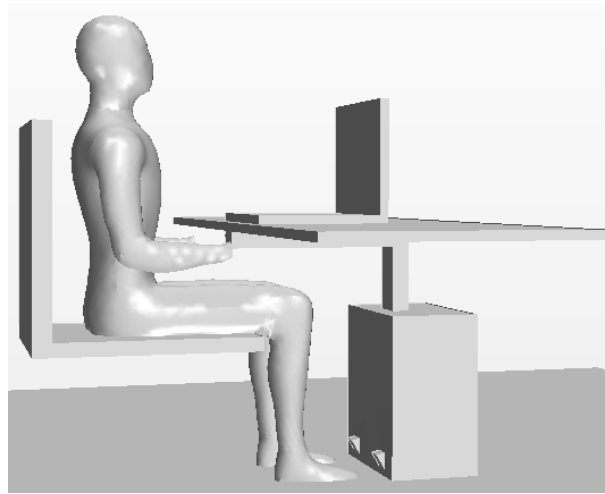


Figure 5-1 Split diffuser to the feet

Table 5-1 Summary of the boundary conditions of split diffuser test

	Case	Room Temperature (°C)	Diffuser Size (m <sup>2</sup> )	Supply Velocity (m/s)	Supply Temperature (°C)	Supply Flow Rate (cfm)
Baseline Case	A	18.9	N/A	N/A	N/A	N/A
	B	21.1	N/A	N/A	N/A	N/A
Velocity Test	C	18.9	$0.0500 \times 0.0500$	0.5	40.0	5.0
	D	18.9	$0.0625 \times 0.0500$	0.4	40.0	5.0
	E	18.9	$0.0833 \times 0.0500$	0.3	40.0	5.0
Supply Combination Test	C	18.9	$0.0500 \times 0.0500$	0.5	40.0	5.0
	F	18.9	$0.0625 \times 0.0500$	0.5	36.8	6.3
	G	18.9	$0.0833 \times 0.0500$	0.5	31.3	8.3

The second part of this work is using a confinement box around occupant's legs with the split diffuser to help improve the heating performance. The confinement box was defined as a well-insulated box with an opening in the front (Figure 5-2 a). A confinement box of

three different sizes - 0.40 m × 0.45 m × 0.50 m, 1.00 m × 0.45 m × 0.50 m, and 1.60 m × 0.45 m × 0.50 m - was tested in this work respectively. The front opening was assumed to be covered with plastic strips made of polyvinyl chloride (PVC). The PVC strip has a thickness of 0.003 m (Figure 5-2 b) which gives a thermal resistance of 0.0158 m<sup>2</sup>·K/W (PVC conductivity is 0.19 W/m·K). Also, because it is assumed that the occupant is going to put their legs through the strip door, the strip door was modeled as porous baffle interface. It was assumed that the strip door could be taken as a perforated screen with a porosity of 0.5. According to Idelchik’s “Hydraulic Resistance Handbook” (Idelchik 1960), the porous media resistance coefficient  $\xi$  was calculated as

$$\xi = \frac{\Delta H}{\frac{\rho v^2}{2g}} \cong \left[ \xi_\varphi + \bar{a}_0^{Re} (\xi_0 - \bar{f})^2 \right] \frac{1}{\bar{f}^2} \quad (5 - 1)$$

where  $\Delta H$  is the pressure loss ( $kg/m^2$ ),  $\rho$  is the air density ( $kg/m^3$ ),  $v$  is the stream velocity ( $m/s$ ),  $g$  is the gravitational acceleration ( $m/s^2$ ),  $\bar{f}$  is the porosity (0.5),  $\xi_\varphi$ ,  $\bar{a}_0^{Re}$ , and  $\xi_0$  are all parameters depending on the Reynolds number  $Re$  and can be found easily in the handbook,

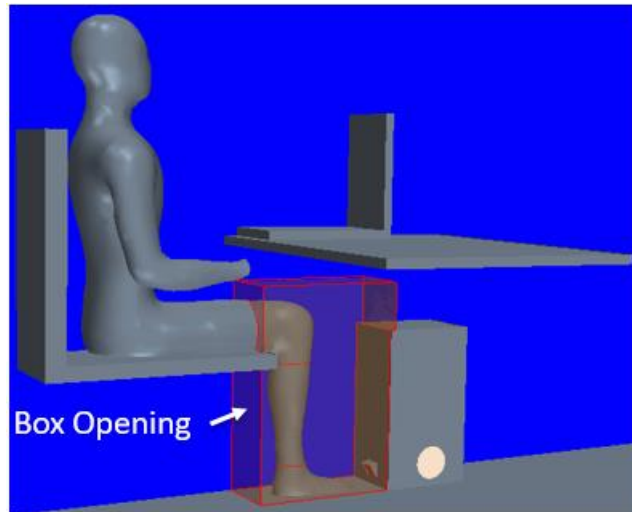
$$Re = \frac{v_0 d_h}{\nu} \quad (5 - 2)$$

where  $v_0$  is the mean velocity of the stream in the orifices,  $d_h$  is the hydraulic diameter of the orifices, and  $\nu$  is the kinematic viscosity. The boundary condition of this first part was summarized in Table 5-2.

Table 5-2 Summary of the boundary conditions using confinement box

Cas e	Room Temperatur e (°C)	Box Size (m <sup>3</sup> )	Box Opening Size (m <sup>2</sup> )	porous media resistance
----------	------------------------------	----------------------------	---------------------------------------	-------------------------------

					coefficient
					$t \xi$
Baseline Case	A	18.9	N/A	N/A	N/A
	B	21.1	N/A	N/A	N/A
Confinement Box Test	H	18.9	0.40m×0.45m×0.50 m	0.40m×0.50 m	4.968
	I	18.9	1.00m×0.45m×0.50 m	1.00m×0.50 m	6.904
	J	18.9	1.60m×0.45m×0.50 m	1.60m×0.50 m	7.344



(a)



(b)

Figure 5-2 Split diffuser with the confinement box (a) CFD model; (b) Example of the strip door (<http://www.ganikpyccurtains.com/>)

The third part of the work is testing a footwarmer to heat the occupants by conduction and radiation. The footwarmer consists of a heating mat under the feet, a reflective box covering the front part of the feet and a heating lamp placed inside the box. The heating mat was

designed to be electrically heated with a heat flux of  $175 \text{ W/m}^2$  uniformly through an area of  $0.50 \text{ m} \times 0.45 \text{ m}$ . The reflective box was assumed to be a box of  $0.45 \text{ m} \times 0.15 \text{ m} \times 0.15 \text{ m}$ , with reflective material covering the interior surface (reflectivity equals to 1). The heating lamp was simulated by a strip ( $0.45 \text{ m} \times 0.024 \text{ m}$ ) placed on the top surface inside the box with a total heat flow rate of  $20 \text{ W}$ . Three tests were conducted, including heating with only the mat, heating with the mat and reflective box, and heating with the mat, reflective box and heating strip.

Table 5-3 Summary of the boundary conditions using footwarmer

	Case	Room Temperature (°C)	Box Size (m <sup>3</sup> )	Mat Heating Flux (W)	Heating Lamp Power (W)
Baseline Case	A	18.9	N/A	N/A	N/A
	B	21.1	N/A	N/A	N/A
Footwarmer Test	K	18.9	N/A	175	0
	L	18.9	$0.45\text{m} \times 0.15\text{m} \times 0.15\text{m}$	175	0
	M	18.9	$0.45\text{m} \times 0.15\text{m} \times 0.15\text{m}$	175	20

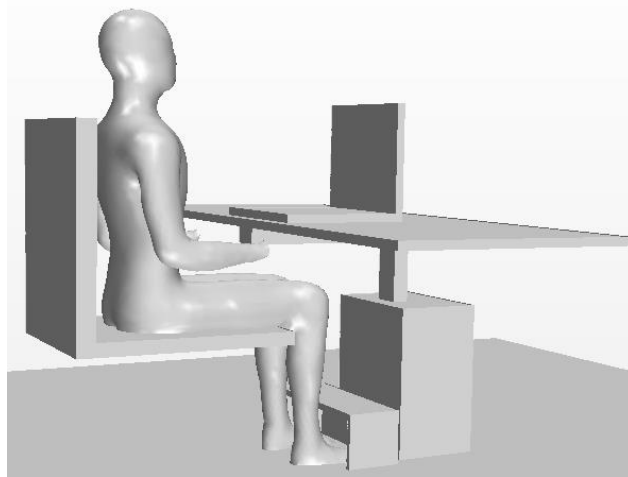


Figure 5-3 Footwarmer heating

### 5.1.2. Clothing Assembly

Usually, when people used CFD to simulate the flow field around the human body, they used either constant surface temperature or heat flux as the boundary condition (Dyger et al. 2009; Nilsson et al. 2007; Russo et al. 2009). Some researchers involved clothing insulation in their simulation but ignored the difference between different segments (Cheng et al. 2012). However, this  $\mu X$  is focused on some particular body parts, where the local resistance matters. ASHRAE Handbook (ASHRAE 2013a) specifies the clothing insulation value of individual garments commonly worn, but these values were previously determined on a whole-body basis. To specify the clothing insulation of each body part, this work converted the whole-body clothing resistance of a clothing element  $i$  ( $R_{cl,whole,i}$ ,  $m^2K/W$ ) to its local clothing resistance ( $R_{cl,local,i}$ ,  $m^2K/W$ ) by:

$$R_{cl,local,i} = \frac{A_t}{A_{cov,i}} R_{cl,whole,i} \quad (5 - 3)$$

where  $A_t$  is the total body surface area ( $m^2$ ) and  $A_{cov,i}$  is the covered body area of clothing element  $i$  ( $m^2$ ) (Lai and Chen 2016). The clothing insulation of all the segments are summarized below (Table 5-4). The total clothing value of the human body is 0.92 clo which is closed to the typical winter clothing value of 1.00 clo.

Table 5-4 Local clothing insulation

	Clothes	Insulation clo	Thermal resistance $m^2.K/W$
Face	None	0.000	0.000
Head			
Chest	Long-sleeve dress shirt + Suit	0.630	0.241
Shoulder			
Back			



Left Upper Arm			
Right Upper Arm			
Left Arm			
Right Arm			
Left Thigh	Straight trousers	0.240	0.090
Right Thigh			
Left Calf	Straight trousers + Calf length socks	0.270	0.111
Right Calf			
Left Foot	Calf length socks + shoes	0.050	0.067
Right Foot			
Whole Body		0.920	

### 5.1.3. Thermal Comfort

To reduce the room temperature from 21.1°C to 18.9 °C, the  $\mu X$  is needed to manage the local thermal envelope to achieve local thermal comfort. How to evaluate the performance of the  $\mu X$  regarding thermal comfort is the critical question for this work. As discussed in Section 2.1.2.2, many models have been developed for predicting the thermal comfort in a certain environment. However, since this work is focused on evaluating the thermal response of the human body to non-uniform static environment and evaporation is not included, the Clothing Independent Thermal Comfort Model was adopted (Nilsson 2007). This model was developed based on equivalent temperature, which is defined as the temperature of an imaginary enclosure with the mean radiant temperature equal to air temperature and still air in which a person has the same sensible heat exchange by convection and radiation as in the actual conditions, and it can be calculated using Eqn. 3-1. However, to make the comfort evaluation clothing independent, Eqn. 5-4 was developed

so that for any clothing combination, the thermal sensation, as a Mean Thermal Vote (MTV), can be evaluated based on the heat loss of individual body part.

$$t_{eq,zone} = t_s - R_T(a_1 + a_2MTV_{zone}) \quad (5 - 4)$$

where  $R_T$  is the total insulation, including resistance of clothing and air layer;  $a_1, a_2$  are the linear regression constants ( Nilsson 2007). Combining Eqn. 3-1 and 5-4, the MTV can be correlated to the local heat loss directly.

In order to evaluate the performance of the  $\mu X$  in the environment of reduced air temperature (18.9 °C), the MTV of each case using different kinds of  $\mu X$  were predicted according to the CFD results of this current study, and compared with the one of the case of regular set-point (21.1°C).

## **5.2. Results and Discussion**

### **5.2.1. Split Diffuser**

#### **5.2.1.1. Effect of the Supply Velocity**

As mentioned before, the first method we tried was using the hot air jet to heat the feet locally. Different from the cooling case, since the surrounding air (18.9 °C) is cooler than the skin temperature (33.9 °C), there is no “free heating” existing like the cooling case. One has to make sure the hot jet can get to the human body before it is mixed with the surrounding air. So first of all, three different supply velocities, 0.3 m/s, 0.4 m/s and 0.5 m/s, were tested when the supply flow rate and temperature were fixed at 0.0024 m<sup>3</sup>/s air at 40 °C. The simulation results are summarized in Table 5-5.

Table 5-5 Summary of heating with hot jet at different velocities

Case	A	B	C	D	E
$\mu$ X Supply Temp (°C)			40	40	40
$\mu$ X Supply Vel (m/s)			0.5	0.4	0.3
$\mu$ X Supply Flow Rate (cfm)			5	5	5
Room Return Temp (°C)	18.9	21.1	18.9	18.9	18.9
Averaged Heat Flux (W/m <sup>2</sup> )	59.3	50.3	56.2	59.1	59.3
Total Heat loss (W)	103.3	87.6	97.8	102.9	103.2
Reduced Heat Loss (W)		15.7	5.5	-0.4	-0.1

Note: Reduced Heat Loss is heat loss difference compared with Case A.

From Table 5-5, When the room air temperature was reduced from 21.1°C to 18.9 °C, the total heat loss was increased from 87.6 W to 103.3 W, which made a 15.7 W difference. After turning on the  $\mu$ X, the total heat loss was reduced by 4.8 W only when the supply velocity was 0.5 m/s. When the supply velocity was set to be 0.4 m/s and 0.3 m/s, the total heat loss was even increased instead of reduced. The reason for that could be seen in Figure 5-4. The surface heat flux was indicated by color. The streamline initiated from the diffuser was also plotted with color to indicate the temperature of the air along the streamline. It can be observed from the figure that 1) the heat flux of each segment was highly affected by the clothing insulation when the  $\mu$ X was off (Case A and B); 2) the air was mixed with the surrounding air quite fast (the streamline turned from red into blue), which means the hot jet can only work in a very short distance from the diffuser (the air temperature has to be higher than the skin temperature to warm the body); 3) with 0.5 m/s supply velocity, the hot jet was blown on most area of the foot, while with 0.4 m/s and 0.3 m/s supply velocity,

the hot jet was deflected upwards by the buoyancy before it got to the foot. This explains why only when the supply velocity was 0.5 m/s, the hot jet started to work.

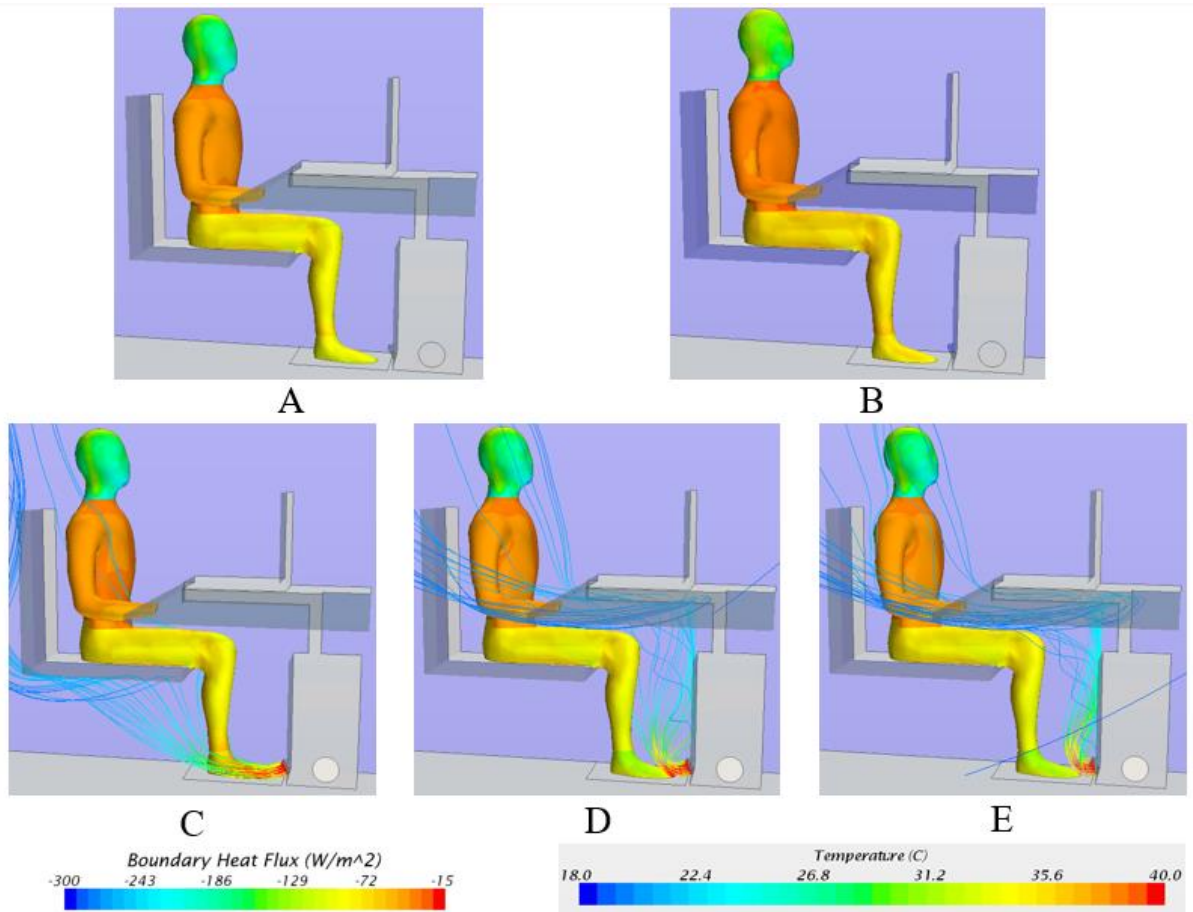


Figure 5-4 Surface heat flux of the cases with different supply velocities

Figure 5-5 shows the predicted MTV of each segment of the occupant when different supply velocities were applied. Without the  $\mu X$ , when the room temperature was reduced from 21.1°C to 18.9 °C, the whole-body MTV was reduced from slightly cool (-0.488) to a little more than cool (-1.166), while all the local MTVs decreased by 0.28 - 0.74. The maximum decrement happened on the face, which is mostly because the face is naked. The second maximum decrement happened on the feet partially confirmed that the feet were

more sensitive in cold environment. There is a big variation of the local MTV (from -2.647 to 0.122 in the 18.9 °C case and from -1.909 to 0.410 in the 21.1°C case) observed when the  $\mu X$  was off. Low MTVs happened on the face, head, calf, and foot; neutral MTVs happened on the torso, arm, and thigh.

When the  $\mu X$  was turned on, the whole-body MTV was changed as well as some local MTVs. However, these changes were only significant when the supply velocity was 0.5 m/s (Case C). Since the hot jet was directed to the foot, the highest increment happened on the feet. With 0.5 m/s supply velocity, the hot air of 40 °C is able to bring the local MTV of the feet from -2.384 (cold) to -0.805 (slightly cool) which is even closer to the neutral than the original environment (Case B), and bring the whole-body MTV from -1.166 (cool) to -0.929 (slightly cool) although it was still lower than the original (Case B). Nevertheless, for the case with 0.4 m/s and 0.3 m/s, the result was disappointing. Compared with the case without the  $\mu X$  (Case A), there was almost no improvement at all for both whole-body MTV and local MTV. This is consistent with the previous heat loss analysis.

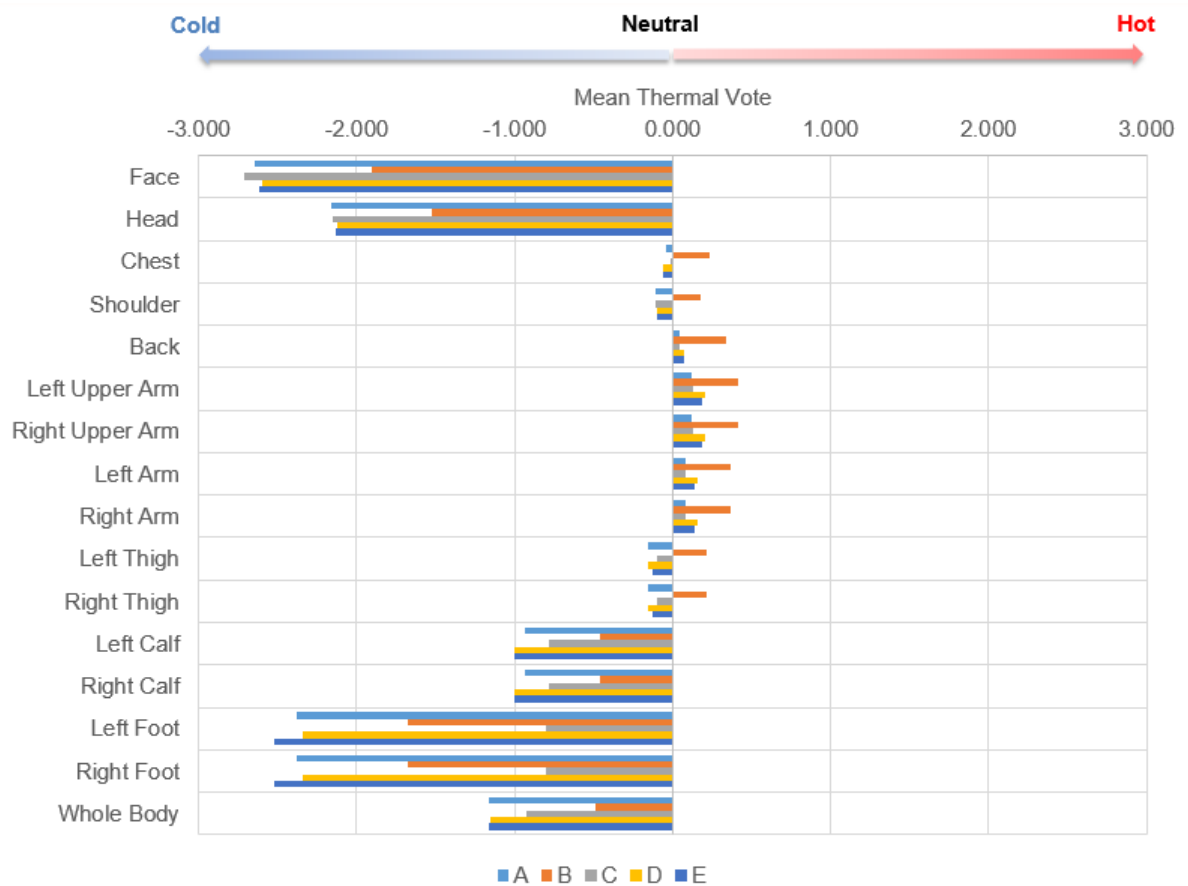


Figure 5-5 Mean Thermal Vote of the cases with different supply velocities

### 5.2.1.2. Determination of Suitable Air Supply Temperature and Flow Rate

Since the supply velocity was decided, similar to the cooling case, the next step was to determine the combination of the supply condition so as to maximize the heating performance to restore thermal comfort. The  $\mu X$  was designed to provide 60 W heating power constantly, and three combinations of supply temperature and velocity were tested. The results are summarized in Table 5-6.

Table 5-6 Summary of heating with hot jet of different supply combinations

Case	A	B	C	F	G
------	---	---	---	---	---

$\mu$ X Supply Temp (°C)			40.0	36.8	31.3
$\mu$ X Supply Vel (m/s)			0.5	0.5	0.5
$\mu$ X Supply Flow Rate (cfm)			5	6.3	8.3
Room Return Temp (°C)	18.9	21.1	18.89	18.89	18.89
Averaged Heat Flux (W/m <sup>2</sup> )	59.3	50.3	56.2	57.2	58.0
Total Heat loss (W)	103.3	87.6	97.8	99.5	100.9
Reduced Heat Loss (W)		15.7	5.5	3.7	2.3

Note: Reduced Heat Loss is heat loss difference compared with Case A.

Table 5-6 indicates that the performance of the  $\mu$ X benefited more from lower supply flow rate, which is opposite to the cooling case. The maximum reduced heat loss 4.8 W is given by the combination of 0.0024 m<sup>3</sup>/s (5 cfm) supply flow rate and 40 °C supply temperature, and it decreased to 3.7 W and 2.3 W when the flow rate was increased to 0.0030 m<sup>3</sup>/s (6.3 cfm) and 0.0039 m<sup>3</sup>/s (8.3 cfm). The reason for that can be better indicated in Figure 5-6. With 0.5 m/s supply velocity, the hot jet could always blow over the top surface of the foot. However, the red area (the area with smaller heat flux) on the foot decreased with the increasing of the flow rate. The first reason is that because the supply temperature decreased with the increasing of the flow rate, Case F and G have smaller temperature differences between the jet air and the skin, which determines the heating capability of the jet. The second reason is that since the supply temperature was lower in Case F and G, the jet started to cool foot earlier than Case C. Therefore, more heat was taken away from the heel.

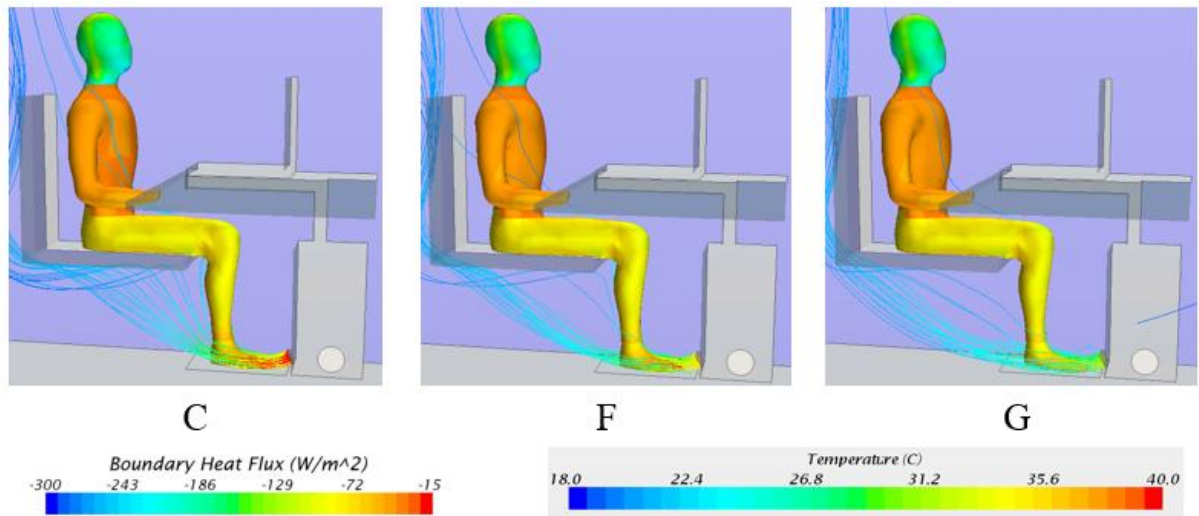


Figure 5-6 Surface heat flux of the cases with different supply combinations

Figure 5-7 shows the predicted MTV of each segment of the occupant when different supply combinations were applied. It is observed that the whole-body MTV were improved by the hot jet compared with Case A and the improvement was the most for Case C ( $\Delta$ MTV = 0.238). The local MTV of the foot were all increased for the three cases compared with Case A, and they were all even better than the original environment (Case B). However, one has to notice that even the best case C could only improve the overall MTV from -1.166 to -0.929, which is far less than -0.488. Therefore, heating with the hot jet alone was proved to be not sufficient.



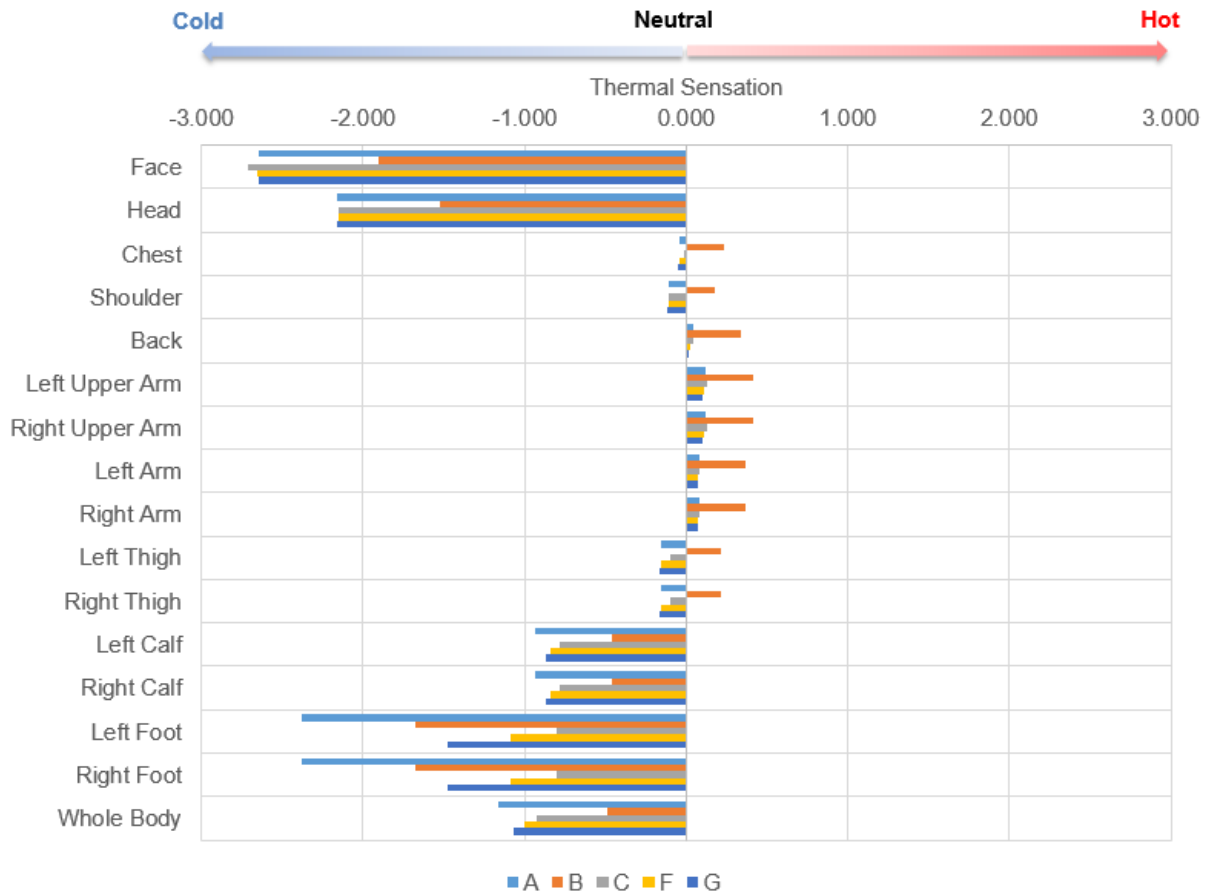


Figure 5-7 Mean Thermal Vote of the cases with different supply combinations

### 5.2.2. Effect of Confinement Box

The idea of using a confinement box with hot air supply came from the idea of slowing down the mixing process between the hot air and surrounding cooler air. The driving force of heat transfer is a temperature difference. However, based on the previous finding, the hot jet mixed too fast with the surrounding air so that its heating performance was severely limited. A well-insulated confinement box of different sizes, containing the feet and calves, was tested in this work. 0.0024 m<sup>3</sup>/s of hot air at 40 °C was supplied at 0.5 m/s. The results are summarized in Table 5-7.

Table 5-7 Summary of heating with hot jet and confinement box

Case	A	B	H	I	J
Box length (m)			0.40	1.00	1.60
Box Width (m)			0.45	0.45	0.45
Box Height (m)			0.50	0.50	0.50
Room Return Temp (°C)	18.9	21.1	18.89	18.89	18.89
Averaged Heat Flux (W/m <sup>2</sup> )	59.3	50.3	51.9	52.8	52.9
Total Heat loss (W)	103.3	87.6	90.3	91.9	92.1
Reduced Heat Loss (W)		15.7	13.0	11.4	11.2

Table 5-7 indicates the idea of using hot air jet with confinement box worked much better than the jet alone regarding the reduced heat loss. The reduced heat loss was increased from 5.5 W to 13.0 W, which is almost three times when the box was 0.40 m long. This is very likely because the hot air was successfully confined in the box and warmed the legs quite a bit. The reduced heat loss decreased with the increasing of the size of the box, which is possibly because when the box was larger, there was more air exchange through the front opening of the box. The reason for that can be better indicated in Figure 5-8. When the box was 0.40 m wide (Case H), the hot air exiting from the diffuser was blown onto the top surface of the foot. However, different with the case without the confinement box, most of it turned upwards, flew around the calf, and left the box from the upper part of the opening. Together with a recirculation region created in the upper front corner of the box, the temperature of the air dropped much more slowly. And therefore, smaller heat flux was observed all over the foot and calf. After the box was enlarged, the opening size of the box

was also enlarged, which resulted in that the hot air escaped from the box faster and more heat exchange between the air inside and outside the box.

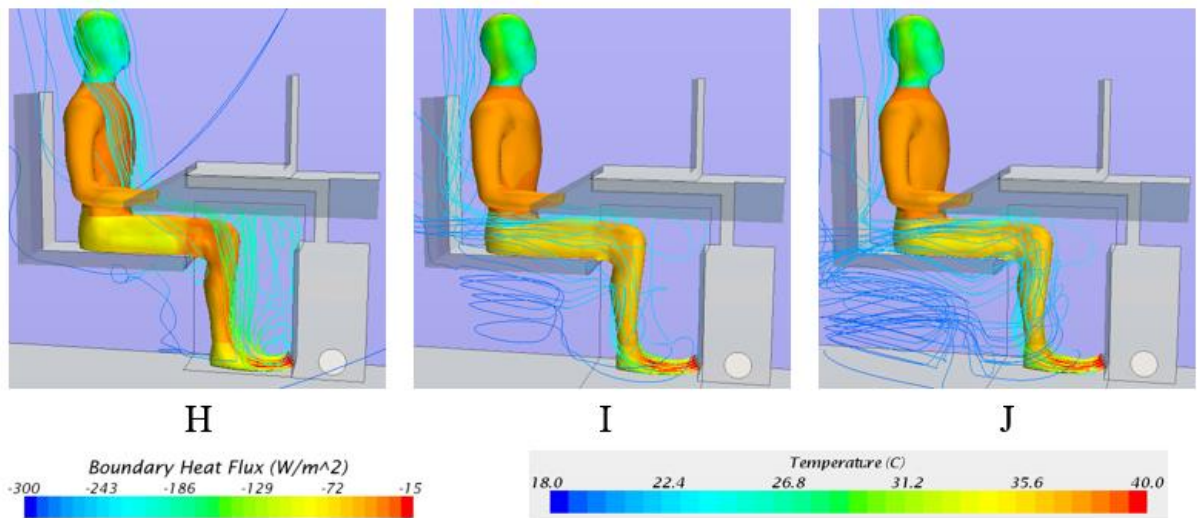


Figure 5-8 Surface heat flux of the cases with confinement box

Figure 5-9 shows the MTV prediction of the cases using the confinement box. For better comparison between the case with and without the box, the MTVs of the Case C are also included. With the confinement box, the  $\mu X$  improved the whole-body MTV from -1.166 (Case A) to -0.606 (Case H) at most which is very close to the original MTV level in normal condition (Case B). Compared with Case C, the confinement box was able to increase the improvement of whole-body MTV from 0.237 to 0.560 with the same amount of heating power. Regarding the local MTVs, the confinement box brought most of the local MTVs, except the head, face, and feet, towards the warm side more or less. It is understandable that the box did not improve the thermal comfort of the head and face. However, it is very interesting that the box made the feet feel cooler than without the box. An explanation is that with the box, on the one hand, the hot air was not able to flow all over the foot, and

like shown in Figure 5-8 the hot air rose upwards and left the box there with entrained air; on the other hand, the cool air outside the box entered from the back of the feet and cool the heel of the feet. Different with the case without the confinement box, the most obvious change happened on the calves. Without the confinement box, the jet could improve the MTV of the calf by only a little, from -0.935 (Case A) to -0.780 (Case C). However, with the confinement box, the improvement was extended to 0.181 (Case H), which is on the warm side.

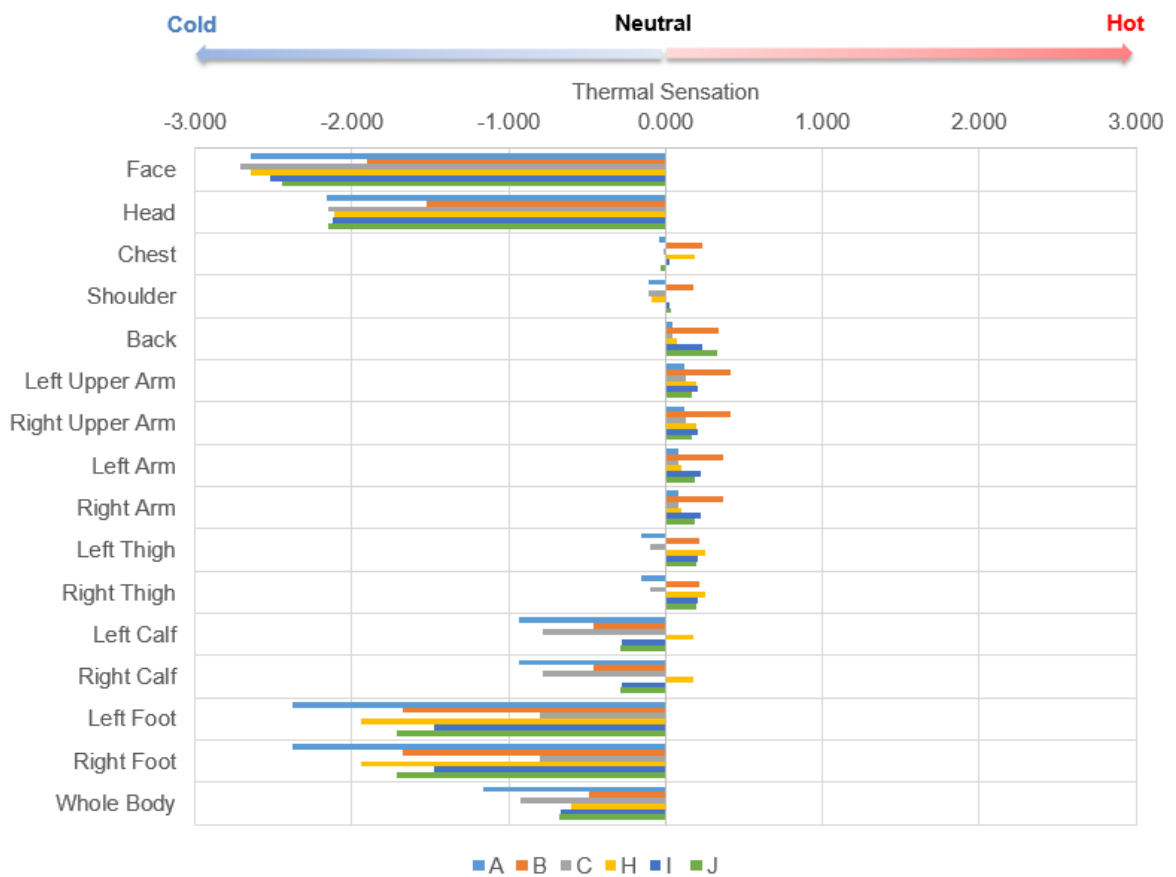


Figure 5-9 Mean Thermal Vote of the cases with confinement box

### 5.2.3. Footwarmer

Although combining the hot jet with the confinement box can improve the thermal comfort in the environment with reduced set-point (18.9 °C), this idea might still be unfavorable because it put too many constraints around the legs. Therefore, another method of using a footwarmer was tested in this section. The principle of this method is heating the feet by conduction and radiation. The primary part of the footwarmer is a 0.50 m × 0.45 m heating mat with a heating flux of 175 W/m<sup>2</sup>. Two additional parts were added to the mat to improve the heating performance: a reflective box and a heating lamp. The results were summarized in Table 5-8.

Table 5-8 Summary of heating with footwarmer

Case	A	B	K	L	M
Mat Heating power (W)			40	40	40
Reflective Box		N/A	×	√	√
Heating Lamp Power (W)			N/A	N/A	20
Room Return Temp (°C)	18.9	21.1	18.89	18.89	18.89
Averaged Heat Flux (W/m <sup>2</sup> )	59.3	50.3	51.1	49.6	45.8
Total Heat loss (W)	103.3	87.6	89.0	86.3	79.8
Reduced Heat Loss (W)		15.7	14.3	16.9	23.4

**Table 5-8** indicates the performance of the footwarmer. By using the heating mat alone, the reduced heat flow rate was as high as 14.3 W which was higher than all the previous cases. With the help of the reflective box, this number was raised to 16.9 W, which is the first time to be able to recover the 15.7 W difference resulted from the reducing of background set-point. One should also note that both case K and case L only used 40 W

heating power, and when the remaining 20 W heating power was used by a heating lamp, another 6.5 W heat loss was reduced from the manikin, which brought the reduced heat loss up to 23.4 W. These results show that, from the reduced heat point of view, the footwarmer heating the occupant in a cooler environment by conduction and radiation is more efficient than convection. More details can be observed in **Figure 5-10**. With only the heating mat, the bottom side of the foot was heated by the heating mat with a constant heat flux of 175 W. Moreover, when the front part of the feet is covered by the reflective box, the radiant heat from the heating mat reflected by the box was transferred to the top surface of the foot. When the heating lamp was added, more radiant heat provided by the heating lamp and reflected by the box was transferred to the foot. In addition, it should be noticed that the reflective box played a role like a small confinement box to hold some part of the convective hot air from the mat and lamp inside the box, and this hot air also exchanged heat with the foot by convection.

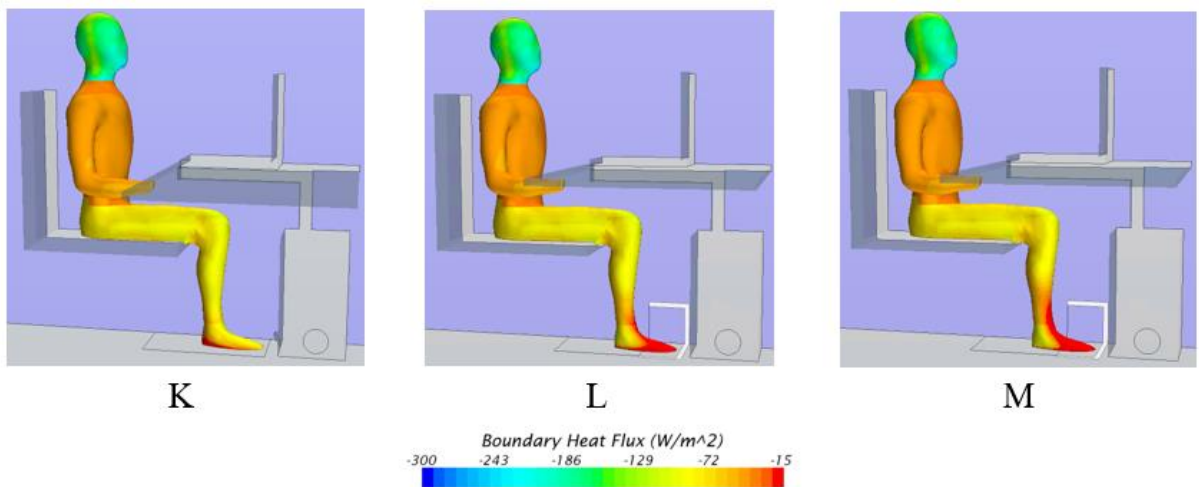


Figure 5-10 Surface heat flux of the cases with footwarmer

**Figure 5-11** shows the MTV prediction of the cases using footwarmer. Case K, L and M successfully recover the whole-body MTV to around the original level (Case B). With only the heating mat, the whole-body MTV was -0.549 which is a little lower than -0.488 (Case B); with the additional reflective box and heating lamp, the whole-body MTV was raised even beyond the original level to -0.433 and -0.154 respectively. Regarding the local MTV, it is obvious that most of the contribution came from the feet and partially from the calves. The heating mat directly brought the MTV of the feet from -2.384 (cold) to 3.003 (hot) with an increment of 5.387 and the MTV of the calves from -0.935 to -0.774 with an increment of 0.161. With the help of the reflective box and heating strip, the local MTV of the feet was brought up to 3.850 (Case L) and 4.162 (Case M), and the local MTV of the calves was brought to -0.633 (Case L) and -0.297 (Case M). The big increment of MTV on the feet is very much due to the heat conducted through the heating mat. Without the heating mat, the feet transferred heat through the socks and the sole of the shoes to the floor with low temperature (18.9 °C). However, with the heating mat, instead of losing heat to the floor, the feet got heat from the mat. This big difference turned over the local thermal sensation of the feet and compensated the whole-body MTV as well.

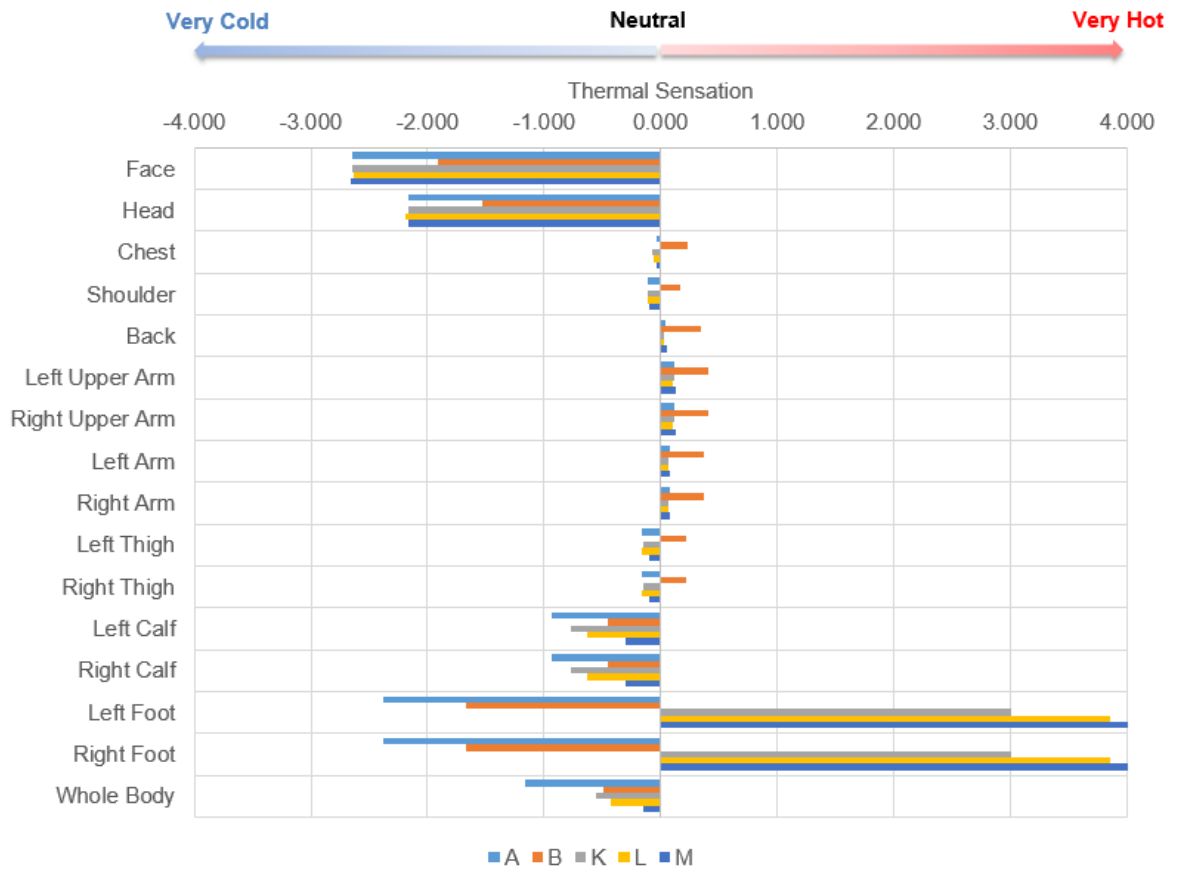


Figure 5-11 Mean Thermal Vote of the cases with footwarmer

### 5.3. Summary and Conclusions

The  $\mu X$  was designed to give constant 60W heating power during the day in winter. Three approaches were evaluated in this study using the previously validated CFD model. It was found:

- 1) Different from the cooling case, heating a person with the hot jet is more complicated, since shooting hot air to an occupant in a cold environment may not be able to make them feel warm because it may entrain cooler air to blow on the human body. Only when supply air temperature was higher than 40 °C, the jet started to heat the person. The supply velocity needs to be at least 0.5 m/s. Lower



supply air velocity made the jet deflected too fast. However, even with this supply condition, the jet can at most reduce the total heat loss by 5.5 W, which is not sufficient to recover the thermal comfort.

- 2) Another idea of using a confinement box to hold the hot air around the legs and feet was proved to be promising. This confinement box was open in front. For holding the hot air, a strip door can be used on the opening. With this confinement box, the hot air can be retained around the legs for a while before it was mixed with the cooler air. This reduced the heat loss to two or three times compared to the single jet air heating approach.
- 3) The best performance was obtained by using a footwarmer to heat occupant's feet. Instead of using convection to heat the body, both conduction and radiation were used. A warming footpad with constant heat flux was put under people's feet. Together with a reflective box covering the front part of the feet and heating lamp placed inside the box, more than 23 W heat loss can be reduced.



## **6. Experimental Evaluation of the Micro-Environmental Control in a Semi-Open Space**

The previous two chapters used validated computational simulation to help evaluate different strategies of using micro-environmental control system with expanded temperature set-point. These studies have shown the excellent predicted performance of the  $\mu X$ . This chapter presents the methods and results of an experimental study in which a dressed manikin sitting in a full-scale chamber was used to evaluate the performance the  $\mu X$ . The study also included the tests on the effects of the cubicle as a semi-open space in combination with  $\mu X$ .

### **6.1. Overview**

#### **6.1.1. Experimental Facility**

Since the effectiveness of the  $\mu X$  for cooling the occupant sitting in an office is highly influenced by the surrounding flow, a full-scale indoor environment quality chamber was used to simulate a real office with a workstation. Figure 6-1 shows a rendering of the experimental facility and its relationship to the surrounding lab space. The experimental setup is the same as described in **Sec. 4.1.1**.

In all tests conducted, a heated anatomically correct multi-segment thermal manikin (Figure 6-2) was placed in the workstation to reproduce the heat loading of an occupant. The manikin was dressed in typical summer clothes and its skin temperature was maintained at a defined set-point (33.9 °C) by a computer-controlled feedback system (Khalifa et al.

2009). The manikin garments are summarized in Table 6-1. The total clothing insulation based on ASHRAE Handbook is 0.43 clo (ASHRAE 2013c).

Table 6-1 Summary of the garment dressing the manikin

Garment	Segment	Recommended clothing insulation (clo)
None	Face Head Left Forearm Right Forearm Left Hand Right Hand	0.00
Short-sleeve polo shirt	Chest Shoulder Back Left Upper Arm Right Upper Arm	0.19
Men's Briefs	Left Thigh Right Thigh	0.04
Straight trousers	Left Thigh Right Thigh Left Calf Right Calf	0.15
Socks	Left Calf Right Calf Left Foot Right Foot	0.03
Shoes	Left Foot Right Foot	0.02
<b>Total</b>		<b>0.43</b>

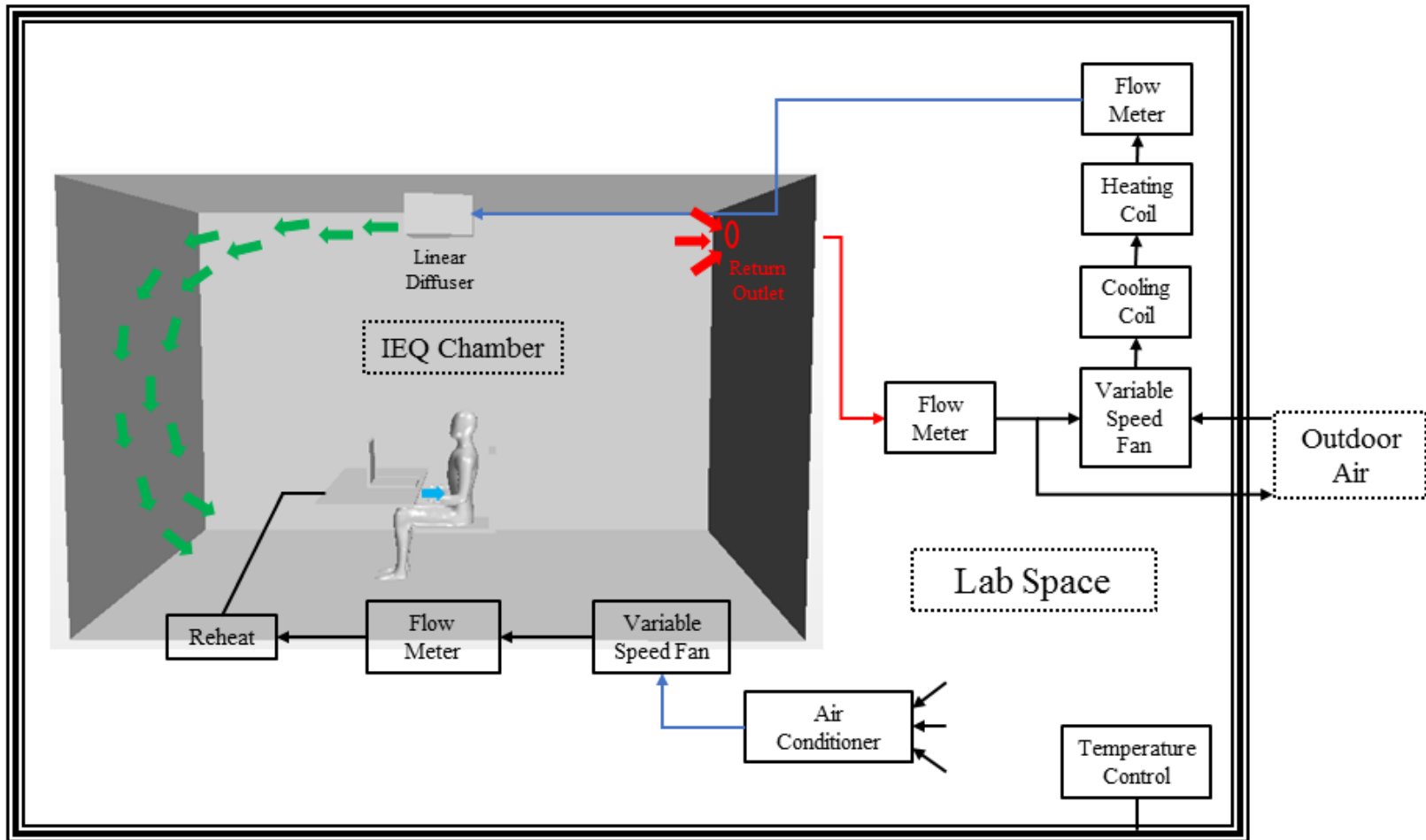


Figure 6-1 Flow diagram of the IEQ chamber

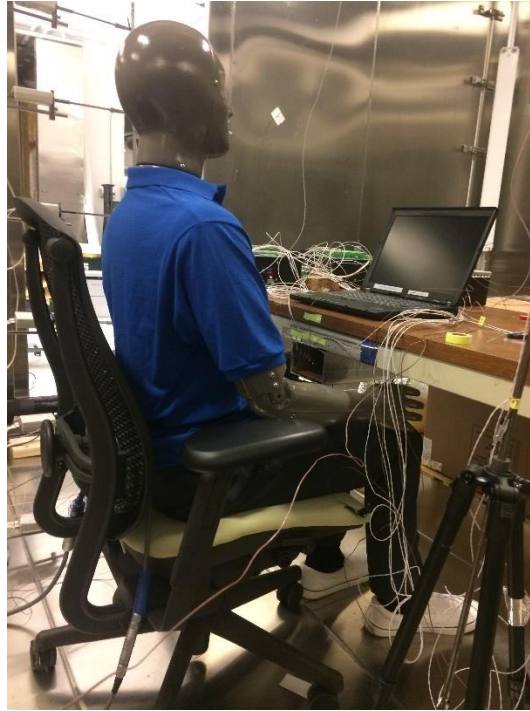


Figure 6-2 Clothed multi-segment thermal manikin

To make the shooting direction adjustable, a car diffuser (Figure 6-3) with adjustable louvers was installed. This diffuser has dimensions of 0.133 m  $\times$  0.064 m with five vertical blades and three horizontal blades, which can direct the jet by  $\pm 10^\circ$  vertically and  $\pm 30^\circ$  horizontally.



Figure 6-3 Diffuser with louvers installed

A common form of the semi-open space in the office is the partitioned cubicle. People use it to provide some private space in large offices. In this study, we looked into the effects of the cubicle space on indoor environment management. A 1.8 m  $\times$  1.8 m cubicle was constructed using partitions made of plywood boards and polystyrene boards (Figure 6-4). The height of the partitions is 1.8 m, and the cubicle was placed around the workstation Figure 6-5a. The cubicle can be opened on all four sides by sliding the partition along a track placed on the floor. Thus, the effects of opening location and openness were investigated by opening the cubicle from the front, side, and back (with respect to the background coming flow) with an opening ratio of 50% and 100% (Figure 6-5b&c).

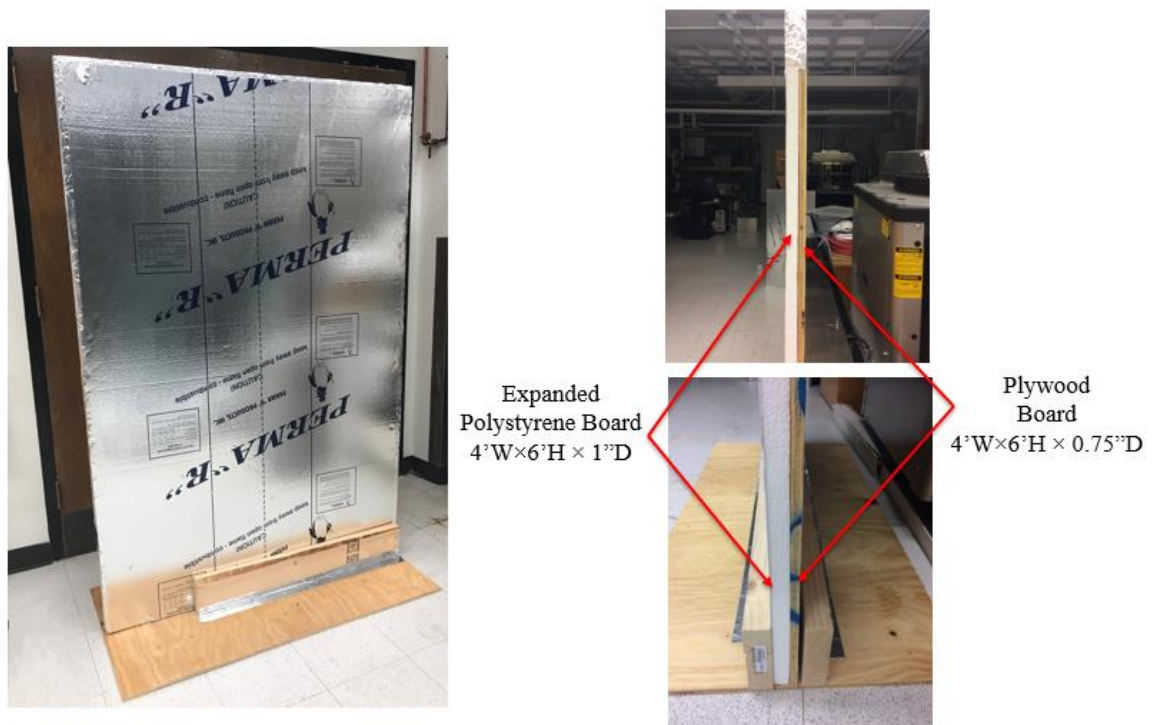
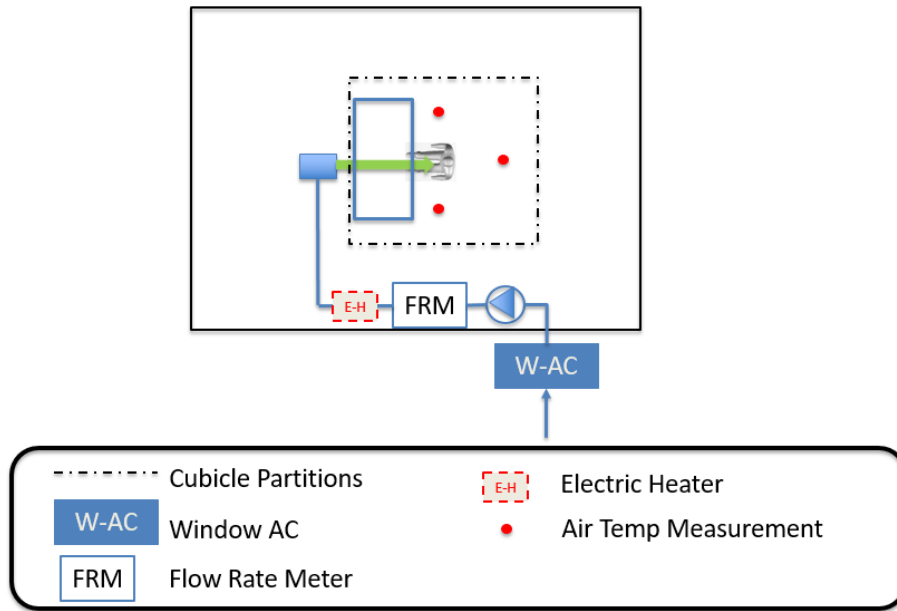


Figure 6-4 Partition of the cubicle

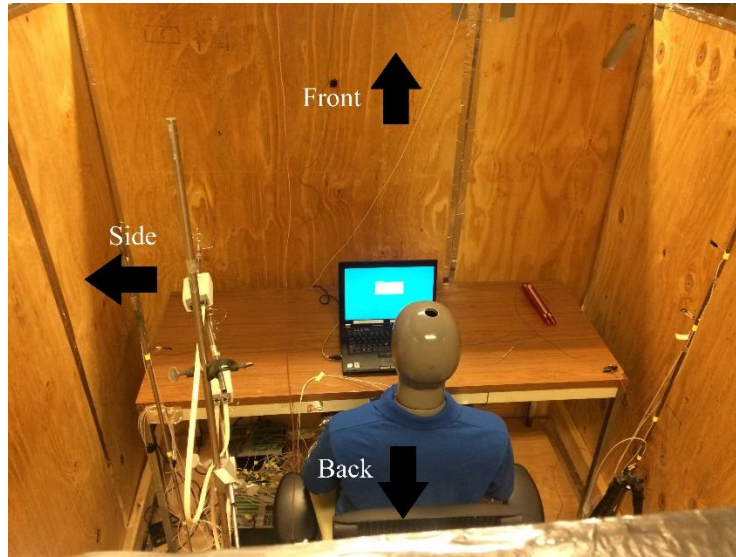


(a)



(b)





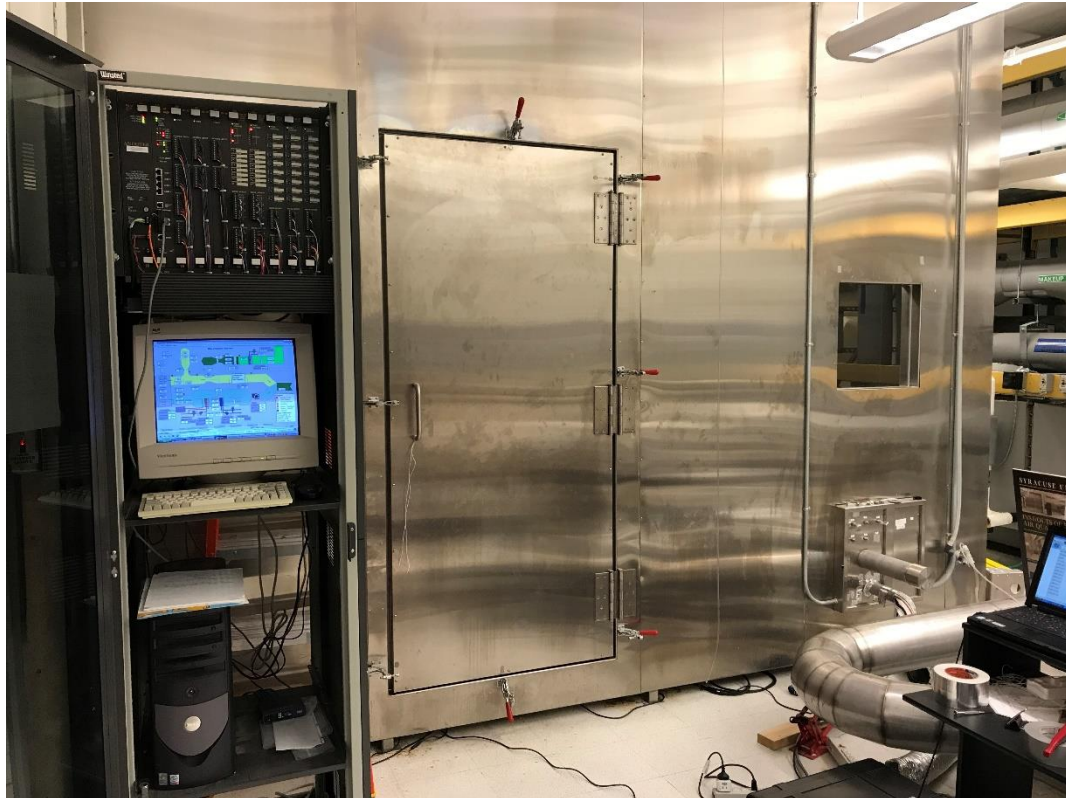
(c)

Figure 6-5 Cubicle around the workstation

### 6.1.2. Experimental Conditions

This chapter mainly consists of two parts: that of testing the  $\mu X$  with a clothed manikin in an open-space office at raised cooling setpoint and that of testing the effect of the cubicle on micro-environmental control. To simulate an open-space office, the workstation with a clothed manikin was placed in the center of the chamber (Figure 6-6a) with a linear diffuser placed above it. The linear diffuser provides background temperature conditioning of the space by blowing conditioned air towards the end wall. In order to minimize the possibility of short circuiting and maximize the mixing of the air, the return outlet was located on the opposite wall. Before each set of tests, the chamber had to be pre-conditioned to the setpoint, and this preparation process usually takes more than 5 hours. The total supply air flow rate was maintained at  $0.075 \text{ m}^3/\text{s}$  which corresponded to an air change rate of  $5 \text{ h}^{-1}$ . The supply air was conditioned by an air conditioning unit (Figure 6-6b) placed by the side

of the chamber to make sure the return air temperature reached the set-point. When the  $\mu X$  was turned off, the chamber was running at a 100% recirculation mode. When the  $\mu X$  was turned on, the chamber supply air flow rate was reduced to make up for the air supplied by the  $\mu X$ .



(a)



(b)

Figure 6-6 IEQ chamber (a) and its HVAC system (b)

The performance of the  $\mu$ X in cooling condition was tested first. The effect of the distance between the diffuser and the manikin, the effect of the shooting angle, the effect of the flow rate, the effect of the supply temperature, and the effect of the clothing were evaluated in sequence. Typically, people sitting in an office have a range of movement with a radius of 0.61 m away from the desk. Therefore, tests with three distances (0.20 m, 0.45 and 0.61 m) between the stomach and the  $\mu$ X diffuser were conducted. The tested shooting angle included  $0^\circ$  and  $10^\circ$ . The effects of the supply flow rate and temperature were investigated separately. The air flow rate supplied by the  $\mu$ X was set at three levels:  $0.0073 \text{ m}^3/\text{s}$  (15.5 cfm),  $0.0139 \text{ m}^3/\text{s}$  (29.4 cfm) and  $0.0189 \text{ m}^3/\text{s}$  (40.0 cfm), and three supply temperatures –

20.0 °C, 23.0 °C, and 26.0 °C - were tested for each flow rate. In the end, in order to explore the effect of the different clothing garment, a tight sports shirt was used to replace the polo shirt. The experimental condition of each set of the test was summarized in Table 6-2.

Table 6-2 Experiment conditions of the  $\mu$ X tests

Case #	Room Return Temp (°C)	Distance from the diffuser (m)	$\mu$ X Shooting Angle (°)	$\mu$ X Supply Flow Rate (cfm)	$\mu$ X Supply Temp (°C)	Upper Body Garment
BL	26.1	N/A				Polo shirt
D1-A0-F2-T2		0.20	0	29.4	23.1	
D2-A0-F2-T2		0.45	0	29.4	23.1	
D3-A0-F2-T2		0.61	0	29.4	23.1	
D1-A1-F2-T2		0.20	10	29.4	23.1	
D2-A1-F2-T2		0.45	10	29.4	23.1	
D3-A1-F2-T2		0.61	10	29.4	23.1	
D1-A0-F1-T1		0.20	0	15.5	20.2	
D1-A1-F1-T1			10	15.5	20.2	
D1-A0-F1-T2			0	15.5	23.1	
D1-A1-F1-T2			10	15.5	23.1	
D1-A0-F1-T3			0	15.5	26.1	
D1-A1-F1-T3			10	15.5	26.1	
D1-A0-F2-T1			0	29.4	20.2	
D1-A1-F2-T1			10	29.4	20.2	
D1-A0-F2-T2			0	29.4	23.1	
D1-A0-F2-T2			0	29.4	23.1	



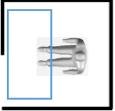
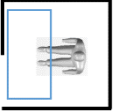
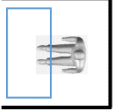
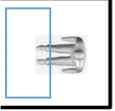
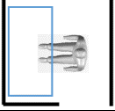
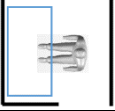
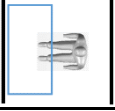
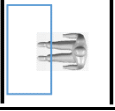
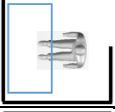
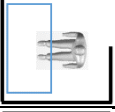
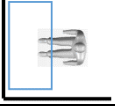
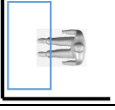
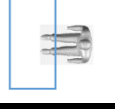
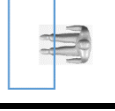
D1-A1-F2-T2			10	29.4	23.1	
D1-A0-F2-T3			0	29.4	26.1	
D1-A1-F2-T3			10	29.4	26.1	
D1-A0-F3-T1			0	40.0	20.2	
D1-A1-F3-T1			10	40.0	20.2	
D1-A0-F3-T2			0	40.0	23.1	
D1-A1-F3-T2			10	40.0	23.1	
D1-A0-F3-T3			0	40.0	26.1	
D1-A1-F3-T3			10	40.0	26.1	
BL-S		N/A				
D1-A0-F2-T2-S		0.20	0	29.4	23.1	Sport Shirt
D3-A0-F2-T2-S		0.61	0	29.4	23.1	


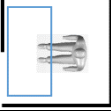
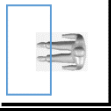
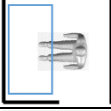
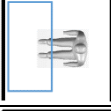
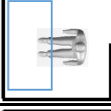
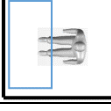
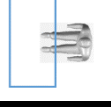
Code explanation: D $\alpha$ -A $\beta$ -F $\gamma$ -T $\delta$ (-S). D (Distance):  $\alpha$ =0-0.2m; 1-0.45m; 2-0.61m. A (Angle):  $\beta$ =0-0°; 1-10°. F (Flowrate):  $\gamma$ =1-15.5cfm; 2-29.4cfm; 3-40.0cfm. T (Supply Temperature):  $\delta$ =1-20.2°C; 2-23.1°C; 3-26.1°C. (-S): Sport Shirt.

After the test of the  $\mu$ X, the cubicle came in. The partitions of the cubicle were placed around the workstation and could be opened on all the four sides. Firstly the cubicle was tested as fully closed, and then the cubicle was opened in half and whole on each side. Without the  $\mu$ X, the cubicle was tested in a simulated total-volume-ventilated room with a set-point of 26.1 °C or 23.9 °C; and after that, it was tested with the  $\mu$ X on as well. In these tests, the manikin was always placed 0.20 m away from the desk edge and dressed in a polo shirt. When the  $\mu$ X was on, 0.0139 m<sup>3</sup>/s (29.4 cfm) of air at 23.0 °C was supplied horizontally (shooting angle = 0°) to the manikin. The manikin surface heat flux from each

segment was recorded as well as the temperature distribution inside the cubicle. The experimental condition of each set of tests was summarized in Table 6-3.

Table 6-3 Experimental conditions of the cubicle tests

Case Code	Cubicle Opening	Room Return Temp (°C)	$\mu X$	Case Code	Cubicle Opening	Room Return Temp (°C)	$\mu X$
FC-0-0-H		26.1	Off	FC-0-1-H		26.1	On
OF-1-0-H				OF-1-1-H			
OF-2-0-H				OF-2-1-H			
OL-1-0-H				OL-1-1-H			
OL-2-0-H				OL-2-1-H			
OB-1-0-H				OB-1-1-H			
OB-2-0-H				OB-2-1-H			
FO-2-0-H				FO-2-1-H			
Case Code	Cubicle Opening	Room Return Temp (°C)	$\mu X$	Case code explanation: XX-A-B-C			

FC-0-0-L		23.9	Off	XX: Opening direction; FC-Fully Closed; OF-Open from the Front; OL-Open from the Left; OB-Open from the Back; FO-Fully Open. A: Opening size; 0-fully closed; 1-half open; 2-fully open. B: $\mu$ X operating condition; 0-off; 1-on. C: Background temperature set-point; H-High (79°F); L-Low (75°F)
OF-1-0-L				
OF-2-0-L				
OL-1-0-L				
OL-2-0-L				
OB-1-0-L				
OB-2-0-L				
FO-2-0-L				

## 6.2. Micro-Environmental Control System in Cooling Condition

### 6.2.1. Effects of the Distance between the Diffuser and the Manikin

To quantify the effects of the distance between the diffuser and the manikin, six sets of experiments were conducted. The supply flow rate and temperature were fixed at 0.0139 m<sup>3</sup>/s (29.4 cfm) and 23.0 °C. The manikin was moved from 0.20 m, to 0.45 m and 0.61 m away from the diffuser. Both 0° and 10° shooting angles were tested in the experiment. The experimental results were summarized in Table 6-4. It was found that with the same shooting angle, the total heat loss increased with the distance. Especially when the shooting angle was 0°, the total heat loss increased from 96.4 W for 0.20 m distance to 102.4 W for

0.61 m distance, which gives a difference of 6.0 W. This is different with what we found previously when the manikin was naked. The possible reason for that was the existence of the clothes changed the surface properties of the manikin. With a loose polo shirt, many wrinkles together with the knit structure changed the flow over the chest and stomach. When the diffuser was closed to the manikin, the jet was narrow and not able to spread thoroughly over the manikin surface because of the wrinkles; however, when the diffuser was far away, the jet was able to develop and blow on larger area of the manikin surface, so even though the jet's spread was constrained, a little more heat was removed. This explanation can be verified by Figure 6-7. When the manikin was further away from the manikin, more heat was removed from the chest, forearms, hands, and thighs.

Table 6-4 Experimental results of the cases with different distances between the diffuser and the manikin

	BL	D1-A0- F2-T2	D1-A1- F2-T2	D2-A0- F2-T2	D2-A1- F2-T2	D3-A0- F2-T2	D3-A1- F2-T2
Distance from the Diffuser (m)	0.20	0.20	0.20	0.45	0.45	0.61	0.61
Shooting Angle (°)		0	10	0	10	0	10
Room Supply Temp (°C)	24.84 (± 0.65)	25.99 (± 0.42)	25.95 (± 0.42)	25.99 (± 0.41)	26.01 (± 0.48)	25.66 (± 0.33)	25.65 (± 0.27)
Room Return Temp (°C)	26.09 (± 0.06)	26.15 (± 0.05)	26.17 (± 0.05)	26.16 (± 0.04)	26.22 (± 0.06)	26.12 (± 0.05)	26.08 (± 0.03)
μX Supply		23.01 (± 0.05)	23.02 (± 0.06)	23.13 (± 0.05)	23.16 (± 0.07)	22.84 (± 0.10)	23.03 (± 0.08)



Temp (°C)							
$\mu$ X Supply Flowrate (cfm)		29.6	29.8	29.4	29.3	29.4	29.5
Averaged Heat Flux (W/m <sup>2</sup> )	41.10 (± 0.39)	53.19 (± 0.18)	54.81 (± 0.22)	53.83 (± 0.23)	56.78 (± 0.21)	56.46 (± 0.23)	56.75 (± 0.16)
Total Heat loss (W)	74.5 (± 0.7)	96.4 (± 0.3)	99.4 (± 0.4)	97.6 (± 0.4)	102.9 (± 0.4)	102.4 (± 0.4)	102.9 (± 0.3)
Extra Heat Loss (W)		<b>21.9</b>	<b>24.9</b>	<b>23.1</b>	<b>28.4</b>	<b>27.8</b>	<b>28.4</b>

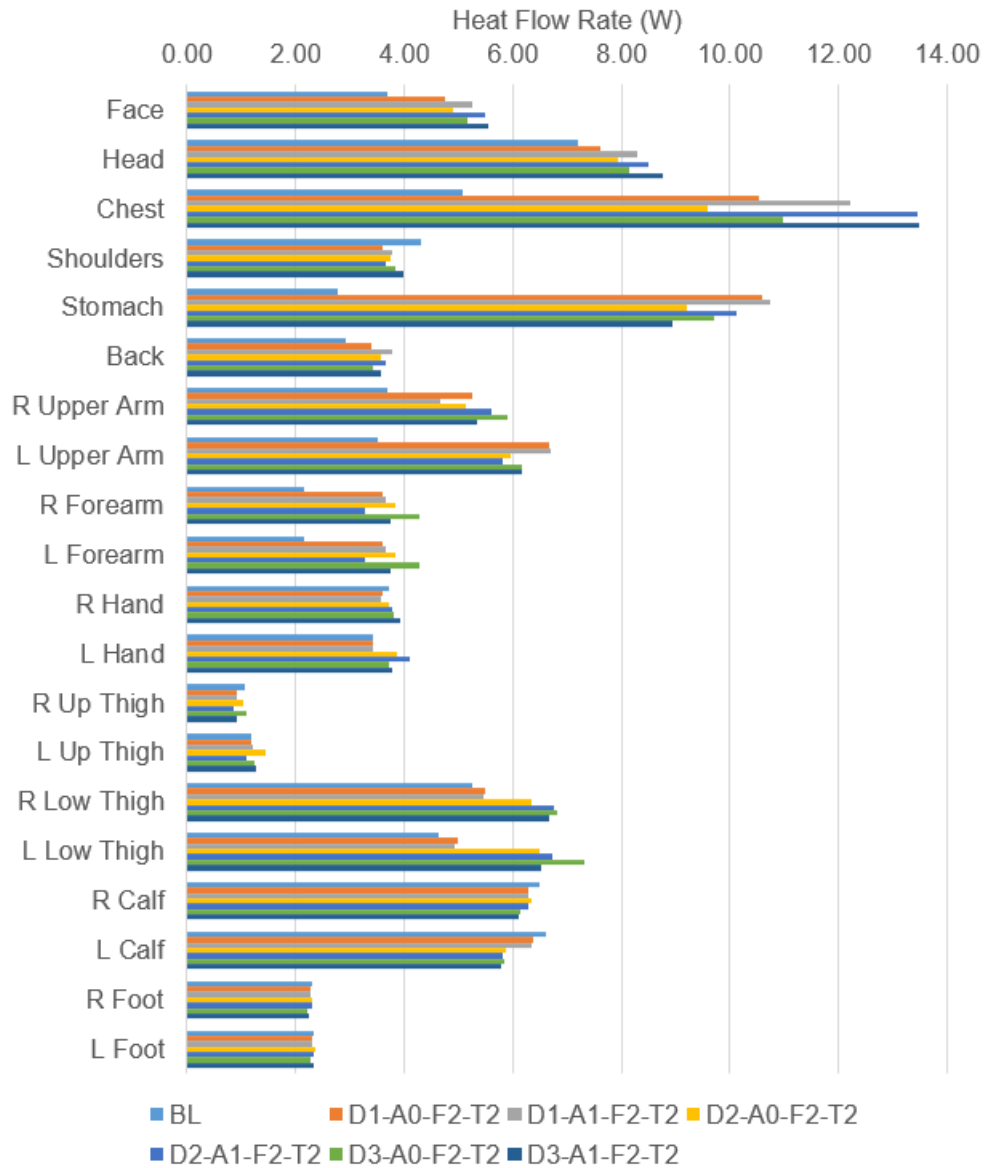


Figure 6-7 Segmental heat flow rates of the cases with different distances

### 6.2.2. Effect of the Shooting Angle

Another interesting finding which we can get from Table 6-4 is that with the same distance the 10° shooting angle removed more heat from the manikin, which is consistent with the previous results found in Sec. 4.2.4. At the distance of 0.20 m, 0.45 m, and 0.61 m, the jet

with a shooting angle of  $10^\circ$  was able to remove 2.9 W, 5.3 W, and 0.5 W more than that of  $0^\circ$  shooting angle. Figure 6-7 shows that most of the difference comes from the stomach and chest. Since the supply air flow rate, supply temperature, and the distance did not change, this increment is exclusively due to a higher convective heat transfer coefficient, which resulted from two reasons: on the one hand, when the shooting angle was changed from  $0^\circ$  to  $10^\circ$  by adjusting the louver, the cross-section of the jet was reduced, and the jet supply velocity was increased; on the other hand, the larger shooting angle made the jet blow onto a larger area of the body. This effect could be confirmed by more test results in Figure 6-8. Note that the extra heat removed is the manikin heat loss difference between the case with the  $\mu X$  and without the  $\mu X$  (Case BL). For all the combinations of supply flow rate and temperature tested except 15.5 cfm + 26.1 °C case, the  $10^\circ$  shooting angle removed more heat than the  $0^\circ$ .

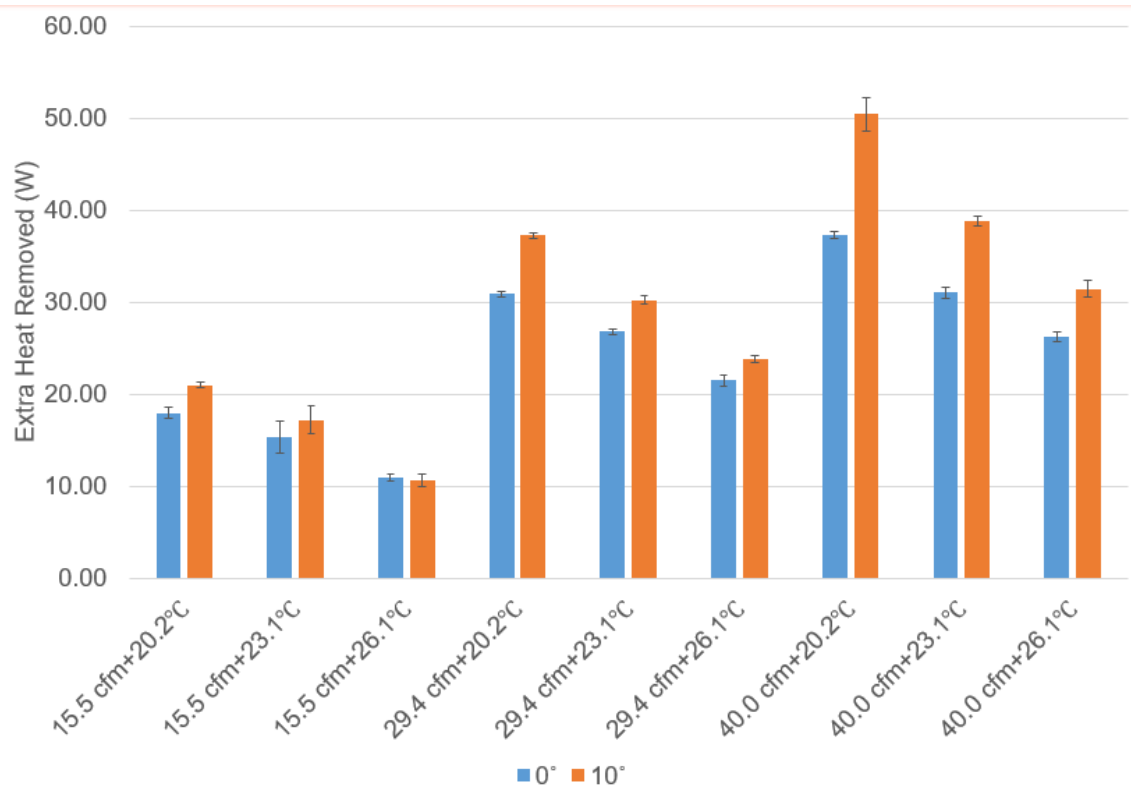


Figure 6-8 Effect of the shooting angle

### 6.2.3. Effect of the Supply Flow Rate and Supply Temperature

In Sec.4.2.3, the effect of the supply flow rate and temperature has been partially investigated by CFD. However, that part of work focused more on the combinatorial effect of them (ensuing 50 W cooling power) instead of the individual effect. This current and the next subsection focused on the individual effect of the supply flow rate and temperature. Figure 6-9 looks into the effect of the supply flow rate for each combination of shooting angle and supply temperature. It was shown that the extra heat flow rate increased with the air flow rate no matter what shooting angle or supply temperature it was. Figure 6-10 looks into the effect of the supply temperature for each combination of shooting angle and supply

flow rate. It shows that the extra heat removed was negatively correlated with the supply temperature.

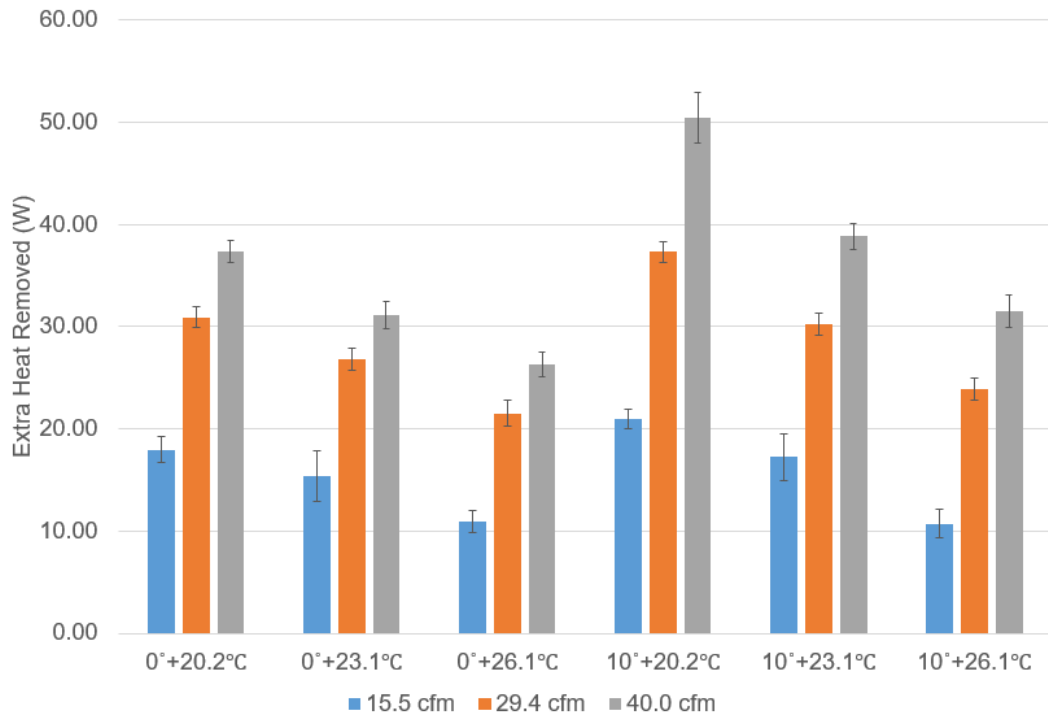


Figure 6-9 Effect of the supply flow rate

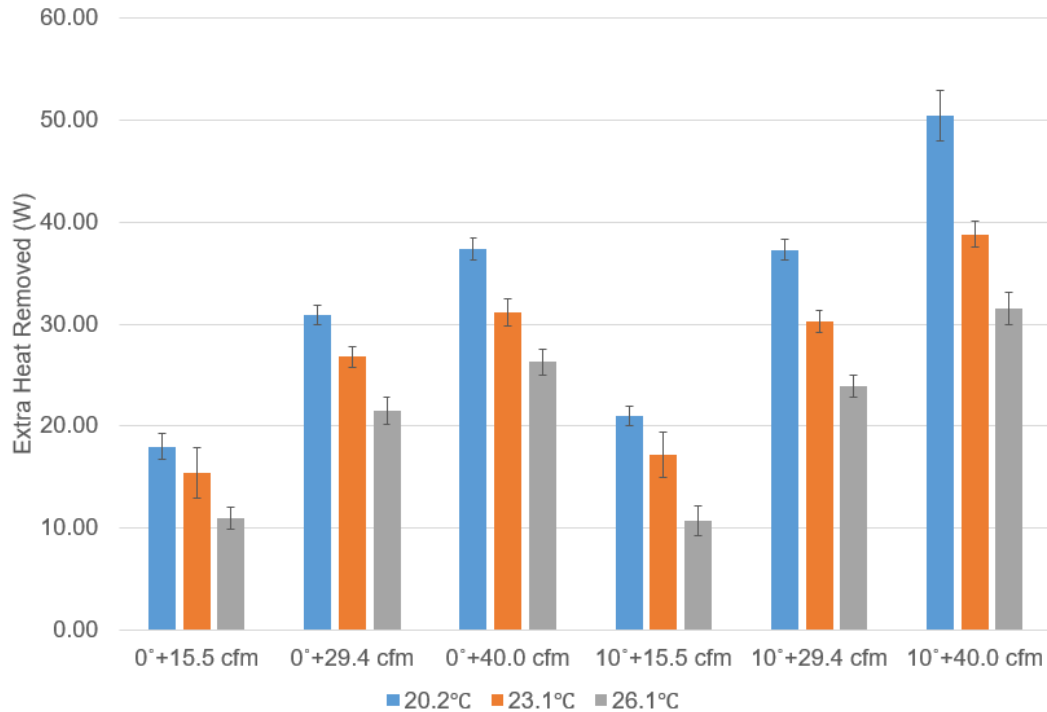


Figure 6-10 Effect of the supply temperature

However, in order to quantify the cooling efficiency, the extra heat loss was divided by the cooling power provided to the  $\mu X$  and the fan power (ebm papst 2017a, 2017b, 2017c) consumed to give us the overall cooling efficiency:

$$\eta = \frac{\dot{Q}_{total,i} - \dot{Q}_{total,BL}}{P} \quad (6 - 1)$$

The results show that the cooling efficiency dramatically increased with the supply temperature (Figure 6-11). With 20.2 C supply temperature, the cooling efficiency was between 25-40%. With 23.1 C supply temperature, the cooling efficiency was between 40-60%. But with 26.1 C supply temperature, the cooling efficiency was way over 300%.

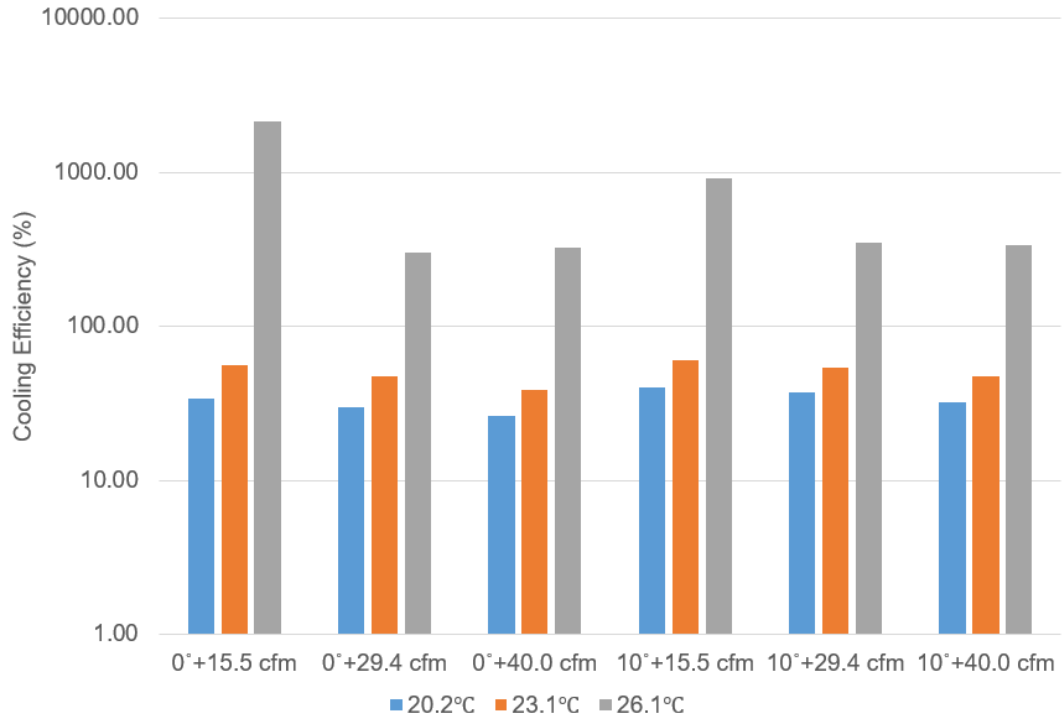


Figure 6-11 Cooling efficiency

#### 6.2.4. Effect of the Clothing Material

As the first layer between the human body and surrounding environment, the clothes play an important role in determining the thermal comfort of the human body. The comfort of the garment is the complex effect of textile properties which are basically dependent on the chemical structure and morphology of the constituent fibers. Comfort properties of textile products such as yarns, fabrics, mats and any other products that are used for wearing purposes embrace different mechanical properties including heat and moisture transfer (Song 2011). This subsection includes the work of testing the  $\mu X$  using a manikin dressed in either a polo shirt or a sports shirt (Figure 6-12). An obvious difference between these two garments is that there are many wrinkles with a loose shirt which create some air

pockets between the skin surface of the manikin and the clothes, while the sports shirt is tightly attached to the skin surface.



Figure 6-12 Manikin dressed in a polo shirt (left) and a sports shirt (right)

The experimental results are summarized in Table 6-5. It was found that the clothing material did affect the heat loss from the manikin a lot. Although both of the two shirts are short sleeve shirt, the manikin with the sports shirt released above 10.0 W more than the manikin with the polo shirt. Another interesting finding is that when the manikin was dressed in a sports shirt, the extra heat loss taken by the manikin was negatively correlated to the distance between the diffuser and the manikin. This is different from the case with a polo shirt. The reason was explained in Sec. 6.2.1 and can be confirmed by Figure 6-13. When the manikin was dressed in the sports shirt, there were no wrinkles, and the clothes surface was as smooth as a naked manikin. When the jet hit on it, regardless of how far the



manikin was away from the diffuser, it was easy for the jet to spread, and because of the development of the jet, its cooling capacity decreased with the distance.

Table 6-5 Experimental results with different clothing material

	BL	D1-A0-F2-T2	D3-A0-F2-T2	BL-S	D1-A0-F2-T2-S	D3-A0-F2-T2-S
Distance from the Diffuser (m)	0.20	0.20	0.61	0.20	0.20	0.61
Shooting Angle (°)		0	0		0	0
Room Supply Temp (°C)	24.84 (± 0.65)	25.99 (± 0.42)	25.66 (± 0.33)	23.54 (± 0.16)	25.00 (± 0.10)	24.97 (± 0.11)
Room Return Temp (°C)	26.09 (± 0.06)	26.15 (± 0.05)	26.12 (± 0.05)	26.10 (± 0.04)	26.12 (± 0.02)	26.12 (± 0.04)
μX Supply Temp (°C)		23.01 (± 0.05)	22.84 (± 0.10)		23.16 (± 0.04)	23.00 (± 0.05)
μX Supply Flowrate (cfm)		29.6	29.4		29.5	29.5
Averaged Heat Flux (W/m <sup>2</sup> )	41.10 (± 0.39)	53.19 (± 0.18)	56.46 (± 0.23)	47.50 (± 0.20)	68.48 (± 0.13)	67.57 (± 0.16)
Total Heat loss (W)	74.5 (± 0.7)	96.4 (± 0.3)	102.4 (± 0.4)	86.1 (± 0.4)	124.2 (± 0.2)	122.5 (± 0.3)
Extra Heat Loss (W)		<b>21.9</b>	<b>27.8</b>		<b>38.0</b>	<b>36.4</b>

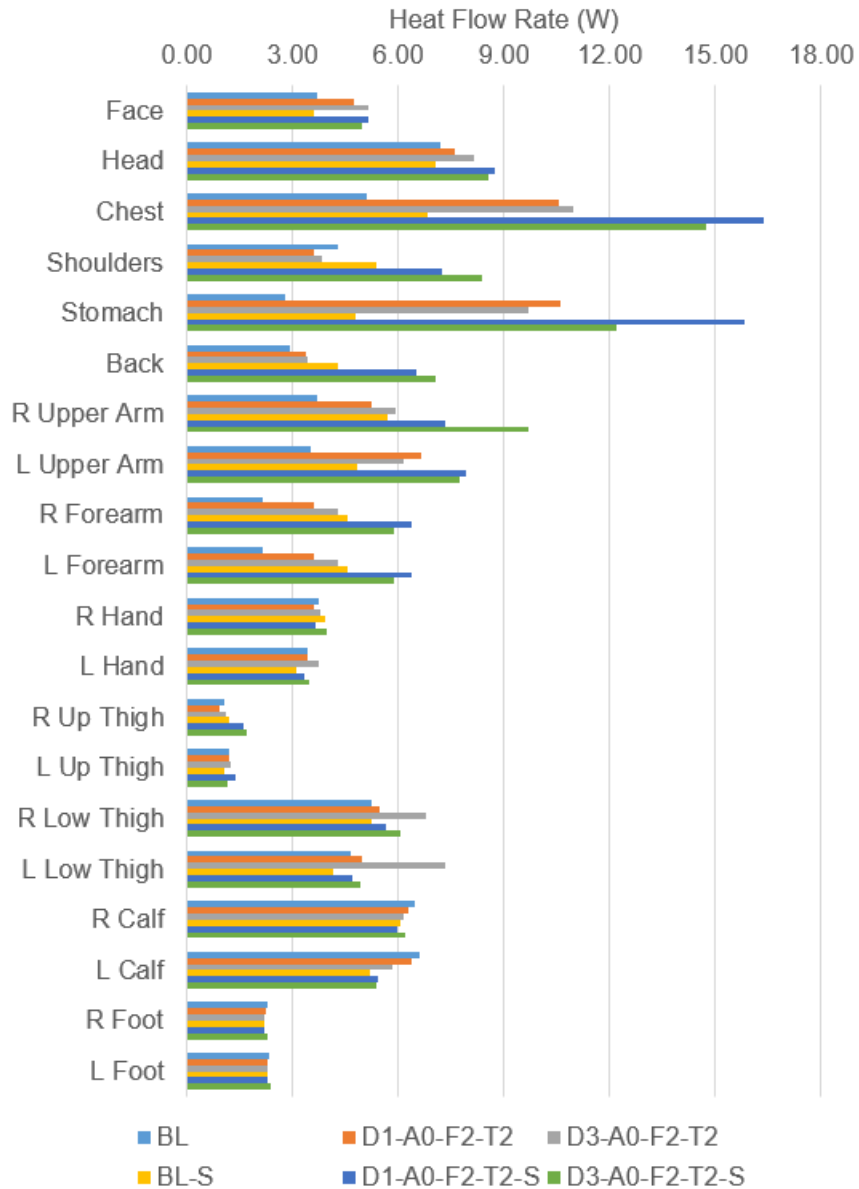


Figure 6-13 Segmental heat flow rates of the cases with different clothing material

### 6.3. Effects of the Semi-Open Space

Office cubicles, as a common form of the semi-open space, have become increasingly popular in the past few decades, because it can give the occupants privacy as well as promote communication and collaboration among them. However, it has drawn attention

from the researchers and engineers that the partitions in the office can lead to a large variation of IAQ and thermal comfort level ( Bauman et al. 1991; Bauman et al. 1992; Lee and Awbi 2004; Posner et al. 2003). Very few studies have been done on this when a micro-environmental control system is used. This section discusses the effects of the cubicle on the thermal environment based on experimental results.

### **6.3.1. With v.s. Without the Cubicle**

The cubicle was tested first under the mixing ventilation. The conditioned air was supplied from the ceiling and entered the occupied space from the front (Figure 6-1). The test was conducted with the cubicle fully closed and then fully opened one side at a time. The test results are summarized in Table 6-6. Without the cubicle, the manikin released 74.5 W heat to the ambiance. However, with the cubicle, the total heat loss of the manikin was reduced by 1 to 8 W depending on the opening direction and opening size. When the cubicle was fully closed (some cubicles have sliding doors), the manikin released only 66.4 W heat with the same return air temperature. There are two reasons for this. On the one hand, the cubicle partitions prevent the background airflow from blowing on the manikin. As shown in Figure 6-14, the spatially averaged velocity was reduced from 0.104 m/s to 0.090 m/s. Especially at the lower level closed to the floor, because the supply air was cooler than the room temperature, the air velocity was always much higher when there was no cubicle. On the other hand, because of the cubicle partition, most of the heat released was kept in the cubicle. Figure 6-15 compares the temperature in the occupied space with and without the cubicle. With the closed cubicle, the temperature measured inside the cubicle were all

higher than the temperature without the cubicle. The average temperature with the cubicle was around 0.4 °C higher than that without the cubicle.

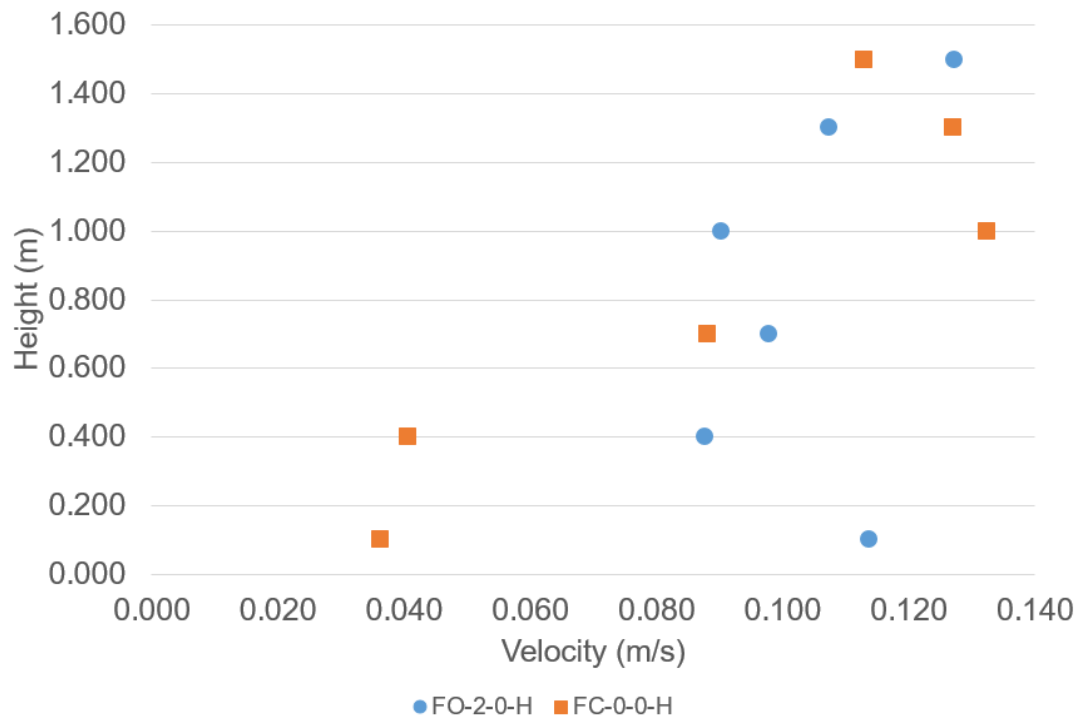


Figure 6-14 Velocity in the occupied space (26.1 °C)

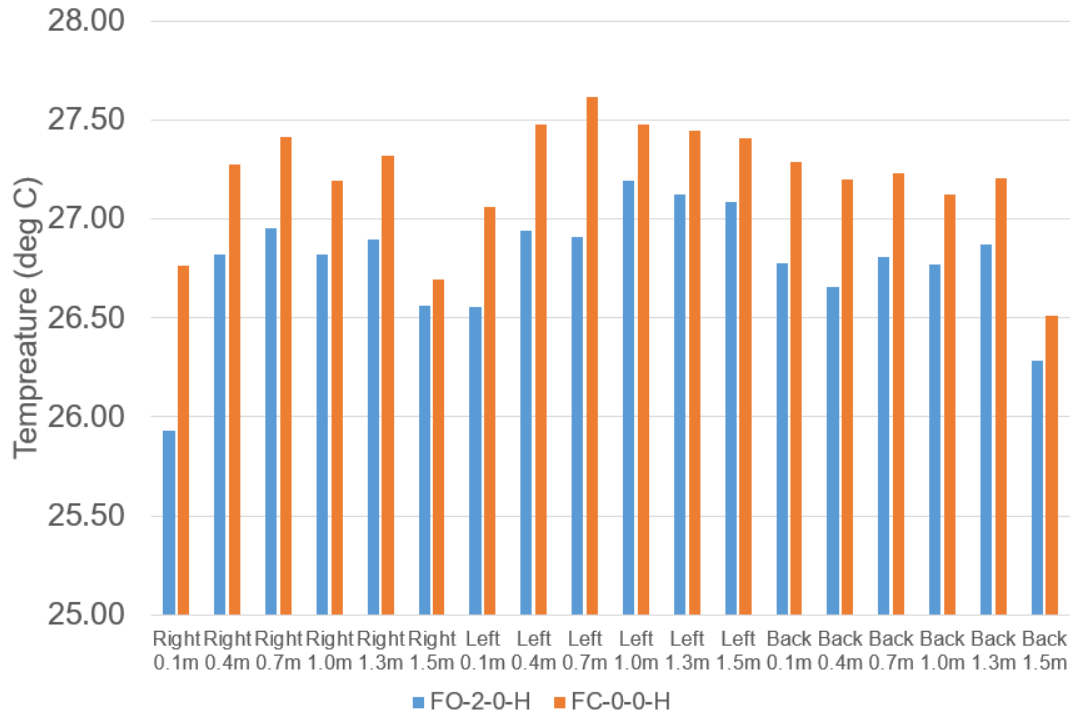


Figure 6-15 Temperature in the occupied space with v.s. without cubicle (26.1 °C)

Similar phenomena can be observed from the results of the cases when the room temperature set-point was 23.9 °C. Table 6-7 shows the test results of the 23.9 °C set-point. With a lower set-point, the difference between the case with a closed cubicle and without a cubicle was even more significant. Without the cubicle, the manikin released 100.24 W heat to the ambience. However, when the cubicle was fully closed (some cubicles have sliding doors), the manikin released only 85.87 W heat with the same return air temperature. The explanation mentioned before is confirmed by these cases. The average velocity was reduced from 0.115 m/s to 0.081 m/s (Figure 6-16), and the average temperature with the cubicle was around 0.6 °C higher than that without the cubicle (Figure 6-17).

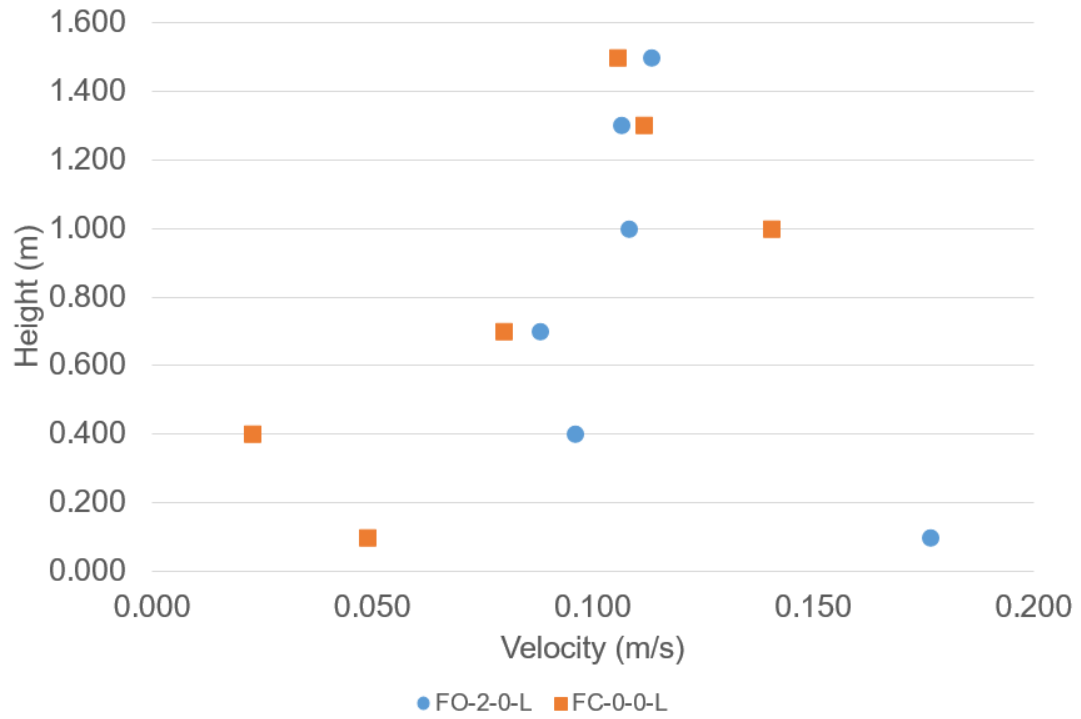


Figure 6-16 Velocity in the occupied space (23.9 °C)

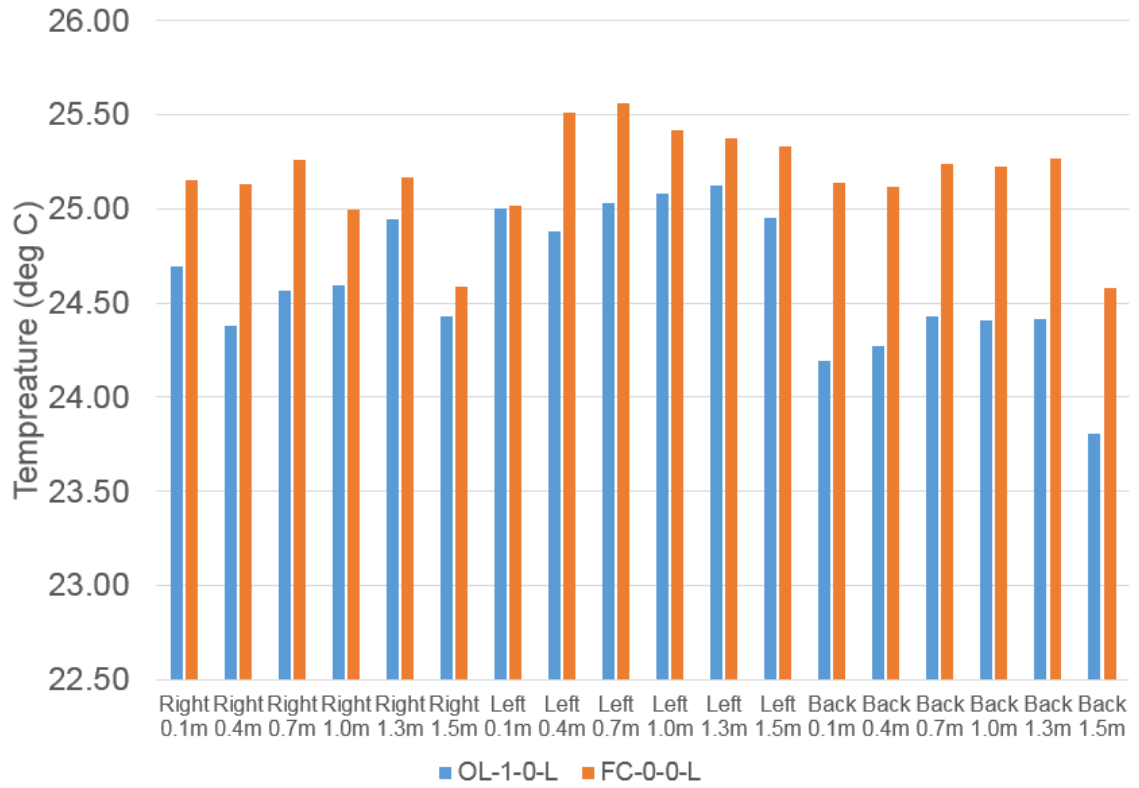


Figure 6-17 Temperatures at different heights from the floor in the occupied space with v.s. without cubicle (return air temperature: 23.9 °C)

Table 6-6 Summarized test results of the partitioned office without  $\mu$ X at 26.1 °C return air temperature

	FC-0-0-H	OL-1-0-H	OL-2-0-H	OB-1-0-H	OB-2-0-H	OF-1-0-H	OF-2-0-H	FO-2-0-H
Open Direction	N/A	Left	Left	Back	Back	Front	Front	Fully
Opening Width (ft)	N/A	3	6	3	6	3	6	6
Room Supply Temp (°C)	23.89 ( $\pm$ 0.73)	23.81 ( $\pm$ 0.57)	23.88 ( $\pm$ 0.39)	23.02 ( $\pm$ 0.71)	23.88 ( $\pm$ 0.34)	23.38 ( $\pm$ 0.41)	23.63 ( $\pm$ 0.35)	24.84 ( $\pm$ 0.65)
Room Return Temp (°C)	26.06 ( $\pm$ 0.08)	26.10 ( $\pm$ 0.07)	26.09 ( $\pm$ 0.05)	25.93 ( $\pm$ 0.08)	26.16 ( $\pm$ 0.05)	26.17 ( $\pm$ 0.05)	26.14 ( $\pm$ 0.05)	26.09 ( $\pm$ 0.06)
$\mu$ X Supply Temp (°C)	N/A							
$\mu$ X Supply Flowrate (cfm)	N/A							
Averaged Heat Flux (W/m <sup>2</sup> )	36.60 ( $\pm$ 0.23)	39.73 ( $\pm$ 0.22)	38.69 ( $\pm$ 0.22)	40.41 ( $\pm$ 0.34)	38.38 ( $\pm$ 0.15)	37.25 ( $\pm$ 0.30)	40.25 ( $\pm$ 0.13)	41.10 ( $\pm$ 0.39)
Total Heat loss (W)	66.4 ( $\pm$ 0.4)	72.0 ( $\pm$ 0.4)	70.1 ( $\pm$ 0.4)	73.3 ( $\pm$ 0.6)	69.6 ( $\pm$ 0.3)	67.5 ( $\pm$ 0.5)	73.0 ( $\pm$ 0.2)	74.5 ( $\pm$ 0.7)
Adjusted Total Heat loss (W)	66.0	72.0	70.1	71.7	70.1	68.1	73.4	74.4



Table 6-7 Summarized test results of the partitioned office without  $\mu$  X at 23.9 °C return air temperature

	FC-0-0-L	OL-1-0-L	OL-2-0-L	OB-1-0-L	OB-2-0-L	OF-1-0-L	OF-2-0-L	FO-2-0-L
Open Direction	N/A	Left	Left	Back	Back	Front	Front	Fully
Opening With (ft)	N/A	3	6	3	6	3	6	6
Room Supply Temp (°C)	20.70 ( $\pm$ 0.21)	20.00 ( $\pm$ 0.29)	20.70 ( $\pm$ 0.20)	20.69 ( $\pm$ 0.19)	20.69 ( $\pm$ 0.27)	20.85 ( $\pm$ 0.86)	20.89 ( $\pm$ 0.62)	20.36 ( $\pm$ 3.19)
Room Return Temp (°C)	23.97 ( $\pm$ 0.05)	23.78 ( $\pm$ 0.05)	23.92 ( $\pm$ 0.03)	24.03 ( $\pm$ 0.05)	23.93 ( $\pm$ 0.05)	23.91 ( $\pm$ 0.07)	23.88 ( $\pm$ 0.05)	23.87 ( $\pm$ 0.28)
$\mu$ X Supply Temp (°C)	N/A							
$\mu$ X Supply Flowrate (cfm)	N/A							
Averaged Heat Flux (W/m <sup>2</sup> )	47.37 ( $\pm$ 0.35)	53.50 ( $\pm$ 0.18)	52.15 ( $\pm$ 0.26)	51.97 ( $\pm$ 0.21)	51.27 ( $\pm$ 0.15)	50.86 ( $\pm$ 0.49)	53.79 ( $\pm$ 0.27)	55.29 ( $\pm$ 2.04)
Total Heat loss (W)	85.9 ( $\pm$ 0.6)	97.0 ( $\pm$ 0.3)	94.6 ( $\pm$ 0.5)	94.2 ( $\pm$ 0.4)	93.0 ( $\pm$ 0.3)	92.2 ( $\pm$ 0.9)	97.5 ( $\pm$ 0.5)	100.2 ( $\pm$ 3.7)
Adjusted Total Heat loss (W)	85.0	94.4	93.0	93.7	91.4	90.4	95.8	100.9

### 6.3.2. Effect of the Opening Size of the Cubicle

The effect of the opening size of the cubicle was tested in the study. The front, left or back sides of the cubicle were either half or fully opened in each pair of the experiments. The test results for the cases with higher temperature set-point were listed in Table 6-6. It was unexpected that the case with half opening on the back side had a total heat loss of 73.3 W, which was the highest of all the six cases. This was partially because the return air temperature of this case was 25.93 °C, which was a little less than that in the other cases. For a better comparison, the total heat loss was adjusted based on the set-point and the measured value of the return air temperature:

$$\dot{Q}_{adj.} = \dot{Q}_{meas.} \cdot \frac{T_{skin} - T_{r,set}}{T_{skin} - T_{r,meas}}$$

where  $\dot{Q}_{adj.}$  is the adjusted total heat loss,  $\dot{Q}_{meas.}$  is the measured total heat loss,  $T_{skin}$  is the manikin skin surface temperature (33.9 °C),  $T_{r,set}$  is the set-point of the return air temperature (26.1 °C), and  $T_{r,meas}$  is the measured return air temperature.

The adjusted total heat loss removes the effect of return air temperature difference and allows the comparison to be focused on the effect of the opening size of the partition. After the adjustment, it is shown that when the cubicle was opened from the left and back side, the total heat loss was within  $71.0 \pm 1.0$  W, with the half open cases a little higher than the fully open cases. However, when the cubicle was opened from the front, a much larger difference was observed between half open and fully open. With half openness, the total heat loss from the manikin was 68.1 W, but this number increased to be 73.4 W with full openness, which is the closest to the number of the fully-open case (FO-2-0-H). It is easy

to understand that when the front side was fully opened, the total heat loss from the manikin was the second highest following the fully-open case (FO-2-0-H) because the cooler supply air could get to the occupied space without any block. However, it is interesting to find that half-open case yielded the second lowest total heat loss, which is even lower than the cases with an opening from the left and back side. A possible explanation can be obtained from Figure 6-18, which compares the temperature distribution in the occupied space when the cubicle was opened half or completely in the front. It can be observed that when the cubicle was half open because the opening was the left half part of the front side cooler air entered the cubicle through the left lower part of the front side – in case OF-1-0-H, Left 0.1m, and Left 0.4m had lower temperatures than OF-2-0-H. However, because either the amount of this part of air was too small or it went out of the cubicle before mixing, the remaining space - especially the right half side of the cubicle – was hotter than the case of OF-2-0-H.



Figure 6-18 Temperature in the occupied space with opening in the front (26.1 °C)

The similar conclusion could be drawn from the results of the cases with lower set-point (Table 6-7). Among all the partially opened cubicle cases, the one fully opened in the front (OF-2-0-L) yielded the highest total heat loss while the one half-opened in the front (OF-1-0-L) yielded the lowest total heat loss. The explanation is the same with that mentioned previously (Figure 6-19).

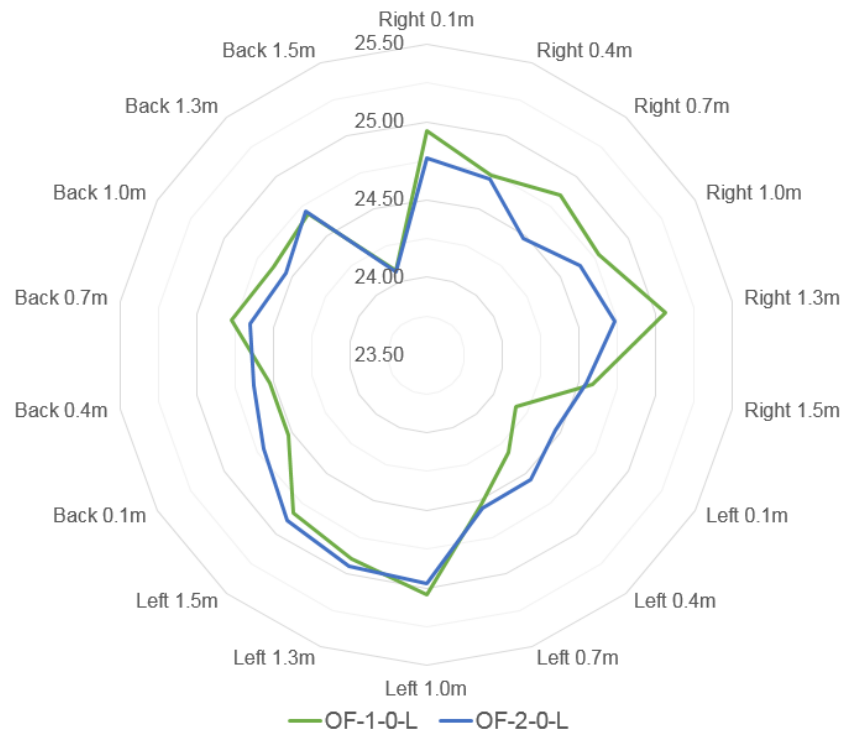


Figure 6-19 Temperature in the occupied space with opening in the front (23.9 °C)

### 6.3.3. Cubicle with $\mu X$

The cubicle was then tested with the  $\mu X$ . The results are summarized in Table 6-8. It can be observed that different from the cases without the  $\mu X$ , the effect of the cubicle on the thermal response of the manikin was not that obvious (Figure 6-20). The difference of the

total heat loss of the manikin between with and without the cubicle was smaller compared with that of the cases without the  $\mu X$ . Figure 6-20 illustrates the percentage of increased heat loss compared with the case with a fully closed cubicle. When the room background temperature was set to be 23.9 °C and without the  $\mu X$ , opening the cubicle resulted in as high as 18.7% increment in the total heat loss. This number was reduced to 12.7% when the room temperature was set to be 26.1 °C and further reduced to 6.9% when the  $\mu X$  was turned on. This means that the  $\mu X$  helps reduce the dependence of the micro-environment of the human body on the background environment, which is the macro-environment.

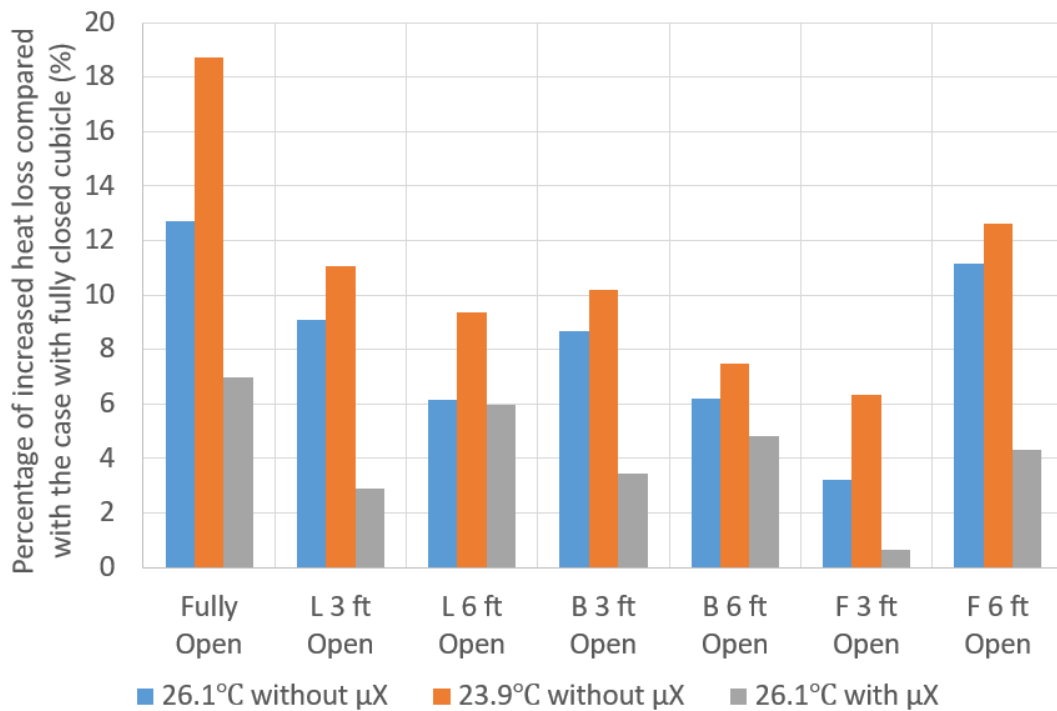


Figure 6-20 Percentage of increased heat loss compared with the case with fully closed cubicle

Table 6-8 Summarized test results of the partitioned office with  $\mu$ X at 26.1 °C return air temperature

	FC-0-1-H	OL-1-1-H	OL-2-1-H	OB-1-1-H	OB-2-1-H	OF-1-1-H	OF-2-1-H	FO-2-1-H
Open Direction	N/A	Left	Left	Back	Back	Front	Front	Fully
Opening With (ft)	N/A	3	6	3	6	3	6	6
Room Supply Temp (C)	24.93 ( $\pm$ 0.50)	24.73 ( $\pm$ 0.22)	24.97 ( $\pm$ 0.21)	25.03 ( $\pm$ 0.30)	25.09 ( $\pm$ 0.88)	25.00 ( $\pm$ 0.21)	24.93 ( $\pm$ 0.63)	28.42 ( $\pm$ 0.10)
Room Return Temp (C)	26.13 ( $\pm$ 0.06)	26.06 ( $\pm$ 0.03)	26.02 ( $\pm$ 0.05)	26.23 ( $\pm$ 0.04)	26.17 ( $\pm$ 0.07)	26.15 ( $\pm$ 0.03)	26.20 ( $\pm$ 0.05)	26.15 ( $\pm$ 0.05)
$\mu$ X Supply Temp (C)	23.21 ( $\pm$ 0.13)	23.04 ( $\pm$ 0.11)	22.86 ( $\pm$ 0.11)	23.12 ( $\pm$ 0.05)	23.10 ( $\pm$ 0.05)	23.17 ( $\pm$ 0.05)	23.18 ( $\pm$ 0.05)	22.96 ( $\pm$ 0.04)
$\mu$ X Supply Flowrate (cfm)	29.3	29.3	29.3	29.5	29.3	29.4	29.4	29.1
Averaged Heat Flux (W/m <sup>2</sup> )	51.87 ( $\pm$ 0.32)	53.36 ( $\pm$ 0.24)	54.97 ( $\pm$ 0.22)	53.66 ( $\pm$ 0.16)	54.38 ( $\pm$ 0.52)	52.21 ( $\pm$ 0.22)	54.11 ( $\pm$ 0.26)	55.48 ( $\pm$ 0.28)
Total Heat loss (W)	94.0 ( $\pm$ 0.6)	96.8 ( $\pm$ 0.4)	99.7 ( $\pm$ 0.4)	97.3 ( $\pm$ 0.3)	98.6 ( $\pm$ 0.9)	94.7 ( $\pm$ 0.4)	98.1 ( $\pm$ 0.5)	100.6 ( $\pm$ 0.5)

#### 6.4. Thermal Response Evaluation

The thermal response of the manikin was evaluated using the Clothing Independent Thermal Comfort Model (Håkan O. Nilsson 2007). The Mean Thermal Vote (MTV) of each segment, as well as the whole body, was predicted based on the heat flux measurement. **Figure 6-21** shows the whole-body MTV prediction of the cases with different distances between the manikin and the diffuser. The case FO-2-0-L represents the case with the normal set-point of 75.0 °F and without the  $\mu X$ , which represents the comfortable scenario (Slightly cool, -0.90). After the set-point was raised to 79.0 °F, the MTV was shifted to the warm side. While with the  $\mu X$ , the whole-body MTV could be drawn back to the cool side and around the number of FO-2-0-L.

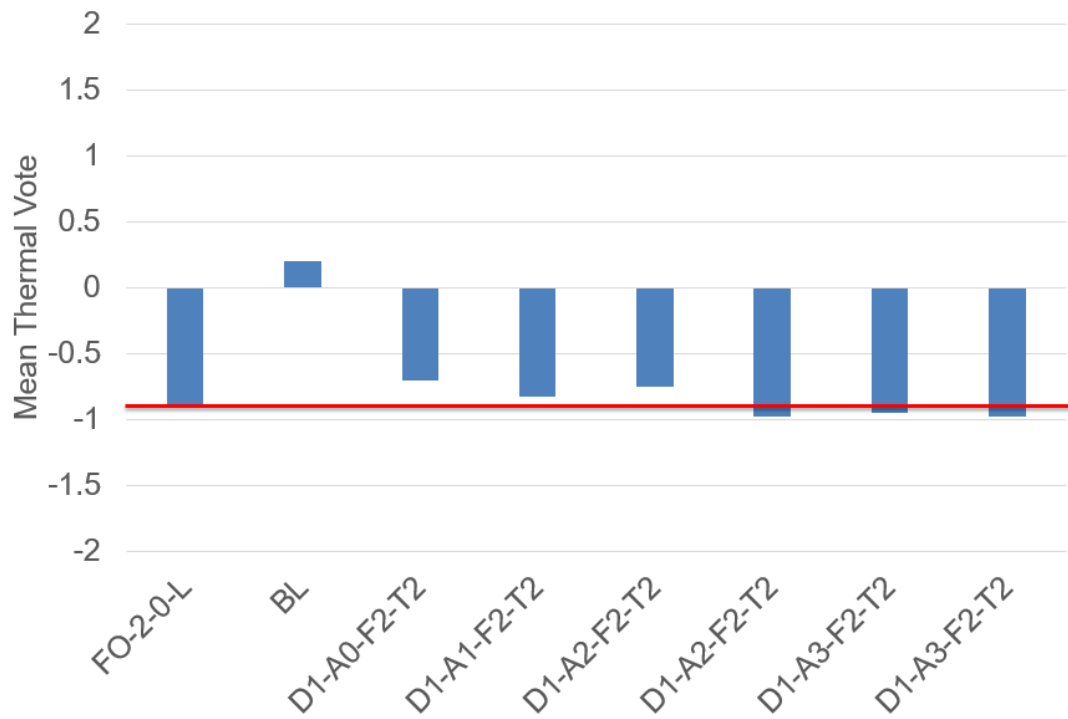


Figure 6-21 Whole-body MTV prediction of the cases with different distances

Figure 6-22 shows the whole-body MTV of the cases with different supply temperatures and flow rates. With 15.5 cfm supply flow rate, the  $\mu X$  brought the MTV to the cool side but was not able to fully recover the thermal sensation level at 75 °F set-point. Even with only 20.0 °C supply temperature, the predicted MTV was at most -0.71 which is closer to the neutral than -0.90. However, with 29.4 cfm supply air, the  $\mu X$  could bring the MTV value to the comfort level except when the supply temperature was 26.0 °C. The cases with 40.0 cfm supply flow rate could bring the whole-body MTV all the way to the cold side of the comfort level (>1). Moreover, when the supply temperature was 20.0 °C, with 10° shooting angle, the MTV level was as low as -1.83.

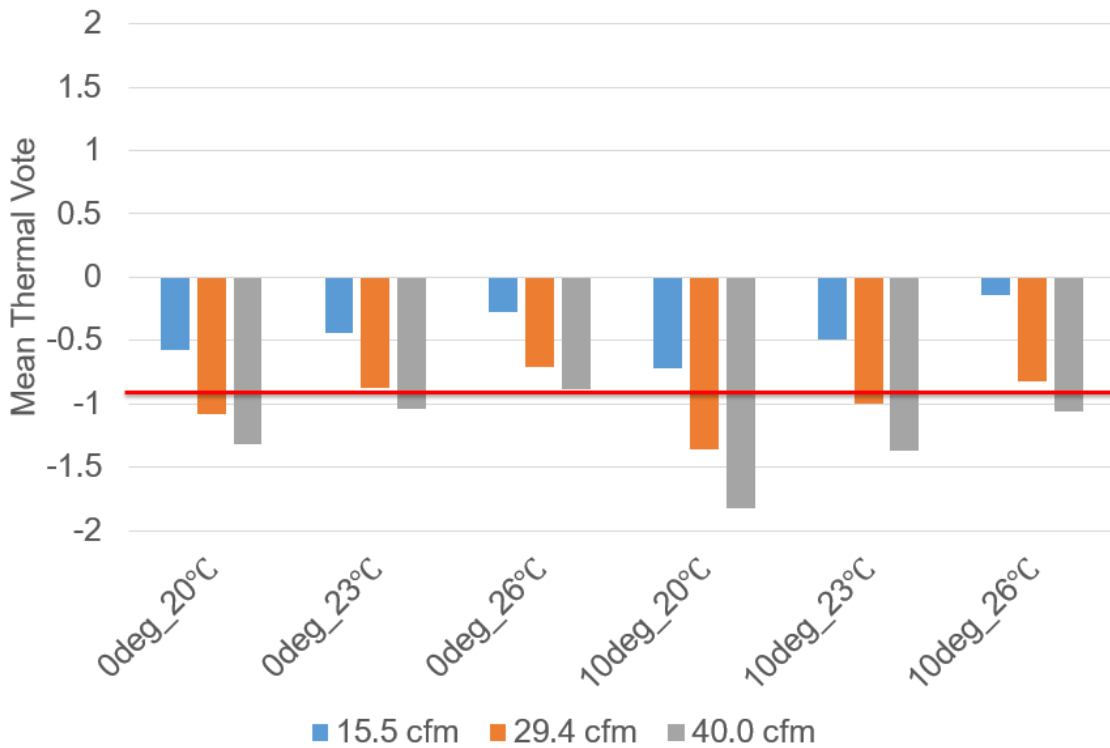


Figure 6-22 Whole-body MTV prediction of the cases with different supply temperatures and flow rates



The cubicle does also change the thermal response of the occupants. Figure 6-23 illustrates the predicted MTV of the cases with and without the cubicle. The effect of the cubicle was more obvious when the cubicle was not equipped with the  $\mu$ X. At 26.1 °C background temperature, a fully closed cubicle raised the MTV from 0.20 to 0.54, which exacerbates the thermal sensation; and at 23.9 °C background temperature, the cubicle could even raise the MTV by 0.7 unit at most. Partially opened cubicle yielded MTVs between the one with fully closed cubicle and the one without cubicle. However, with the  $\mu$ X, the predicted MTV was much around the same level, no matter how the cubicle was opened.

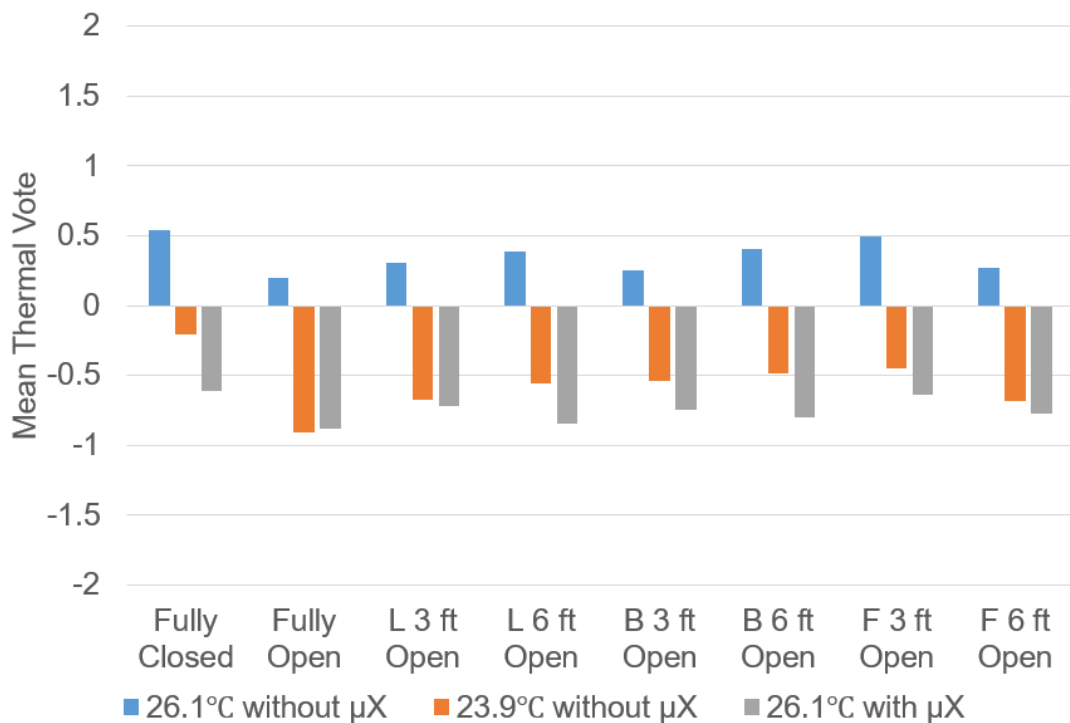


Figure 6-23 Whole-body MTV prediction with and without the cubicle

## 6.5. Summary and Conclusions

Experiments using a thermal manikin and a full-scale chamber were conducted to evaluate the performance of the  $\mu$ X under different conditions and investigate the effects of the cubicle as a semi-open space on the thermal environment of occupants. The results indicate that

- 1) The heat loss by the manikin is sensitive to the distance between the diffuser and the manikin as well as the clothing material. With a loose polo shirt, the heat loss from the manikin increased with the distance, while with a tight sports shirt, the heat loss from the manikin decreased with the distance, when the distance was changed from 0.20 m to 0.61 m.
- 2) Increasing the shooting angle from  $0^\circ$  to  $10^\circ$  resulted in additional heat loss from the manikin. This is attributed to a higher supply air velocity due to a smaller jet cross section and a larger surface area of the manikin which the jet blew onto.
- 3) The heat loss from the manikin was found to be positively correlated with the supply air flow rate, but negatively correlated with the supply temperature. However, the overall cooling efficiency dramatically increased with the supply temperature.
- 4) The existence of the cubicle was found to be able to “protect” the occupants from the background air flow by reducing the average velocity and increasing the average temperature in the occupied space. The openness of the cubicle weakened the “protection” of the cubicle to different extends depending on the opening direction and size. Fully opening against the coming air flow weakened the “protection” the most while half opening against the coming air flow had the least effect on the “protection” among the experimental configurations tested.

- 5) The cubicle equipped with the  $\mu$ X could help reduce the dependence of the micro-environment around the occupant on the background environment, which is the macro-environment, regardless how the cubicle was opened.
- 6) The Clothing Independent Thermal Comfort Model was used in this study to predict the thermal response of occupants under the different test conditions. The  $\mu$ X was proved to be able to restore the thermal sensation level at higher ambient temperature. The combination of supply temperature at 23.1 °C and supply flow rate of 29.4 cfm and the combination of supply temperature at 26.1 °C and supply flow rate of 40.0 cfm yielded the same level of thermal sensation of the comfort condition.
- 7) Although the existence of the cubicle helped protect the occupants from the background air flow, it also exacerbated the thermal condition of the occupied space. The involvement of the  $\mu$ X proved to be able to restore the thermal condition in the cubicle.

## **7. CFD Study of the Ventilated Semi-Open Space**

The experimental results of the effect of the Semi-Open Space, the cubicle, on the thermal response of the occupant were discussed in the last Chapter. This Chapter discusses how the Semi-Open Space would affect the air quality. In this chapter, this effect will be studied using the validated CFD model.

### **7.1. Overview**

A CFD model based on the guidelines given by Russo's validated CFD case (Russo 2011) was developed and further validated by the experimental work presented in Chapter 4. A cubicle with the same dimensions as the one tested in Chapter 6 was built into the CFD model. The air quality in all regions in the room was compared for scenarios with and without a cubicle. The effect of the openness of the cubicle was also investigated as well as the opening direction. This chapter also included the studies on the effects of the cubicle as an SOS in combination with a  $\mu X$  with local air purification.

The room and cubicle configurations modeled are the same as those used in Chapter 1 and 0. A 1.8 m  $\times$  1.8 m cubicle was created symmetrically around the desk and seated occupant. The height of the cubicle partition was 1.8 m. Same with the experiments, the cubicle could be half or fully opened from four sides. The boundary condition of each segment of the manikin was set to be constant heat flux. The heat flux value came from the experimental results. The room wall was set to be the same with the indoor temperature set-point – 26.1 °C for the cases with the  $\mu X$  and 23.9 °C for the case without the  $\mu X$ . The room air temperature (supply air temperature) was set to be 26.0 °C with the  $\mu X$  and 22.8°C without the  $\mu X$ .

Since this work focuses on how the cubicle configuration, as well as the micro-environmental control system, affects the indoor air quality instead of the actual distribution of certain contaminant, a tracer gas (sulfur hexafluoride, SF<sub>6</sub>) was used to represent the pollutant emission. Two emission sources, the wall and the desk, were simulated in this chapter (Figure 7-1). The emission from the wall is used to present the case in which pollutant sources are outside the cubicle and that from the desk to represent the sources inside the cubicle. The  $\mu$ X placed under the table has two openings on both sides of it. When the  $\mu$ X is on, the air purification starts to work by taking in contaminated air and supplying clean air.

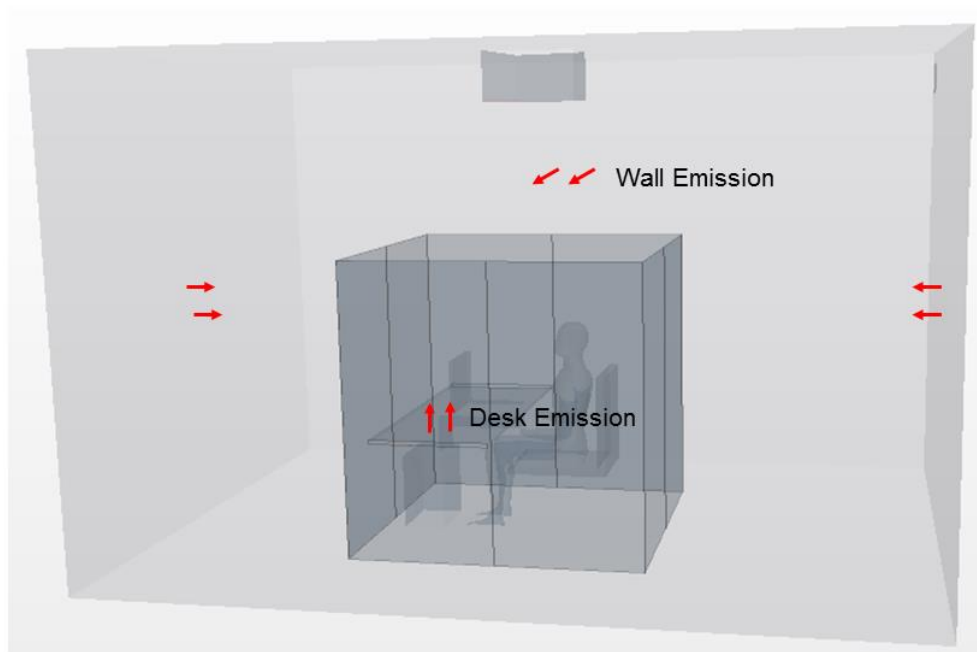


Figure 7-1 Simulation domain with SOS

Sec. 2.2 introduced several analysis methods for air quality. In the current work, the Contaminant Removal Efficiency (also called Ventilation Efficiency,  $\varepsilon$ ) and Blocking

Coefficient ( $\beta$ ), were used to quantify the performance of the ventilation strategies and SOS. The Contaminant Removal Efficiency or Ventilation Efficiency was calculated using Eqn. 2-11 where  $C_p$  is the pollutant concentration in the breathing zone, which is conventionally defined as the zone within a 0.3 m radius of a worker's nose and mouth (**Figure 7-2**, OJIMA 2012). Blocking Coefficient was calculated using Eqn. 2-13 where  $C_{SOS}$  is represented by the volume averaged SF6 concentration in the cubicle.

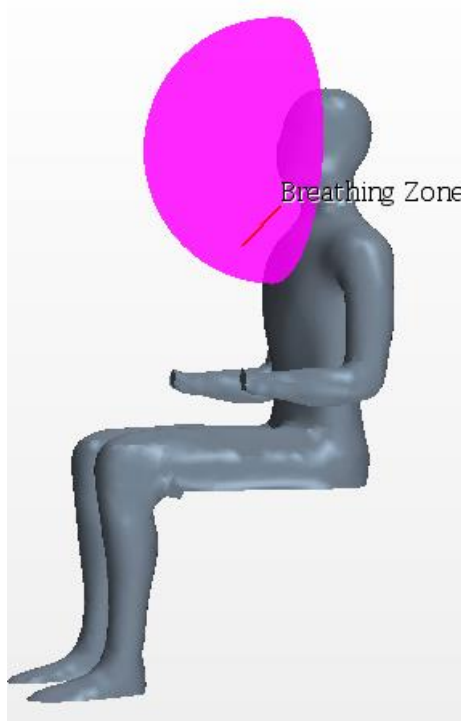


Figure 7-2 Sampling grid in the breathing zone

## 7.2. Effects of the SOS

The partitions around the workstation changes the airflow pattern around it, hence the contaminant distribution. However, the performance of the cubicle is dependent on many

factors, including the opening direction and size of the cubicle, location of the contaminant source, as well as whether the  $\mu X$  is on or off.

### **7.2.1. Pollutant Mass Fraction Level in the Breathing Zone and the Cubicle**

Pollutant mass fraction in the occupied space is a direct indication of the air quality. **Figure 7-3** shows the mass fraction level of the  $SF_6$  when the pollutant was emitted from the desk. When the  $\mu X$  was off, no local air purification was provided and the case with a fully closed cubicle gave the highest pollutant mass fraction in the breathing zone, which is because the emission source was inside the cubicle and the partitions prevented the pollutant from going outside. When the cubicle was fully opened, the pollutant in the breathing zone was diluted and removed so that the mass fraction was reduced by a half. When the cubicle was partially open, the pollutant concentration in the breathing zone was dependent on the direction and the size of the opening that determined the air flow inside the cubicle and were all lower than the one for the fully closed case. Since the emission source (desk) was very closed to the breathing zone, the pollutant concentration in the breathing zone was sometimes high when the air carrying pollutant flew towards the breathing zone (OF-2 and OL-1) and sometimes low when the air carrying pollutant was pushed away from the breathing zone (OB-1, OB-2, and OL-2). After turning on the  $\mu X$ , the effect of local purification was obvious regardless whether there was a cubicle. The pollutant mass fraction was reduced to different extents, and the biggest improvement was found in the fully closed cubicle. With the local air purification, even though the clean air was not supplied to the breathing zone directly, the pollutant in the breathing zone had still been diluted because after hitting

on the body some part of the clean air was spread or transported by the thermal plume upward to the breathing zone.

**Figure 7-4** shows the mass fraction level of the SF<sub>6</sub> in the breathing zone when the pollutant was emitted from the wall. Different from the cases of desk source, the pollutant mass fraction in the breathing zone was quite close to each other among the cases without local purification. This is because when the emission was from the walls, the distribution of the pollutant was very uniform and the air was well mixed before it entered the cubicle. When the  $\mu$ X was turned on with local purification, regardless how the cubicle was arranged, the mass fraction was reduced by almost the same amount.

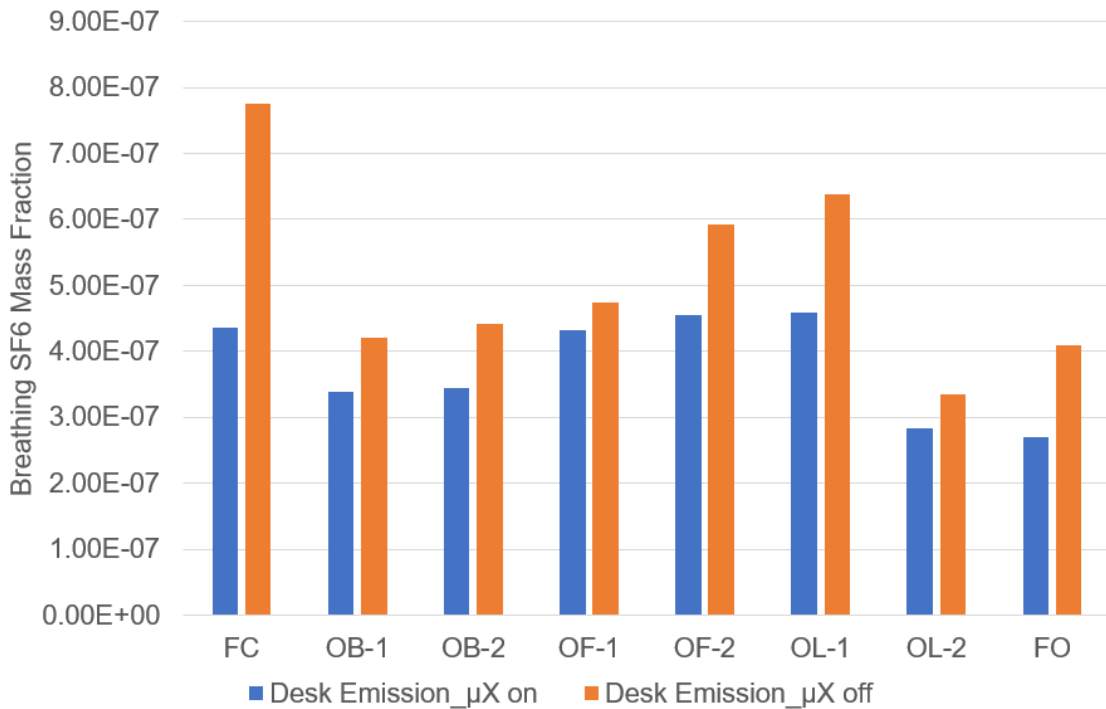


Figure 7-3 SF<sub>6</sub> mass fraction in the breathing zone with desk emission



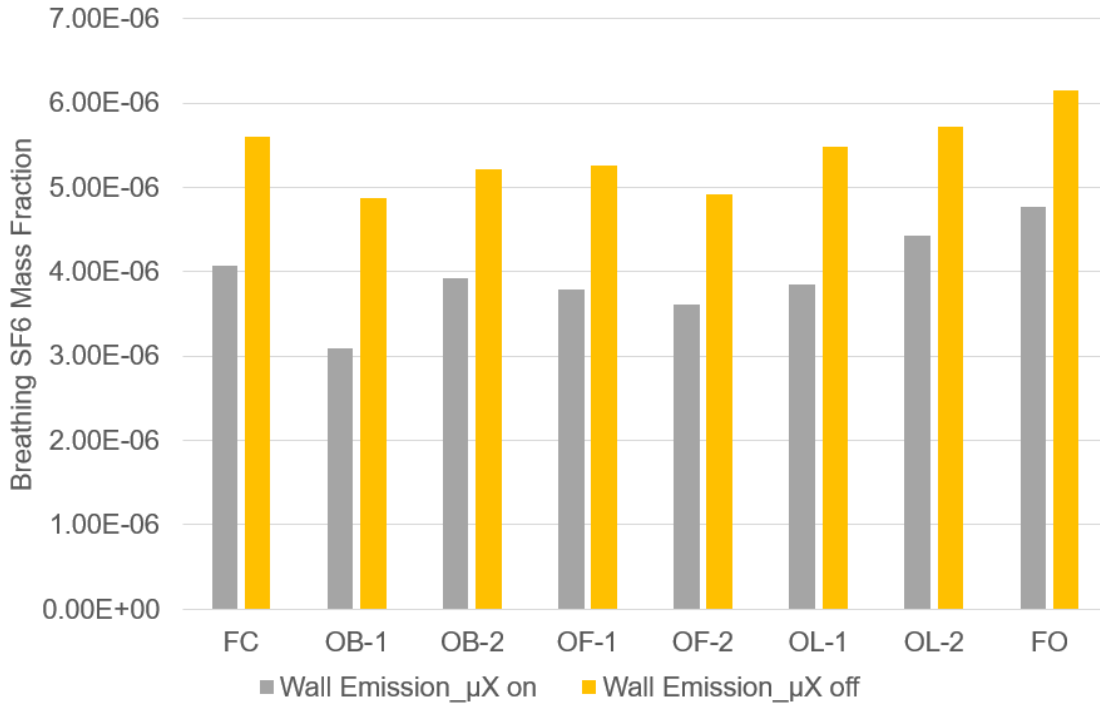


Figure 7-4 SF<sub>6</sub> mass fraction in the breathing zone with wall emission

The pollutant mass fraction in the cubicle is also a very important parameter for evaluating the air quality since the occupant may not sit in the chair all the time. Figure 7-5 shows the mass fraction level of the SF<sub>6</sub> in the cubicle when the pollutant was emitted from the desk. When the μX was off, the fully closed (FC) cubicle gave the highest SF<sub>6</sub> mass fraction, while the fully open (FO) cubicle reduced the mass fraction by half and the other cases in which the cubicle was partially opened gave the mass fractions between them and closer to the FO case. The explanation for that is the cubicle partition played a role in confining the pollutant in the cubicle and opening the cubicle either partially or completely allowed the fresh air to enter and dilute the air in the cubicle. Among those cases with partially or fully opened cubicles, the FO case worked the best because it allowed the air to enter the cubicle from all the directions, and then the case with a cubicle open from the front (OF-1 and OF-

2) worked the second best which allowed most of the upcoming air (from the front) to enter the cubicle. Different from the mass fraction behavior in the breathing zone, because both the emission source and the  $\mu X$  (local purification) were inside the cubicle, turning on the  $\mu X$  could reduce the level of the pollutant concentration by almost the same amount regardless of the opening configurations.

**Figure 7-6** shows the mass fraction level of the SF<sub>6</sub> in the cubicle when the pollutant was emitted from the wall. Since as mentioned before the air in the space was well-mixed both inside and outside the cubicle, the pollutant mass fraction level is highly similar with the one in the breathing zone (Figure 7-4). Among all the cases, the  $\mu X$  could reduce the mass fraction by the same amount.

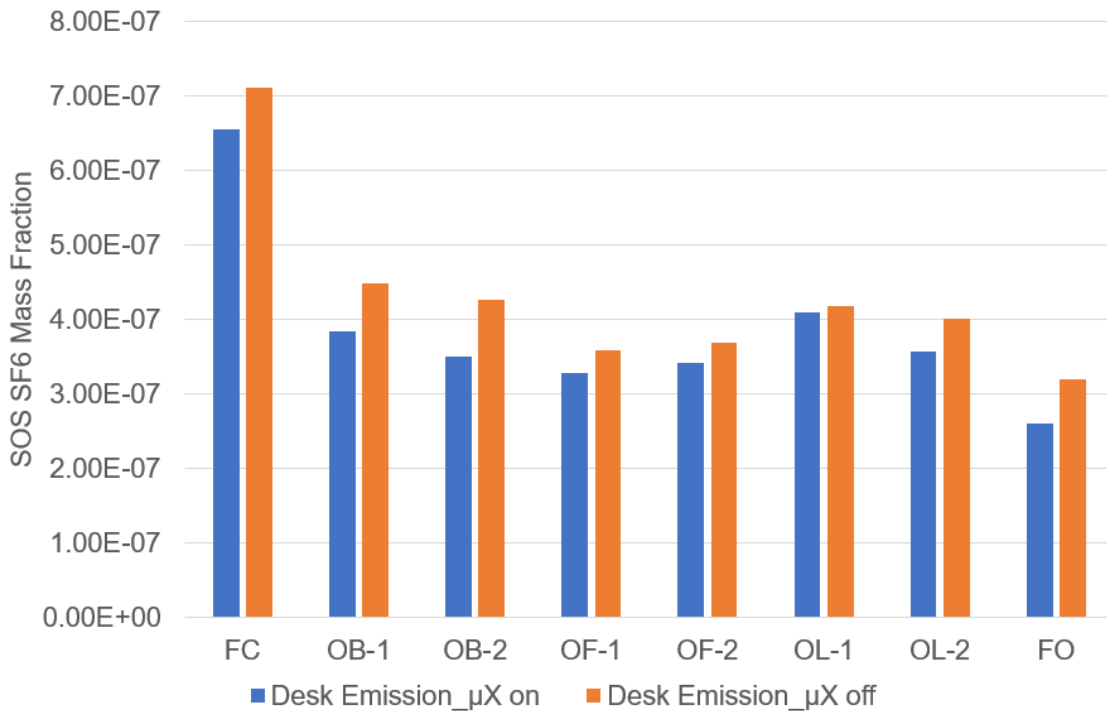


Figure 7-5 SF6 mass fraction in the cubicle with desk emission

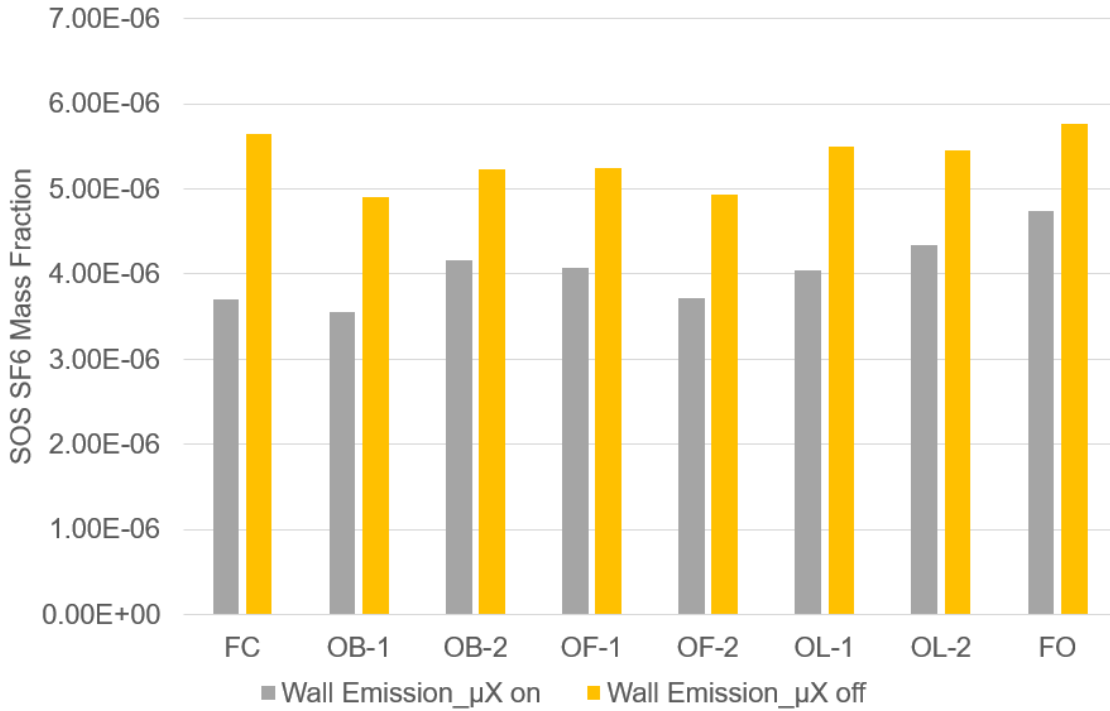


Figure 7-6 SF6 mass fraction in the cubicle with wall emission

### 7.2.2. Contaminant Removal Efficiency

In order to examine the performance of the ventilation system under different configurations of the cubicle and with or without the  $\mu$ X, Contaminant Removal Efficiency ( $e$ ) was calculated at the breathing zone. **Figure 7-7** shows the calculated Contaminant Removal Efficiency in the breathing zone of all the cases with the desk or wall source. Note that an  $e$  of 100% represents well-mixed air quality, a value greater than 100% shows cleaner air is present than well-mixed air and a value less than 100% shows dirtier air is present than well-mixed air. The results show that when the pollutant was emitted from the desk, the air quality in the breathing zone was not well mixed for any of the cases with or without the  $\mu$ X. The worst efficiency was given by the FC case. And the use of the  $\mu$ X could improve the efficiency by more than 20 percent when there was a fully closed cubicle

or no cubicle at all. However, when the cubicle was opened partially the advantage of using the  $\mu$ X became unclear and sometimes negative (OB-1 and OF-1). This means that when the cubicle was partially opened, adding a local purification in the  $\mu$ X is not necessarily better than adding purification process in the background mixing ventilation. When the pollutant was emitted from the wall, as mentioned before, a well-mixed condition was established in the room including the cubicle, so the  $e$  in the breathing zone of any cases was a little higher than 100%. However, different from the case of the desk source, the use of the  $\mu$ X with local purification always brought an improvement of the air quality in the breathing zone. Comparing the cases with the desk emission and wall emission, the ventilation system (with and without the  $\mu$ X) always worked better (mostly two times) when the pollutant was emitted from the wall than the one when the pollutant was emitted from the desk.

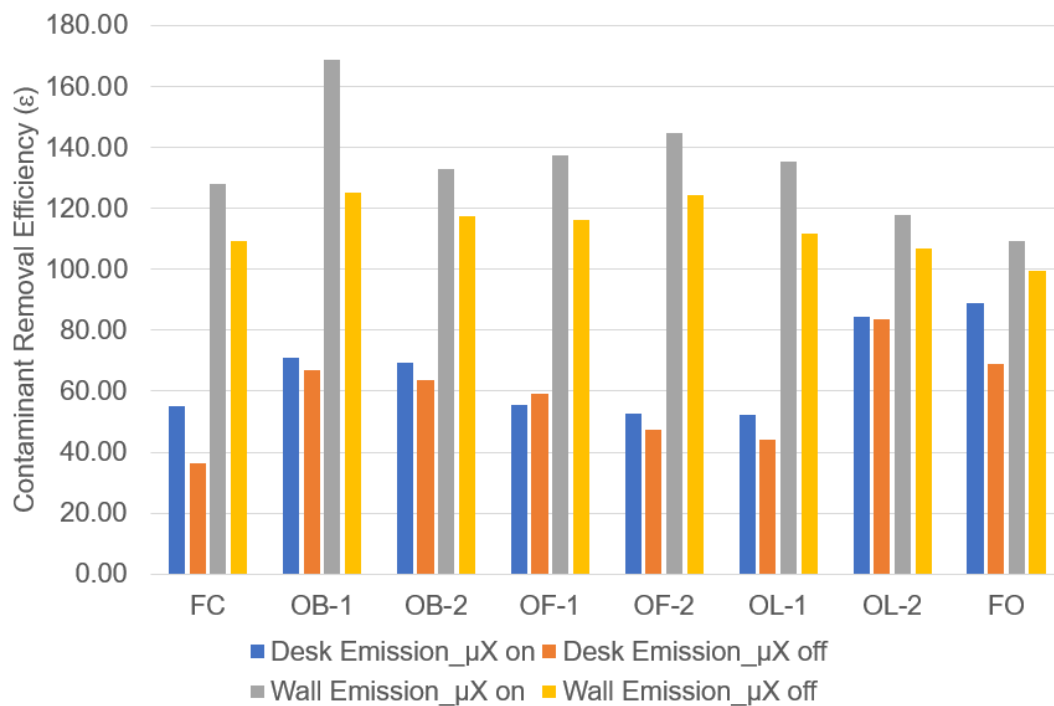


Figure 7-7 Contaminant Removal Efficiency in the breathing zone

**Figure 7-8** shows the Contaminant Removal Efficiency contours for the cases with desk emission. The contours show a range from 0 to 200%. The dark blue region indicates cleaner than well-mixed air and the red regions indicate dirtier air. It was demonstrated that the pollutant distribution in the cubicle was highly non-uniform, especially in the region closed to the desk. The breathing zone was located in the region with large gradient and dirtier air, which explains why the contaminant removal efficiency of these cases were always low. The dirty air carrying the pollutant from the desk was mixed with the surrounding air in the cubicle and then was pulled out of the cubicle due to the entrainment of the supply jet of the background mixing ventilation. The make-up air entered the cubicle in different ways depending on the opening direction and size of the manikin and diluted the air in the breathing zone. A local jet of clean air was observed when the  $\mu X$  was turned on. However, since the local supply air was maintained at a lower temperature than the ambient room air for improving thermal comfort, most of the local clean air, instead of entered the breathing zone, was transported downward to the lower region and mixed with the dirty air carrying the pollutant from the bottom side of the desk. This may be the reason why the  $\mu X$  brought little improvement of the air quality in the breathing zone.

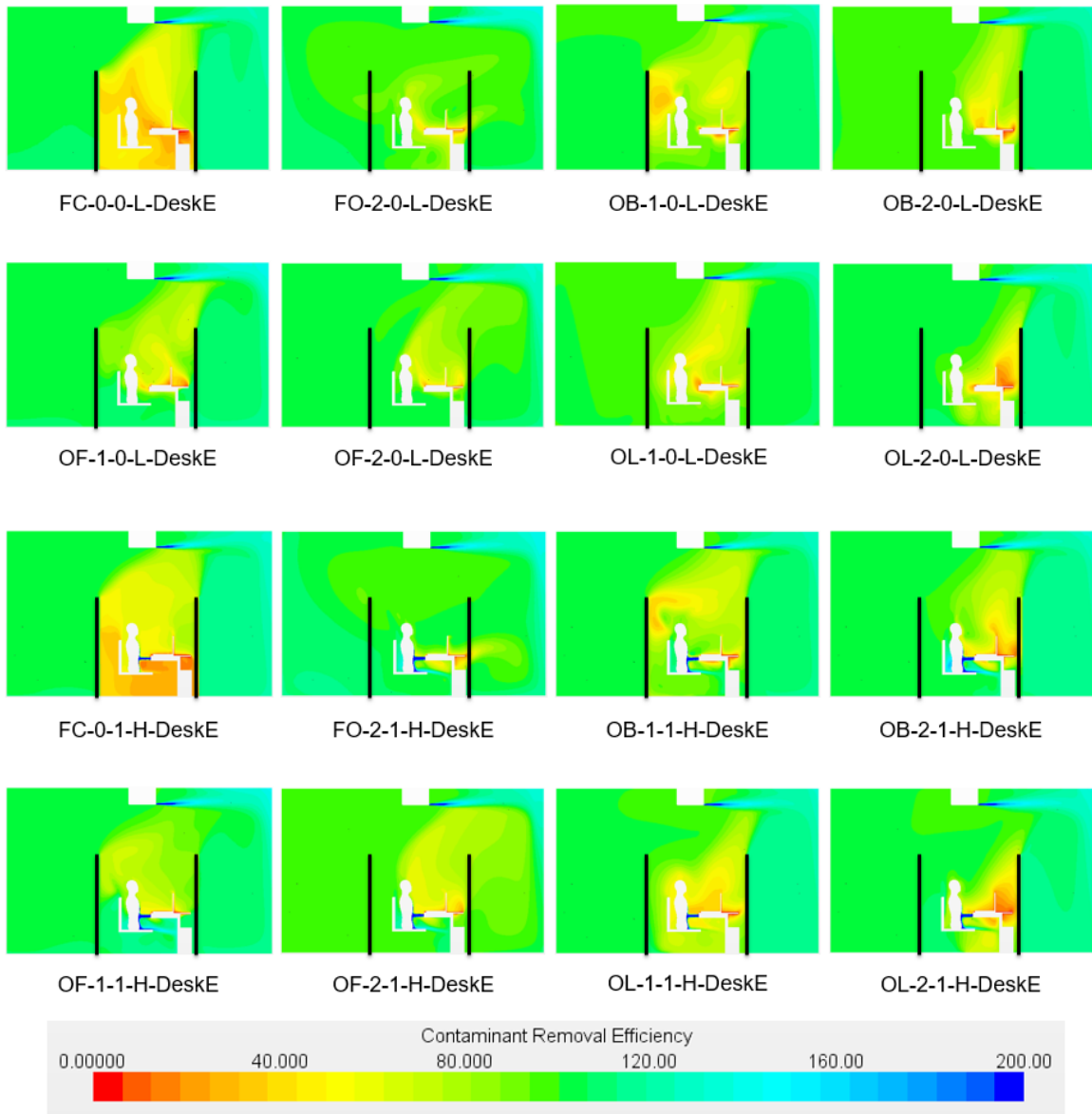
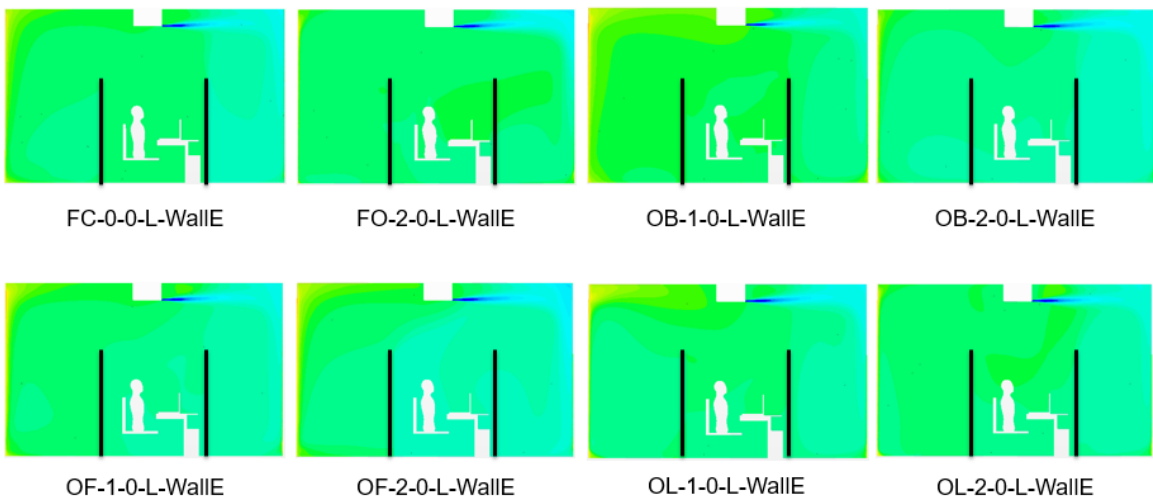


Figure 7-8 Contaminant Removal Efficiency with desk emission

**Figure 7-9** shows the Contaminant Removal Efficiency contours for the cases with wall emission. Different from the cases of desk emission, the pollutant distribution of the wall emission cases was much more uniform, especially inside the cubicle. This is because the pollutant was emitted from the four side walls uniformly and the mixing ventilation did a

good job in mixing the room air. Nevertheless, when the  $\mu X$  was turned on, a clean jet, as well as a clean region, showed up around the occupant. This clean region effectively reduced pollutant concentration in the breathing zone and increased the contaminant removal efficiency. Comparing these cases with the cases with desk emission, the reason why this time the  $\mu X$  could improve the air quality more effectively is that in the lower region of the cubicle there was no pollutant source and therefore the cooler clean air remained clean before it was taken by the thermal plume to the breathing zone.



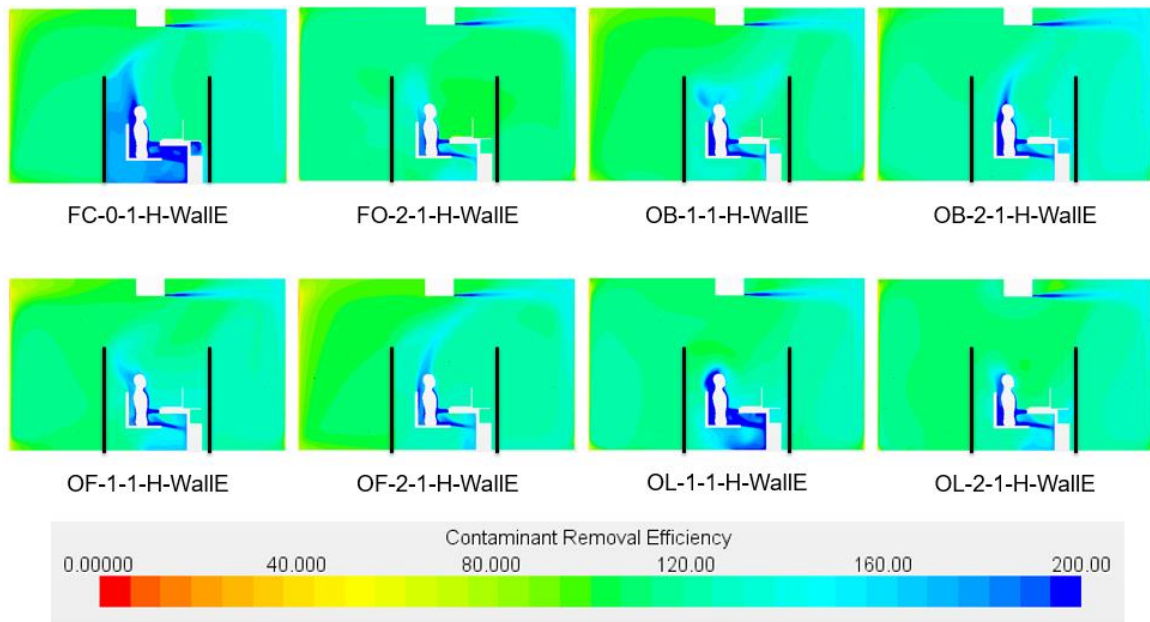


Figure 7-9 Contaminant Removal Efficiency with wall emission

### 7.2.3. Blocking Coefficient

Blocking Coefficient ( $\beta$ ) was an index to quantify the performance of the SOS. It is a ratio between the exhaust pollutant concentration and the pollutant concentration in the SOS.

**Figure 7-10** illustrates the blocking coefficient of the cubicle of all the cases with the desk or wall source. Note that a  $\beta$  of 100% represents the cubicle did not have any blocking effect, a value greater than 100% shows cleaner air is contained in the cubicle and a value less than 100% shows dirtier air is contained in the cubicle. When there was no cubicle, the blocking coefficient was always around 100% regardless where the emission source was. When the pollutant was emitted from the desk,  $\beta$  was always less than 100%. A fully closed cubicle (FC) gave a blocking coefficient less than 40%, and a partially opened cubicle gave a blocking coefficient between 60% and 80%. In this case, the  $\mu X$  did not make a big difference because it reduced the pollutant level in the cubicle as well as the pollutant level



in the exhaust. When the pollutant was emitted from the wall, the  $\beta$  was always higher than 100%. Without the  $\mu X$ ,  $\beta$  was a little higher than 100% with a maximum at around 120%. Turning on the  $\mu X$  could significantly improve the blocking coefficient, and the most improvement was given by the fully closed cubicle in which the blocking coefficient was increased by 30%. This is because the fully closed cubicle could hold most of the clean air made by the  $\mu X$  inside the cubicle.

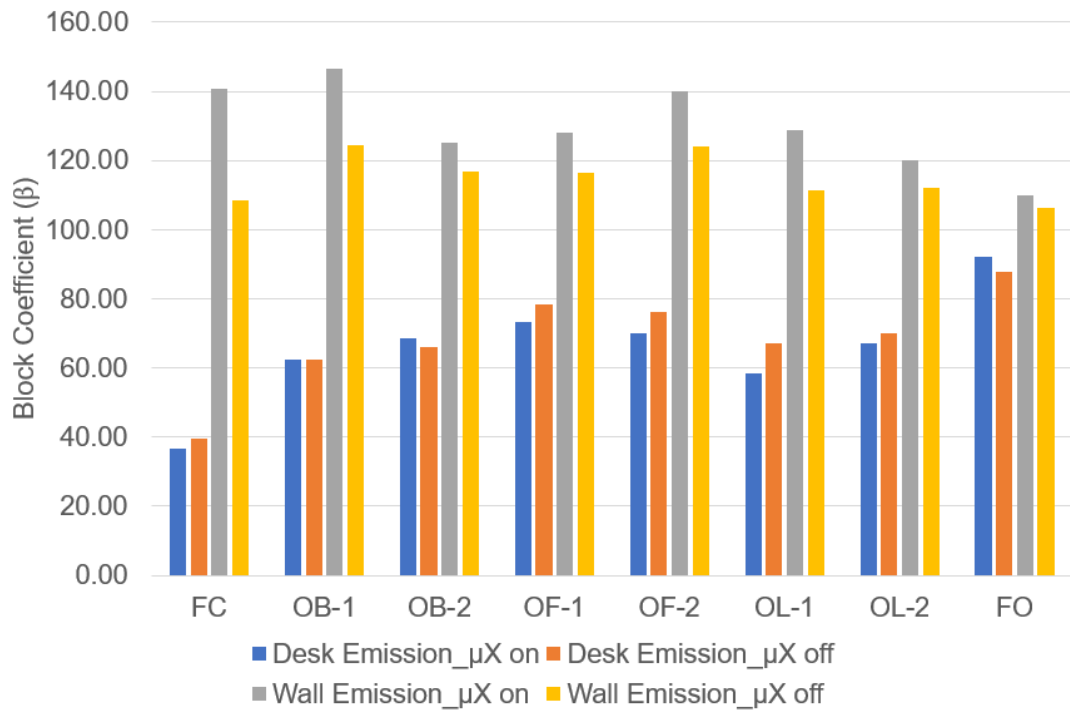


Figure 7-10 Blocking Coefficient of the cubicle

### 7.3. Summary and Conclusions

Simulations using the previously-validated CFD model were conducted to investigate the effects of the cubicle as a semi-open space on the indoor air quality and evaluate the performance of the  $\mu X$  with air purification in combination with the cubicle. The results indicate that

- 1) The effect of the cubicle on the pollutant distribution is highly dependent on the location of the pollutant source. The pollutant level of the breathing zone is highly sensitive to the cubicle configuration. When the pollutant was emitted inside the cubicle and close to the breathing zone (from the desk), a fully closed cubicle could make the pollutant level in the breathing zone twice as the case without a cubicle. The opening direction and opening size of the cubicle changed the flow field inside it and therefore yielded different levels of pollutant concentration in the breathing zone. However, when the pollutant was emitted outside the cubicle (in this case it was emitted from the wall, but it could also represent the emission from other cubicles or office appliances in the hall way), the cubicle did not make a big difference in the air quality in the breathing zone because the pollutant distribution is fairly uniform in the space.
- 2) The pollutant level in the cubicle is also highly sensitive to the cubicle configuration. When the pollutant was emitted inside the cubicle, similar with the breathing zone, the pollutant concentration in a fully closed cubicle was twice as the one without cubicle. However, different from the breathing zone, partially opened cubicle did not show that big variation in the pollutant concentration level in the cubicle. The averaged pollutant concentration in the partially opened cubicle was only a little higher than the one without a cubicle. The pollutant concentration in the cubicle with wall emission was almost the same as the one in the breathing zone since the concentration field was very uniform in this case.
- 3) The combination of using the  $\mu X$  and the cubicle was tested with desk or wall emission. When the pollutant was emitted from the desk, turning on the  $\mu X$  could

reduce the pollutant level in the breathing zone, but was not necessarily as efficient as the background mixing ventilation. Only when the cubicle was fully closed or fully opened (without a cubicle), the  $\mu X$  showed a significant advantage. This means that when the cubicle was partially opened, the  $\mu X$  with local purification may not provide better air quality than cleaning more return air. However, when the pollutant was emitted from the walls (outside the cubicle), the  $\mu X$  with air purification could improve the air quality by almost the same amount regardless of opening configurations in terms of the Contaminant Removal Efficiency.

- 4) The performance of the cubicle was quantified by using Blocking Coefficient. When the pollutant was emitted from the desk, the cubicle had a negative effect on the air quality inside the cubicle. A fully closed cubicle made the pollutant concentration inside the cubicle twice as much as the well-mixed condition, and partially opened cubicle increased the pollutant level by a half compared with the well-mixed condition. However, when the pollutant was emitted from the wall, the performance of the cubicle had been reversed, and the positive effect was even further increased when the  $\mu X$  was applied.

## **8. Performance Evaluation of the Selected Cooling/Heating Delivery Devices**

Chapter 4, and 5 used CFD simulation to investigate the performance of different air terminal devices (ATDs) and heating delivery devices (HDDs) under the conditions of expanded temperature set-point. The current chapter presents results from the full-scale chamber and thermal manikin experiments that were performed to confirm that the selected cooling/heating delivery devices can maintain the heat balance for restoring occupants' thermal comfort while the set-point temperature for the ambient space air is increased in the cooling season or decreased in the heating season. It is noted that this part of the work was driven by an ARPA-E project which looks for techniques to restore occupant's thermal comfort while reducing building energy by relaxing indoor temperature set-point. ARPA-E defines the problem in the way presented in Sec. 4.1.5, and the objective is *“when the ambient temperature is raised from 75 °F to 79 °F, a removal of 23 W is needed to be taken by the  $\mu X$  system; when the ambient temperature is lowered from 70 °F to 66 °F, a supply of 18 W is needed to be provided by the  $\mu X$  system”* (ARPA-E 2014).

### **8.1. Performance Evaluation of Three Different ATDs for Cooling**

Three different ATDs were tested in the full-scale chamber with a workstation and a thermal manikin for the ARPA-E project for selecting one to incorporate into the final design of  $\mu X$ . An HVAC system was used for conditioning the chamber, and the room temperature was controlled to be 79 °F by the return air temperature. The manikin was dressed in typical summer clothing (a short-sleeve sports shirt, men's briefs, trousers, socks, and shoes) with a constant skin temperature at 33.9 °C. Air at conditions similar to those produced by  $\mu X$  was supplied to the diffusers through a laboratory system comprising a

window air conditioning unit, an orifice flange flow meter, an in-duct fan, an electric heater, an air diffuser, and connecting ducts was constructed (Figure 4-2). Three different diffusers were tested including a single diffuser, split round diffusers and split rectangular diffusers (Figure 8-2). The air of three combinations of air flow rate and supply temperature which contains 50 W cooling power (according to Eqn. 4-1) were supplied by the laboratory cooling system.

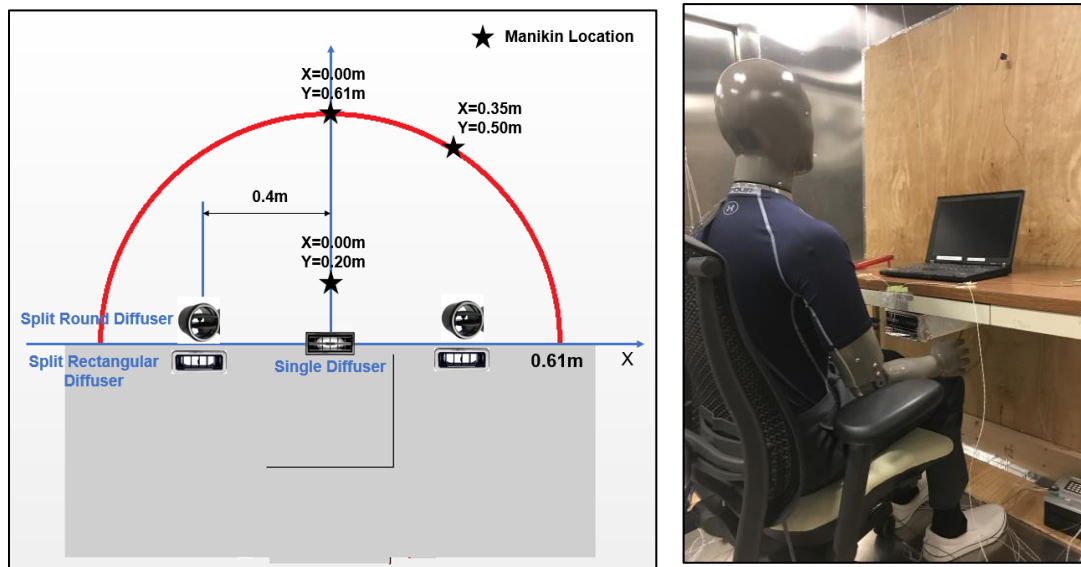


Figure 8-1 Layout of diffuser/manikin experiment



Figure 8-2 Three types of diffusers (ATDs) tested

The heat loss from the manikin was recorded with and without the  $\mu$ X surrogate system active. The test results for the single rectangular diffuser at 50 W of air cooling and 29 cfm of air flow are summarized in Table 8-1. The extra heat loss was a lot above 23 W with a minimum at 36.4 W when the manikin was placed 0.61 m away from the diffuser.

Table 8-1 Performance of single rectangular diffuser at 23 cfm and 50 W

Single Diffuser 13.3 cm × 6.4 cm	79 °F			
	$\mu$ X off	$\mu$ X on	$\mu$ X on	$\mu$ X on
X (m)	0	0	0	0.35
Y (m)	0.2	0.2	0.61	0.5
Room Supply Temp (°F)	74.4 (±0.3)	77.0 (±0.2)	77.0 (±0.1)	76.08 (±0.2)
Exhaust Temp (°F)	79.0 (±0.1)	79.0 (±0.1)	79.0 (±0.1)	79.1 (±0.1)
$\mu$ X Supply Temp (°F)	N/A	73.7 (±0.1)	73.6 (±0.1)	73.4 (±0.1)
$\mu$ X Supply Flowrate (cfm)	N/A	29.5	29.5	29.4
Averaged Heat Flux (W/m <sup>2</sup> )	47.50 (±0.20)	68.48 (±0.13)	67.57 (±0.16)	73.70 (±0.22)
Extra Heat Removed (W)	N/A	38.04	36.4	47.51

Table 8-2 shows the test results for the single rectangular diffuser and the split round diffusers at 50 W of air cooling and 23 cfm of air flow, showing the reduced performance resulting from lowering the air flow rate from 29 to 23 cfm. It can be seen that while both types of diffusers can remove well in excess of 23 W of extra heat from the manikin. In the 23 cfm case, the split round diffuser delivered a higher performance. This can be attributed to two factors: (1) jets issuing from round diffusers usually have a longer core region, thus project the cold air further, and (2) split diffusers discharge air from two sides of the manikin and cover a larger surface area of the manikin than the single central diffuser.

Table 8-2 Performance of single rectangular and split round diffusers at 23 cfm and 50 W

<b>Single Diffuser 13.3 cm × 6.4 cm</b>	<b>79 °F</b>			
	<b>μX off</b>	<b>μX on</b>	<b>μX on</b>	<b>μX on</b>
X (m)	0	0	0	0.35
Y (m)	0.2	0.2	0.61	0.5
Room Supply Temp (°F)	74.4 (±0.3)	77.8 (±0.2)	77.8 (±0.2)	77.7 (±0.4)
Exhaust Temp (°F)	79.0 (±0.1)	79.0 (±0.1)	79.0 (±0.1)	79.1 (±0.1)
μX Supply Temp (°F)	N/A	72.0 (±0.1)	72.0 (±0.2)	72.0 (±0.2)
μX Supply Flowrate (cfm)	N/A	22.7	23	22.8
Averaged Heat Flux (W/m <sup>2</sup> )	47.50 (±0.20)	66.08 (±0.23)	64.51 (±0.30)	70.72 (±0.25)
Extra Heat Removed (W)	N/A	33.69	30.85	42.09
<b>Split Round Diffuser D=6.87 cm</b>	<b>79 °F</b>			
	<b>μX off</b>	<b>μX on</b>	<b>μX on</b>	<b>μX on</b>
X (m)	0	0	0	0.35
Y (m)	0.2	0.2	0.61	0.5
Room Supply Temp (°F)	74.4 (±0.3)	77.3 (±0.3)	77.7 (±0.3)	77.6 (±0.3)
Exhaust Temp (°F)	79.0 (±0.1)	79.1 (±0.1)	79.2 (±0.1)	79.1 (±0.1)
μX Supply Temp (°F)	N/A	71.9 (±0.2)	72.2 (±0.1)	72.0 (±0.1)
μX Supply Flowrate (cfm)	N/A	23.2	22.8	23
Averaged Heat Flux (W/m <sup>2</sup> )	47.50 (±0.20)	71.99 (±0.11)	72.95 (±0.20)	67.18 (±0.25)
Extra Heat Removed (W)	N/A	42.38	44.13	35.68

Table 8-3 presents the test results for the single rectangular diffuser and the split round and rectangular diffusers at 50 W of air cooling and 17 cfm of air flow. It was found that all the three diffusers could fulfill the requirement of removing an extra 23 W from the manikin when 50 W of cooling was supplied through the diffuser air flow.

Table 8-3 Performance of single rectangular and split round diffusers at 17 cfm and 50 W

<b>Single Diffuser 13.3 cm × 6.4 cm</b>	<b>79 °F</b>			
	<b>μX off</b>	<b>μX on</b>	<b>μX on</b>	<b>μX on</b>
X (m)	0	0	0	0.35
Y (m)	0.2	0.2	0.61	0.5
Room Supply Temp (°F)	74.4 (±0.3)	78.9 (±0.2)	78.4 (±0.2)	78.4 (±0.2)
Exhaust Temp (°F)	79.0 (±0.1)	79.1 (±0.1)	79.1 (±0.1)	79.1 (±0.1)
μX Supply Temp (°F)	N/A	69.7 (±0.1)	69.7 (±0.1)	69.6 (±0.1)
μX Supply Flowrate (cfm)	N/A	16.9	17.1	16.9
Averaged Heat Flux (W/m <sup>2</sup> )	47.50 (±0.20)	62.71 (±0.22)	61.02 (±0.28)	62.93 (±0.45)
Extra Heat Removed (W)	N/A	27.58	24.51	27.97
<b>Split Round Diffuser D=6.87 cm</b>	<b>79 °F</b>			
	<b>μX off</b>	<b>μX on</b>	<b>μX on</b>	<b>μX on</b>
X (m)	0	0	0	0.35
Y (m)	0.2	0.2	0.61	0.5
Room Supply Temp (°F)	74.4 (±0.3)	77.4 (±0.3)	77.7 (±0.3)	77.7 (±0.3)
Exhaust Temp (°F)	79.0 (±0.1)	79.1 (±0.1)	79.1 (±0.1)	78.9 (±0.1)
μX Supply Temp (°F)	N/A	69.8 (±0.1)	69.8 (±0.1)	69.7 (±0.1)
μX Supply Flowrate (cfm)	N/A	17	16.8	17.2
Averaged Heat Flux (W/m <sup>2</sup> )	47.50 (±0.20)	65.40 (±0.11)	65.65 (±0.23)	64.63 (±0.19)
Extra Heat Removed (W)	N/A	32.45	32.91	31.06
<b>Split Rectangular Diffuser 9.84 cm × 3.97 cm</b>	<b>79 °F</b>			
	<b>μX off</b>	<b>μX on</b>	<b>μX on</b>	<b>μX on</b>
X (m)	0	0	0	0.35
Y (m)	0.2	0.2	0.61	0.5
Room Supply Temp (°F)	74.4 (±0.3)	77.8 (±0.3)	77.8 (±0.3)	77.6 (±0.3)



Exhaust Temp (°F)	79.0 (±0.1)	79.1 (±0.1)	79.1 (±0.1)	79.0 (±0.1)
μX Supply Temp (°F)	N/A	69.7 (±0.1)	69.7 (±0.1)	69.7 (±0.3)
μX Supply Flowrate (cfm)	N/A	17	17	17
Averaged Heat Flux (W/m <sup>2</sup> )	47.50 (±0.20)	62.26 (±0.20)	62.39 (±0.33)	60.72 (±0.43)
Extra Heat Removed (W)	N/A	26.75	27.00	23.97

It was concluded that the split round diffusers could always give the best performance regarding extra heat removed while all the three diffusers could remove more than 23 W heat from the manikin with at least 17 cfm air flow rate.

## 8.2. Performance Evaluation of the Heating Delivering Device (HDDs)

The performance of the Heating Delivering Device (HDD) was tested in a full-scale chamber with a workstation and a thermal manikin for the ARPA-E project to make sure the proposed HDD could fulfill the requirement of reducing 18 W heat loss. An HVAC system was used for conditioning the chamber, and the room temperature was controlled to be 66 °F by the return air temperature. The manikin was dressed in typical winter clothing (a long-sleeve T-shirt, a suit, men’s briefs, trousers, socks and shoes, **Figure 8-3**) with a constant skin temperature at 33.9 °C. A heating foot mat with a reflective box covering the front part of the feet was tested with a heating power of at most 60 W. An infrared heating bulb of maximum 20 W was installed in the reflective box to provide an extra option for heating. The heating mat is electrically heated and of a dimension 45 cm × 45 cm. The reflective box is 50 cm × 15 cm × 15 cm and with reflective material and insulation on both interior and exterior side (**Figure 8-4**).



Figure 8-3 Manikin test with the heating delivering device



Figure 8-4 Heating delivering device

The heat loss from the manikin was recorded with and without the HDD active. The test results for using only the heating mat were summarized in **Table 8-4**. The heating power of the mat was increased from 0 to 40 W with the heating bulb turned off. The reduced heat loss was increased from 0 to a little above 10 W. It is observed that after the heating power reached 30 W, the reduced heat loss stopped increasing. This is because the manikin surface temperature was controlled by electric heaters and after the heating power from the mat reached 30 W, the heater on the feet of the manikin stopped generating heat. Therefore, the performance of the heating mat with heating power higher than 30 W was predicted by linear regression using the data below 30 W heating power. It was shown that with only the heating mat, the HDD could reduce around 19.4 W heat loss from the manikin, which is higher than the 18 W ARPA-E requirement (**Figure 8-5** Error! Reference source not found.).

Table 8-4 Test results of the heating mat only

Case	66 °F							
	μX off	μX on	μX on	μX on	μX on	μX on	μX on	μX on
Room Supply Temp (°F)	55.5 (±1.2)	57.2 (±0.9)	54.5 (±0.9)	58.1 (±0.9)	54.6 (±0.9)	56.0 (±1.0)	54.6 (±0.9)	56.1 (±2.0)
Exhaust Temp (°F)	66.0 (±0.1)	66.1 (±0.1)	66.1 (±0.1)	66.1 (±0.1)	66.2 (±0.1)	66.3 (±0.1)	66.3 (±0.1)	66.3 (±0.1)
Mat Heating power (W)		10	15	20	25	30	35	40
Reflective Box	N/A	√	√	√	√	√	√	√
Heating Bulb Power (W)		N/A	N/A	N/A	N/A	N/A	N/A	N/A
Averaged Heat Flux (W/m <sup>2</sup> )	67.44 (±0.34)	65.09 (±0.29)	64.26 (±0.14)	64.52 (±0.36)	63.13 (±0.32)	61.78 (±0.25)	61.51 (±0.14)	61.80 (±0.21)

Total Heat Loss (W)	122.27 (±0.62)	118.01 (±0.53)	116.51 (±0.25)	116.98 (±0.65)	114.45 (±0.57)	112.00 (±0.45)	111.52 (±0.26)	112.05 (±0.38)
Reduced Heat Loss (W)	N/A	4.26	5.76	5.29	7.82	10.27	10.75	10.22

The infrared heating bulb was installed inside the reflective box to provide another option of heating since it was reported that the heating bulb could provide enough heating in a cooler environment (Zhang et al. 2015). The experiment results were presented in **Table 8-5**. The heating bulb was always turned on at 20 W, and the heating power from the mat was increased from 0 to 25 W. After the heating power reached 25 W, the heater in the feet was turned off, and the linear regression was used to determine the performance of the heating mat with an infrared bulb. The results were shown in **Figure 8-5**. The performance of the heating bulb was less effective than the heating mat. With 20 W heating bulb and 40 W heating mat, the HDD could only reduce the heat loss by 14 W.

Table 8-5 Test results of the heating mat and bulb

Case	66 °F					
	μX off	μX on	μX on	μX on	μX on	μX on
Room Supply Temp (°F)	55.5 (±1.2)	55.6 (±1.0)	57.9 (±0.7)	54.3 (±0.9)	54.3 (±0.9)	54.2 (±0.9)
Exhaust Temp (°F)	66.0 (±0.1)	66.0 (±0.1)	66.1 (±0.1)	66.1 (±0.1)	66.2 (±0.1)	66.2 (±0.1)
Mat Heating power (W)	N/A	0	10	15	20	25
Reflective Box		√	√	√	√	√
Heating Bulb Power (W)		20	20	20	20	20

Averaged Heat Flux (W/m <sup>2</sup> )	67.44 (±0.34)	64.57 (±0.23)	64.05 (±0.21)	62.60 (±0.16)	62.10 (±0.19)	61.83 (±0.17)
Total Heat Loss (W)	122.27 (±0.62)	117.07 (±0.42)	116.12 (±0.37)	113.49 (±0.29)	112.59 (±0.35)	112.10 (±0.30)
Reduced Heat Loss (W)	N/A	5.20	6.15	8.78	9.68	10.17

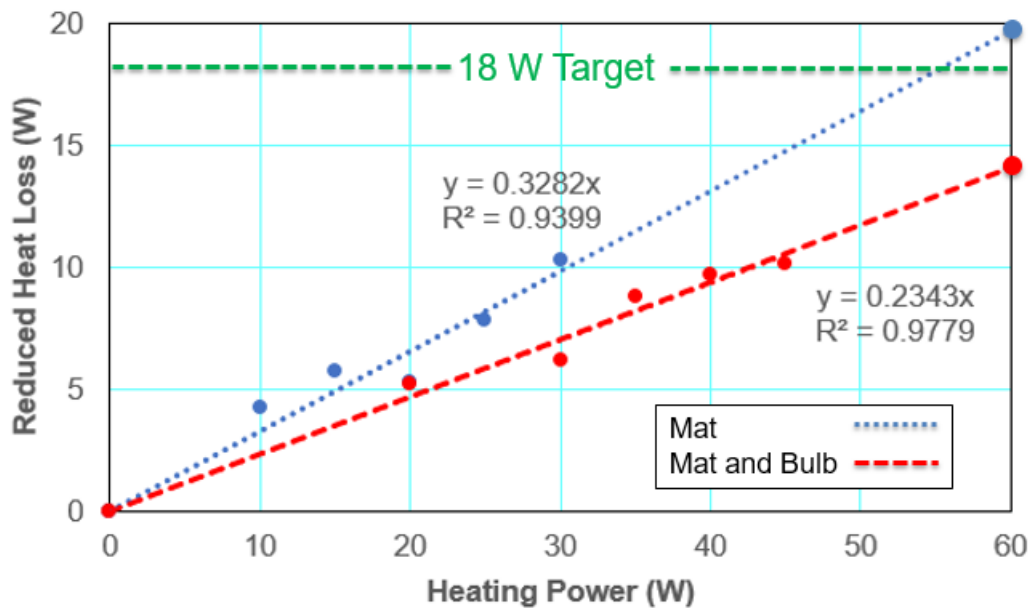


Figure 8-5 Prediction of the performance of the HDD using linear regression

### 8.3. Summary and Conclusions

This chapter summarizes the results of the tests in the full-scale environmental chamber with the thermal manikin to compare the performance of the 3 diffuser ATD layouts and the 2 HDDs. Results show that all diffuser configurations are capable of achieving or exceeding the target 23W of extra heat removal from the thermal manikin within the specific range of movement (0.61m). The essential part of the HDD is a heating foot mat

with a reflective box. An additional infrared bulb was also tested with them. The results show that the combination of using the heating mat with the reflective box can reduce more than 18W heat loss from the manikin, but the combination with the infrared bulb cannot achieve the target of 18W.

## **9. Conclusions and Recommendations for Future Study**

The primary goal of this study is to investigate why and how micro-environmental control system ( $\mu$ X) and semi-open space (SOS) can improve thermal comfort and IAQ while saving energy. As a secondary goal, the ability of the CFD model to adequately predict the local heat transfer from the human body and its limitation are also investigated.

### **9.1. Effects of the SOS and $\mu$ X on Thermal Comfort and Air Quality Conditions**

Although it has been widely recommended throughout the world to save the energy consumption of the buildings by relaxing the indoor temperature set-point (increasing the set-point in summer and reducing it in winter), it is always arguable that occupant's productivity may be reduced thereby. This current work used both simulation and experiments to evaluate several candidate methods for restoring thermal comfort in the environment with extended ranges of temperature set-points.

During summer time, the room temperature was raised to 26.1 °C for energy saving while a cooler air was supplied locally. This concept was tested by CFD simulation first and then by full-scale experiments. It has been shown by CFD simulation and then verified by experiments that the cooling performance increased more by increasing the supply air velocity than reducing the supply air temperature when the total cooling power is constant, and the cooling performance of the Air Terminal Devices (ATDs) is highly dependent on the shooting angle – the best performance always happened when the jet was aimed at the stomach. The experiments further show that the overall cooling efficiency was positively correlated with the supply temperature. In addition, both the simulation and experimental

work has demonstrated that the heat loss by the manikin was sensitive to the distance between the diffuser and the manikin. However, this effect was also related to the clothing material on the manikin because it determined the surface condition (curvature, porosity, and smoothness) and hence heat transfer coefficient. Three different ATDs were evaluated by CFD simulation, and the best performance was given by the Type I ATD (single diffuser in the center). The thermal comfort analysis was conducted based on both heat balance analysis and the Clothing Independent Thermal Comfort Model. The combination of supply air temperature of 23.1 °C and supply flow rate of 29.4 cfm and the combination of supply temperature of 26.1 °C and supply flow rate of 40.0 cfm yielded the same level of thermal sensation of the comfortable condition.

While many studies have focused on providing local thermal comfort in hot environment, very few looks into providing local heating in a cool environment. This work used the validated CFD model to evaluate several heating methods when an occupant with typical winter clothing was sitting in an office of reduced set-point at 18.9 °C for energy saving. This amount of heating power could be converted to a blow of hot air to heat the occupant by convection, conductive heat from a foot-warmer or radiant heat from an infrared heating bulb. The idea of heating a person with warm air was tested first. With 60 W of heating power, a jet with a temperature of at least 40 °C was able to heat the occupant (reduce heat loss). The minimum supply velocity is 0.5 m/s. Velocity below that made the jet deflected too fast to reach the surface of the manikin. However different from cooling the occupants with air jet, since shooting hot air to an occupant in a cold environment may entrain cooler air to blow on the human body, it was not that efficient and could only reduce the heat loss



by no more than 5.5 W. The addition of a confinement box was demonstrated to be able to improve the heating performance of the warm air jet to two or three times by retaining the hot air around the legs and feet for a while before it was mixed with the surrounding cooler air. This new idea is promising to restore occupants' thermal comfort but can be ergonomically disadvantageous because it might put too many constraints around the legs. Inspired by the work done other researchers who concluded that feet were the most sensitive part of the body to a cold environment, another method of using a foot-warmer was tested. The results showed that a warming foot mat with constant heat flux was very effective. Together with a reflective box covering the front part of the feet, the heating mat consuming 40 W electricity could reduce the heat loss by 16.9 W, which would fully recover the whole-body thermal comfort. To further improve the thermal comfort, an additional 20 W heating bulb was shown to be able to bring the overall Mean Thermal Vote (MTV) closer to the neutral level.

Full-scale chamber experiments with a clothed thermal manikin were conducted specially for confirming that the selected ATDs and HDDs were able to restore the heat balance when the room temperature set-point was relaxed for saving energy. It was shown that all diffuser configurations, with as low as 17 cfm flow rate, were capable of achieving or exceeding the target 23W of extra heat removal from the thermal manikin within the specified range of movement (0.61m), and the combination of using the heating mat with the reflective box can reduce more than 18W heat loss from the manikin.

The cubicle commonly used in the open-floor office is a typical Semi-Open Space (SOS). Usually, the cubicle is partially open on one or at most two sides. The existence of the cubicle partition significantly changes the airflow pattern in the office, and hence the thermal environment and air quality distribution. The effects of the cubicle on the thermal environment were evaluated using full-scale experiments. The results indicate that the cubicle could “protect” the occupants from the background air flow by reducing the average velocity as well as increasing the average temperature in the occupied space. The openness of the cubicle weakened the “protection” of the cubicle depending on the opening direction and size. Fully opening toward the incoming air flow weakened the “protection” the most while half opening toward the incoming air flow had the least effect on the “protection.” One should also note that the “protection” may not be favored in terms of thermal comfort especially in summer, because it weakened the cooling performance of the background ventilation. However, this negative effect can be mitigated by equipping the cubicle with the  $\mu X$ , which could also help reduce the dependence of the micro-environment on the background environment.

The effects of the cubicle and the combination of the  $\mu X$  with air purification in the cubicle on the air quality were evaluated using CFD simulation. The results indicate that the performance of the cubicle was highly sensitive to the location of the emission location and it should be used and designed with caution. When the pollutant was emitted inside the cubicle, the use of the cubicle was unfavored since it prevented the contaminant from being diluted by the mixing ventilation. However, when the pollutant was emitted from outside cubicle, the use of it should be encouraged since it helps prevent the contaminant from

entering the cubicle. The use of the  $\mu X$  with local purification could always improve the air quality in the breathing zone, and especially when the emission source was outside the cubicle, it demonstrated a big advantage. However, this combination might not be more efficient than adding the same amount of purified return air to the background mixing ventilation system when the emission source was inside the cubicle. In general, the use of the  $\mu X$  with local purification is beneficial regarding improving the air quality in the breathing zone and the cubicle.

## **9.2. Validity of CFD Models**

Not only are the results of the  $\mu X$  and SOS assessment study significant to this line of work, but also the validation work stands out on its own. Before this work, several studies have been conducted to provide the guidelines for modeling indoor environment using CFD. However, there were no studies previously on validating the CFD models with a micro-environment control system against the fully-scale experiments. The validated computational model can further be used to investigate other indoor configurations and identify potential problems and risks, and provide the guideline for the future work. Specifically,

- 1) The CFD cases, to predict the whole-body and local heat transfer from a manikin of constant surface temperature with or without the  $\mu X$ , was compared with the experiments, in which a naked thermal manikin with constant surface temperature setting was sitting in an environment with or without the  $\mu X$ . The results showed that the overall heat loss of the manikin without the  $\mu X$  predicted by the CFD agreed

extremely well with the experiment (CFD 0.5% higher than the experiment), while with the  $\mu X$ , the CFD result became 5.9% less than the experiment, which is still good. The heat transfer discrepancy of each segment of the manikin between the CFD and the experiment varied depending on the segment and the  $\mu X$  status. The variation of the discrepancy among all the segments is mostly due to the difference of the geometry and small uncertainty in the location of each segment.

- 2) The presence of the furniture has been reported to affect the development of the thermal plume and the supplying jet. In this study, the effect of the seat backrest was evaluated. A difference of the heat flux ( $\sim 10 \text{ W/m}^2$ ) was observed at the back due to the seat backrest. The reason for that is the solid backrest stopped the jet from detouring to the back to enhance the heat transfer. Other than the furniture, the clothing insulation is another challenge of using CFD for prediction. In Chapter 4, the effect of the clothing was represented by a temperature reduction on the manikin surface (except head, face, forearms, and hands) from the constant skin surface temperature at  $33.9 \text{ }^\circ\text{C}$ . However, this assumption might not be able to give the best match especially when people are wearing heavy clothes since the clothes surface temperature would change with the micro-environment (immediate ambient temperature,  $\mu X$  supply conditions, etc.). Another widely-used method is to model the clothing insulation as a layer of thermal resistance with constant value as Chapter 5. Usually, researchers use the value recommended by ASHRAE, but this recommended value could be very rough since it does not account for different

clothing materials and wrinkles or possible air pocket between the clothes and the skin.

- 3) When the manikin was exposed to a running  $\mu X$ , a significant discrepancy was observed for the stomach between the CFD and experiment. In the previous study, people always trust the experiments and tried to find the reasons from the CFD side. The effects of the grid size, selection of the turbulence model and the boundary condition have been studied. However, nobody has questioned the experiments, for example, whether the experiment maintained the same conditions as specified. In Chapter 1, the fidelity of the surface temperature control of the experiment was examined, and it was found that the surface temperature of the manikin was not as uniform as expected. There was at least a 1.0 °C surface temperature difference found on almost all the segments when the manikin was sitting in a room without the  $\mu X$ . This is because each segment of the manikin was controlled by a single heater to make sure the average surface temperature to reach the set-point and there was always an inevitable difference of heat transfer coefficient over each segment. This non-uniformity would become even more obvious when there is a local cooling or heating effect on any one of the segments, which made the experimental results different from the CFD results.

### **9.3. Recommendations for Future Work**

While this work has shown many encouraging results of using micro-environmental control system for maintaining thermal comfort and useful knowledge about the performance of

the semi-open space in the office environment, it also identifies certain issues that would provide useful guidelines for future work.

1. This work conducted the CFD simulations as well as the experiments in a lab space, where the conditions were always assumed ideal, for example, the tested chamber has a clean enclosure surface (no windows); there is only one workstation, no other heat source existed, etc. Also, in both the CFD simulations and the experiments, the occupant was always simulated with constant and uniform skin temperature, which does not account for the thermoregulation process of the human body. These issues will affect the micro-environment of the human body and possibly alter some of the conclusions found in this work.
2. The performance of the  $\mu X$  was predicted and evaluated either by CFD or experiments with a manikin, the conclusions about using it to restore thermal comfort of occupants in the environment of relaxing set-point need to be reinforced using human subject test.
3. As mentioned above, in order to further validate the CFD model, a manikin with higher fidelity is needed. One possible solution would be dividing the manikin into more segments to ensure more uniform condition on each of them.

4. An appropriate way to model the clothes on the manikin is needed in the future if one would like to get more reliable results of modeling occupants' thermal response using CFD simulations.
  
5. The effects of the cubicle on the air quality have been studied by using CFD simulations. The model needs to be further validated, and the conclusion needs to be confirmed by using experiments.

## Reference

- Ahmed Chérif Megri, Mark Snyder, M. M. 2005. Building zonal thermal and airflow-A review. *International Journal of Ventilation*, 4(2).
- Arens, E., T. Xu, K. Miura, H. Zhang, M. Fountain, and F. Bauman. 1998. A study of occupant cooling by personally controlled air movement. *Energy and Buildings*, 27(1):45–59.
- Arens, E., H. Zhang, and C. Huizenga. 2006a. Partial- and whole-body thermal sensation and comfort - Part II: Non-uniform environmental conditions. *Journal of Thermal Biology*, 31(1–2 SPEC. ISS.):60–66.
- Arens, E., H. Zhang, and C. Huizenga. 2006b. Partial- and whole-body thermal sensation and comfort — Part I : Uniform environmental conditions, 31:53–59.
- ARPA-E. 2014. *Delivering efficient local thermal amenities (DELTA) FOA*. Washington D.C.
- ASHRAE. 2013a. *ASHRAE Handbook Thermal comfort*. Atlanta, GA, USA.
- ASHRAE. 2013b. *ASHRAE Handbook-Fundamentals Chapter 18 Nonresidential Cooling and Heating Load Calculations*. Atlanta, GA, USA: ASHRAE.
- ASHRAE. 2013c. *ASHRAE Standard 55 Thermal environmental conditions for human occupancy*. Atlanta, GA, USA.
- ASHRAE. 2013d. *ASHRAE standard 62.1\_Ventilation for air quality*.
- Azer, N. Z., and S. Hsu. 1977. The prediction of thermal sensation from a simple model of human physiological regulatory response. *ASHRAE Transaction*, 83(1).
- Bauman, F. S., D. Faulkner, E. a. Arens, W. J. Fisk, L. P. Johnston, P. J. McNeel, D. Pih, and H. Zhang. 1992. Air movement, ventilation, and comfort in a partitioned office



- space. *ASHRAE Transaction: Symposia*, 98(1):0–13.
- Bauman, F. S., D. Faulkner, E. A. Arens, W. J. Fisk, L. P. Johnston, P. J. McNeel, D. Pih, and H. Zhang. 1991. *Air movement, comfort and ventilation in workstations*. Berkeley.
- Bauman, F., H. Zhang, E. A. Arens, and C. Benton. 1993. Localized comfort control with a desktop task conditioning system: laboratory and field measurements. *ASHRAE Transaction*, 99:733–749.
- Bennett, D. H., T. E. McKone, J. S. Evans, W. W. Nazaroff, M. D. Margni, O. Jolliet, and K. R. Smith. 2002. Defining intake fraction. *Environmental Science & Technology*, 36(9):207A–211A.
- Bolashikov, Z., A. Melikov, and M. Krenek. 2010. Control of the free convective flow around the human body for enhanced inhaled air quality: Application to a seat-incorporated personalized ventilation unit. *HVAC&R Research*, 16(2):161–188.
- Brasche, S., M. Bullinger, R. Schwab, H. Gebhardt, V. Herzog, and W. Bischof. 2004. Comparison of risk factor profiles concerning self-reported skin complaints and objectively determined skin symptoms in German office workers. *Indoor Air*, 14(2):137–143.
- Cao, G., H. Awbi, R. Yao, Y. Fan, K. Sirén, R. Kosonen, and J. (Jensen) Zhang. 2014. A review of the performance of different ventilation and airflow distribution systems in buildings. *Building and Environment*, 73:171–186.
- Cao, G., P. V. Nielsen, R. L. Jensen, P. Heiselberg, L. Liu, and J. Heikkinen. 2015. Protected zone ventilation and reduced personal exposure to airborne cross-infection. *Indoor Air*, 25(3):307–319.
- CD-Adapco. 2015. STAR-CCM + ® Documentation.

- Cermak, R., A. Melikov, L. Forejt, and O. Kovar. 2006. Performance of Personalized Ventilation in Conjunction with Mixing and Displacement Ventilation. *HVAC&R Research*, 12(2):295–311.
- Charles, K. E. 2003. *Fanger's Thermal Comfort and Draught Models Fanger's Thermal Comfort and Draught Models IRC Research Report RR-162*. Institute for Research in Construction. Ottawa, Canada.
- Chen, Q. 2009. Ventilation performance prediction for buildings: A method overview and recent applications. *Building and Environment*, 44(4):848–858.
- Cheng, Y., J. Niu, and N. Gao. 2012. Thermal comfort models: A review and numerical investigation. *Building and Environment*, 47(1):13–22.
- Cho, Y., H. B. Awbi, and T. Karimipناه. 2008. Theoretical and experimental investigation of wall confluent jets ventilation and comparison with wall displacement ventilation. *Building and Environment*, 43(6):1091–1100.
- Croitoru, C., I. Nastase, F. Bode, A. Meslem, and A. Dogeanu. 2015. Thermal comfort models for indoor spaces and vehicles - Current capabilities and future perspectives. *Renewable and Sustainable Energy Reviews*, 44:304–318.
- Dalewski, M., H. E. Khalifa, and A. K. Melikov. 2013. Performance of Ductless Personalized Ventilation in Open-Plan Office - Field Survey. In *11th REHVA World Congress and 8th International Conference on Indoor Air Quality, Ventilation and Energy Conservation in Buildings*.
- Dang, T. Q. 2008. Personalized ventilation system using combined jet nozzle and flow suction.pdf. U.S.A.
- de Dear, Richard J., Brager, G. S. 1998. Developing an Adaptive Model of Thermal

- Comfort and Preference. *ASHRAE Transaction*, 104(Part 1).
- de Dear, R., T. Akimoto, E. A. Arens, G. Brager, C. Candido, K. W. D. Cheong, N. Nishihara, S. C. Sekhar, S. Tanabe, J. Toftum, H. Zhang, and Y. Zhu. 2013. Review Article Progress in thermal comfort research over the last twenty years. *Indoor Air*, 23:442–461.
- de Dear, R., E. A. Arens, H. Zhang, and M. Oguro. 1997. Convective and radiative heat transfer coefficients for individual human body segments. *International Journal of Biometeorol*, 40:141–156.
- de Dear, R. J., J. W. Ring, and P. O. Fanger. 1993. Thermal sensations resulting from sudden ambient temperature changes. *Indoor Air*, 3(3):181–192.
- Deevy, M., Y. Sinai, P. Everitt, L. Voigt, and N. Gobeau. 2008. Modelling the effect of an occupant on displacement ventilation with computational fluid dynamics. *Energy and Buildings*, 40(3):255–264.
- Demetriou, D., O. Ozdemir, H. E. Khalifa, and C. Isik. 2008. Distributed demand controlled ventilation for improving IAQ. In *11th International Conference on Indoor Air Quality and Climate. Copenhagen, Denmark*.
- Deng, Q., R. Wang, Y. Li, Y. Miao, and J. Zhao. 2016. Human thermal sensation and comfort in a non-uniform environment with personalized heating. *Science of the Total Environment*.
- Dygert, R. K., and T. Q. Dang. 2012. Experimental validation of local exhaust strategies for improved IAQ in aircraft cabins. *Building and Environment*, 47(1):76–88.
- Dygert, R. K., T. Q. Dang, J. S. Russo, and H. E. Khalifa. 2009. Modeling of the human body to study the personal micro environment. *HVAC&R Research*, 115.

- ebm papst. 2017a. *3300 Axial Fans*.
- ebm papst. 2017b. *3314 NH axial fan*.
- ebm papst. 2017c. *Fan Performance Graph*.
- EIA. 2014. EIA - Annual Energy Outlook 2014 Early Release.
- Fanger, P. O. 1970. *Thermal Comfort*. Copenhagen: Danish Technical Press.
- Fiala, D., K. J. Lomas, and M. Stohrer. 1999. A computer model of human thermoregulation for a wide range of environmental conditions: the passive system. *Journal of Applied Physiology*, 87(5):1957–1972.
- Fiala, D., K. J. Lomas, and M. Stohrer. 2001. Computer prediction of human thermoregulatory and temperature responses to a wide range of environmental conditions, 143–159.
- Foda, E., and K. Sirén. 2012. Design strategy for maximizing the energy-efficiency of a localized floor-heating system using a thermal manikin with human thermoregulatory control. *Energy and Buildings*, 51:111–121.
- Gagge, A. P. 1973. Rational temperature indices of man's thermal environment and their use with a 2-node model of his temperature regulation. *Federation Proceedings*, 32(5):1572–1582.
- Gagge, A. P., A. P. Fobelets, and L. Berglund. 1986. A standard predictive index of human response to the thermal environment. *ASHRAE Transaction*, 92(CONF-8606125-).
- Gao, N., and J. Niu. 2004. CFD study on micro-environment around human body and personalized ventilation. *Building and Environment*, 39(7):795–805.
- Gao, N., and J. Niu. 2005. Modeling the performance of personalized ventilation under different room airflows. In *Ninth International IBPSA Conference. Building*

- Simulation Group 2005*. (pp. 327–334). Montreal, Canada.
- Gao, N., and J. Niu. 2006. Transient CFD simulation of the respiration process and inter-person exposure assessment. *Building and Environment*, 41(9):1214–1222.
- Givoni, B., and R. F. Goldman. 1971. Predicting metabolic energy cost. *Journal of Applied Physiology*, 30(3):429 LP-433.
- Givoni, B., and R. F. Goldman. 1972. Predicting rectal temperature response to work, environment, and clothing. *Journal of Applied Physiology*, 32(6):812 LP-822.
- Guan, Y. D., M. H. Hosni, B. W. Jones, and T. P. Giolda. 2003. Literature review of the advances in thermal comfort modeling. In *ASHRAE Transactions* (pp. 908–916).
- Haghighat, F., Y. Li, and A. C. Megri. 2001. Development and validation of. *Annals of Internal Medicine*, 36:1039–1047.
- Halvonova, B., and A. Melikov. 2010. Performance of Ductless Personalized Ventilation in Conjunction with Displacement Ventilation: Impact of Workstations Layout and Partitions. *HVAC&R Research*, 16(1):75–94.
- Hang, J., and Y. Li. 2011. Age of air and air exchange efficiency in high-rise urban areas and its link to pollutant dilution. *Atmospheric Environment*, 45(31):5572–5585.
- Hayashi, T., Y. Ishizu, S. Kato, and S. Murakami. 2002. CFD analysis on characteristics of contaminated indoor air ventilation and its application in the evaluation of the effects of contaminant inhalation by a human occupant. *Building and Environment*, 37(3):219–230.
- Hensen, J. L. M. 1990. Literature review on thermal comfort in transient conditions. *Building and Environment*, 25(4):309–316.
- Hospital wards. 2014.

- Houdas, Y., and E. Ring. 1982. *Human Body Temperature: Its measurement and regulation*. New York: Plenum Press.
- Houghton, F. C. 1923. Determining lines of equal comfort. *Transactions of Am. Soc. of Heat-Vent. Engineers*, 29:163–176.
- Hoyt, T., E. Arens, and H. Zhang. 2015. Extending air temperature setpoints: Simulated energy savings and design considerations for new and retrofit buildings. *Building and Environment*, 88:89–96.
- Hoyt, T., K. H. Lee, H. Zhang, E. Arens, and Tom Webster. 2009. Energy savings from extended air temperature setpoints and reductions in room air mixing. In *International Conference on Environmental Ergonomics* (pp. 0–5). Boston.
- Huang, L., Q. Ouyang, Y. Zhu, and L. Jiang. 2013. A study about the demand for air movement in warm environment. *Building and Environment*, 61:27–33.
- Huizenga, C., S. Abbaszabeh, L. Zagreus, and E. A. Arens. 2006. Air quality and thermal comfort in office buildings : Results of a large indoor environmental quality survey Air Quality and Thermal Comfort in Office Buildings : In *Healthy Building 2006*. Lisboa; Portugal: Healthy Buildings.
- Idelchik, I. E. 1960. *Handbook of hydraulic resistance (3rd edition)*. Israel Program for Scientific Translations.
- Indraganti, M., R. Ooka, and H. B. Rijal. 2015. Thermal comfort in offices in India: Behavioral adaptation and the effect of age and gender. *Energy and Buildings*, 103(December):284–295.
- Jiang, Z., F. Haghghat, and Q. Chen. 1997. Ventilation Performance and Indoor Air Quality in Workstations under Different Supply Air Systems: A Numerical Approach.

- Indoor and Built Environment*, 6(3):160–167.
- Kaczmarczyk, J., A. Melikov, Z. Bolashikov, L. Nikolaev, and P. O. Fanger. 2006. Human response to five designs of personalized ventilation. *HVAC&R Research*, 12(2):367–384.
- Kaczmarczyk, J., A. Melikov, and D. Sliva. 2010. Effect of warm air supplied facially on occupants' comfort. *Building and Environment*, 45(4):848–855.
- Kaczmarczyk, J., a Melikov, and P. O. Fanger. 2004. Human response to personalized ventilation and mixing ventilation. *Indoor Air*, 14 Suppl 8(Suppl 8):17–29.
- Karjalainen, S. 2012. Thermal comfort and gender: A literature review. *Indoor Air*, 22(2):96–109.
- Kato, S., S. Murakami, and H. Kobayas. 1994. New scales for evaluating ventilation efficiency as affected by supply and exhaust openings based on spatial distribution of contaminant. *12th ISCC in Yokohama, 1994*, 177–186.
- Khalifa, H. E. 2006. Computation of occupant exposure in an office cubicle. In *Proceedings of the A and WMA Indoor Environmental Quality: Problems, Research and Solutions Conference 2006* (Vol. 2, pp. 904–917).
- Khalifa, H. E. 2017. Micro Environmental Control System. U.S.A.
- Khalifa, H. E., M. I. Janos, and J. F. Dannenhoffer. 2008. Energy-neutral personal ventilation. In *Indoor Air 2008*. Copenhagen, Denmark.
- Khalifa, H. E., M. I. Janos, and J. F. Dannenhoffer. 2009. Experimental investigation of reduced-mixing personal ventilation jets. *Building and Environment*, 44(8):1551–1558.
- Khalifa, H. E., S. J. Prescod, and B. Elhadidi. 2006. Computation of an occupant exposure

- in an office cubicle. In *AWMA/EPA Conference: Indoor Air Quality - Problems, Research and Solutions* (pp. 1–14). Durham, NC.
- Kim, J., R. de Dear, C. Candido, H. Zhang, and E. Arens. 2013. Gender differences in office occupant perception of indoor environmental quality (IEQ). *Building and Environment*, 70:245–256.
- Kohri, I., and T. Mochida. 2002. Evaluation Method of Thermal Comfort in a Vehicle with a Dispersed Two-Node Model Part 1—Development of Dispersed Two-Node Model. *Journal of the Human-Environment System*, 6(1):19–29.
- Kohri, I., and T. Mochida. 2003. Evaluation Method of Thermal Comfort in a Vehicle with a Dispersed Two-Node Model Part 2-Development of New Evaluation. *Journal of the Human-Environment System*, 6(2):77–91.
- Kong, M., J. Zhang, B. Guo, and K. Han. 2016. Measurements of grease emission and heat generation rates of electric countertop appliances (RP-1631, part 1). *Science and Technology for the Built Environment*, 4731(August):1–21.
- Kong, M., J. Zhang, P. V. Nielsen, J. Wang, and L. Wang. 2014. Experimental study of chair ventilation in office cubicles. In *Roomvent 2014*. Sao Paolo.
- Kong, M., J. Zhang, and J. Wang. 2015. Air and air contaminant flows in office cubicles with and without personal ventilation: A CFD modeling and simulation study. *Building Simulation*, 8(4).
- Kong, M., J. Zhang, and J. Wang. 2015. Air and air contaminant flows in office cubicles with and without personal ventilation: A CFD modeling and simulation study. *Building Simulation*, 8(4):381–392.
- Lai, D., and Q. Chen. 2016. A two-dimensional model for calculating heat transfer in the



- human body in a transient and non-uniform thermal environment. *Energy & Buildings*, 118:114–122.
- Lan, L., P. Wargoeki, and Z. Lian. 2012. Optimal thermal environment improves performance of office work. *Indoor Environment*, (January):12–17.
- Lee, H., and H. B. Awbi. 2004. Effect of internal partitioning on indoor air quality of rooms with mixing ventilation - Basic study. *Building and Environment*, 39(2):127–141.
- Li, X., and Y. Jiang. 1998. 用计算流体力学方法求解通风房间的空气年龄. 清华大学学报, 38(5):28–31.
- Licina, D., J. Pantelic, A. Melikov, C. Sekhar, and K. W. Tham. 2014. Experimental investigation of the human convective boundary layer in a quiescent indoor environment. *Building and Environment*, 75:79–91.
- Lomas, K. J., D. Fiala, and M. Stohrer. 2003. First principles modeling of thermal sensation responses in steady-state and transient conditions. *ASHRAE Transaction*.
- Martinho, N., A. Lopes, and M. Silva. 2008. CFD modelling of benchmark tests for flow around a detailed computer simulated person. *The 7 Th International Thermal Manikin and Modeling Meeting*, 2007(September):3–8.
- Matsunaga, K., F. Sudo, S. Tanabe, and T. L. Madsen. 1993. Evaluation and measurement of thermal comfort in the vehicles with a new thermal manikin. *SAE Technical Paper Series*.
- Megri, A. C., and F. Haghghat. 2007. Zonal Modeling for Simulating Indoor Environment of Buildings: Review, Recent Developments, and Applications. *HVAC&R Research*, 13(6):887–905.
- Melikov, A. K. 2004. Improving comfort and health by personalized ventilation. In

- Roomvent 2004*. Coimbra, Portugal.
- Melikov, A. K. 2004. Personalized ventilation. *Indoor Air, Supplement, 14*(SUPPL. 7):157–167.
- Melikov, A. K., R. Cermak, and M. Majer. 2002. Personalized ventilation: evaluation of different air terminal devices. *Energy and Buildings, 34*(8):829–836.
- Melikov, A. K., and V. Dzhartov. 2013. Advanced air distribution for minimizing airborne cross-infection in aircraft cabins. *HVAC&R Research, 19*(8):926–933.
- Melikov, A. K., and G. L. Knudsen. 2007. Human Response to an Individually Controlled Microenvironment. *HVAC&R Research, 13*(4):645–660.
- Melikov, A. K., B. Krejciríková, J. Kaczmarczyk, M. Duszyk, and T. Sakoi. 2013. Human response to local convective and radiant cooling in a warm environment. *HVAC&R Research, 19*(8):1023–1032.
- Mendonça, K., and C. Inard. 2002. A zonal model for predicting simultaneous heat and moisture transfer in buildings. *Proceedings: ...*, 1–6.
- Mills, A. F. 1999. *Heat Transfer* (Second). Upper Saddle River, NJ: Prentice Hall, Inc.
- Nicol, F., and M. Humphreys. 2007. Maximum temperatures in European office buildings to avoid heat discomfort. *Solar Energy, 81*(3):295–304.
- Nicol, J. F., and I. A. Raja. 1997. Indoor thermal comfort: the Pakistan study. *Energy for Sustainable Development, 3*(5):50–60.
- Nielsen, P. V. 1980. The influence of ceiling-mounted obstacles on the air flow pattern in air-conditioned rooms at different heat loads. *Building Services Engineering Research & Technology, 1*(4):199–203.
- Nielsen, P. V. 2006. Comparison between Different Air Distribution Systems Slovene

Klima Forum , Hidria Institute Klima , Godovic , Slovenija.

Nielsen, P. V. 2007. Analysis and Design of Room Air Distribution Systems. *HVAC&R Research*, 13(6):987–997.

Nielsen, P. V. 2011. The “Family Tree” of Air Distribution Systems. *Roomvent 2011*.

Nielsen, P. V., E. Barszcz, and T. Czarnota. 2008. The influence of draught on a seat with integrated personalized ventilation. In *International Conference on Indoor Air Quality and Climate* (p. 2). Copenhagen.

Nielsen, P. V., N. Bartholomaeussen, E. Jakubowska, H. Jiang, O. Jonsson, K. Krawiecka, A. Mierzejewski, S. Thomas, K. Trampczynska, M. Polak, and M. Soennichsen. 2007. Chair with integrated personalized ventilation for minimizing cross infection. In *Proceedings of Roomvent*.

Nielsen, P. V., C. Damsgaard, L. Liu, and R. L. Jensen. 2013. Test of different air distribution concepts for a single-aisle aircraft cabin. In *CLIMA 2013*. Prague, Czech Republic.

Nielsen, P. V., C. E. Hyldgaard, A. Melikov, H. Andersen, and M. Soennichsen. 2007. Personal Exposure Between People in a Room Ventilated by Textile Terminals—with and without Personalized Ventilation. *HVAC&R Research*, 13(4):635–643.

Nielsen, P. V., T. S. Larsen, and C. Topp. 2003. Design methods for air distribution systems and comparison between mixing ventilation and displacement ventilation. In *7th International Conference on Healthy Buildings 2003* (p. Vol. 2). Singapore.

Nielsen, P. V, and E. Jakubowska. 2009. The Performance of Diffuse Ceiling Inlet and other Room Air Distribution Systems The Performance of Diffuse Ceiling Inlet and other Room Air Distribution Systems. In *COLD CLIMATE HVAC 2009*.

- Nilsson, H., H. Brohus, and P. V Nielsen. 2007. *Annex 20: Benchmark test for a computer simulated person - manikin heat loss for thermal comfort evaluation.*
- Nilsson, H. O. 2004. *Comfort climate evaluation with thermal manikin methods and computer simulation models.*
- Nilsson, H. O. 2007. Thermal comfort evaluation with virtual manikin methods. *Building and Environment*, 42(12):4000–4005.
- Nilsson, H. O., H. Brohus, and P. V Nielsen. 2007. CFD Modeling of Thermal Manikin Heat Loss in a Comfort Evaluation Benchmark Test CFD Modeling of Thermal Manikin Heat Loss in a Comfort Evaluation Benchmark Test.
- Office cubicles. 2014.
- OJIMA, J. 2012. Gaseous Contaminant Distribution in the Breathing Zone. *Industrial Health*, 50(3):236–238.
- Pasut, W., E. Arens, H. Zhang, and Y. Zhai. 2014. Enabling energy-efficient approaches to thermal comfort using room air motion. *Building and Environment*, 79:13–19.
- Pasut, W., H. Zhang, E. A. Arens, S. Kaam, and Y. Zhai. 2013. Effect of a heated and cooled office chair on thermal comfort. *HVAC&R Re*, 19:574–583.
- Pasut, W., H. Zhang, E. Arens, and Y. Zhai. 2015. Energy-efficient comfort with a heated /cooled chair : Results from human subject tests. *Building and Environment*, 84:10–21.
- Peng, L., P. V. Nielsen, X. Wang, S. Sadrizadeh, L. Liu, and Y. Li. 2016. Possible user-dependent CFD predictions of transitional flow in building ventilation. *Building and Environment*, 99:130–141.
- Posner, J. D., C. R. Buchanan, and D. Dunn-Rankin. 2003. Measurement and prediction of

- indoor air flow in a model room. *Energy and Buildings*, 35(5):515–526.
- Residential kitchens. 2014.
- Restroom blocks. 2014.
- Russo, J. 2011. A Detailed and Systematic Investigation of Personal Ventilation Systems.
- Russo, J., T. Dang, and H. E. Khalifa. 2008. Computational analysis of personal ventilation jets. In *Indoor Air 2008*. Copenhagen, Denmark.
- Russo, J., and H. E. Khalifa. 2010. CFD analysis of personal ventilation with volumetric chemical reactions. *HVAC and R Research*, 16(6):799–812.
- Russo, J. S., T. Q. Dang, and H. E. Khalifa. 2009. Computational analysis of reduced-mixing personal ventilation jets. *Building and Environment*, 44(8):1559–1567.
- Russo, J. S., and H. Ezzat Khalifa. 2010. CFD assessment of intake fraction in the indoor environment. *Building and Environment*, 45(9):1968–1975.
- Sandberg, M. 1981. What is ventilation efficiency? *Building and Environment*, 16(2):123–135.
- Seppanen, O., W. J. Fisk, and D. Faulkner. 2004. Control of Temperature for Health and Productivity in Offices. U.S.
- Shaw, C. Y., F. Vaculik, J. S. Zhang, R. J. Magee, and M. N. Said. 1993. Effect of air diffuser layout on the ventilation conditions of a workstation. Part II: Air change efficiency and ventilation efficiency. *ASHRAE Transactions*, 99(2):133–143.
- Shaw, C. Y., J. S. Zhang, M. N. Said, F. Vaculik, and R. J. Magee. 1993. Effect of air diffuser layout on the ventilation conditions of a workstation. Part I: Air distribution patterns. *ASHRAE Transactions*, 99(2):125–132.
- Skistad, H., E. Mundt, P. V. Nielsen, K. Hagstrom, and J. Railia. 2002. Displacement

- ventilation in non-industrial premises. In *In REHVA Huidebook No.1*.
- Song, G. 2011. *Improving comfort in clothing*. Philadelphia, PA, USA: Woodhead Publishing Limited in association with The Textile Institute.
- Sørensen, D. N., and L. K. Voigt. 2003. Modelling flow and heat transfer around a seated human body by computational fluid dynamics. *Building and Environment*, 38(6):753–762.
- Stolwijk, J. A. 1971. A mathematical model of physiological temperature regulation in man. NASA Contractor Report CR-1855. *NASA Contractor Report, CR-1855(August):77*.
- Summer, W. 1971. *Odour pollution of air, Causes and control (Chemical and process engineering series)*. London: TBS The Book Service Ltd.
- Tanabe, S., T. Tsuzuki, K. Kimura, and S. Horikawa. (n.d.). *Numerical Simulation Model of Thermal Regulation of Man with 16 Body Parts of Evaluating Thermal Environment (Part 1 Heat Transfer at Skin Surface and Comparison with SET\* and Stolwijk Model)*. *Summaries of Technical Papers of Annual Meeting, Architectural Institute of Japan*.
- Taniguchi, Y., H. Aoki, K. Fujikake, H. Tanaka, and M. Kitada. 1992. Study on Car Air Conditioning System Controlled by Car Occupants' Skin Temperatures - Part 1: Research on a Method of Quantitative Evaluation of Car Occupants' Thermal Sensations by Skin Temperatures. *SAE Technical Paper Series*.
- Teshome, E., and F. Haghghat. 2004. Zonal Models for Indoor Air Flow. A Critical Review. *International Journal of Ventilation*, 3(May):119–129.
- Verhaart, J., M. Veselý, and W. Zeiler. 2015. Personal heating: effectiveness and energy

- use. *Building Research & Information*, 43(3):346–354.
- Wang, L., J. Zhang, X. Bai, and M. Kong. 2014. Local heat flux distribution over human body : literature review and analysis. In *Roomvent 2014* (pp. 1–10). Sao Paolo.
- Wang, X. 1994. *Thermal comfort and sensation under transient conditions*. The Royal Institute of Technology, Sweden.
- Watanabe, S., A. K. Melikov, and G. L. Knudsen. 2010. Design of an individually controlled system for an optimal thermal microenvironment. *Building and Environment*, 45(3):549–558.
- Webb, C. G. 1959. An analysis of some observations of thermal comfort in an equatorial climate. *British Journal of Industrial Medicine*, 16(4):297–310.
- Wurtz, E., F. Haghghat, L. Mora, and K. C. Mendonca. 2006. An integrated zonal modelk to predict transient indoor humidity distribution.pdf. *ASHRAE Transaction*, 112(2):175–186.
- Xu, W., and Q. Chen. 2001a. A two-layer turbulence model for simulating indoor airflow - Part I. Model development. *Energy and Buildings*, 33(6):613–625.
- Xu, W., and Q. Chen. 2001b. A two-layer turbulence model for simulating indoor airflow Part II. Applications. *Energy and Buildings*, 33:627–639.
- Yaglou, C. P., and D. Minaed. 1957. Control of heat casualties at military training centers. *Arch. Indust. Health*, 16(4):302–316.
- Yang, J., S. Kato, and J. Seo. 2009. Evaluation of the convective heat transfer coefficient of the human body using the wind tunnel and thermal manikin, (November):563–569.
- Yi, L., L. Fengzhi, L. Yingxi, and L. Zhongxuan. 2004. An integrated model for simulating interactive thermal processes in human – clothing system, 29:567–575.

- YOKOYAMA, S., N. KAKUTA, T. TOGASHI, Y. HAMADA, M. NAKAMURA, and K. OCHIFUJI. 2000. Development of prediction computer program of whole body temperatures expressing local characteristic of each segment: part 1-bio-heat equations and solving method. *Transactions of the Society of Heating, Air-Conditioning and Sanitary Engineers of Japan.*, (77):1–12.
- Yokoyama, S., N. Nakuta, and K. Ochifuji. 1997. Development of a new algorithm for heat transfer equation in human body and its applications, *16(4):153–59*.
- Zeiler, W., M. Vesely, D. Vissers, and R. Li. 2015. Thermal response of different body parts: The fingertip as control sensor for personalized heating. *Energy Procedia*, 78:2766–2771.
- Zhai, Y., C. Elsworth, E. Arens, H. Zhang, Y. Zhang, and L. Zhao. 2015. Using air movement for comfort during moderate exercise. *Building and Environment*, 94(P1):344–352.
- Zhai, Y., H. Zhang, Y. Zhang, W. Pasut, and E. Arens. 2013. Comfort under personally controlled air movement in warm and humid environments. *Building and Environment*, 65:109–117.
- Zhang, H. 2003. *Human thermal sensation and comfort in transient and non-uniform thermal environments*. University of California, Berkeley.
- Zhang, H., E. Arens, S. A. Fard, C. Huizenga, G. Paliaga, G. Brager, and L. Zagreus. 2007. Air movement preferences observed in office buildings. *International Journal of Biometeorology*, 51(5):349–360.
- Zhang, H., E. Arens, C. Huizenga, and T. Han. 2010a. Thermal sensation and comfort models for non-uniform and transient environments : Part I: Local sensation of



- individual body parts. *Building and Environment*, 45(2):380–388.
- Zhang, H., E. Arens, C. Huizenga, and T. Han. 2010b. Thermal sensation and comfort models for non-uniform and transient environments , part II: Local comfort of individual body parts. *Building and Environment*, 45(2):389–398.
- Zhang, H., E. Arens, C. Huizenga, and T. Han. 2010c. Thermal sensation and comfort models for non-uniform and transient environments , part III: Whole-body sensation and comfort. *Building and Environment*, 45(2):399–410.
- Zhang, H., E. Arens, D. Kim, E. Buchberger, F. Bauman, and C. Huizenga. 2010. Comfort , perceived air quality , and work performance in a low-power task – ambient conditioning system. *Building and Environment*, 45(1):29–39.
- Zhang, H., E. Arens, M. Taub, D. Dickerhoff, F. Bauman, M. Fountain, W. Pasut, D. Fannon, Y. Zhai, and M. Pigman. 2015. Using footwarmers in offices for thermal comfort and energy savings. *Energy and Buildings*, 104:233–243.
- Zhang, S., H. E. Khalifa, and J. F. Dannenhoffer. 2007. Flow between adjacent cubicles due to occupant-controlled floor diffusers. In *Roomvent 2007 Conference, Helsinki, Finland*.
- Zhang, Y. F., D. P. Wyon, L. Fang, and A. K. Melikov. 2007. The influence of heated or cooled seats on the acceptable ambient temperature range. *Ergonomics*, 50(4):586–600.

# VITA

**Name of the Author:** Meng Kong

**Place of Birth:** Kaifeng, Henan, Chian

**Date of Birth:** April 28, 1988

**Graduate and undergraduate school attended:**

Syracuse University, Syracuse, NY, USA

Beijing University of Civil Engineering and Architecture, Beijing, China

**Degree Awarded:**

M.S. Mechanical and Aerospace Engineering, 2013, Syracuse University, USA

B.S. Building Environment and Equipment Engineering, 2010, Beijing University of  
Civil Engineering and Architecture, China

**Awards and Honors:**

ASHRAE Graduate Student Grant-In-Aid for 2015-2016 academic year, 2015

Research assistant scholarship at Syracuse University, 2014-2017

Teaching assistant scholarship at Syracuse University, 2013

Supreme-class China Artificial Environmental Engineering scholarship, 2009

National Merit-based Scholarship of China, 2008

**Professional Experience:**

Research assistant at Syracuse University, Department of Mechanical and Aerospace  
Engineering, 2014-2017

Teaching assistant at Syracuse University, Department of Mechanical and Aerospace  
Engineering, 2013

